REHVA COMMUNITY OF YOUNG PROFESSIONALS

BOOK OF PAPERS

2024

ISTANBUL, TÜRKIYE

HVAC WORLD STUDENT COMPETITION 2024

REHVA STUDENT COMPETITION 2024

Our Sponsors

BOOK OF PAPERS

2024

Istanbul, Türkiye

© REHVA, 2024
All rights reserved.
www.rehva.eu

Table of content

Introduction

The Book of papers is presented by RCYP (REHVA Community of Young Professionals). The RCYP aims to facilitate professional activities and knowledge exchange between young professionals (below 35 years) in the fields of indoor climate, HVAC, building physics, and building services. In the current book, the papers written by the participants of the REHVA Student Competition and the ones from the HVAC World Student Competition are presented. The winners of each competition are also shown at the beginning. At the end of the book, the photos of the events can be found.

REHVA Student Competition

Ever since 2005, REHVA has been organizing a yearly international competition to award the best HVAC students in Europe. REHVA member associations nominate one entry per country to the competition after having organized their national level competitions. The submitted works are based on a Master or Bachelor work and can cover any topic in the fields related to REHVA. The Student competitions are organized during the REHVA Annual Meetings and the Students receive a trophy with their names engraved in it, which is then handed over next year to the next winner. The trophy has been traveling long in the past decade, carrying the names of all the proud winners since 2005.

HVAC World Student Competition

In 2013, REHVA founded a World Student competition with several its international partner associations. Ever since 2016, the HVAC World Student Competition has been taking place between students nominated by REHVA (EU), ASHRAE (United States), CAHVAC (China), FAIAR (South America), ISHRAE (India), SAREK (South Korea) and SHASE (Japan). Each association may send one candidate from their region or continent. REHVA's candidate in the HVAC World Student Competition is the winner from REHVA Student Competition. The other MoU partners organise the HVAC World Student Competition according to the same rules around the world with the participation of REHVA in the jury. The first competition was held in 2016 by REHVA in Denmark. REHVA co-finances the participation of the European candidate in these global competitions

REHVA Student Competitions 2024

REHVA Student Competition 2024 took place in Istanbul during REHVA's Annual Meeting on May 16, 2024. This event brought together 15 students from various parts of Europe who gathered in Turkey to showcase their research projects before a distinguished panel of jury members.

Jury members :

The jury team members included Livio Mazzarella (AiCARR-Italy), Maja Todorović (KGH-Serbia), Uwe Schulz (Die Planer – Switzerland), Yangang Xing (CIBSE-UK), Murat Çakan (TTMD – Turkey), Michal Krajcik (SSTP – Slovakia).

Here is the final result and the subject of their project:

The 1st place and the trophy were awarded to João Mota, from Portugal, for his work titled "Acoustic Assessment of a Novel Visor Concept with Aerodynamic Sealing for Medical Protection”.

Marco Bizzarri secured second place for his paper on "Building Heating Load Prediction for Optimal Control of Hybrid Heat Pumps: Evaluation of an Autoregressive Model and Energy Analysis“, while the French team, Ninon Gauthier and Roxane Viala, came third with their study on "Monte-Carlo modeling of input uncertainly in ELECTRE-Tri Multi Criteria Decision Analysis“. Angelika Václavová won the "best poster" category.

HVAC World Student Competitions 2024

The HVAC World Student Competition 2024 took place in Korea, on June 20th, 2024.

The first prize was awarded to João Mota (Portugal) with his work on the topic " Acoustic Assessment of a Novel Visor Concept with Aerodynamic Sealing for Medical Protection“. Junhyeok Jang and Hyejun You – SAREK/Korea, arrived second. Yashu Zhao – CAHVAC/China secured the third place, and Tatsuya Miyata – SHASE/Japan won the prize for best poster. The HVAC World Student Competition 2024 was the 5th time that REHVA's representative won the 1st prize.

About RCYP (REHVA Community of Young Professionals)

The RCYP was founded in 2020 by REHVA and coordinated by Arash Rasooli, the first winner of REHVA and HVAC World Student Competition (2016). REHVA seeks the objective of advancing its programs and services for young engineers, helping them build their professional foundations and career. REHVA organises courses for students and young professionals and promotes their participation in the REHVA network event by discounts. REHVA will support the joint activities defined together with the RCYP members and offer advantages relying on the existing REHVA knowledge sources and services, such as free or discounted access to REHVA guidebooks, events and trainings, publication possibility in the REHVA Journal, specific sessions at REHVA events for the community.

The CLIMA World Congresses are inviting young researchers to submit abstracts. If students team-up and purchase REHVA guidebooks, they receive a discount. RCYP is building an online community and information hub tailored to the interest of community members. For any inquiries, feel free to contact us at rcyp@rehva.eu.

Results

REHVA Student Competition 2024

Marco Bizzarri
Italy

2

João Mota
Portugal

1

Ninon Gauthier – Roxane Viala
France

3

HVAC World Student Competition 2024

Junhyeok Jang – Hyejun You
SAREK

2

João Mota
REHVA

1

Yashu Zhao – Suxian Jiang
CAHVAC

3

1st Place
REHVA
Student Competition

João Mota
Portugal

2024

REHVA Federation of European Heating, Ventilation and Air Conditioning Associations

SPONSORED BY:

EUROVENT CERTIFIED PERFORMANCE www.eurovent-certification.com

Acoustic Assessment of a Novel Visor Concept with Aerodynamic Sealing for Medical Protection

João Pedro Sousa Mota[1*]
Supervisors: Adélio Manuel Rodrigues Gaspar[1**], Nuno Cláudio Ferreira Rosa[1**]

1: University of Coimbra, ADAI, Department of Mechanical Engineering, Rua Luís Reis Santos, Polo II, 3030-788 Coimbra, Portugal.
* e-mail: joao.mota@adai.pt, ** e-mail: adelio.gaspar@dem.uc.pt, ***e-mail: nuno.rosa@uc.pt

Accepted on 8 July 2023

Abstract—This paper details the acoustic evaluation and optimization of a new solid visor with aerodynamic sealing for medical care. This novel personal protective equipment (PPE) ensures effective aerodynamic sealing of the breathing zone, reducing the risk of inhaling infectious droplets and aerosols. To mitigate considerable noise from the air supply system, various solutions were investigated, including adjustments to air flow rate, tube diameter, tube insulation, tube splitter configurations, and the addition of physical barriers and a sound muffler. These optimizations reduced noise levels by 34.1 dBA for an air flow rate of 25 l/min, with a final prototype producing a noise level of 44.3 dBA. Speech Intelligibility Index (SII) significantly improved across all flow rates, reaching values close to 1. Comparison with surgical masks and FFP2 respirators was conducted to evaluate speech transmission, demonstrating the potential for enhanced acoustic performance this type of PPE.

Index Terms—Air-curtain, Air-sealed visor, Acoustic assessment, Speech Intelligibility Index, PPE

Introduction

The COVID-19 pandemic has prompted the adaptation of safety measures in healthcare systems worldwide, emphasizing the importance of personal protective equipment (PPE) like masks, respirators, and face shields to mitigate airborne transmission risks.

Given the potential for future pandemics [1], [2], there's a growing demand for reliable PPE to safeguard essential workers. While traditional face masks have limitations [3], [4], visors provide enhanced comfort and eye protection [5]–[7]. However, their protection effectiveness compared to masks and respirators is typically lower [8], driving ongoing developments to improve PPE design for better comfort and effectiveness.

In response to the pandemic, novel PPE designs, including air-curtain sealed devices, have emerged [9]–[11]. Air curtains, initially introduced for protecting against aerosols and droplets, also show promise in industrial settings for safeguarding against gaseous contaminants and particulate matter [12], [13]. Positioned in front of the face, they effectively intercept and redirect potential contaminants, improving air quality. However, integrating air curtains into visors can produce significant noise, which can adversely affect human health and cause issues related to prolonged use of such PPE [14]–[16].

Among these innovative designs is the MASK4MC (Mask for Medical Care) [17], and its evolution, the VV4MC (Ventilated Visor for Medical Care), designed to offer additional protection against airborne transmission. This study focuses on evaluating and optimizing the acoustic performance of such novel air-curtain sealed PPE, considering noise levels, frequency characteristics, speech intelligibility, and the impact on speech transmission. This study aims to offer design solutions for future devices, aiding healthcare workers in preventing the spread of new viruses.

II. Methods

A. Description of the air curtain personal protective equipment

The design of the personal protective equipment (PPE) for medical professionals, as depicted in Figure 1, ensures comfort and safety in clinical settings. With its solid face shield (A in Figure 1) and air curtain provided by a two-chamber plenum (B in Figure 1), this PPE offers reliable protection against various airborne particles while seamlessly integrating with essential gear such as surgical masks, respirators, and goggles. The robust support system (C and D in Figure 1) not only guarantees a secure fit but also acts as a structural component, helping its assembly with the shield and plenum through screws (J in Figure 1). As air is channeled through the main tube (E in Figure 1) and directed by the T-shaped splitter (F in Figure 1), it encounters polymeric barriers (I in Figure 1) to establish a stable air curtain, vital for safeguarding against contaminants. An airflow rate of 24.5 l/min was found to be optimal for stability and protection efficiency [18], achieving a velocity of approximately 0.5 $m.s^{-1}$ across the frontal jet outlets. The subsequent analysis will focus on evaluating the PPE's efficacy at an air flow rate of 25 l/min. Further details can be found in references [18], [19] and a complete analysis for more air flow rates can be also be found in reference [20].

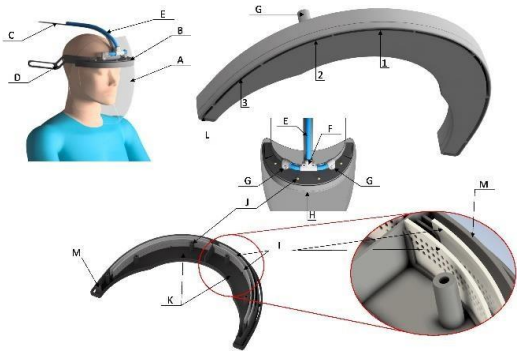

Figure 1 – MASK4MC illustration. Source: [20]

B. Experimental setup and procedures

The aim is to experimentally evaluate the acoustic performance of the PPE prototype and optimize it. Figure 2 illustrates the experimental setup used for measuring A-weighted Noise Equivalent Level, Third-Octave Frequency Distribution, and the Speech Intelligibility Index. Experiments were conducted in a controlled low-noise room during nighttime to mitigate external interferences.

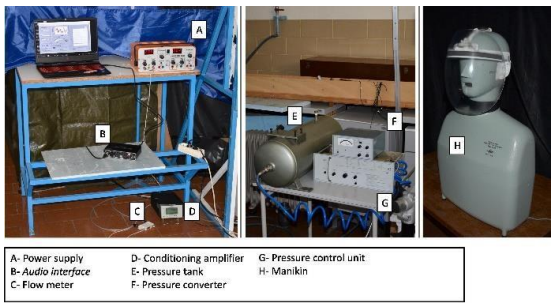

Figure 2 – Illustration of the experimental setup. Source: [20].

An acoustic manikin (Brüel & Kjær Sound Quality Head and Torso Simulator Type 4100) with built-in condenser microphones and a preamplifier within each ear was used for data acquisition of sound signals. The air supply system utilized the building's compressed air network, comprising an additional air compressor tank, a pressure converter, a pressure control unit, and a flow meter.

LabView-based software applications [21]–[23] were employed for data acquisition of sound signals and analysis. A-weighted sound levels were used to account for human hearing sensitivity across the audible frequency spectrum. The A-weighting slightly amplifies the mid-range frequencies, where human hearing is most sensitive, while significantly attenuating the low-frequency region, where the sensitivity is reduced. The application of this weighting to the measurements is noticeable in the frequency spectra, particularly in the low-frequency range where the negative values indicate that sound levels, although present, fall below the human hearing threshold in those specific frequencies. The first experiment aimed to assess the impact of the PPE on ambient noise by measuring the values and one-third octave spectra over a 30 s period. The measurements were conducted under two conditions: without the PPE and with the manikin wearing the PPE, but without the air supply. The assessment of the PPE acoustic performance was initiated by measuring the sound levels without the air curtain flow and establishing the initial conditions (t = 0 s) for each experiment. After approximately 45 s, the air supply was then activated, and the desired air flow rate was set. To ensure the stabilization of the short-term equivalent continuous sound pressure level ($Lp_{eq,T}$), data was acquired continuously over a period of 105 s. The total time for each experiment is 150 s. The equivalent continuous pressure levels for both the ambient noise (Leq_{room}) and total noise (Leq_{tot}) were calculated using equation (1). The calculations were performed using data collected from t = 15 to 45 s, for ambient noise, and from 120 to 150 s, for total noise.

The evaluation of noise levels was based on the following equations:

$$Leq = 10\log_{10}\left(\frac{1}{n}\sum_{i=1}^{n} 10^{\frac{Lp_i}{10}}\right)\ [\text{dBA}], \quad (1)$$

$$Leq_{PPE} = 10\log_{10}\left(10^{\frac{Leq_{tot}}{10}} - 10^{\frac{Leq_{room}}{10}}\right)\ [\text{dBA}] \quad (2)$$

n is the total number of sound pressure levels (Lp_i) recorded over each measurement, Leq_{tot} represents the measured total equivalent continuous sound pressure level, when air supply is turned on, and Leq_{room} the measured ambient equivalent continuous sound pressure level, when air supply is turned off. To obtain the Leq_{PPE}, the equivalent continuous sound pressure level generated by the PPE, equation (2) is used.

The Speech Intelligibility Index (SII) was calculated following ANSI/ASA 3.5–1997 [24] standard.

To assess the impact of wearing the VV4MC on speech transmission, a comparative study using white noise was conducted considering other commonly used PPE. Figure 3 illustrates the experimental setup for the speech transmission study. A microphone was placed 2 meters apart from the manikin, which had a loudspeaker inside its head to emit the white noise (set to 67 dBA) (a in Figure 3). Figure 3 also depicts the different scenarios considered, including without any mask or visor (b in Figure 3), with a surgical mask (c in Figure 3), with an FFP2 respirator (d in Figure 3), and with the optimized version of the VV4MC (e in Figure 3).

Figure 3 – Experimental setup to assess the impact of PPEs on speech levels. Source: [20].

C. Noise reduction strategies

Acoustic optimization strategies for the novel PPE encompass several approaches, as shown in Figure 4.

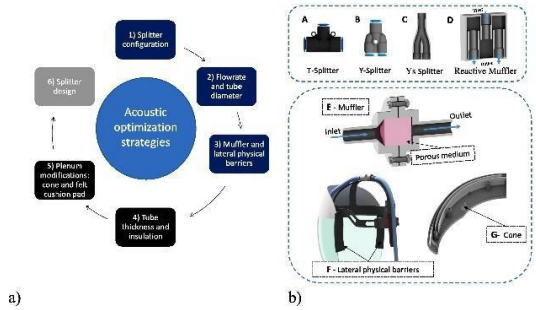

Figure 4 – a) Flowchart of the design optimization process and b) Proposed solutions sketches. Source: [20].

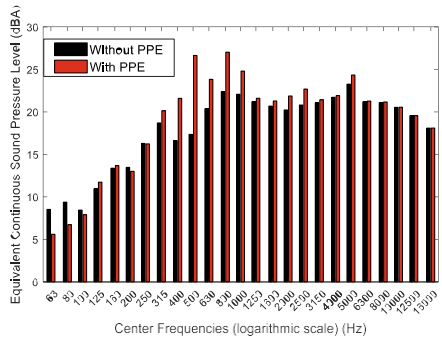

Figure 5 – Ambient A-weighted noise equivalent level. Adapted from [20].

Initially, replacing the T-shaped splitter (A in Figure 4b) with a Y-shaped one (B in Figure 4b) minimizes air disturbance and eliminates sharp corners, reducing airflow disruptions. Additionally, experiments explore the impact of tube diameter and air flow rate on noise levels. As already mentioned, the complete study including all air flow rates tested is available in reference [20]. Further noise reduction components include a muffler (E in Figure 4b) with porous material placed upstream of the splitter to absorb and reflect sound waves [25], [26]. Lateral physical barriers (sideguards) (F in Figure 4b) enhance protection efficiency and further reduce noise from the jet slots [19]. Tube thickness variations (8 mm inner diameter, 1 and 2-mm thickness) are also tested, as well as the application of a layer of tube insulation.

Within the plenum, strategies involve covering the floor with a cushion pad (3 mm height) to absorb sound energy and installing a cone (G in Figure 4b) to diffuse air and minimize pressure fluctuations. Computational Fluid Dynamics simulations ensured that both these changes inside the plenum geometry would not compromise efficiency [20].

The final stage explores alternative splitter designs, including the Ys (Y streamlined) splitter (C in Figure 4b) and the Reactive Muffler Splitter (RMS) (D in Figure 4b). The RMS, similar to an automotive muffler, reflects sound waves to reduce noise within the inlet and outlet tubes [27].

Both the Ys and RMS are non-commercial components, custom-designed and 3D printed in-house for this specific application.

III. Data Presentation And Discussion

A. PPE impact on ambient noise

The effect of wearing the novel PPE on ambient A-weighted noise equivalent level, measured at the manikin's ears, was evaluated by analyzing $Lp_{eq,T}$ values and one-third octave spectra. Figure 5 shows the results of the ambient one-third octave bands frequency spectra with and without the PPE. The results indicate that the PPE impact on A-weighted noise equivalent level was minimal, as $Lp_{eq,T}$ remained consistent at ≈34.8 dBA. However, slight effects were noted in the spectra at the mid-frequency range (Figure 5).

B. Acoustic optimizations

As depicted in Figure 4, the design optimization process was iterative, with adopted solutions leading to incremental improvements throughout the study. TABLE I provides a description of each optimization iteration, serving as a guide for analyzing the results presented in Figure 6, Figure 7, and Figure 8. The results in these figures are depicted with a color gradient ranging from red, indicating the worst result, to bright green, indicating the best.

As previously noted, the analysis only considers an airflow rate of 25 l/min. However, a comprehensive analysis for other airflow rates, as well as a detailed frequency analysis of each tested solution, can be found in reference [20].

Furthermore, detailed analysis of tube thickness variation, plenum modifications, and tube insulation are also available in reference [20].

Iterations 1, 3, 4, and 8 employ the same type of splitter (Y) but feature varying tube internal diameters, which increase accordingly. Notably, increasing the tube diameter while maintaining the same airflow rate, i.e. reducing air flow velocity, leads to an improvement in acoustic performance. Simply adjusting the tube internal diameter resulted in a reduction of the noise level from 78.4 to 59.1 dBA and an increase in the Speech Intelligibility Index (SII) from 0.17 to 0.53 (Figure 6 and Figure 7). While increasing the tube diameter improves the acoustic performance, excessive increases often coincide with greater tube thickness, potentially compromising flexibility and adding weight, therefore, the tube internal diameter was not further increased.

Regarding noise reduction components, the ones that are analyzed in this work are the muffler (E in Figure 4b) and the sideguards (F in Figure 4b). Comparing optimization iterations 4, 5, and 6, for a tube internal diameter of 8 mm, highlights the acoustic performance improvements brought by these components. Introducing these solutions separately allowed to assess the noise reduction capability of each one. Notably, the muffler demonstrated a higher impact on noise reduction compared to the sideguards, reducing noise levels from 62.0 dBA to 54.9 dBA, while the sideguards reduced noise levels to 57.8 dBA (Figure 6). Although the muffler outperformed the sideguards in noise reduction, both components showed equivalent improvements in SII, increasing this value from 0.44 to

0.64 (Figure 7). The variations in improvement can be attributed to the different spectral attenuation achieved by each component. This is further detailed in reference [20].

Combining both components brings further improvements of both noise levels and speech intelligibility. Comparing optimization iterations 4 and 7 shows that this combined solution results in noise levels reduction from 62.0 dBA down to 51.4 dBA and an improvement of the SII from 0.44 up to 0.80. Now comparing optimization iterations 7 and 11, where the only difference is in the tube internal diameter, which increased from 8 to 10 mm, the improvements are more pronounced, with noise levels decreasing to 47.8 dBA and SII increasing to 0.92 (Figure 6 and Figure 7). This marks a significant achievement in the optimization process, reaching a point where the VV4MC guarantees good speech intelligibility, as defined by the guidelines in ANSI/ASA S3.5-1997 (R2020) [24], where values above 0.75 characterize a good communication system.

In the final stage of this optimization process, there was a concern regarding the contribution of the splitter (F in Figure 1) to the noise. This concern was caused by an earlier modification from a T-shaped splitter to a Y-shaped one (optimization iteration 2 and 3), which resulted in a reduction of noise levels from 69.1 to 66.9 dBA and an increase in the SII from 0.17 to 0.25 (Figure 6 and Figure 7).

Therefore, two new components, the Ys and the RMS, were designed and 3D-printed to further improve the acoustic performance (C and D in Figure 4b, respectively).

As the improvements observed from iteration 2 to 3 were attributed to reduced air flow disturbances by eliminating sharp corners in the air flow path, the Ys was designed in a way that could further minimize these disturbances and improve the acoustic performance.

However, this solution did not yield the expected results. Comparing the results of optimization iterations 8 and 9, the introduction of the Ys splitter led to an increase in noise levels, from 59.1 to 62.2 dBA, and a decrease in the SII, from 0.53 down to 0.44 (Figure 6 and Figure 7). These results suggested that this design actually facilitated noise propagation from upstream due to reduced disturbance, when compared with the commercial Y-splitter (B in Figure 4b).

To address this issue, and motivated by the positive impact of the muffler, the RMS was designed. Its design aimed to reflect sound waves back upstream and within itself, reducing upstream noise propagation. The impact of this solution can be seen by comparing iterations 8 and 10. This comparison reveals the impact of this solution, with the RMS alone reducing noise levels from 59.1 to 54.9 dBA and increasing the SII from 0.53 to 0.71. When integrated with the muffler and sideguards in iteration 12, the results showed a further reduction of noise levels down to 44.3 dBA and an increase of the SII to 0.99 (Figure 6 and Figure 7), close to its maximum value (1.0).

Iteration 12 represents the final prototype of the VV4MC, incorporating the RMS, the muffler, and the sideguards, with a tube internal diameter of 10 mm. Comparing the frequency spectra of the first and the final iterations of this optimization process (Figure 8), reveals a striking difference which shows how the entire frequency spectrum was attenuated, resulting in an overall noise levels reduction of 34.1 dBA, from 78.4 dBA down to 44.3 dBA, and an increase of the SII from 0.17 to 0.99. Moreover the noise levels generated by the VV4MC are considered safe and well below the recommended occupational noise limits set by the World Health Organization (WHO) [28], the National Institute for Occupational Safety and Health (NIOSH) [29], and European directives [30].

TABLE I.
OPTIMIZATION ITERATION DESCRIPTION WITH TUBE INTERNAL DIAMETER (Ø), SPLITTER DESIGNS AND OTHER NOISE REDUCTION COMPONENTS.

Optimization iteration	Description
1	Ø4 mm (Y)
2	Ø5.5 mm (T)
3	Ø5.5 mm (Y)
4	Ø8 mm (Y)
5	Ø8 mm (Y + Muffler)
6	Ø8 mm (Y + Sideguards)
7	Ø8 mm (Y + Muffler + Sideguards)
8	Ø10 mm (Y)
9	Ø10 mm (Ys)
10	Ø10 mm (RMS)
11	Ø10 mm (Y + Muffler + Sideguards)
12	Ø10 mm (RMS + Muffler + Sideguards)

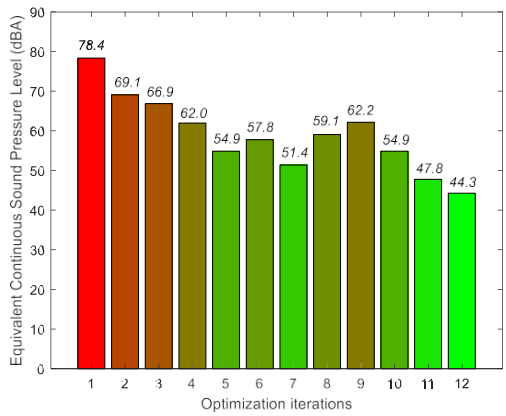

Figure 6 – Equivalent Continuous Sound Pressure Level (Leq) evolution throughout the study (for 25 l/min).

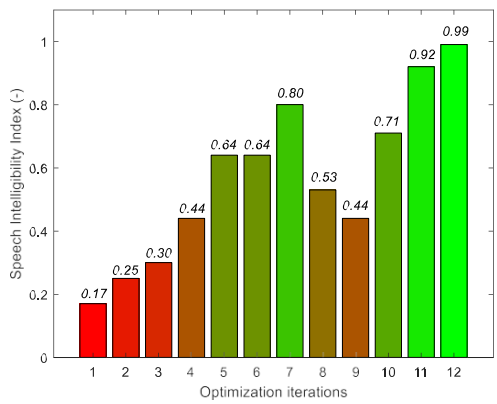

Figure 7 – Speech Intelligibility Index (SII) evolution throughout the study (for 25 l/min).

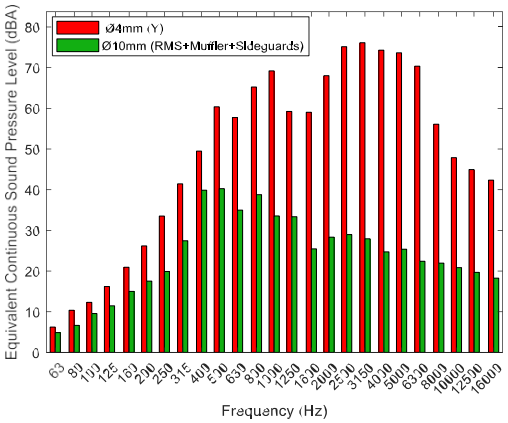

Figure 8 – One-Third Octave Frequency Spectra comparison between the first optimization iteration (1) and the last (12).

C. Speech Attenuation of different PPE

PPEs can impact have a negative impact in communication, especially in critical work settings where clear communication is essential to carry out procedures and maintain high performance [3].

This study addresses this concern by assessing the impact of wearing the VV4MC in speech transmission. This is done by comparing how different PPE attenuate the white noise attenuation emitted by a speaker. The experimental setup for this purpose can be seen in Figure 3. Evaluation of white noise attenuation with different PPE revealed reductions ranging from 2.2 dBA for the surgical mask, close to those of Goldin et al. [31], 3.7 dBA for the FFP2 respirator, and 4.7 dBA for the VV4MC (Figure 9). These results demonstrate that the VV4MC has a higher impact on speech transmission and that this issue still needs to be properly addressed.

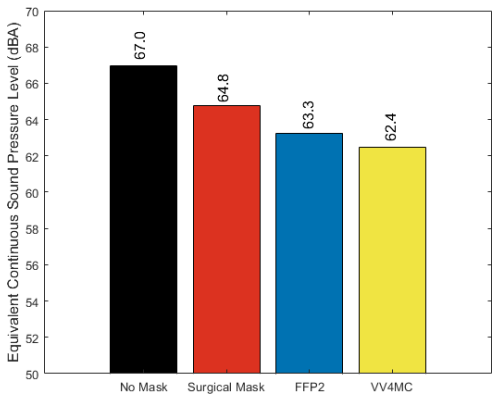

Figure 9 – White noise attenuation of the different PPE. Adapted from [20].

IV. CONCLUSIONS

This paper presents the assessment and optimization of the acoustic performance of a novel visor concept with aerodynamic sealing. Methods include measuring A-weighted Noise Equivalent Level, conducting frequency analysis, evaluating Speech Intelligibility Index (SII), and assessing speech attenuation of the final PPE prototype. The primary noise source is the air supply system, mitigated through various strategies to prevent noise propagation. Implementation of strategies such as increasing tube diameter, adding a muffler, new splitter designs, and a lateral physical barrier resulted in a 34.1 dBA reduction in noise level for an air flow rate of 25 l/min. The final PPE configuration achieved an A-weighted Noise Equivalent Level at 44.3 dBA, with excellent speech intelligibility (0.99). In speech attenuation tests, the final prototype showed lower results compared to surgical masks and FFP2 respirators. Future work should focus on usability tests in real working conditions, incorporating survey testing for user feedback to refine PPE design and functionality.

ACKNOWLEDGEMENT

This work was funded by FEDER - European Regional Development Funds through the operational program Centro 2020 of Portugal 2020 according to Support System for Scientific and Technological Research (SAICT) in the framework of the project "VV4MC – A new type of ventilated visor for medical care" (CENTRO-01-0145-FEDER-181248) and was sponsored by national funds through FCT – Fundação para a Ciência e a Tecnologia, under project LA/P/0079/2020, DOI: 10.54499/LA/P/0079/2020 (https://doi.org/10.54499/LA/P/0079/2020).

REFERENCES

[1] M. Marani, G. G. Katul, W. K. Pan, and A. J. Parolari, "Intensity and frequency of extreme novel epidemics," *Proc. Natl. Acad. Sci. U. S. A.*, vol. 118, no. 35, p. e2105482118, Aug. 2021, doi: 10.1073/pnas.2105482118.

[2] K. E. Jones *et al.*, "Global trends in emerging infectious diseases," *Nat. 2008 4517181*, vol. 451, no. 7181, pp. 990–993, Feb. 2008, doi: 10.1038/nature06536.

[3] Y. Li *et al.*, "Effects of wearing N95 and surgical facemasks on heart rate, thermal stress and subjective sensations," *Int. Arch. Occup. Environ. Health*, vol. 78, no. 6, pp. 501–509, Jul. 2005, doi: 10.1007/s00420-004-0584-4.

[4] B. V. Shenal, L. J. Radonovich, J. Cheng, M. Hodgson, and B. S. Bender, "Discomfort and exertion associated with prolonged wear of respiratory protection in a health care setting," *J. Occup. Environ. Hyg.*, vol. 9, no. 1, pp. 59–64, Jan. 2012, doi: 10.1080/15459624.2012.635133.

[5] M. Abboah-Offei, Y. Salifu, B. Adewale, J. Bayuo, R. Ofosu-Poku, and E. B. A. Opare-Lokko, "A rapid review of the use of face mask in preventing the spread of COVID-19," *Int. J. Nurs. Stud. Adv.*, vol. 3, p. 100013, Nov. 2021, doi: 10.1016/j.ijnsa.2020.100013.

[6] D. K. Chu *et al.*, "Physical distancing, face masks, and eye protection to prevent person-to-person transmission of SARS-CoV-2 and COVID-19: a systematic review and meta-analysis," *Lancet (London, England)*, vol. 395, no. 10242, pp. 1973–1987, Jun. 2020, doi: 10.1016/S0140-6736(20)31142-9.

[7] J. Brainard *et al.*, "A mixed methods study on effectiveness and appropriateness of face shield use as COVID-19 PPE in middle income countries," *Am. J. Infect. Control*, vol. 50, no. 8, pp. 878–884, Aug. 2022, doi: 10.1016/j.ajic.2022.01.019.

[8] L. Li, M. Niu, and Y. Zhu, "Assessing the effectiveness of using various face coverings to mitigate the transport of airborne particles produced by coughing indoors," *Aerosol Sci. Technol.*,

vol. 55, no. 3, pp. 332–339, 2020, doi: 10.1080/02786826.2020.1846679.

[9] H. Clack, "Personal cold plasma 'air curtain' design for COVID-19 protection moves forward | University of Michigan News." Accessed: Mar. 14, 2023. [Online]. Available: https://news.umich.edu/personal-cold-plasma-air-curtain-design-for-covid-19-protection-moves-forward/

[10] A. S. Sakharov and K. Zhukov, "Study of an Air Curtain in the Context of Individual Protection from Exposure to Coronavirus (SARS-CoV-2) Contained in Cough-Generated Fluid Particles," *Phys. 2020, Vol. 2, Pages 340-351*, vol. 2, no. 3, pp. 340–351, Jul. 2020, doi: 10.3390/PHYSICS2030018.

[11] D. Keisar, A. Garzozi, M. Shoham, and D. Greenblatt, "Development and evaluation of a fluidic facemask for airborne transmission mitigation," *Exp. Therm. Fluid Sci.*, vol. 141, p. 110777, Feb. 2023, doi: https://doi.org/10.1016/j.expthermflusci.2022.110777777.

[12] X. Wei, D. Yi, W. Xie, J. Gao, and L. Lv, "Protection against inhalation of gaseous contaminants in industrial environments by a personalized air curtain," *Build. Environ.*, vol. 206, p. 108343, Dec. 2021, doi: 10.1016/J.BUILDENV.2021.108343.

[13] J. Ma, H. Qian, F. Liu, and X. Zheng, "Performance analysis of a novel personalized air curtain for preventing inhalation of particulate matters in industrial environments," *J. Build. Eng.*, vol. 58, p. 105014, Oct. 2022, doi: 10.1016/j.jobe.2022.105014.

[14] T. Y. Chang, C. S. Liu, L. H. Young, V. S. Wang, S. E. Jian, and B. Y. Bao, "Noise frequency components and the prevalence of hypertension in workers," *Sci. Total Environ.*, vol. 416, pp. 89–96, Feb. 2012, doi: 10.1016/j.scitotenv.2011.11.071.

[15] Y. Huang, G. Di, Y. Zhu, Y. Hong, and B. Zhang, "Pair-wise comparison experiment on subjective annoyance rating of noise samples with different frequency spectrums but same A-weighted level," *Appl. Acoust.*, vol. 69, no. 12, pp. 1205–1211, Dec. 2008, doi: 10.1016/J.APACOUST.2007.10.006.

[16] M. Pawlaczyk-Łuszczyńska, A. Dudarewicz, M. Waszkowska, W. Szymczak, and M. Śliwińska-Kowalska, "The impact of low frequency noise on human mental performance," *Int. J. Occup. Med. Environ. Health*, vol. 18, no. 2, pp. 185–198, 2005, [Online]. Available: https://pubmed.ncbi.nlm.nih.gov/16201210/

[17] S. . G. Pais, J.; Jesus, L.; Silva, H.; Lopes, A.; Ramos, J.; Costa, J. J.; Gameiro da Silva, M.; Martinho, N.; Rosa, N.; Matos, "Viseira de vedação aerodinâmica. Modelo de utilidade como EPI de categoria III, Ref. DP/02/2021/76885. Desenvolvido no âmbito do projeto Mask4MC – Mask for Medical Care (Dispositivo de proteção individual para cuidados médicos), projeto em copromoção liderado pela SETsa -Sociedade de Engenharia e Transformação S.A. e tendo com copromotores a ADAI -Associação para o Desenvolvimento da Aerodinâmica Industrial e a FMUC -Faculdade de Medicina da Universidade de Coimbra." 2021 [Online]. Available: https://patents.google.com/patent/PT12042U/pt?q=(Viseira+de+vedação+aerodinâmica)&oq=Viseira+de+vedação+aerodinâmica

[18] N. Rosa *et al.*, "Experimental and numerical evaluation of a new visor concept with aerodynamic sealing to protect medical professionals from contaminated droplets and aerosols," *Indoor Air*, vol. 32, no. 9, p. e13114, Sep. 2022, doi: 10.1111/ina.13114.

[19] N. Rosa, A. R. Gaspar, J. J. Costa, A. G. Lopes, J. Sabino Pais, and M. G. da Silva, "Experimental assessment of an air curtain-sealed personal protective equipment for medical care: Influence of breathing and thermal plume," *Exp. Therm. Fluid Sci.*, vol. 148, p. 110955, Oct. 2023, doi: 10.1016/j.expthermflusci.2023.110955.

[20] J. Mota, N. Rosa, A. R. Gaspar, J. J. Costa, A. G. Lopes, and M. Gameiro da Silva, "Acoustic assessment of a novel visor concept with aerodynamic sealing for medical care," *Appl. Acoust.*, vol. 217, no. January, p. 109852, 2024, doi: 10.1016/j.apacoust.2024.109852.

[21] M. C. Gameiro da Silva, "Virtual Laboratories for a Course on Indoor Environmental Quality," *Int. J. Online Biomed. Eng.*, vol. 5, no. 6, p. 20, Oct. 2009, doi: 10.3991/ijoe.v5s2.1107.

[22] M. C. G. da Silva and M. L. O. S. Mateus, "Desenvolvimento de um conjunto de aplicações computacionais para emolução de equipamentos de medição e análise sonora," in *V Congresso Ibérico de Acústica, Accoustics European Symposium*, Coimbra, Portugal, 2008.

[23] M. C. Gameiro da Silva, "Sound Measuring Virtual Instruments", in *Proceedings of 4th International Conference on Remote Engineering and Virtual Instrumentation*, Porto, Portugal, 2007.

[24] American National Standards Institute, *ANSI/ASA S3.5-1997 (R2020), Methods For Calculation Of The Speech Intelligibility Index*.

[25] R. A. Scott, "The absorption of sound in a homogeneous porous medium," *Proc. Phys. Soc.*, vol. 58, no. 2, p. 165, Mar. 1946, doi: 10.1088/0959-5309/58/2/303.

[26] L. Cao, Q. Fu, Y. Si, B. Ding, and J. Yu, "Porous materials for sound absorption," *Compos. Commun.*, vol. 10, pp. 25–35, Dec. 2018, doi: 10.1016/J.COCO.2018.05.001.

[27] J. H. Chaudhri, B. S. Patel, and S. A. Shah, "Muffler Design for Automotive Exhaust Noise Attenuation-A Review," *J. Eng. Res. Appl.*, vol. 4, no. 1, pp. 220–223, 2014, Accessed: May 15, 2023. [Online]. Available: www.ijera.com

[28] WHO, "Occupational noise: assessing the burden of disease from work-related hearing impairment at national and local levels," *Environ. Burd. Dis. Ser.*, no. 9, pp. 1–33, 2004, Accessed: Mar. 06, 2023. [Online]. Available: http://www.who.int/quantifying_ehimpacts/national/en%5Cnhttp://www.ncbi.nlm.nih.gov/pubmed/22183164

[29] W. J. Murphy and J. R. Franks, "Revisiting the NIOSH Criteria for a Recommended Standard: Occupational Noise Exposure," *J. Acoust. Soc. Am.*, vol. 111, no. 5_Supplement, pp. 2397–2397, May 2002, doi: 10.1121/1.4778162.

[30] EU-OSHA, *Directive 2003/10/EC - noise | Safety and health at work EU-OSHA*. 2021. Accessed: May 22, 2023. [Online]. Available: https://osha.europa.eu/en/legislation/directives/82

[31] A. Goldin, B. Weinstein, and N. Shiman, "How Do Medical Masks Degrade Speech Reception?," *Hear. Rev.*, vol. 27, no. 5, pp. 8–9, 2020, [Online]. Available: https://hearingreview.com/hearing-loss/health-wellness/how-do-medical-masks-degrade-speech-reception

2nd Place
HVAC World
Student Competition

Junhyeok Jang -
Hyejun You
Korea

2024

Heat transfer enhancement of drain water heat recovery systems using TPMS (Triply Periodic Minimal Surfaces) heat exchangers

Junhyeok Jang[1,*], Hyejun You[2], Yongchan Kim[2]
[1]*Department of Smart Convergence, Korea University, Seoul 02841, Republic of Korea;*
[2]*Department of Mechanical Engineering, Korea University, Seoul 02841, Republic of Korea*
junhyeogj04@gmail.com; hjyou367@naver.com; yongckim@korea.ac.kr
Received approval August 2023

Abstract— The enhancement of heat transfer efficiency in heat recovery systems is required for residential buildings owing to the poor performance of renewable energy in apartments, which account for 60% of domestic buildings. The existing drain water heat recovery (DWHR) exchangers with coil-type have limitations in high-capacity applications because of their low efficiency. The triply periodic minimal surfaces (TPMS) have a potential to replace the DWHR with coil-type because of its high surface area-to-volume ratio and enhanced turbulence intensity, substantially improving heat exchange efficiency. In this study, the heat transfer performance of DWHR exchangers with TPMS type was investigated. The simulation was set in transient conditions, and the Realizable k- s model was adopted. The inlet temperature of cold water was 279 K and the temperature of stored hot water was set to 308 K. The time to reach the maximum temperature of cold water decreased in the TPMS- type compared to the coil-type, which was 30 s and 150 s, respectively. The recovered heat in the TPMS-type was 17% higher than that in the coil-type. The difference in the time to reach the target temperature of 290 K significantly decreased by 85% as the flow rate increased from 3 to 6 LPM. Additionally, the time to reach the target temperature in TPMS-type with a thickness of 15 mm was 750% shorter than that of 7.5 mm at a flow rate of 6 LPM.

Index Terms— Numerical analysis, Triply periodic minimal surfaces (TPMS), Heat exchanger, Drain water heat recovery (DWHR).

I. Introduction

The heat recovery systems are essential for residential buildings owing to the poor performance of renewable energy in apartments, which account for 60% of domestic buildings. The conventional drain water heat recovery (DWHR) exchangers with coil-type have limitations when supplying high-capacity water because the size of the heat exchanger proportionally increases with the coil size to increase the capacity of the cold water. The triply periodic minimal surfaces (TPMS) have been paid attention to overcome this issue because they offer a high surface area-to-volume ratio and enhanced turbulence intensity, substantially improving heat exchange efficiency. Recently, extensive studies on TPMS heat exchangers have been conducted for various applications, including cold storage systems [1], and electric vehicles [2]. However, although the heat transfer characteristics of TPMS-type heat exchangers in DWHR systems should be analyzed for practical applications, they have rarely been studied in the literature.

In this study, the heat transfer performance of DWHR exchangers with TPMS-type was investigated by numerical simulations under various flow rate conditions and compared with that of the conventional coil-type. Additionally, the effects of wall thickness of TPMS were investigated.

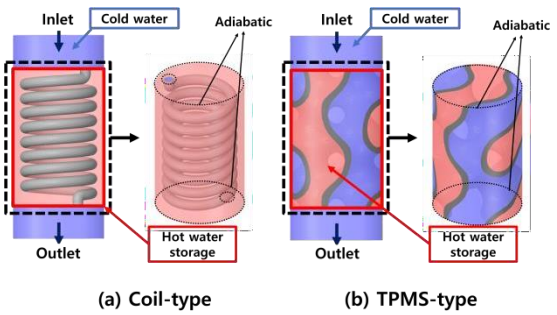

Figure 1. Geometries and boundary conditions of (a) coil-type, and (b) TPMS-type heat exchanger.

TABLE 1
Geometry details for coil-type and TPMS-type heat exchangers.

	Coil-type	TPMS-type
Diameter (mm)	220	
Height (mm)	330	
Volume of exchanger (mm^3)	12,544,379	
Volume of cold water (mm^3)	1,862,182	5,789,449

II. Methods

A. Model geometries and simulation settings

The geometries of the conventional coil-type heat exchanger and the TPMS-type heat exchanger are shown in Fig. 1. The inlet cold water temperature of 279 K was preheated through the heat exchanger and drained at 308 K. As shown in Fig. 1(a), cold water was supplied through the coil in the coil-type heat exchanger. As shown in Fig. 1(b), the Gyroid-sheet structure separated the hot drained water and the cold water in the TPMS-type heat exchanger. The details of the heat exchanger geometry are listed in Table 1. The volume of the cold water in the TPMS-type

was approximately 2.8 times greater than that in the coil-type.

The simulation was set in transient conditions, and the Realizable k-ε model was adopted for the simulation. The working fluid and solid region were set as water and copper, respectively. The cold water was set to a constant velocity and a temperature of 279 K at the inlet of the DWHR. The constant pressure was set at the outlet of the DWHR. The initial temperature of the heat source and drained water was set at 308 K. The outer walls of the heat exchanger were set as adiabatic conditions.

B. Model validation

The optimum number of grids was adopted for the coil-type and the TPMS-type, which were 1,102,951 and 898,258, respectively. The grids were composed of polyhedral type, and the number of boundary layers was set to 5. The deviations of the outlet temperature of cold water and pressure drop between acceptable grids and the finest grids were less than 0.9% at 180 s, representatively.

III. DATA PRESENTATION AND DISCUSSION

A. Performance comparison between the coil-type and TPMS-type heat exchangers

Fig. 2 shows the variations of cold and hot water temperature with time in coil-type and TPMS-type. The temperature of the hot water in both types decreased almost identically, with a difference of 0.2%. However, the time to reach the maximum temperature of cold water was shorter in the TPMS-type than that in the coil-type, which was 30 s and 150 s, respectively. The maximum temperature of cold water in TPMS-type was also 3 K higher.

The recovered heat of cold water over time is depicted in Fig. 3. The maximum recovered heat in the TPMS-type and coil-type were 4110 W, and 3508 W at 150 s, respectively, exhibiting a difference of 17%.

As shown in Fig. 4, the swirl and vortex in the TPMS-type enhanced the convective heat transfer, resulting in a higher heat recovered by the cold water.

B. Effect of inlet flow rates

The turbulence intensity was investigated at 3, 6, 9, and 12 LPM by comparing the average velocity relative to the

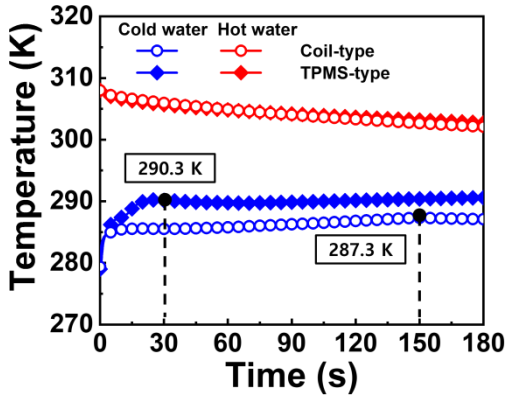

Figure 2. Temperature variation of cold water and hot water according to time.

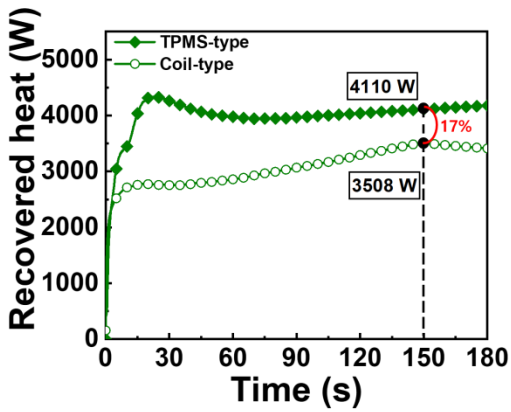

Figure 3. Recovered heat of cold water according to time.

inlet velocity of cold water. The turbulence intensity exhibited its highest increase of 2% as the flow rate increased from 3 to 6 LPM. However, the turbulence intensity exhibited a variation within 0.1% for flow rates above 6 LPM.

Fig. 5 shows the temperature variation of cold water under various flow rates with time. The times to reach the target temperature of 290 K decreased by 138, 20, 13, and 10 s when the inlet flow rates increased by 3, 6, 9, and 12 LPM, respectively. The time to reach the target temperature significantly decreased by 85% as the flow rate increased from 3 to 6 LPM. The variation in turbulence intensity at 6 LPM caused a significant difference in the convective heat transfer performance of cold water.

C. Effect of wall thickness

The heat transfer performance of the TPMS-type with wall thicknesses of 7.5 and 15 mm was investigated. Fig. 6 shows the temperature variation of cold water in TPMS-type with wall thicknesses of 7.5 and 15 mm at the inlet flow rates of 3 and 6 LPM. As the wall thickness of TPMS-type increased, the average velocity of cold water increased by 12% and 20% under the flow rates of 3 LPM and 6 LPM, respectively. The times to reach the target temperature of

290 K decreased by 750% from 170 to 20 s with wall thickness of 7.5 mm and 15 mm, respectively, at a flow rate of 6 LPM. However, as the thickness increased at a flow

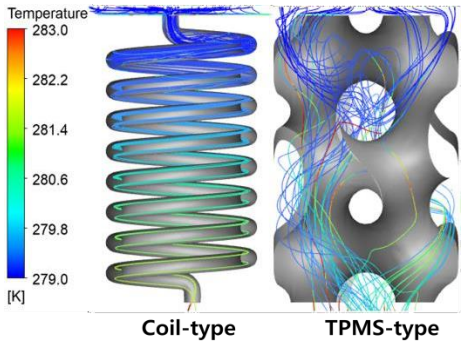

Figure 4. Velocity streamlines and flow temperature of the heat exchangers at 150 s.

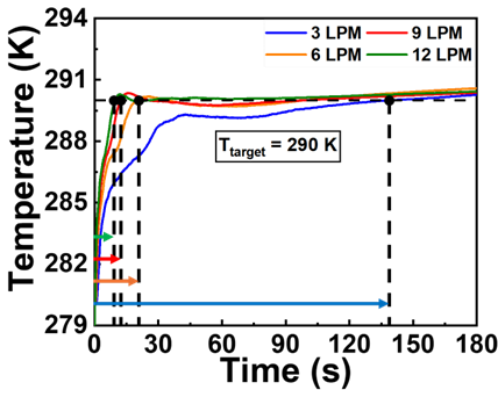

Figure 5. Temperature variation of cold water according to time under various flow rate conditions.

rate of 3 LPM, it decreased by 4% because the development of velocity significantly increased in the initial region at 6 LPM compared to 3 LPM.

In Fig. 7, the recovered heat of cold water with time is depicted. As the wall thickness increased from 7.5 to 15 mm, the maximum recovered heat increased by 6% and 10% at the flow rates of 3 LPM and 6 LPM, respectively. The increased average velocity and higher temperature of cold water led to an increase in recovered heat in TPMS-type with a thickness of 15 mm.

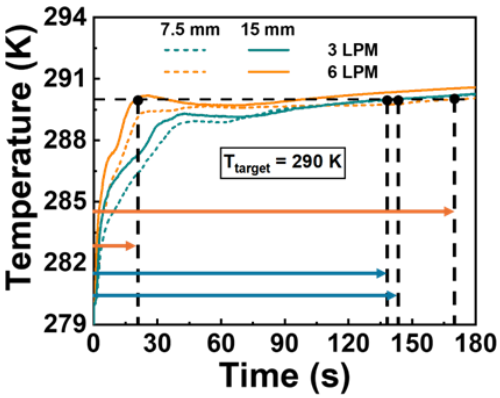

Figure 6. Temperature variation of cold water under various thickness and flow rate conditions according to time.

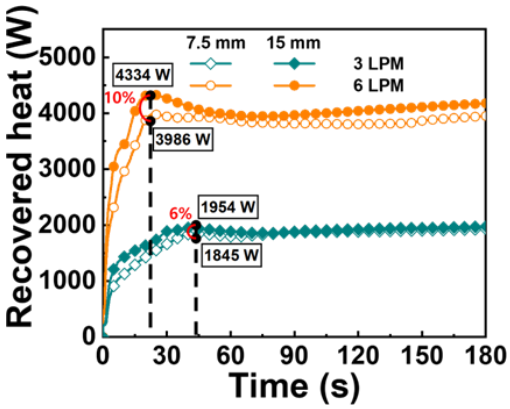

Figure 7. Recovered heat amount of cold water according to time under various thickness and flow rate conditions.

IV. CONCLUSIONS

In this study, the heat recovery performance of the TPMS-type DWHR heat exchanger was investigated by numerical simulations. The time to reach the target temperature in the TPMS-type was faster than that in the coil-type by 120 s at 6 LPM. Additionally, the amount of recovered heat of the TPMS-type was 17% higher than that of the coil-type. As the flow rate increased from 3 to 6 LPM, the time to reach the target temperature significantly decreased by 85%. The time to reach the target temperature in the TPMS-type with a thickness of 15 mm was 750% shorter and the maximum recovered heat increased by 10% compared to that of 7.5 mm at 6 LPM. Therefore, the TPMS-type heat exchanger enhanced the heat recovery performance with optimally designed thickness and flow rate conditions.

REFERENCES

1 W. Li, W. Li, and Z. Yu, “Heat transfer enhancement of water-cooled triply periodic minimal surface heat exchangers,” Applied Thermal Engineering, vol. 217, 119198, August 2022.

2 R. Attarzadeh, S. Attarzadeh, and C. Duwig, “Multi-objective optimization of TPMS-based heat exchangers for low-temperature waste heat recovery,” Applied Thermal Engineering, vol. 212, 118448, April 2022.

2nd Place
REHVA
Student Competition

Marco Bizzarri
Italy

2024

SPONSORED BY:

REHVA Federation of European Heating, Ventilation and Air Conditioning Associations

EUROVENT CERTIFIED PERFORMANCE www.eurovent-certification.com

Building Heating Load Prediction for Optimal Control of Hybrid Heat Pumps: Evaluation of an Autoregressive Model and Energy Analysis

Marco Bizzarri[1], Paolo Conti[1], Eva Schito[1], Daniele Testi[1]

[1]Department of Energy, Systems, Territory and Constructions Engineering (DESTEC), University of Pisa, 56122 Pisa, Italy

E-mail: marco.bizzarri@phd.unipi.it, paolo.conti@unipi.it, eva.schito@unipi.it, daniele.testi@unipi.it.

Work presented as Master Thesis in October 2022.

Abstract—The present work presents a predictive control strategy for the optimal operation of a hybrid heat pump, namely, a single generation unit made of an electric heat pump and a condensing boiler. The control strategy is based on the short-term prediction of the heating load and supply water temperature, using an autoregressive technique and a grey-box model. The predictions are then used as input to the generator models to evaluate their expected performance and to choose the best technology to be used in the next operating period to meet the heating demand. The predictive accuracy and related energy savings of the proposed autoregressive control strategy have been tested on some benchmark dwellings, representative of the Italian residential building stock. Results show good predictions for non-renovated buildings, although some limitations emerge in case of highly- variable indoor occupancy profiles and heat gains. Nevertheless, even in these cases, the proposed predictive control strategy leads to savings of up to 20% in operating costs compared to the typical control strategy currently used in commercially available hybrid heat pumps (e.g., weather compensation). Conversely, the proposed approach does not produce improvements in well-insulated houses with low- temperature emitters. This is due to the major relevance of highly variable internal and solar inputs compared to the thermal losses associated with the outdoor temperature evolution. The significant dynamic variation of the thermal demand leads to a deterioration of the forecast, which in turn affects the activation profile of the generators and the associated energy savings. Finally, the prediction method was also tested on experimental data collected in real buildings, leading to an early validation of the prediction model in field applications.

Index Terms— Hybrid heat pumps, load forecasting, machine-learning, model-based control.

I. Introduction, State of the Art, and Goals

The efficient control of HVAC (Heating Ventilation and Air Conditioning) systems in buildings is a widely discussed issue. Buildings are a major source of final energy consumption and CO_2 emissions [1], and this is why international treaties and policies are setting strict requirements to increase the efficiency of the sector [2], [3]. In particular, the residential sector is the largest contributor to emissions and one of the most difficult to decarbonize, being characterized by a large number of scattered and heterogeneous buildings. Therefore, to tackle the energy efficiency problem in residential buildings, policy makers, researchers, and industrial operators should adopt a large-scale perspective, focusing on the necessity of broad coverage of new efficient solutions and measures.

The installation of new and high-performance HVAC systems, such as Heat Pumps (HPs), has significant potential that can be further enhanced through advanced control strategies. Focusing on hydronic heating, which is the most common system configuration employed in residential buildings, the current control strategies used for heat generators are extremely straightforward. Typically, the water supply temperature is controlled with a fixed set-point or with weather compensation strategies. Besides, thermal comfort is ensured by on-off or PID controls, following the indication of the internal thermostat or thermostatic valves [4], [5]. Although some procedures are available for determining the best weather compensation curve [6], in practical applications, the relationship between outdoor conditions and water supply temperatures is typically set to the device's default configuration or is the outcome of a trial-and-error calibration by the installer. Still, given the arbitrariness of the process, most residential buildings are likely to have non-optimal control of the heating and cooling systems operation [7], which could lead to significant energy waste. As a result, a clear need for more advanced HVAC control strategies emerged, suitable for large-scale implementation. The use of self-learning methods, in particular, could overcome the need for manual tuning of heating systems, enabling them to operate more efficiently and avoid energy waste.

In this context, the present work aims to develop a control strategy to seek the optimal operation of a specific HVAC system, the so-called Hybrid Heat Pump (HHP) or hybrid system. The HHP technology integrates a gas boiler and an Air Source Heat Pump (ASHP), with the two heat generators working conjointly to meet the thermal demand, leveraging their respective strengths for optimal performance and efficiency. For instance, one of the main problems with ASHPs is the reduced heating capacity and low efficiency in cold outdoor conditions, when the building heating load is at its maximum. And, on the opposite range of operation, they can suffer from cycling losses at low-capacity ratios. With the use of HHPs, these conditions are effectively covered by the activation of the boiler to support the heat pump in all the moments when it would not properly work.

Hybrid systems have experienced remarkable growth in the domestic heating market in recent years, as international

policies are gradually pushing conventional gas boilers out of the market [3]. Among the others, HHP penetration is particularly significant in Italy, which is reported to be the leading country in Europe for installations [8].

Initial studies on HPPs [9], [10], [11] assessed the benefits of their use: despite the variability of their economic feasibility depending on the specific scenario, HHPs have been found capable of significantly reducing the energy-related emissions and primary energy use of the building sector. The studies [12], [13], [14] also evaluated the benefits at the urban scale, as HHPs can simultaneously save energy and relieve the electrical grid that would otherwise be overloaded by widespread HP installations.

Two operating schemes for HHP are possible: integrative, where the two heat generators can contribute synchronously to meet the heating load, or alternative, where the two generators always operate asynchronously [15], [16]. Whichever configuration is chosen, the control method plays a key role in the actual efficiency of these systems. Several methodologies for HHPs control have been developed, simulated, and compared [17], [18], [19], [20]. While Model Predictive Control (MPC) is generally reported to be the best alternative in terms of energy efficiency, its need for highly accurate models and data input that often hinders practical and broad application in real buildings.

In the present research, we pursued the development of a data-driven predictive control procedure for HHPs, with the aim of making it easily implementable on the normal microprocessors currently used in commercial heat generators, requiring only on-board readings of operating temperatures and mass flows, avoiding advanced but computationally expensive techniques (e.g. artificial neural networks [21]). We opted for model-based control, implementing a simple and straightforward AutoRegressive (AR) model, that was reported to provide a fair trade-off between ease of implementation and predictive accuracy [22]. The predictions of heating load and supply temperature were then used within the generator models to evaluate their performance and subsequently select the most appropriate generator to meet the heating demand, employing an HHP alternative operation. As a data-driven approach, the control system can self-learn the information needed for optimal operation. That is why this predictive technique is particularly suitable for characterizing building systems with limited information available, making it a useful and widely applicable solution, unlike classical MPCs.

In the paper we present the development of this novel control application for HHPs, together with the seasonal energy assessment on several simulated case studies, in order to obtain a general evaluation of achievable benefits in the Italian residential scenario. We analyzed different building types and climates through the dynamic energy simulation of both building thermal loads and HHP performances. Additionally, the AR prediction accuracy was tested on real data collected during the winter operation of real buildings placed all over the Italian territory.

The procedure described here was developed as part of a research grant in collaboration with the Italian company Immergas S.p.A., one of the European leaders in heating system manufacturing. Jointly, we registered the proposed predictive control methodology at the European Patent Office.

Figure 1 shows the scheme of the HHP controller developed in the study.

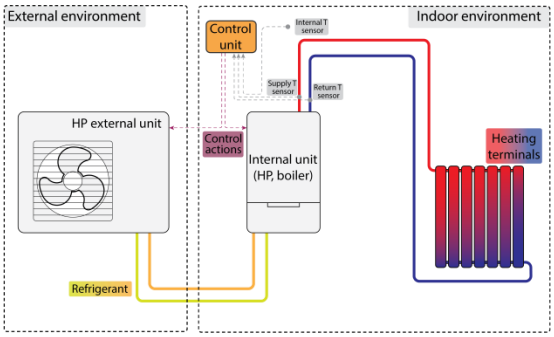

Figure 1: Schematic representation of the hybrid heat pump control application developed.

II. METHODS

A. Proposed Predictive Control Method for HHP

To optimize the operation of the HHP and minimize energy costs, the proposed supervisory data-driven predictive control was based on the 1-hour ahead forecast of the building heat demand. The obtained information was then used to estimate the efficiency of the boiler and heat pump, allowing for the selection and activation of the most cost-effective heater. The choice for hourly thermal load prediction fell on an autoregressive system, because of its simple implementation and low computational cost. The AR prediction estimates the thermal demand only considering n previous values of hourly heating loads and combining them through a linear relationship:

$$Q_{(t+1)} = \phi_1 Q_{(t-n+1)} + \phi_2 Q_{(t-n+2)} + \ldots + \phi_n Q_{(t)} \quad (1)$$

Like all data-driven techniques, the AR forecast first requires a period of training. During this time frame, a large database of j values is collected and used to calculate the coefficients ϕ_i that best fit the known Q_i values (see Eq. 1), through least-square approximation. To have an accurate estimate throughout the entire heating season, the values of the autoregressive coefficients were periodically updated every m timesteps. The methodology is presented in Figure 2.

A sensitivity analysis was conducted on the indexes j, n and m to identify the values that provide the best results in terms of accuracy, for each scenario.

Besides the prediction of the heating load, to achieve optimal control, a straightforward method was also needed to evaluate the corresponding supply temperature at the heater outlet.

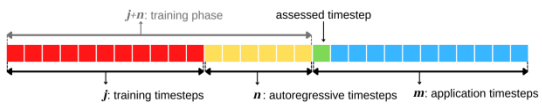

Figure 2: Graphical representation of the timesteps used to train and apply the autoregressive model.

A hybrid grey-box model was considered to represent the physics of the heat emitters:

$$Q_{t+1} = c_1(T_{supply,t+1} - T_{indoor})^{c_2}, \quad (2)$$

where the internal space temperature T_{indoor} is equal to the indoor set-point, and Q_{t+1} represents the predicted heat load. By applying the logarithm to both sides, the formula was linearized, and the coefficients c_1 and c_2 were determined through least-square approximation. The two coefficients were also re-updated every m timesteps.

Then, for the application of the predictive control, modeling of the two heat generators was also needed. Any modeling method could be acceptable: for the present study, the condensing boiler was characterized by the procedure described in the Italian technical standard UNI/TS 11300-2 [23], based on EN 15316-4-1 [24], in which partial and full load efficiency are properly interpolated and corrected, while the HP performance was characterized through the equation:

$$COP = f\left(\frac{T_{supply}}{T_{external}}\right) \cdot g\left(\frac{f_{compr}}{f_{max,T}}\right) \cdot \left(\frac{T_{supply}}{T_{supply} - T_{external}}\right), \quad (3)$$

with f and g being polynomial functions depending on supply and external temperatures and on the load factor of the compressor. We calculated the polynomial coefficients by performing a best-fit regression on the data collected during a previous experimental campaign. Still, other methodologies such as EN 15316-4-2 [25] could be easily adapted in Eq. 3.

Finally, the switching logic between the two heaters was characterized. The HP and the gas boiler are operated asynchronously, with a threshold set based on a cost effectiveness criterion. The controller's objective is then to choose the value of the Boolean HP_{ON}, which defines the activation of the heat pump, such that the value of the hourly cost function is minimized:

$$cost_i = \frac{Q_i}{COP_i} \cdot c_{el} \cdot (HP_{ON}) + \frac{Q_i}{\eta_i} \cdot c_{gas} \cdot (1 - HP_{ON}), \quad (4)$$

where c_{el} and c_{gas} represent the electricity and gas prices, respectively. Therefore, an accurate forecast was needed to correctly identify the most cost-effective generator and use it at the proper temperature.

B. Application of the Proposed Control to a Set of Residential Buildings

As reported in the literature, both climatic conditions and building insulation levels have a relevant impact on HHP performance. In the present work, several climates and dwelling types were considered for a more comprehensive and general analysis.

Our primary assessment relied on a matrix dataset of 18 test cases, which were dynamically simulated using TRNSYS 17 modeling software. The resulting hourly building energy needs were used to create the reference heat load profile to train the AR model and to evaluate the accuracy of the forecast. The test cases refer to three cities: Parma (HDD=2502), Florence (HDD=1821), and Bari (HDD=1185). These locations can be classified as having a cold, mild, and hot climate, respectively, and can be considered as representative of the three primary climate zones in Italy. The simulation utilized climate data from the Typical Meteorological Year (TMY). For each climatic scenario, three typical dwellings were considered. These were: an apartment in a multi-family house built in the 1980s with radiators (80 m^2), a detached single-family house built in the 1990s with radiators (140 m^2), and a newer detached house built in the 2000s (130 m^2) with a higher level of thermal insulation and radiant panels as heating terminals. We also considered different typical domestic use profiles and related occupancy, heat gains, and set-point profiles for each housing typology. Additionally, we introduced potential unexpected variations in the baseline occupancy profiles by partially randomizing the hourly occupancy schedules. This introduction of randomized profiles resulted in a more variable heat load, which is more realistic and potentially more challenging for the model.

Along with the heating demand, the ideal hourly value of the supply temperature was also estimated solving heat-transfer equations for the hydronic heat emitters.

The proposed control system was compared with three other configurations from an energy and cost-saving perspective. Overall, the scenarios analyzed were:

- Baseline case: condensing boiler alone.
- Current case: weather compensation control of supply water temperature and switch between boiler and HP at fixed temperature (i.e., -15°C).
- Ideal case: optimal control, based on the ideal thermal load and supply temperature prediction.
- Forecast case: near-optimal control, based on AR forecasts of the thermal load and supply temperature.

The "Current case", given the extremely low switch temperature, can be considered an HP priority mode.

Additionally, in every situation, the internal thermostat would still operate to maintain the internal temperature at the desired set-point. This is what also enables the predictive strategy to constantly respect the actual hourly heating demand. In our simulation we considered this aspect by integrating a post-strategy to correct prediction errors and coherently adjust the energetic consumption.

C. Load Prediction on Real Building Data

Besides the simulative analysis, the predictive step of the control was also tested on a database of real-world building data, recorded during the operation of 31 actual houses spread throughout the Italian territory. This provided a more reliable validation of the AR model, since real data are highly affected by unpredictable events, such as the many possible behaviors that might occur in a real house, or the non-ideal operation and control of the heat generator.

Starting from the original data provided by the generator monitoring system (from December 2021 to March 2022), the information was preprocessed before being fed to the AR algorithm. Thus, data cleaning and data transformation phases were applied. First, outliers and missing values were corrected. Data aggregation was also necessary because the original measurements were taken with a 10-

minute sampling time, and the AR algorithm requires a 1-hour discretization.

The measured variables consisted of supply and return temperatures, along with the mass flow value. A trigger value was also retrieved to determine whether or not the heat generator was operating at a specific time. With all this information, the hourly load provided by the heat generator could be retrieved.

III. RESULTS AND DISCUSSION

A. *Forecasting and Control Results on TRNSYS Case Studies*

After the complete definition of the models and the different case studies, the computational process was carried out using a code written in the MATLAB environment. The evaluation of forecasting algorithms began with an assessment of their accuracy. Subsequently, the predictions were utilized within the control system, and a simulation of the actual heating season operation was conducted to evaluate the achievable benefits.

The Mean Average Percentage Error (MAPE) was used to quantify prediction accuracy of the AR algorithm. It reads:

$$MAPE = \frac{1}{n}\sum_{i=1}^{n} \left| \frac{Q_{forecast,i} - Q_{observed,i}}{Q_{observed,i}} \right|, \qquad (5)$$

where $Q_{forecast,i}$ and $Q_{observed,i}$ represent the hourly load forecast and the actual value, respectively.

The sensitivity analysis on the j, n, and m values revealed that minimum $MAPEs$ are obtained with trainings from 3 to 7 weeks, but often 4-6 weeks are sufficient. The optimal number of days of autoregression, n, appears to be large in the case studies with regular occupancy profiles, but when randomized occupancy profiles were introduced, 2-4 days were the best options. In contrast, the value of m seemed irrelevant. The similar optimal values of j, n, and m indexes for all the case studies are promising in light of a general application to all types of domestic buildings, without the need for tailored calibration. Table 1 presents the corresponding MAPE values for the optimal j, n, and m combination obtained in each scenario.

TABLE I
BEST RESULTS IN TERMS OF PREDICTIVE ACCURACY (MAPE) OBTAINED IN EACH CASE STUDY

		1980s flat		1990s villa		2000s villa	
Parma (cold)	Regular	6.3%	Regular	9.8%	Regular	16.8%
	Random	12.7%	Random	20.3%	Random	30.1%
Florence (mild)	Regular	8.7%	Regular	11.7%	Regular	21.6%
	Random	14.4%	Random	20.8%	Random	31.6%
Bari (hot)	Regular	9.9%	Regular	12.1%	Regular	20.8%
	Random	22.2%	Random	27.8%	Random	35.4%

Similar results were also obtained for supply temperature prediction. Good predictive accuracy is evident especially in older buildings (1980s and 1990s), while a deterioration in accuracy was obtained in newer buildings and with the introduction of randomized heat gain profiles. Figure 3 visually shows the predictive ability of the model on a selected case study.

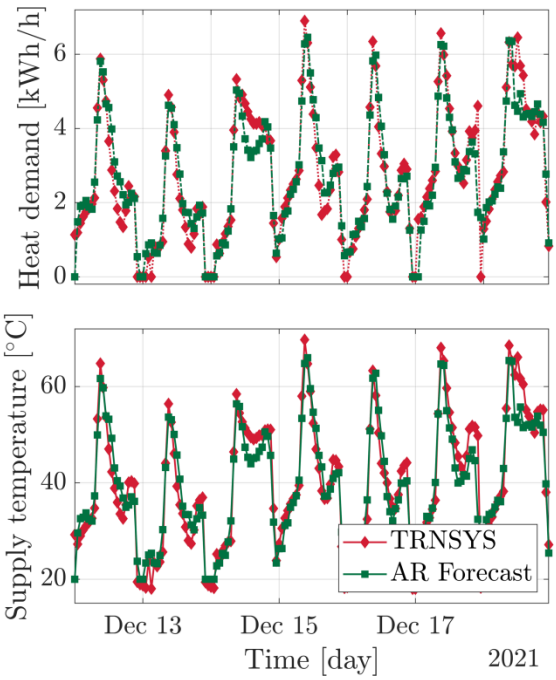

Figure 3: Predictive accuracy of the model in a week in January - Florence, 1990s villa with randomization of occupancy.

Once the forecast was completed, the energy implications of the proposed control strategy were examined. A whole heating season was simulated for each case study. The achievable savings can be observed in Figure 4, where the reduction in energy expenses is shown through comparison with the benchmark case, i.e. the boiler alone.

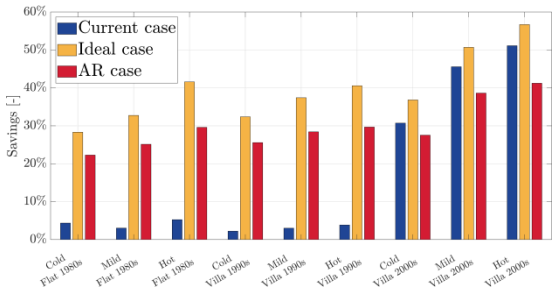

Figure 4: Seasonal cost savings obtained in the different case studies with randomization of occupancy, compared to the reference case (boiler only).

To summarize, the case studies from the non-renovated buildings of the 1980s and 1990s showed significant savings due to increased usage of HP. Choosing the appropriate water supply extended the working hours

within the HP operating limits, reducing the need for boiler use. In newer buildings with low-temperature radiant terminals, HP was already widely used with a favorable COP, and the proposed control was instead penalized by inaccuracies in prediction, leading to greater boiler use. In these buildings, the use of the HP decreased with respect to the "Current case", but it was still used with higher seasonal COPs. Nevertheless, achieving this goal alone did not guarantee savings in this building category.

When considering primary energy consumption, applying the primary energy factors of the Italian scenario, the AR control always allowed significant reductions (60-70%) compared to the boiler alone. Regarding the current control, significant savings in primary energy usage were present both in older and newer buildings. Specifically, in newer buildings, the current control, which is practically an HP-alone configuration, allowed more primary energy savings than the HHP predictive control, similar to what has been observed in the literature for other HHP control methods [11].

Nevertheless, the application of the AR predictive control procedure to newer homes with radiant heating systems could lead to other possible indirect advantages: in our simulated "Current case", we considered the most correct climate compensation curve. However, in practice, this is not always the case, as the device's configuration is often set to the default or calibrated through trial-and-error. Therefore, the self-learning capabilities of the method could still be of some benefit in this sense.

B. Preliminary Experimental Validation of the Forecasting Algorithm

Finally, a preliminary analysis has been attempted on data measured on real buildings. Real data, in terms of thermal power and supply temperature to the emissive system, showed a very discontinuous system's operation, with frequent on-offs and significant power peaks in the morning, in order to quickly reach the internal set-point after the night pause.

For the present work, only the predictive accuracy was evaluated. The results show a notable increase in errors caused by the more irregular behavior, but in Figure 5 it is showed how the model can still qualitatively follow the actual load and temperature trends.

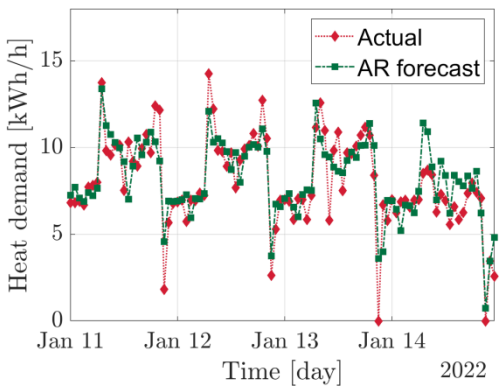

Figure 5: Comparison of real-building data and prediction on 4 days in January 2022 ($MAPE = 26.6\%$).

However, not all real buildings resulted adapt to be modelled with an AR algorithm. For instance, in our database, numerous houses seemed to be utilized infrequently, with the boiler operating for only a few hours per day or even per week. With so many off periods, the AR was not able to train and predict properly. Therefore, we deemed it essential to create a quality indicator for the dataset collected in any given building. The chosen indicator was:

$$MAPE_{MA} = \frac{1}{k}\sum_{i=1}^{k} \left| \frac{Q_{measured,i} - Q_{measured,MA_i}}{Q_{measured,i}} \right|, \qquad (6)$$

which represents the deviation of the observed value from the 3-hour moving average of the heat load time series. Correlation with the autoregressive MAPE, already used to characterize the prediction error, was investigated. The results indicate a good fit with the linear regression, as shown in Figure 6.

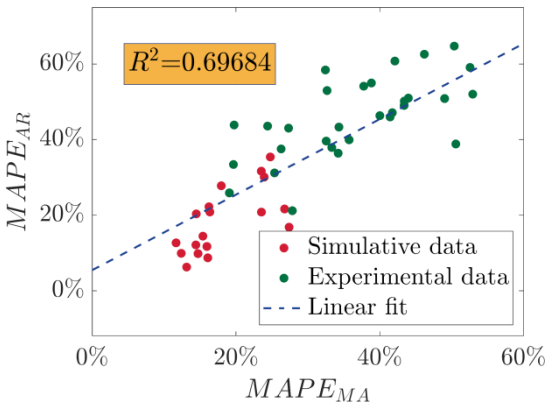

Figure 6: Correlation between input data variability (difference, over the first two weeks, compared to moving average data) and forecasting error with the AR algorithm.

The correlation is clearly established with only two weeks of observation. Simply by measuring the heat load in this time window, and after evaluating the error index $MAPE_{MA}$, a clear idea of the expected predictive ability in a specific case study can thus be derived. This could provide a useful indication for the practical diffusion of this HHP control procedure.

IV. CONCLUSIONS

In the present work, a predictive control method is developed to identify the optimal control of HHPs. It includes the building heating load prediction and the following evaluation of the appropriate supply temperature. This allows for an estimation of the expected performances of the two heaters, enabling the selection of the most suitable one for activation in the upcoming period. We proposed a simple AR forecast method as was found it to be a valuable trade-off between computational effort, required input data, and expected results.

The accuracy of the AR prediction was fully acceptable for 1980s apartments or 1990s villas, with an average prediction error of less than 15%, but was poorer for 2000s buildings, where the greater insulation made the

contribution of internal and solar loads more relevant, which are difficult to predict. Accuracy was worse when partially randomized hourly occupancy profiles were considered within the simulations, due to the more variable evolution of the heat demand. In such cases the MAPE values doubled, reaching more than 35% in the worst scenarios. The predictive ability also worsened under warmer climatic conditions, although not significantly.

From the application of the proposed control methodology, the HHP resulted cost-effective in all the considered case studies, except for those set in the 2000s houses. The controller provided superior performance in the 1980s apartments and 1990s villas, both in terms of economics and primary energy, and the results obtained were very close to those that could have been obtained with an ideal load and supply temperature prediction. Savings were mainly achieved through greater use of the heat pump, which, due to the better choice of supply temperature, was able to turn on in a greater number of instances. The application to the more recent villas, which was already critical in terms of load and temperature prediction, was found to be economically inconvenient compared to the current control. In fact, in newer buildings, the gap between the ideal control strategy and the current one was extremely narrow, as the HP was already the most advantageous generator thanks to the low-temperature emitters. Therefore, forecasting errors caused higher boiler utilization, penalizing the whole performance.

Although the overall procedure has not yet been fully experimentally tested for HHP control, by evaluating the predictive accuracy on real-world data we were able to establish a criterion for easily verifying the potential feasibility of the methodology.

ACKNOWLEDGEMENT

The authors wish to acknowledge the company Immergas S.p.A., who provided the input on this topic and made available useful data and information for the analysis. Jointly, the company and the DESTEC department registered the application at the European Patent Office (EP4266134).

REFERENCES

[1] IEA, “World energy outlook 2022,” Paris, France, 2022.

[2] Conference of the Parties of the UNFCCC, “Report of the Conference of the Parties on its twenty-seventh session, held in Sharm el-Sheikh from 6 to 20 November 2022. Addendum. Part two: Action taken by the Conference of the Parties at its twenty- seventh session, Decisions adopted by the Conference of the Parties,” Sharm el-Sheikh, 2022.

[3] “Directive 2010/31/EU of the European Parliament and of the Council of 19 May 2010 on the energy performance of buildings (recast),” OJ L 153 18.6.2010. p. 13.

[4] T. Q. Péan, J. Salom, and R. Costa-Castelló, “Review of control strategies for improving the energy flexibility provided by heat pump systems in buildings,” J Process Control, vol. 74, pp. 35–49, Feb. 2019.

[5] Z. Liao and A. L. Dexter, “The potential for energy saving in heating systems through improving boiler controls,” Energy Build, vol. 36, no. 3, pp. 261–271, Mar. 2004.

[6] H. Madani, J. Claesson, and P. Lundqvist, “A descriptive and comparative analysis of three common control techniques for an on/off controlled Ground Source Heat Pump (GSHP) system,” Energy Build, vol. 65, pp. 1–9, Oct. 2013.

[7] L. Peeters, J. Van der Veken, H. Hens, L. Helsen, and W. D’haeseleer, “Control of heating systems in residential buildings: Current practice,” Energy Build, vol. 40, no. 8, pp. 1446–1455, Jan. 2008.

[8] European Heating Industry, “Heating Market Report 2021,” 2021.

[9] F. Li, G. Zheng, and Z. Tian, “Optimal operation strategy of the hybrid heating system composed of centrifugal heat pumps and gas boilers,” Energy Build, vol. 58, pp. 27–36, Mar. 2013.

[10] H. Park, K. H. Nam, G. H. Jang, and M. S. Kim, “Performance investigation of heat pump–gas fired water heater hybrid system and its economic feasibility study,” Energy Build, vol. 80, pp. 480–489, Sep. 2014.

[11] K. Klein, K. Huchtemann, and D. Müller, “Numerical study on hybrid heat pump systems in existing buildings,” Energy Build, vol. 69, pp. 193–201, Feb. 2014.

[12] C. Vuillecard, C. E. Hubert, R. Contreau, A. mazzenga, P. Stabat, and J. Adnot, “Small scale impact of gas technologies on electric load management – µCHP & hybrid heat pump,” Energy, vol. 36, no. 5, pp. 2912–2923, May 2011.

[13] S. R. Asaee, V. I. Ugursal, and I. Beausoleil-Morrison, “Techno-economic feasibility evaluation of air to water heat pump retrofit in the Canadian housing stock,” Appl Therm Eng, vol. 111, pp. 936–949, Jan. 2017.

[14] G. Bennett, S. Watson, G. Wilson, and T. Oreszczyn, “Domestic heating with compact combination hybrids (gas boiler and heat pump): A simple English stock model of different heating system scenarios,” Building Services Engineering Research and Technology, vol. 43, no. 2, pp. 143–159, Mar. 2022.

[15] G. Bagarella, R. Lazzarin, and M. Noro, “Annual simulation, energy and economic analysis of hybrid heat pump systems for residential buildings,” Appl Therm Eng, vol. 99, pp. 485–494, Apr. 2016.

[16] M. Dongellini, C. Naldi, and G. L. Morini, “Influence of sizing strategy and control rules on the energy saving potential of heat pump hybrid systems in a residential building,” Energy Convers Manag, vol. 235, p. 114022, May 2021.

[17] Y. Ma and M. Zaheeruddin, “Dynamic modeling, adaptive control and energy performance simulation of a hybrid hydronic space heating system,” Building Services Engineering Research and Technology, vol. 39, no. 4, pp. 406–429, Jul. 2018.

[18] G. Li, “Parallel loop configuration for hybrid heat pump – gas fired water heater system with smart control strategy,” Appl Therm Eng, vol. 138, pp. 807–818, Jun. 2018.

[19] F. D’Ettorre, P. Conti, E. Schito, and D. Testi, “Model predictive control of a hybrid heat pump system and impact of the prediction horizon on cost-saving potential and optimal storage capacity,” Appl Therm Eng, vol. 148, pp. 524–535, Feb. 2019.

[20] E. Zanetti, R. Scoccia, S. Garone, M. Aprile, M. Motta, and L. Mazzarella, “Energy Saving Potentials of a Centralized Hybrid Heating System via Adaptive Model Predictive Control in a Northern Italy Residential Building,” pp. 2925–2932.

[21] E. T. Maddalena, Y. Lian, and C. N. Jones, “Data-driven methods for building control — A review and promising future directions,” Control Eng Pract, vol. 95, p. 104211, Feb. 2020.

[22] P. Dagnely, T. Ruette, T. Tourwé, E. Tsiporkova, and C. Verhelst, “Predicting Hourly Energy Consumption. Can Regression Modeling Improve on an Autoregressive Baseline?,” 2015, pp. 105–122.

[23] UNI - Ente Italiano di Normazione, UNI/TS 11300 - 2, 2019.

[24] EN – European Standards, EN 15316-4-1, 2017.

[25] EN – European Standards, EN 15316-4-2, 2017.

3rd Place
HVAC World
Student Competition

Yashu Zhao -
Suxian Jiang
China

2024

REHVA
Federation of European Heating, Ventilation and Air Conditioning Associations

Optimized design and experimental study of near dew point indirect evaporative cooling air conditioning heat exchanger for domestic use

Author: Yashu Zhao(zyszzt960@163.com), Suxian Jiang(1073101237@qq.com) ***Year:*** January 2024. ***Institute:*** Xi'an Polytechnic University(XPU), No.19, Jinhua South Road, Xincheng District, Xi'an, Shaanxi, China.
Supervisors: Prof. Xiang Huang(huangx@xpu.edu.cn), Dr. Junjie Chu (chujunjie2010@foxmail.com).

Abstract—For residential building air-conditioning, a new type of double countercurrent dew-point indirect evaporative cooler is proposed. This technology combines a double countercurrent design and efficient wet channel material, with the aim of achieving a greater cooling temperature difference and reducing the size of the dew point core. By simulating the working conditions in Xi'an (dry-bulb temperature 35 ℃, wet-bulb temperature 25.8 ℃) in the double enthalpy-difference laboratory, the results show that when the secondary/primary air volume ratio is 0.9, the wet-bulb efficiency reaches 104%, the dew- point efficiency reaches 79%, and the cooling capacity reaches 1.76kW. The use of a small air volume miniaturized dew point cooler will better meet the needs of the residential construction sector.

Index Terms—residential building; double countercurrent; wet channel material; dew point indirect evaporative cooling; performance experiments

1 Introduction

The rapid increase in global energy consumption within buildings has become a significant concern due to the depletion of energy resources and the impact on global climate change [1]. In developed nations, heating, ventilation, and air conditioning (HVAC) systems alone consume approximately 50% of the total energy utilized in buildings, constituting roughly 20% of overall energy consumption. Conversely, in certain developing nations like China, HVAC systems are responsible for 50–70% of the total energy consumption in buildings [2,3]. Cooling constitutes a crucial aspect of HVAC systems, with energy consumption for cooling varying significantly, ranging from 10% to 90% of the total HVAC system, depending on factors such as geographical location, occupancy density, building type, and function [4,5].

With the rapid development of social economy and the continuous increase of residential buildings, the scale of usage of domestic air conditioning still has a large upward space, the existing mechanical compression refrigeration method often brings high energy consumption and environmental pollution and other problems. Therefore, a more energy-efficient, low-carbon, economical and healthy green air conditioning technology-evaporative cooling technology is receiving more and more attention. It plays a crucial role in helping China achieve dual carbon goals. It addresses climate change and reduces greenhouse gas emissions and drives economic transformation and promotes green and sustainable development.

In 2003, Valeriy Maisotenko et al. proposed "indirect evaporative cooling thermal cycle form" [6], that is, dew point indirect evaporative cooling technology, which can further improve the refrigeration efficiency of indirect evaporative cooling. Dew point indirect evaporative cooler is a high-efficiency form of refrigeration. In the wet channel, heat transfer and mass transfer are coupled together, and the mass transfer also accelerates the transfer of heat, while the heat transfer enhances the evaporation of the liquid membrane surface, and its heat transfer and mass transfer process is complex [7].

Bruno [8] constructed a flat-plate cross-flow thermal mass exchanger using a special medium with high water retention and hygroscopic properties for the wet channel and a moisture impermeable membrane for the dry channel. Tests showed that the exchanger had a dew point efficiency of 75%. Zhan et al. [9] conducted a comparative study into the M-cycle counter-flow and cross-flow flat-plate heat exchangers for indirect evaporative coolers (IEC), indicating that the counter-flow exchanger have approximately 20% higher cooling capacity, 15-23% higher dew point and wet bulb efficiencies, and 10% lower COP. Zhan et al. [10] carried out a numerical study on a cross-flow dew point cooling heat exchanger, indicating that the average air velocities in dry and wet channels should be less than 1.77 m/s and 0.7 m/s respectively, the optimum working-to-product air ratio was 50%, the channel's length-to-height ratio should be in the range 100-300, while its height should be in the range 4 mm-6 mm. Xu Peng et al. [11,12] developed a dew point indirect evaporative cooler with ultra-high performance. The test results showed that the wet-bulb efficiency can reach 114% and the dew-point efficiency can reach 75% at a dry-bulb temperature of 37.8℃. When the optimal air volume ratio was 0.364, COP reached a maximum of 52.5. Duan Zhiyin et al [13] studied a counter-flow dew point indirect evaporative cooler, tested the temperature, humidity and flow rate at the inlet, outlet and exhaust of the cooler and measured different inlet conditions, water supply temperature and evaporation rate respectively. According to the test results, the cooler had wet-bulb efficiency ranging from 55% to 106% and EER ranging from 2.8 to 15.5. Chu Junjie et al. [14] developed a new type of counter-flow dew point indirect evaporative cooler, and tested and analyzed performance of the cooler by simulating various environmental conditions. The results showed that under the standard drying conditions, when the secondary/primary air volume ratio was 1.1, the cooler wet-bulb efficiency was up to 105.6%, the dew point efficiency reached 76%, and the cooling capacity was 2.83kW, dry-bulb temperature drop can reach 15.2 ℃.

At present, dew point indirect evaporative cooling technology has been adopted because of the greater

temperature drop, mainly used in industrial buildings, but it is not widely used in residential buildings. Its volume is limited, and the efficiency needs to be further improved to reduce the size of the dew point core. In this paper, an indirect evaporative cooler is developed. The cooler adopts double countercurrent structure, which can improve efficiency and reduce heat exchanger size. It uses polymer core with the hydrophilic membrane, providing a more efficient and water-saving spraying scheme.

2 Principle analysis

As shown in Figure 1, indoor air enters the dry channel on both sides from the air inlets and is blown along the dry channel. The air is divided into two parts: Part of the air enters the wet channel through the small hole at the end of the corresponding dry channel. In the process of passing through the wet channel, it reduces the temperature by evaporating water, and exchanges heat with the indoor air blown in the dry channel to cool it down. The other part of the indoor air is blown into the room from the air supply outlet after passing through the air outlet, and the humidity of this part of the air is basically unchanged and the temperature is lower than that of the indoor air.

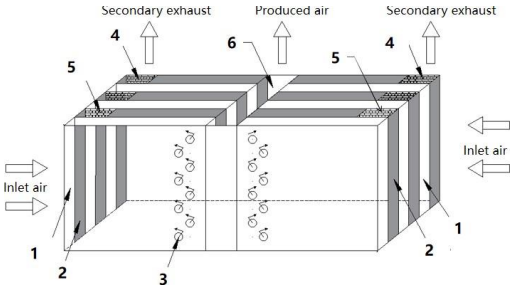

1-dry channel, 2-wet channel, 3-pinhole, 4-baffle, 5-exhaust opening, 6-air inlet,

Figure1. Structural design of double countercurrent dew-point indirect evaporative cooler

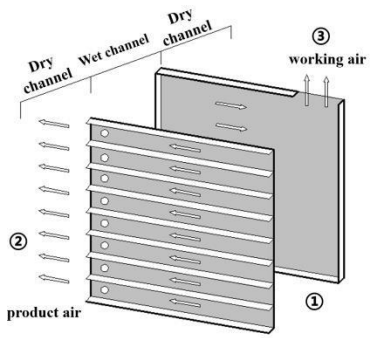

①Air inlet ②Air outlet ③Exhaust air

Figure2. Layout of the measuring points of a countercurrent dew point evaporative cooler.

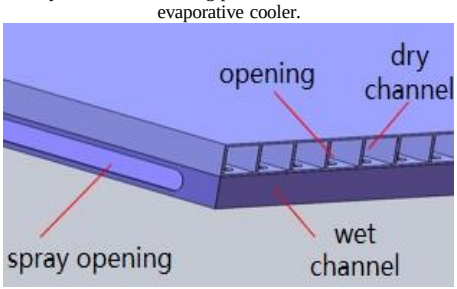

Figure3. Structure of polymer core with hydrophilic membrane

The structure of this dew point indirect evaporative cooler using a polymer core with hydrophilic membrane for higher wet-bulb efficiency is double countercurrent [15] (Figure 2 and 3), for which the wet-bulb efficiency is optimal when the length of the unilateral dry channel is 600 mm and the spacing of the partitions is 8 mm [16]. Table I shows the specific parameters of the cooler.

TABLE I.
COOLER PARAMETERS

Project	Unit	Parameter
Design total air volume	m^3/h	1000
Cooler length	mm	1350
Cooler height	mm	200
Cooler width	mm	400
Individual channel width	mm	8

The dry and wet channels inside the cooler are made of polymer material with hydrophilic membrane. The smooth surface is dry channel, the rough surface is wet channel, the flow distribution of the dry channel on both sides of the primary air volume is 1:1, and there are 100 pieces of core materials inside.

Firstly, the cooling amplitude should be expanded. The dew point core adopts the form of countercurrent heat transfer, that is, the air flow in the opposite direction across the dry channel air and wet channel. The heat transfer potential difference between the two channels of air is smaller, and the heat transfer will be more adequate, and the heat transfer efficiency is relatively higher [17]. Therefore, it can produce more cooling capacity with high wet-bulb efficiency and dew-point efficiency. At the same time, compared with the fork-flow type, the counter-flow dew point indirect evaporative cooler will require less secondary air volume and evaporated water when both coolers have the same cooling capacity. This is because the fact that the air temperature at the outlet of the counter-flow wet channel is closer to the air temperature at the inlet of the dry channel, while the relative humidity of the air at the outlet of the wet channel is closer to 100%.

Secondly, under the premise of ensuring cooling capacity, by adopting a double countercurrent structure (that is, both the left and right sides are air inlets), compared with a single countercurrent structure, when the air volume is same, changing the inlet size of the core and the inlet air speed has a greater impact on heat and mass transfer and flow resistance performance [18].

The increase of wind speed in dry channel will lead to the decrease of heat transfer efficiency. The main reason for this is that as the wind speed in the dry channel increases, the heat transfer time between the air and the air in the wet channel becomes shorter. As a result, the heat transfer process is insufficient, resulting in a decline in heat transfer efficiency [19]. The cooler mainly relies on evaporation mass transfer in the wet channel to drive heat transfer to complete the cooling process. In this process, the contact between the water membrane and the air causes the vaporization of water molecules at the interface. When the water temperature and air temperature is extremely close, and the partial pressure of water vapor in the air is high, so that the water is in a non-saturated or nearly saturated state, at this time, the heat and mass transfer within the water

membrane to drive the heat transfer is quite weak, because the temperature difference and humidity difference at the water-air interface are also small. Therefore, the main heat and mass transfer driving force of the system depends on the flow of air in the wet channel.

Air flow affects water evaporation and heat and mass transfer in four ways: (1) By increasing the fluctuation frequency and amplitude of water membrane, air partial pressure is generated on the surface of water membrane, resulting in the phenomenon of "capillary induced evaporation", which can significantly increase heat transfer [20]; (2) Accelerating the renewal process of the contact surface between air and water membrane, and increasing the intensity of heat and mass exchange; (3) Increasing the relative velocity of the water-gas interface to reduce the interface vapor pressure, increasing the saturation degree of supercooled water, so that the water chemical potential increases, while enhancing the degree of air turbulence. (4) Removing the water vapor and heat so that the water vapor pressure in the air is maintained at a low level, and keeping the heat and mass transfer driving force at a high level.

3 Performance evaluation method

The main evaluation indexes related to the cooling performance of dew point indirect evaporative coolers include: wet-bulb efficiency, dew-point efficiency, cooling capacity, power consumption, coefficient of performance (COP), and water consumption rate [17].

（1） Wet-bulb efficiency

$$\varepsilon_{wb} = \frac{(t_{g1}-t_{g2})}{(t_{g1}-t_{w1})} \times 100\% \qquad (1)$$

t_{g1}—Dry-bulb temperature of primary air inlet, ℃;

t_{g2}—Dry-bulb temperature of primary air outlet, ℃;

t_{w1}—Wet-bulb temperature of primary air inlet, ℃。

（2） Dew point efficiency

$$\varepsilon_{db} = \frac{(t_{g1}-t_{g2})}{(t_{g1}-t_{d1})} \times 100\% \qquad (2)$$

t_{d1} — The dew-point temperature of the primary air inlet, ℃;

（3） Cooling capacity

$$Q = \frac{c_{p,a}\rho_a V(t_{g1}-t_{g2})}{3600} \qquad (3)$$

Q—Cooling capacity, kW;

$c_{p,a}$—Specific heat of air at constant pressure, kJ/(kg·℃);

ρ_a—Air density, kg/m³;

V—Primary air flow, m³/h。

（4） Coefficient of performance (COP)

$$COP = \frac{Q}{W} \qquad (4)$$

W—Total power of cooler, kW。

4 Experimental research

The experimental platform is built in the national double enthalpy-difference laboratory of the industry-university-research cooperative enterprise, which includes a test environment room with two sets of air treatment system and one set of water system.

The air processor can be adjusted to regulate the cold source, heat source, and wet source when controlling the dry and wet bulb temperature of the laboratory environment. The ambient dry-bulb temperature is controlled by adjusting the number of compressors and electric heating inputs for the evaporation coil in the air processor. The ambient wet-bulb temperature is controlled by adjusting the amount of electric heating for the humidifier nozzles in the humidifier box in the air processor, that is, adjusting the wet source of the air processor. The test room is equipped with a set of air volume measurement device, equipped with 9 Φ189 nozzles, for each Φ189 nozzle, the air volume measurement range is 1545 ~ 3535m³ /h; It is equipped with a set of test machine water system, used for the test machine water, and the flow measurement range is 0 ~ 300kg/h.

The experimental platform is mainly composed of fan, air supply pipeline, double countercurrent dew point indirect evaporative cooling core, secondary exhaust fan, circulating water pump, circulating water tank and other equipment.

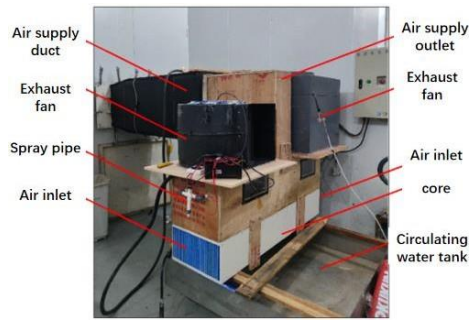

Figure4. Physical Figure of the experimental bench

Figure5. Physical diagram of double countercurrent dew point indirect evaporative cooling core

According to the principle of four-region division [21], three representative cities in Northwest China, namely Urumqi, Lanzhou and Xi 'an, are selected. According to GB 50736-2012 [22] and GB 25860-2010 [23], the outdoor design dry and wet bulb temperature for summer air conditioning in each city as well as the standard dry and standard high humidity conditions are taken as the experimental conditions to be simulated in this experiment, as shown in Table II. The temperature error of wet and dry bulb simulated in enthalpy-difference laboratory is ±0.5℃.

TABLE II.
SIMULATION CONDITIONS IN THE ENTHALPY DIFFERENCE LABORATORY

Climate zone	Sub-area indicators /℃	Standard working conditions	Dry-bulb temperature /℃	Wet-bulb temperature /℃	Dew-point temperature /℃
Ventilated area	$t_w < 20$	Urumqi	33.5	18.2	8.6
High adaptive zone	$20 \le t_w < 23$	Lanzhou	31.3	20.1	14.5

adaptive zone	$23 \le t_w < 28$	Xi 'an	35.1 25.8 22.5
-	-	Standard drying condition	38.0 23..0 16.4
		Standard high humidity condition	38.0 28.0 25.8

5 different values such as 0.7, 0.9, 1.1, 1.3 and 1.5 were selected for the secondary/primary air volume ratio, as shown in Table III, different secondary/primary air volume ratio under different conditions was tested.

TABLE III.
SECONDARY / PRIMARY AIR VOLUME RATIO SETTING

Secondary airflow rate m^3/h	Primary airflow rate m^3/h	total airflow rate m^3/h	Secondary/ primary air volume ratio
390	550	940	0.7
495	550	1045	0.9
605	550	1155	1.1
715	550	1265	1.3
825	550	1325	1.5

The following is the uncertainty analysis of the experimental tests. In order to verify the accuracy of the experimental results, the heat transfer results in the dry and wet channels were obtained from the following equations. The accuracy of the experimental apparatus as shown in Table 3, the energy balance was satisfied within ±10% in most cases, with an average of ±6% .[24]

$$Q_d = m_d(i_{d,in} - i_{d,out}) \quad (5)$$

$$Q_w = m_w(i_{w,out} - i_{w,in}) \quad (6)$$

The uncertainty of the validity measurement can be obtained by the following equation.

$$\frac{\Delta s}{s} = \sqrt{\sum_i \left(\frac{1}{s}\frac{\partial s}{\partial y_i}\Delta y_i\right)^2} \quad (7)$$

$$y_i = T_{d,in}, T_{d,out} D_{d,in}$$

y_i—The measured values in the experiment, including t_{g1}、$t_{g2}$and t_{w1};

Δy_i—Uncertainty per measurement.

TABLE IV.
ACCURACY OF THE EXPERIMENTAL INSTRUMENTS

Name of instrument	Test content	Measurement range	Precision
Portable temperature and humidity self-calculator	Dry-bulb temperature /Relative humidity	0-50℃/1-99%	±0.6℃/±3%
Electronic digital thermometer	Circulating water temperature	50℃-105℃	±1℃
Vane anemometer	Wind speed/Pressure	0.4~20.0m/s	±(0.2m/s +2%)
Three-phase electric parameter digital measuring instrument	Power	0~250kW	±(0.4~0.1%)

5 Experimental results and performance analysis

1.Performance analysis of the cooler under Xi'an working condition

1. Intermittent spraying

The experiment employed a spiral nozzle with a 2mm aperture positioned 150mm above the upper part of the core, and the injection angle of the nozzle was set at 85°. Consequently, each individual nozzle covered a circular area with a radius of 120mm. To ensure complete coverage of the spraying cross-sectional area, a total of eight nozzles were utilized. The test procedure involved continuous spraying for 15 minutes upon activation to fully saturate the core material. Subsequently, five different conditions were tested: continuous spraying; spraying for 15s followed by a pause of 60s; spraying for 15s followed by a pause of 90 s; spraying for 15s followed by a pause of 120s; and finally, spraying for 15s followed by a pause of 180s. Various intermittent spray methods were analyzed. Taking Xi 'an as an example, when the inlet air parameters were stable, the cooling range and wet-bulb efficiency of the outlet air were observed. It can be seen from Figure 6 that the wet-bulb efficiency and cooling range of 15s and 60s are the largest, which are 104.3% and 9.5℃ respectively.

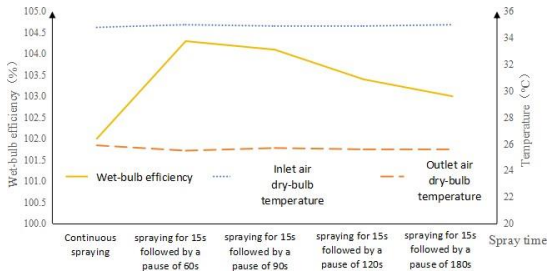

Figure6. Changes of wet-bulb efficiency with different spraying methods

The core material of the cooler has the function of water absorption and water retention, when the spraying water exceeds the evaporation amount, the hydrophilic membrane stores water, and when the spray water is less than the evaporation amount, the hydrophilic membrane releases water. The intermittent spraying method has a more important impact on water consumption and unit power. On the one hand, it can reduce water consumption to a great extent. In order to ensure uniform wetting, the common metal core needs to be uninterruptedly sprayed, resulting in the recycling of excess water, causing scaling, increasing the flow resistance, reducing the heat transfer coefficient, and affecting the evaporative cooling effect. In this test, the polymer material of water absorbing membrane is used, so that the core can form superficial and internal water membrane during the water absorbing process. After the water on the surface of the core evaporates, the internal water is automatically replenished, and the heat and humidity exchange is carried out with the surrounding air in the form of water vapor to maintain dynamic balance. This helps to reduce the frequency of water replacement and reduce water consumption. On the other hand, water is sprayed into the wet channel of the core by means of a circulating pump, and this process comes at the cost of electrical energy consumption. Therefore, the energy consumption of the water replenishment unit will be significantly lower than that with continuous spraying.

5.1.2 Water consumption

Under Xi 'an condition, the water consumption of the above 5 different spraying methods was tested by rotor flowmeter, and each test group was run for 1h. The water consumption corresponding to the five spraying methods was measured to be 5, 1, 0.7, 0.6 and 0.4L/h. As shown in

Table V, the spraying method with 15s stop for 60s has the highest wet-bulb efficiency and lower water consumption, and the unit's performance parameters were relatively good.

TABLE V.
WATER CONSUMPTION AND WET-BULB EFFICIENCY AT DIFFERENT SHOWER INTERVALS

Spraying time /s	Spray time interval /s	Spray frequency	Water consumption L/h	Wet-bulb efficiency /%
15	0	-	5.0	102.0
15	60	48	1.0	104.3
15	90	35	0.7	104.1
15	120	27	0.6	103.4
15	180	19	0.4	103.0

5.1.3 Performance parameters under different air volumes

As shown in Figure 7, the dry-bulb temperature drop of the inlet and outlet air and the cooling capacity change with the airflow ratio. Taking Xi 'an as an example, when the optimal air volume ratio is 1.1, the cooling capacity of the cooler can reach up to 1.94kW, and with the air volume ratio rising from 0.7 to 1.1, the temperature drop is also increasing. When the air volume ratio exceeds 1.1, both the cooling capacity and the inlet and outlet air dry-bulb temperature drop begin to decline. Its COP reaches the maximum value when the air volume ratio is 0.9. This phenomenon occurs because with the increase of the secondary/primary air volume ratio, the exhaust fan power also increases, resulting in a decrease in COP.

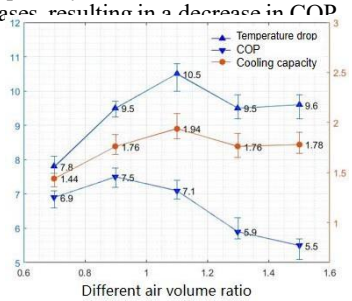

Figure7. Temperature drop and cooling capacity at different air volumes

5.1.4 Current and Power

As can be seen from Figure 8, The current and power at different airflow ratios were tested under Xi'an working condition, and the results show that when the total voltage is maintained at 380V, the current and power increase with the increase of the secondary/primary air volume ratio.

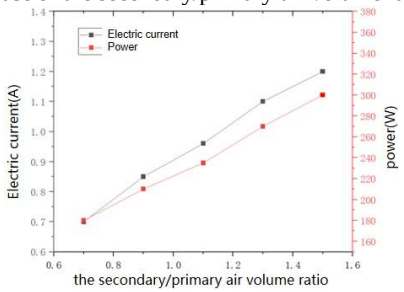

Figure8. Change of current and power consumption at different air volumes

5.2 Performance comparison under different conditions

5.2.1 Option of optimum secondary/primary air volume ratio

After the environment condition was stable, the test prototype began to be tested to obtain different air volume ratios by ensuring that the primary airflow rate was 550m³/h and adjusting the frequency of the secondary exhaust fan.

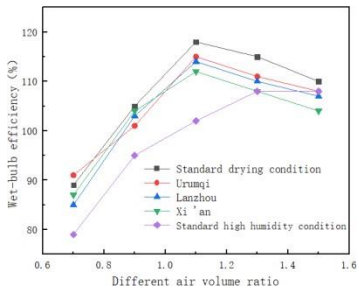

Figure9. Changes of wet-bulb efficiency with different air volume ratios

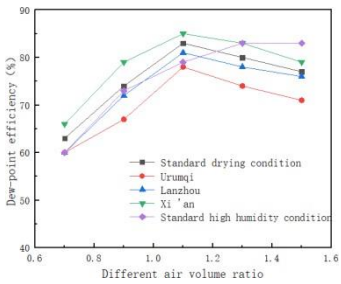

Figure10. Changes of dew-point efficiency with different air volume ratios

As shown in Figure 9, the change of secondary airflow rate has a significant effect on the heat transfer process while keeping the primary airflow rate constant. The wet-bulb efficiency shows an increasing and then decreasing trend with the increase of the secondary/primary air volume ratio. However, air volume ratios at which the wet-bulb efficiency reaches its maximum point are not the same under different environmental conditions. In Lanzhou, Urumqi, Xi'an and standard dry conditions, the wet-bulb efficiency has reached the highest value when the ratio of secondary/primary air volume is 1.1, while in standard high humidity conditions, the wet-bulb efficiency reaches the largest when the secondary/primary air volume ratio is 1.3.

The reason is that in dry areas, the dry and wet bulb temperature difference of the outdoor air is large and the cooling drive is strong. When the secondary/primary air volume ratio is between 0.7 and 1.1, the cooling capacity of the secondary air obtained after evaporation is enough to take away the heat of the primary side. In the high humidity area, the relative humidity of the secondary air is higher, and the water vapor molecules can be contained and carried by the secondary air are significantly reduced when exchanging heat and moisture with the water membrane in the secondary flow channel. Therefore, more secondary airflow rate is needed to take away the latent heat formed by the evaporation in the secondary side and further cool the primary air.

As shown in Figure 10, When the secondary/primary air volume ratio exceeds 1.1, the wet-bulb efficiency and dew-

point efficiency of Lanzhou, Urumqi, Xi 'an and standard drying conditions decreases with the increase of secondary airflow rate. This is because the wind speed on the secondary side is too high at this time, and the heat exchange with the water membrane cannot be fully carried out in the wet channel, and it is quickly discharged by the exhaust fan.

5.2.2 Cooling capacity

Figure 11 shows the variation of the cooling capacity of the cooler with the secondary/primary air volume ratio under five operating conditions. When the secondary /primary air volume ratio is 1.1, the cooling capacity of the cooler is the highest. The cooling capacity is related to the magnitude of the temperature drop. The cooling capacity of the cooler increases as the dry-bulb temperature drop between the inlet and outlet air increases, assuming a constant air supply. Under standard dry and Urumqi conditions, the temperature difference between the dry and wet bulb is maximized, ensuring that the cooler maintains a high level of cooling capacity.

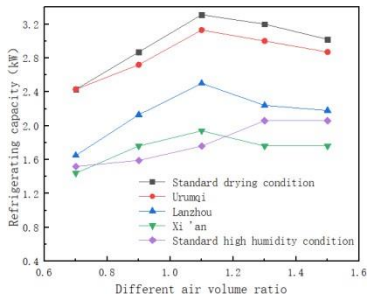

Figure11. cooling capacity with different air volume ratios

6 Conclusion

The design, construction and experimental testing of a double countercurrent dew-point indirect evaporative cooler in a medium humidity region with a cooling capacity of 1.5kW were carried out. The performance of the cooler was analyzed under simulated different environmental conditions, and the conclusions were drawn as follows:

(1)The experimental data show that under the operating conditions of Xi 'an, when the secondary/primary air volume ratio is 1.1, the wet-bulb efficiency reaches 104%, the dew-point efficiency reaches 79%, the cooling capacity reaches 1.76kW, and the dry-bulb temperature difference between the inlet and outlet air is 9.5℃.

(2)A new dew-point indirect evaporative cooler using polymer material with absorbent membrane was studied, and a more efficient and water-saving indirect spraying scheme was provided, which can enhance the hydrophilic ability of the wet channel surface, and its lower power consumption of fans and pumps and higher COP performance also verify that the cooler is suitable for residential buildings.

(3)Experiments simulating different environmental conditions show that the optimal secondary/primary air volume ratio is not the same in different regions. . In the standard dry conditions and Urumqi conditions, the cooler shows excellent performance, and this result also verifies that the dew-point indirect evaporative cooling technology has a huge competitive advantage and a wide range of application prospects in the dry region of Northwest China.

References

1 Pérez -Lombard L, Ortiz J, et al. A review on buildings energy consumption information. Energy Build 2008; 40:394–8.

2 Jiang Y. Chinese building energy consumption situation and energy efficiency strategy, New Architecture; 2008 [in Chinese].

3 Chua KJ, Chou SK, Yang WM, Yan J. Achieving better energy-efficient air conditioning – A review of technologies and strategies. Appl Energy2013;104:87–104.

4 Barnard N, Jaunzens D. Low energy cooling – technology selection and early design guidance. London: Building Research Estabilishment Ltd; 2001.

5 Behne M. Alternatives to compressive cooling in non-residential buildings to reduce primary energy consumption. Berkeley, California: Final report Lawrence Berkeley National Laboratory; 1997.

6 Maisotsenko V，Gillan L E，Heaton T L，et al. Method and plate apparatus for dew point evaporative cooler：U.S.Patent 6，581，402［P］.2003-6-24.

7 Zhou Xiaoqing, Chen Peilin. Thermal analysis of the indirect evaporative cooler [J].HVAC,2000(01):39-42.

8 Bruno F. On-site experimental testing of a novel dew point evaporative cooler. Energy and Buildings 2011; 43(12):3475-3483.

9 Zhan C, Duan Z, Zhao X, Smith S, Jin H, Riffat S. Comparative study of the performance of the M-cycle counter-flow and cross-flow heat exchangers for indirect evaporative cooling – Paving the path toward sustainable cooling of buildings. Energy 2011; 36(12):6790-6805.

[10] Zhan C, Zhao X, Smith S, Riffat SB. Numerical study of a M-cycle cross-flow heat exchanger for indirect evaporative cooling. Building and Environment 2011; 46(3):657-668.

[11] XU Peng,MA Xiaoli,ZHAO Xudong,et al. Experimental investigation of a super performance dew point air cooler[J].Applied Energy,2017,203:761－777.

[12] XU Peng,MA Xiaoli,DIALLO T M O， et al. Numerical investigation of the energy performance of a guideless irregular heat and mass exchanger with corrugated heat transfer surface for dew point cooling[J].Energy,2016,109:803－817.

[13] Duan Z, Zhan C, Zhao X, Dong X. Experimental study of a counter- flow regenerative evaporative cooler. Building and Environment 2016; 104:47-58.

[14] Chu J, Xu W, Fu Y, Huo H. Experimental research on the cooling performance of a new regenerative dew point indirect evaporative cooler. Journal of Building Engineering 2021; 43.

[15] Qu Mingxun,Huang Xiang,Jin Yangfan,etc.Experimental Research on Indirect Evaporative Cooling Heat Exchange Core Based on Two Different Materials[J].Refrigeration and Air Conditioning (Sichuan),2022,36(01):67-72+104.

[16] Wang Yucao.Study on Heat Transfer Performance of Plate in Counter-flow Plate Dew Point IndirectEvaporative Cooler[D].Zhengzhou University of Light Industry,2019.

[17] Huang Xiang. Principle and equipment of evaporative cooling air conditioning[M].Beijing: Machinery Press,2019.05.

[18] Jiang Xiang, Zhu Dongsheng, Tang Guangdong,etcEffect of the inflow velocity distribution on the performance of the evaporative condenser[J].Joumal of Souh China University of Technology(Natural Science Edition)

[19] Lin Yongjun, Zhang Xuewei, Cui Zihua,etc.Study on Performance of Indirect Evaporative Plate Heat Exchanger[J].REFRIGERATION.2022,41(02):26-31.

[20] Guo Zengyuan,Huang Suyi.Field synergy principle and the new technology of enhanced heat transfer[M].Beijing:China Electric Power Publishing House,2004.

[21] Di Yuhui, Liu Jiaping, Huang Xiang.Climate demarcating for application of evaporative cooling air conditioning[J].HVAC,2010,40(2):108-111.

[22] Code for design of heating, ventilation and air regulation for civil buildings: GB 50736- -2012 [S]. Beijing: China State Engineering and Construction Press, 2012.

[23] Evaporative air cooler: GB / T 25860- -2010 [S]. Beijing: China Standards Press, 2010.

3rd Place
REHVA
Student Competition

Ninon Gauthier -
Roxane Viala
France

2024

REHVA
Federation of European Heating, Ventilation and Air Conditioning Associations

Monte-Carlo modeling of input uncertainly in ELECTRE-Tri Multi Criteria Decision Analysis

Ninon Gauthier, Roxane Viala

Abstract—Important decisions in building energy retrofitting occur in early design stages, where data are imprecise, and objectives are unclear. This paper introduces a new method, pELECTRE-Tri, which integrates probabilistic distributions of inputs and Monte Carlo simulation into the ELECTRE Tri method. The method was tested on a retrofitting project with three buildings (around 70 apartments). The method's strengths lie in its decision process being clear, verifiable, and repeatable. However, its primary drawback is the substantial amount of information it requires. Over time, the effective management and systematic organization of data can mitigate this challenge. Adopting this method illuminates a path forward for refining energy retrofitting processes, emphasizing the value of structured data collection and analysis.

Implemented in Python, pELECTRE-Tri method is openly available on Zenodo (DOI: 10.5281/zenodo.7967656).

Key words—ELECTRE Tri, Energy retrofitting, multi- criteria decision making, Sustainability.

Introduction

In the building sector, where existing buildings are the primary consumers of energy, adopting retrofitting measures and policy recommendations can lead to significant reductions in energy consumption and carbon dioxide emissions, offering a pathway to substantial global energy savings.

The most important decisions in energy retrofitting are taken during the early design stages when information is scarce and imprecise. Renovation solutions are dynamic systems that bring together many actors, many factors with long-term applications and a lot of uncertainty. Evaluating retrofits is complex due to various criteria like economic, technical, ecological, and social. Retrofitting methods encompass improved thermal insulation, solar shading, and renewable energy technologies, benefiting the environment, economy, and society. Challenges include uncertainties like climate change and policy shifts, financial constraints, and interdependent building subsystems. Retrofit projects involve trade-offs between stakeholder interests, such as government priorities versus other stakeholders' concerns. Comfort, especially thermal, visual, and acoustic, is crucial. Considering embodied emissions, operational emissions, occupant comfort, and investment costs is essential.

Multi-criteria Decision Analysis (MCDA) is a decision support protocol for ranking elements by evaluating them on different criteria. It deals with a problem that has several aspects depending on the wishes of a decision maker. MCDA makes a problem more understandable, transparent, and accessible. MCDA has already been used in energy retrofitting but with crisp values for the inputs.

To consider the uncertainty et variations of the input data in retrofitting projects, this paper uses probabilistic distributions for inputs and ELECTRE-Tri MCDA with Monte-Carlo simulation. The implementation of this new procedure is tested with a case study. The energy renovation of 3 buildings located in the Lyon area was requested by a company. Field data was collected and an initial ELECTRE-Tri decision-support method was applied [1]. The study detailed in this article was then carried out with a view to incorporating variations in the input data into the analysis.

I. Methods

ELECTRE-Tri serves the objective of categorizing alternatives in energy retrofitting projects. As a result of this method, alternatives, representing various possibilities in a decision-making process, are systematically ranked into predefined categories based on evaluations across diverse criteria. The evaluation involves several criteria, each reflecting perspectives of different natures. As input data, the method requires the identification of the criteria weights that will be used to evaluate the alternatives and the assessment of each alternative according to each criterion. All this data is compiled into a table called the performance matrix, which will be the single input to the method. Throughout its process, input data is juxtaposed against reference profiles, delineating the category boundaries for each criterion. Figure 1 represents an overview of the comparison of performances of an alternative compared to the reference profiles b_i, with i going from 1 to 5, delimitating five categories C for n criteria G_j, with j going from 0 to n.

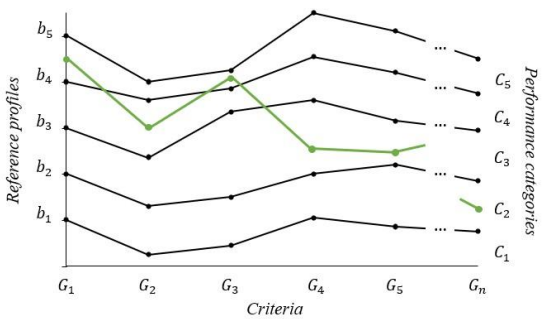

Figure 1: Schematic representation of the performance of an alternative represented in green.

The comparisons between alternatives and profiles yield preference relations, elucidating the relationship of an alternative to a profile. This method yields an optimistic and pessimistic arrangement of alternatives based on the classification direction [3].

This categorization possesses several noteworthy aspects pertinent to the analysis of the decision-making process for optimal renovation alternatives. Primarily, the method independently classifies alternatives within performance categories. By evaluating each alternative's score against category limits for each criterion, a thorough performance assessment is achieved. Importantly, this methodology allows for the incorporation or removal of new alternatives into the process without altering the ranking of existing alternatives, a significant advantage in the decision-making process for energy refurbishment solutions, given the continual emergence of new solutions.

Decision-makers may supplement the category limits with a veto threshold, mitigating the compensation phenomenon. This threshold signifies the maximum distance between a category limit and a data point concerning a criterion. If this distance is surpassed, the alternative can never be classified within the category limited by the threshold due to its significant deviation on a specific criterion. Consequently, if an alternative exhibits exceptionally poor performance in one criterion, it cannot be compensated by an exceptionally good performance in another criterion.

There are two important ways to model imprecision: fuzzy logic and probability theory. The former addresses the vagueness inherent in available information. In ELECTRE-Tri, the imprecision of reference profiles is considered by employing linear variation for concordance and discordance indexes. The latter deals with the variability in outcomes, where the exact outcome of an event is unknown, but probabilities can be assigned to different possible outcomes. This paper proposes to model the uncertainty of inputs in ELECTRE-Tri MCDA by using probability distributions.

II. PROBABILISTIC APPROACH

This paper presents a pioneering methodology in the definition of input data uncertainty in order to bolster the robustness and reliability of the decision-making process. The modeling of uncertainty is done through two key elements:

- Representation of data as probability density functions (PDFs), as opposed to crisp values.
- Application of the Monte Carlo method, a statistical technique utilizing random sampling, to these probability distributions.

A. *Probability density functions (PDFs)*

The integration of data fluctuation into the performance matrix is achieved through the utilization of the Probability Density Function (PDF) [4]. A Probability Density Function is a mathematical expression that characterizes the probability distribution of a continuous random variable [5]. These mathematical curves enable the articulation and quantification of the knowledge embedded in the input data based on their specified parameters. Although any PDF can be employed, this study opts for the normal distribution. The decision to adopt the normal distribution is rooted in two primary considerations. The normal distribution is widely employed to model real-world values, particularly in fields such as economics, social sciences, and natural sciences, where the exact distribution of the data is often unknown. Furthermore, when numerous samples are taken, the normal distribution frequently serves as an effective approximation for the data distribution, even if it doesn't precisely represent the true underlying distribution [6]. Statisticians like Pierre-Simon Laplace have demonstrated through experimentation across various fields that the normality of data tends to increase with sample size.

The normal distribution, denoted as $N(\mu, \sigma^2)$, is characterized by two parameters: the mean value (μ) and the standard deviation (σ), with the variance (v) being expressed as $v = \sigma^2$. Consequently, calculations in this context are conducted using the mean value (μ) and the variance (v) as the defining parameters.

B. *Monte Carlo approach*

The Monte Carlo method, a statistical technique, is employed for estimating operations in intricate systems reliant on random sampling and statistical modeling. This method is particularly useful for applying a set of probability functions by iteratively generating data. The approach involves sampling one data point from each distribution to form a performance matrix. By repeating this process numerous times, the method produces results representative of the underlying distributions of input data. This allows for the incorporation of uncertainty into the decision-making process.

The implementation of the proposed method involves the following steps:

Step 1: Select values from Probability Distribution Functions (PDFs)

The performance of an alternative (a) concerning a criterion (j) is given by:

$$S_a(C_j) = F_j(x)$$

where F_j is the probability density function of the criterion j.

The initial step involves selecting a value from each distribution, forming a new performance matrix using the chosen values.

Step 2: ELECTRE Tri implementation

Once the data set is obtained, ELECTRE Tri is employed to calculate the optimistic and pessimistic rankings for each set of alternatives.

Step 3: Obtaining a set of outcomes.

The final step involves iteratively repeating the first two steps to generate multiple optimistic and pessimistic rankings. The number of times each alternative is classified in each category is recorded, resulting in a distribution of alternatives within the categories. These rankings are then converted into percentages to create tables illustrating the probability of each alternative ranking in each category.

An automated computational algorithm has been developed to streamline the probabilistic ELECTRE-Tri method, ensuring rapid and efficient processing [1]. Python programming language is selected for method implementation due to its readability, user-friendliness, popularity, and versatility in terms of computer support. The method categorizes alternatives into different ranking categories (C_k) defined by upper and lower boundary reference profiles (B_k). Decision-makers have the flexibility to define these boundary reference profiles, and their performance is instrumental in establishing the ranking categories. They also must provide the Performance Matrix, containing for each criterion and each alternative mean value (μ) and the variance (v) as the defining parameters of their assessment.

III. DATA PRESENTATION AND DISCUSSION

A. Case Study

The Multi Criteria Analysis ELECTRE-Tri was firstly applied to a project of refurbishment of three buildings consisting of about 70 apartments to pinpoint the most beneficial renovation approaches for a social landlord [6]. An exploration of renovation options was conducted, which considered a variety of elements presented in Table 1. These identified possibilities were then compiled to create 28 distinct renovation scenarios.

Class	Options
Existing electric floor heating	Connected
	Disconnected
Auxiliary heating	Smart and connected electric storage heater
	Low temperature hot water radiators
	Automated towel warmer
Domestic hot water production	Existing individual electric hot water tank
	Smart and connected individual electric hot water tank
	Smart and connected individual thermodynamic hot water tank
	Individual condensing gas boiler
	Collective thermodynamic
	Individual solar hot water tank with centralized solar hot water tank
Ventilation system	Existing controlled mechanical ventilation
	Controlled mechanical ventilation with single-flow and a humidity-sensitive extract unit
Local energy production	None
	Roof photovoltaic solar panels
	Roof thermal solar panels
	Roof hybrid solar panels
External joinery replacement	None
	All external joinery double gazing
	All external joinery triple gazing
	Only on the balcony windows double glazing
External wall insulation	Existing wall insulation
	External thermal insulation

Table 1: Renovation options

Dimension	Criteria
Economic	Investment cost
	Reinvestment cost over a period of 30 years
	Possibility of financial subsidy
	Operating cost
	Energy cost effectiveness of the solution
Technical	Ease to integrate into existing building
	Implementation in occupied space
	Maintenance/Serviceability
	Ease of monitoring/Energy management
Social	Impact on the cost for the tenants
	Level of thermal comfort
	Level of acoustic comfort
	Aesthetics and space requirements
Environmental	Energy consumption reduction
	Carbon dioxide emissions avoided
	Production place

Table 2 : Evaluation criteria

Each renovation alternative was assessed across four critical dimensions: economic viability, societal impact, technical feasibility, and environmental sustainability (Table 2). This multi-criteria assessment aimed to ensure a holistic evaluation of the potential of each scenario.

In the probabilistic approach conducted, a variance was systematically introduced to the performance scores for each criterion to accurately reflect the complexities and uncertainties inherent in such an analysis. This addition of variance was a deliberate methodological choice, designed to incorporate the natural fluctuations and uncertainties into the decision-making matrix, thus allowing for a more nuanced and informed assessment process. The

performance matrix, containing the performance of each scenario against each criterion and the variance associated with each criterion was then used as the input data of the method.

Using the new performance matrix as input data, the method has been implemented in Python to quickly assess the results. The code creates a distribution for each performance and allows the implementation of the method multiple times to obtain a distribution of the scenarios in the performance categories. The code is openly available on Zenodo (DOI: 10.5281/zenodo.7967656).

B. Results

The result obtained is a distribution of the alternatives in the categories. Instead of ranking the alternatives in one category as in the traditional MCDA method (Table 3), a percentage of the ranking of each alternative in each category is given (Table 4).

The proposed new procedure adds information by providing the percentage of ranking for each alternative within each category, which allows for a more nuanced differentiation of alternatives.

	C1	C2	C3	C4	C5
S1.1		X			
S1.2			X		
S1.3			X		
S1.4			X		
S2.1			X		
S2.2					X
S2.3				X	
S2.4				X	
S3.1			X		
S3.2				X	
S3.3				X	
S3.4				X	
S4.1			X		
S4.2			X		

Table 3 : Previous results with the traditional ELECTRE Tri method applied to the case study

	C1	C2	C3	C4	C5
S1.1		100%			
S1.2		28.4%	71%	0.6%	
S1.3		0.7%	65.8%	33.3%	0.2%
S1.4		41.9%	58%	0.1%	
S2.1		14.5%	82.6%	2.9%	
S2.2		0.2%	3.1%	53.9%	42.8%
S2.3		2.2%	7.3%	65.7%	24.8%
S2.4		0.1%	3%	57.8%	39.1%
S3.1		14.4%	82.3%	3.3%	
S3.2		1.3%	4.3%	94.4%	
S3.3		7.4%	34.9%	57.7%	
S3.4			6.4%	93.6%	
S4.1			100%		
S4.2		0.4%	99.6%		

Table 4: Results obtained with the probabilistic approach applied to the case study

Scenarios are distributed differently over the different categories. It facilitates the comparison of alternatives that were previously ranked at the same level, thereby providing a more precise examination of the performance of individual actions within scenarios. The selected scenario for the refurbishment of the three budlings was the scenario S2.4, a scenario that was not the best classified with the classical method (Table 3). The probabilistic approach enables us to understand that the performance of the scenario S2.2 and S2.4 are nearly equal when the uncertainty of the input data is taken into account. This phenomenon can be explained by the proximity of the input data with the reference profiles, alternatively classifying the scenario in a category or another. Other scenarios are uniformly classified in one category. This can be explained by the performance of a scenario being too weak against one criterion, classifying it in a low category. In the case study, hybrid solar panels are too expensive and thus the scenarios with these options are not well classified.

Furthermore, the probabilistic procedure can be effectively combined with other multi-criteria decision analysis methods to ensure that no important information is overlooked. The same performance matrix is used to group the input data. In the implementation of the method on Python, probability distributions enable to form numerous performance matrix. By generalizing the use of probability distributions, instead of crisp values, this method allows for a more comprehensive understanding of the sensitivity of the results to the input data and can help identify a wider range of potential outcomes.

IV. CONCLUSION

Multi-criteria decision analysis (MCDA) methods are a valuable tool for understanding complex environmental problems, considering a variety of evaluation criteria and the multiplicity of different alternatives. Despite the availability of reliable data, it is essential to recognize the uncertainty and variability inherent in this information. To account for these uncertainties, it is proposed to represent the analysis data by probability distributions. These probability distributions and data fluctuations can be handled efficiently by integrating multi-criteria decision analysis methods, such as ELECTRE Tri, with a Monte Carlo implementation.

This proposed new procedure adds significant information by providing the ranking percentage for each alternative in each category. First and foremost, it facilitates the comparison of alternatives that were previously ranked at the same level, enabling a more detailed examination of the performance of individual actions in the scenarios. In addition, because it uses the same performance matrix to group the inputs to the analysis process, this procedure can be effectively combined with other multi-criteria decision analysis methods to ensure that no important information is overlooked. Last, this method allows for a more comprehensive understanding of the sensitivity of the results to the input data and can help identify a wider range of potential outcomes by generalizing the use of probability distributions rather than crisp values.

However, to take full advantage of this method, decision-makers first need to understand the process. Criteria and their associated weights need to be carefully defined to best represent the wishes of decision-makers. In addition, an understanding of the method is needed to select consistent parameters to define the probability functions.

Development areas can therefore be considered to refine the method. An analysis of other probability density functions would add significant information on the choice of the adequate distribution that would best represent certain criteria. Another axis could be the study of the choice of thresholds for category baselines, the impact of integrating the Monte Carlo method on them, and a methodology for estimating them as accurately as possible. The thresholds are key elements on the method as they are defining the performance categories. Their choice should be meticulously made to enhance the advantages of the method. Finally, a study of the definition of the variance as a function of the level of uncertainty and knowledge of the data would further enhance the robustness of the results obtained.

Utilizing a multicriteria analysis method to choose the best building renovation scenario eases decision-making for stakeholders who often lack technical, economic, environmental, and social expertise. While they may not possess specialized knowledge, these decision-makers are actively engaged in the decision-making process, evaluating the impact of each criterion they value. This approach not only enhances the decision-making process but also ensures that diverse perspectives are considered. In the realm of energy-efficient building renovations, where the stakes are high both environmentally and economically, this method becomes a powerful tool, allowing for informed decisions and fostering sustainable practices in the construction industry.

V. ACKNOWLEDGEMENT

We extend our gratitude to the following individuals who played a crucial role in the completion of this project:

1. Christian Ghiaus: Our dedicated tutor, whose guidance and expertise significantly shaped the direction of this research. His insightful feedback and unwavering support were very valuable.
2. Souleymane Daniel: For his assistance during data collection and analysis.
3. Majid Baseer: His precious insights and thoughtful discussions enriched our project.

VI. REFERENCES

1 Daniel, S.; Ghiaus, C. Multi-Criteria Decision Analysis for Energy Retrofit of Residential Buildings: Methodology and Feedback from Real Application. *Energies* 2023, 16, 902.

2 Almeida-Dias, J.; Figueira, J.R.; Roy, B. Electre Tri-C: A multiple criteria sorting method based on characteristic reference actions.

3 Van de Schoot, R.; Kaplan, D.; Denissen, J.; Asendorpf, J.B.; Neyer, F.J.; Van Aken, M.A. A gentle introduction to Bayesian analysis: Applications to developmental research. *Child Dev.* 2014, 85, 842–860.

4 Cramér, H. Random Variables and Probability Distributions; *Cambridge University Press,* Cambridge, UK, 2004.

5 Br. J. Philos. Sci. Why are normal distributions normal? Lyon, A. 2014, 65, 621–649.

6 Baseer, M.; Ghiaus, C.;Viala, R.; Gauthier, N.; Daniel, S.pELECTRE-Tri: Probabilistic ELECTRE-Tri Method—Application for the Energy Renovation of Buildings. *Energies 2023*, 16, 5296

HVAC World
Student Competition

Other Participants' Contribution

Tatsuya Miyata	**Japan**
Ahmad Faiz Khan	**USA**
Amanda Webb	**USA**

Enhancement of Fault Diagnosis for Chiller Plant: Visualization and Impact Estimation for Multiple Faults

Tatsuya Miyata[1]

[1] Department of Architecture, Faculty of Engineering, University of Tokyo,

***Abstract*— Research on fault diagnosis of HVAC systems is a highly significant topic in reducing energy loss in buildings, and previous studies have proposed methods to diagnose single faults with high accuracy. However, it has been pointed out that in real systems, multiple faults occur with various degrees of severity, which increases the need of enhancements of existing methods. The objective of this paper is to diagnose multiple faults and estimate their impact using a Variational Auto Encoder (VAE). By learning the behavior of the system during fault occurrences, and mapping such data onto the latent space, it is possible to estimate the fault type and degree of fault impact. By applying this method to the system, single fault types could be diagnosed with an average accuracy of over 97%. In addition, fault impact could be estimated with high accuracy, averaging an error of 1.26%. Next, assuming the simultaneous occurrence of two types of faults, we conducted the diagnosis of multiple faults by mapping data into a higher-dimensional latent space. As a result, although the proportion of jointly diagnosed faults was about 70%, at least one of the faults could be diagnosed with very high accuracy. In the future, reconsidering the method of creating fault data and devising maintenance plans can further improve the diagnostic performance.**

***Index Terms*— Fault diagnosis; Fault impact; Multiple faults; Variational Auto Encoder; HVAC systems**

Introduction

In Japan, building sector accounts for about 40% of energy consumption, necessitating greater emphasis on energy efficiency in design, construction, and operation phases [1]. Building systems, particularly Heating, Ventilating, and Air Conditioning (HVAC) systems, contributes significantly to energy consumption, accounting for about half in the operation phase [2]. Therefore, enhancing the efficiency of building systems is crucial for energy conservation. However, due to equipment degradation, control failures, sensor inaccuracies, and other factors, various types of faults may occur within HVAC systems, and these faults can lead to a decrease in efficiency ranging from 5% to 30% across the entire system [3-5]. Therefore, Automated Fault Detection and Diagnosis (AFDD) in HVAC are crucial technologies for inspecting inefficient operation and reducing unnecessary energy consumption during the operational phase.

In previous studies, proposed AFDD methods have achieved high accuracy in detecting and diagnosing single faults, such as Miyata et al., utilizing Convolutional Neural Networks (CNN) [6]. However, it has been noted that in real systems, multiple faults occur simultaneously with various magnitudes [7].

Therefore, this study aims to develop a method capable of diagnosing and estimating the severity of multiple faults, as well as just single faults. More specifically, we applied Variational Auto Encoder (VAE), which can visualize data features in latent space [8] and verified the diagnostic performance of multiple faults. The rest of the manuscript is organized as follows: In section 2, fault data was created using a simulation program of the target system to generate training data for the VAE model. In section 3, the features of single faults were learned by inputting fault data to VAE model, and using this model, our proposed method was able to diagnose which faults occurred and was also able to estimate their impact with high accuracy. In section 4, we assumed that two types of faults occurred simultaneously. By increasing the dimension of the latent space within the model, diagnosing multiple faults became possible. Additionally, we evaluated performance of this method, and demonstrated that this model can diagnose multiple faults with state-of-the-art precision, with lower computational load. Finally, Section 5 presents some concluding remarks.

Target system and fault dataset generation

A. The chiller plant targeted in this study

In this study, we focus on a factory located in Sendai, Miyagi Prefecture. Fig.1 illustrates the thermal source system of this factory. The system comprises two refrigeration units, one primary chilled water pump, three secondary chilled water pumps, two cooling water pumps, and two cooling towers, constituting a relatively small-scale and simple configuration.

The system is equipped with sensors for measuring the flow rate and temperature of both chilled water and cooling water, as well as sensors for outdoor temperature and humidity, as shown in Fig.1. The data obtained from these sensors are recorded every 15 minutes by the Building Energy Management System (BEMS). Through it, we were able to acquire the 15-minute interval measurement data of this system as well as control data for the entire day of January 20, 2019. This study will mainly analyze these data.

B. Fault dataset generation

In this study, we constructed a simulation model of the thermal source system based on the model used in previous research [9], while adhering to equipment specifications

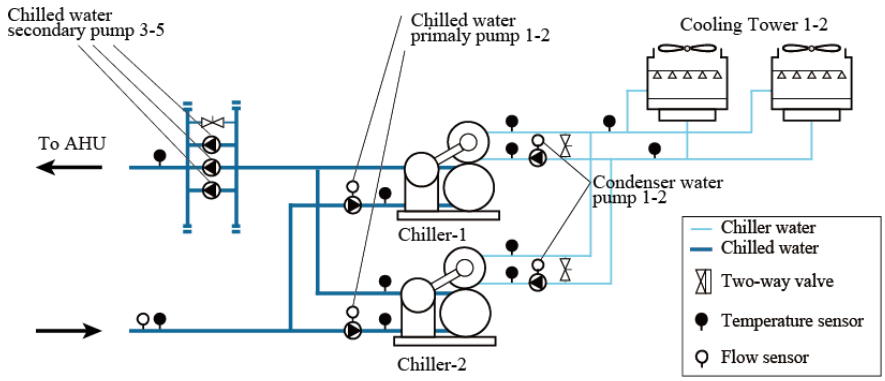

Figure 1. Target heat source system

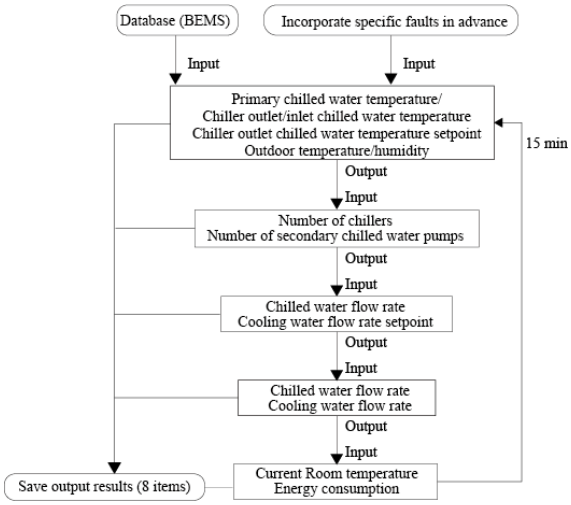

Figure 2. System model calculation flow

and control specifications. The schematic diagram of the simulation flow in this study is presented above (See Fig.2).

Some specific data such as outdoor temperature and indoor heat loads in the target system is obtained by BEMS and provided as boundary conditions to the simulation program. The simulation allows for the calculation of various output results, such as chilled water flow rate, temperature, and the number of operating refrigeration units. It is capable of faithfully reproducing the behavior under normal/fault conditions.

By pre-incorporating elements that could cause malfunctions into the simulation, it becomes possible to calculate the behavior of the system under specific conditions when certain faults occur (fault data). As shown in Table 1, this study targets a total of 8 types of faults and conducts diagnostics on them.

Furthermore, even for the same type of fault, it is assumed to occur in various magnitudes in the real system [10]. Therefore, for each of the 8 types of faults, the magnitude is varied incrementally from the minimum (Lv.1) to the maximum (Lv.10), creating 10 sets of fault data. The detailed progression is shown in Table 1.

Table 1. Assumed faults for the system

Label	Fault target	Conditions	
		Min (Lv.1)	Max (Lv.10)
F1	Sensor offset for primally chilled water flow	-3%	-30%
F2	Sensor offset for secondary chilled water flow control	-3%	-30%
F3	Sensor offset for outdoor relative humidity	-3%	-30%
F4	Sensor offset for secondary chilled water inlet temperature	-0.3℃	-3℃
F5	Sensor offset for TR chilled water inlet temperature	-0.3℃	-3℃
F6	Sensor offset for CT condenser water outlet temperature	-0.3℃	-3℃
F7	Lower limit of condenser water flow control	+6%	+40%
F8	Heat exchange efficiency	-3%	-30%

C. Fault analysis

When various faults occur within the system, it is important to analyze how they affect the output results of the system. Fig.3 illustrates the results of simulations conducted for the cooling tower fan rotation ratio at different levels of F8 (heat exchange rate of the cooling tower), using data from January 20, 2019. As the heat exchange rate of the cooling tower decreases compared to the normal condition (Lv.0), it is observed that the fan rotation ratio increases. This is because more outdoor air needs to be drawn in to lower the temperature of the cooling water.

On the other hand, the cooling water outlet temperature at the cooling tower shows little variation even as the heat exchange rate decreases (See Fig.4). This is probably because the increase in fan rotation compensates for the decrease in heat exchange rate. It should be noted that automated control of HVAC system exhibits such robustness, aiming to stabilize the system and minimize the impact of faults on the overall system performance.

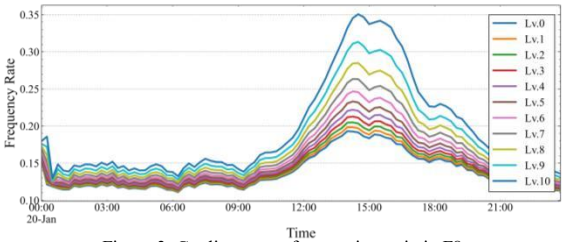

Figure 3. Cooling tower fan rotation ratio in F8

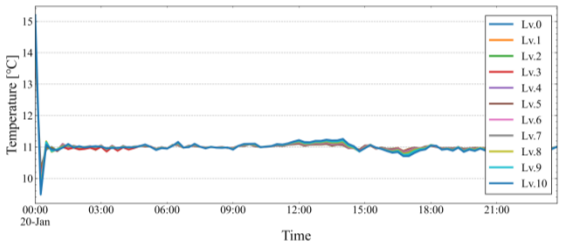

Figure 4. Chilled water outlet temperature in F8

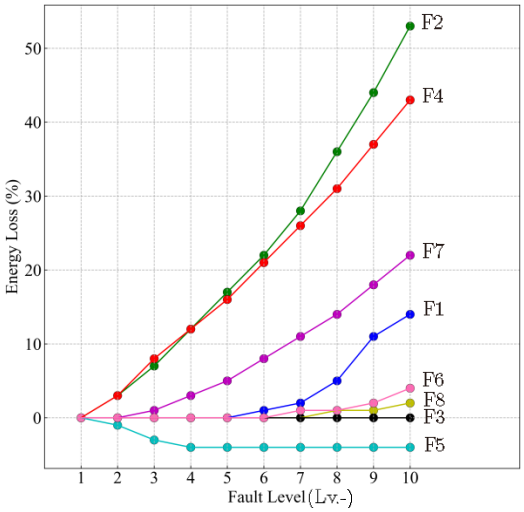

Figure 5. Energy loss at each occurrence of fault (F1-F8)

D. Fault impact on the system

In this study, "impact" of each fault is defined as the energy loss incurred due to the occurrence of the fault. The daily behavior of the target system during each fault occurrence in the simulation is calculated, and the total power consumption during that period is determined.

Subsequently, using normal situation as a reference point, the proportion of additional energy consumption required due to fault occurrence is calculated as energy loss. The results are depicted in Fig.5. With few exceptions, a trend of monotonically increasing energy loss with increasing severity was observed in most type of faults.

As an exception, regarding F5 (error in refrigeration unit's cooling water inlet temperature), the energy loss value was negative, indicating a lower energy consumption than during normal operation. This is probably because the coefficient of performance (COP) of the refrigeration unit generally increases with lower cooling water temperature [11], and F5 led to a decrease in the cooling water temperature. Since the coefficient of performance (COP) of the chiller unit generally increases with lower cooling water temperature, it is presumed that energy consumption decreased as fault impact increases. However, it should be noted that in actual thermal source systems, protective shutdown functions are typically implemented to prevent excessive cooling water temperature reduction.

Single fault diagnosis using VAE

A. Pre-Processing

Simulation results such as temperature and flow rate obtained from the simulation were normalized to a range between 0 and 1, using the following formula (1). The normalized results are then aggregated into a 28×28-sized grayscale image data, which serves as the input data for training the VAE model. Since each of the 8 types of faults has 10 levels of impact, a total of 80 types of image data was created. However, in real-world systems, subtle errors occur due to inaccuracies of model, influence of disturbances, and other causes [12]. Therefore, Gaussian noise with a standard deviation of 0.03 is added to the images. Additionally, by adding noise to the 80 types of data, we could augment the original dataset to 8,000 training data and 1,000 validation data. It should be noted that the values of energy loss remain the same as those in the original data before adding noise.

$$x_{norm} = \frac{x - \min(x)}{\max(x) - \min(x)} \quad (1)$$

B. VAE model construction with originally proposed loss function

VAE consists of two multi-layer neural networks: an encoder and a decoder [8], and each function includes parameters ϕ and θ, as shown in Fig.6. First, the input data $\boldsymbol{X}$ is provided, and the encoder calculates the conditional probability $q_\phi(\boldsymbol{Z}|\boldsymbol{X})$ of the latent variable $\boldsymbol{Z}$. Latent variable can be interpreted as a mapping of the input data $\boldsymbol{X}$ to a lower-dimensional space (latent space). The obtained $\boldsymbol{Z}$ is then input to the decoder. Contrary to the encoder, the decoder calculates the conditional probability distribution $p_\theta(\boldsymbol{X}|\boldsymbol{Z})$ for estimating $\boldsymbol{X}$. Through this process, the reconstructed data $\boldsymbol{X'}$ is obtained from original $\boldsymbol{X}$. Using the reconstruction error of $\boldsymbol{X}$ and $\boldsymbol{X'}$, the parameters ϕ and θ are tuned, and by repeating this process the VAE model can be trained.

We originally defined the loss function *Loss* for learning as (2) and (3): The first and second terms in (3) adjust the latent variable to move away from the center in the latent space as the abnormality of the corresponding input data increases.

On the other hand, the third term in (3) uses the cosine similarity between the latent variable $\boldsymbol{Z}$ and the axis $\boldsymbol{u_m}$ corresponding to each type of anomaly, in the latent space (See Fig.7). It corrects so that similar fault data are mapped close to each other.

$$\cos\theta = \frac{\boldsymbol{Z}\cdot\boldsymbol{u_m}}{|\boldsymbol{Z}|\cdot|\boldsymbol{u_m}|} \quad (2)$$

$$Loss = -E_q[\log p_\theta(\boldsymbol{X}|\boldsymbol{Z})] + D(q_\phi(\boldsymbol{Z}|\boldsymbol{X})||\, p(\boldsymbol{Z})) + \gamma \cdot \sum \cos\theta \quad (3)$$

According to [13] and other papers, equation (3) can be solved by computing the gradients of each neural network and using Stochastic Gradient Descent (SGD) for optimization.

C. Single Fault Diagnosis and Impact Estimation

Through VAE training, the training dataset was successfully mapped in the latent space as shown in Fig.8. The eight axes correspond to each type of faults, and the shades of color represent the fault impact as indicated by energy loss. Fig.8 shows that the larger the impact of the fault is, the farther the latent variables are plotted from the center.

In addition, regarding fault impact, Fig.9 illustrates the correlation between the distance from the center of the latent space and the energy loss. It should be noted that even if the distance from the center is the same, the energy loss may vary for different fault types.

When diagnosing unknown data, we can utilize the following hypothesis: The direction of the point from the center represents the fault type occurring in the system, while the distance from the center represents the impact of the fault. For example, if the position of the latent variable in a certain state of the system is represented by the black dot in Fig.8, we can estimate that the type of fault is F1. Furthermore, referring to the regression curve of F1 in Fig.9, we can diagnose that its energy loss is approximately 2%.

D. Validation

Using this method, automated diagnosis was performed on 1,000 test datasets, and the diagnostic accuracy was verified (See Table 2). The average F-score was approximately 97.1%, indicating a sufficiently high diagnostic accuracy overall. However, for F3, F7, and F8, the F-score fell below 95%, suggesting relatively lower diagnostic accuracy for these faults.

The lower recall observed for F3 and F8 can be attributed to the fact that the characteristics of these faults were not well represented in the input data, due to compensation by other elements. This made it challenging to detect the actual occurrence of these faults. On the other hand, the lower precision observed for F7 suggests that

Table 2. Diagnostic performance for single faults

Label	Accuracy [%]	Precision [%]	Recall [%]	F-measure [%]	RSME
F1	99.7	99.4	1.93	99.6	1.93
F2	91.8	95.9	0.257	93.8	0.257
F3	99.9	94.7	2.74	97.2	2.74
F4	90.1	99.4	0.0	94.5	0.0
F5	100.0	90.0	1.46	94.7	1.46
F6	98.6	100.0	2.28	99.3	2.28
F7	100.0	98.6	1.02	99.3	1.02
F8	96.7	99.9	0.365	98.3	0.365
Ave.	97.1	97.2.	1.26	97.1	1.26

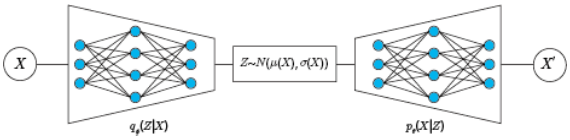

Figure 6. Encoder and Decoder in VAE

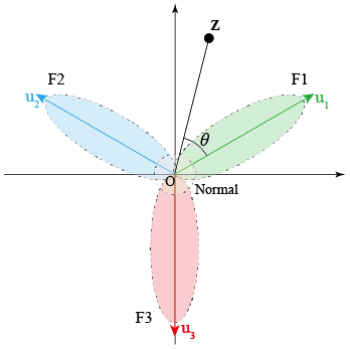

Figure 7. Calculation of *Loss* in the latent space

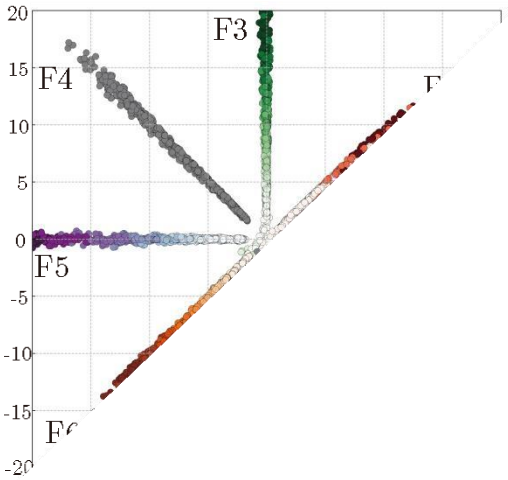

Figure 8. The latent space obtained through learning from 8 types of fault data

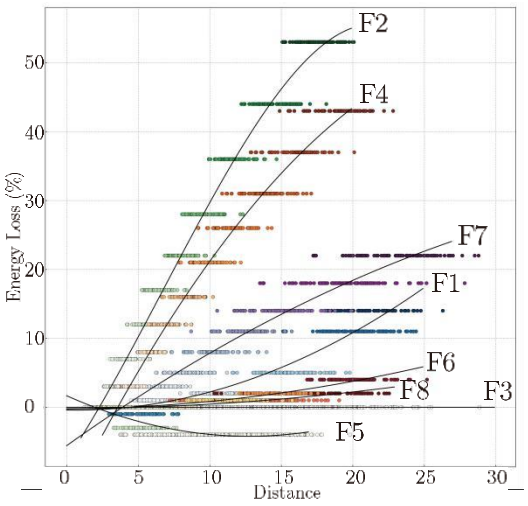

Figure 9. The distribution of each fault: the distance from the origin on the horizontal axis and energy loss on the vertical axis

the influence of F7 is significant, and its characteristics are widely represented in the input data, leading to frequent misdiagnosis with other faults.

Regarding the fault impact, the average RMSE was 1.26%, which indicates a very high level of accuracy in estimation. It should be noted that for F3, the RMSE value is 0%, which is because the energy loss caused by F3 is consistently 0%. On the other hand, faults like F2 and F4 exhibit relatively high RMSE values of over 2%, suggesting slightly less accurate estimation for these faults.

Multiple fault diagnosis using VAE

A. Multiple Fault plots

The term "multiple faults" refers to a situation in which two or more faults occur simultaneously within a system. For example, consider a situation where faults F2 and F7 occur simultaneously. Each individual fault has a severity ranging from Level 1 to Level 10. Therefore, we consider ten levels of multiple faults, denoted as M1 to M10, by varying their severity levels as shown in Table 3.

To diagnose multiple faults, the latent space is dimensionally expanded to ensure that each axis corresponding to each fault is orthogonal to one another. When there are N types of fault candidates, an N-dimensional latent space is introduced such that each axis forms an orthogonal basis for the latent space. For example, if there are three types of fault candidates, F2, F4, and F7, the latent space would be a three-dimensional space (See Fig.10).

The multiple faults M1 to M10 were fed into a VAE model, and the coordinating plots in a 3-dimensional latent space is shown in Fig.10. In the 3-dimensional space, multiple faults are plotted in the intermediate region sandwiched between the two axes of F2 and F7. In the case of M1, since the fault of F2 is predominantly present, it is plotted near the axis of F2. In contrast, for M10, since the fault of F7 is predominantly present, it is plotted near the axis of F7. For other fault impacts, points gradually transition through the intermediate space between the two axes.

This is probably because the latent variables of the VAE are governed by probability distributions. Multiple faults consisting of two types of faults can exert combined effects on the system, incorporating characteristics from both types of faults. On the latent space, their probability distributions overlap, thereby being plotted in the intermediate region between the two axes.

B. Multiple faults diagnosis and validation

In the automated diagnosis of multiple faults, the goal is to automatically diagnose both two faults when fed into a pre-trained VAE model. A total of 28 combinations were created by selecting 2 out of 8 fault types. Additionally, like section 2, data augmentation was performed by applying Gaussian noise, resulting in a total of 28,000 validation datasets. We conducted diagnosis of them and calculated diagnosis accuracy.

Fig.11 is the box plot that presents percentages of cases where at least one of the two faults was diagnosed and where both faults were diagnosed for each of the 28 combinations. The percentage of being able to diagnose at least one of the two multiple faults was highly satisfactory, averaging at 99.4%. Next, regarding the ability to diagnose both faults, while it exceeded 90% for 7 of 28 cases, the overall average was 69.8%, which is not sufficiently high. Notably, the accuracy rates for combinations of F1 and F2, as well as F5 and F6, were notably low, with only 1.7% and 14.2% of cases being diagnosed for both faults, respectively.

C. Fault diagnosis Analysis

First, we will discuss the combination of F1 and F2. F1 (indicating an error in the primary chilled water flow rate) leads to a decrease in chilled water flow rate as it overestimates the flow rate in the primary chilled water pump. On the other hand, F2 (representing an error in the secondary chilled water flow rate) results in an increase in the flow rate of chilled water on the primary side by overestimating the flow rate on the secondary side, thereby causing excess heat load. Consequently, since these faults exert opposing effects on the system, it is presumed that their impacts counterbalanced each other.

Next, we will discuss the multiple faults involving F5

Table 3. Generating multiple faults of F2 and F7

Label	M1	M2	M3	M4	M5	M6	M7	M8	M9	M10
F2	Lv.10	Lv.9	Lv.8	Lv.7	Lv.6	Lv.5	Lv.4	Lv.3	Lv.2	Lv.1
F7	Lv.1	Lv.2	Lv.3	Lv.4	Lv.5	Lv.6	Lv.7	Lv.8	Lv.9	Lv.10

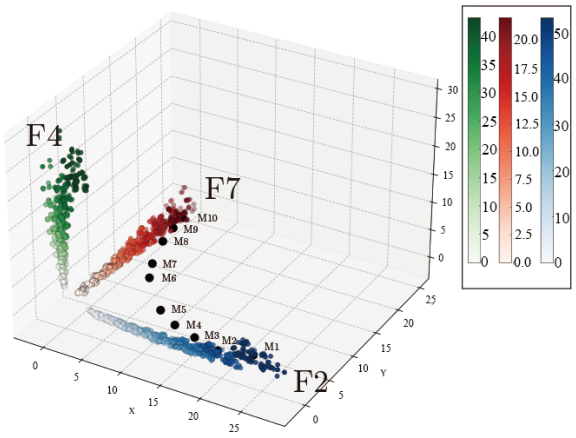

Figure10. Three dimensional latent space for F2,F4,F7

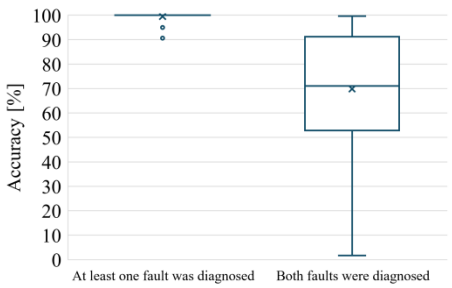

Figure11. Diagnosis results of multiple faults: at least one fault /both faults were diagnosed

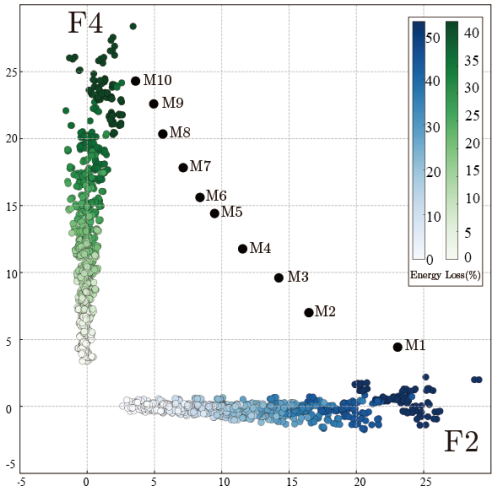

Figure12. The result of plotting multiple malfunctions of F2 and F4 on the latent space

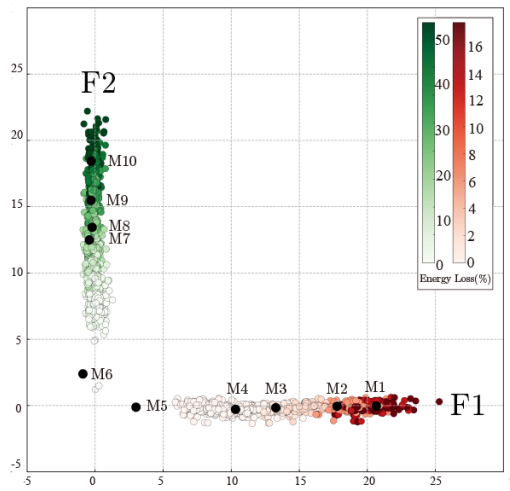

Figure13. The result of plotting multiple malfunctions of F1 and F2 on the latent space

(the error in the cooling water inlet temperature of the chiller) and F6 (the error in the cooling water outlet temperature of the cooling tower). When analyzing diagnostic results, it becomes evident that there is a notable incidence of misdiagnosing F8 (indicative of a decrease in cooling tower heat exchange efficiency). This high misdiagnosis rate can be attributed to both temperature sensors installed in the piping from the cooling tower outlet to the chiller inlet measuring temperatures higher than the true values. Consequently, the combination of F5 and F6 exhibits behavior similar to when the efficiency of the cooling tower decreases, leading to frequent misdiagnoses of F8.

Finally, both the results of F2 and F3, which exhibited relatively high diagnostic accuracy, and those of F1 and F2, which showed lower accuracy, were projected onto the two-dimensional latent space (See Fig.12 and Fig.13). The former were well plotted within the intermediate region of orthogonal axes, whereas the latter's plots were nearly aligned along the two axes. In the latter case, therefore, it is presumed that diagnosing both faults was difficult due to the consistent dominance of one axis over the other.

Conclusion

In this study, we aimed to extend the capability of fault diagnosis for HVAC systems by proposing new method using Variational Autoencoder (VAE) for diagnosing and estimating the impact of multiple faults. We trained the model to map latent variables onto the latent space, ensuring that the direction of these variables represents the type of fault, while the distance from the center signifies the severity of the fault. Consequently, we achieved high-performance diagnosis of multiple faults consisting of two types, based on the position of points in the latent space. Revising the diagnosis model so that it can diagnose several cases with low diagnostic accuracy observed in this study, as well as proposing optimal maintenance plans based on the diagnosis results, will be future tasks.

REFERENCES

1 QJUDE Qdr. Benefits of demand response in electricity markets and recommendations for achieving them. US Dept. Energy, Washington, DC, USA, Tech. Rep, Vol. 2006, p. 95, 2006.

2 Chen, C., Watanabe, T., Ryuu, Y., & Akashi, T. (1997). A study on energy consumption for air conditioning in various commercial facilities. Journal of Architecture, Planning and Environmental Engineering, Vol. 62, No. 501, pp. 61–68. (In Japanese)

3 Carlos E Garcia and Manfred Morari. Internal model control. a unifying review and some new results. Industrial & Engineering Chemistry Process Design and Development, Vol. 21, No. 2, pp. 308–323, 1982.

4 Manfred Morari and Jay H Lee. Model predictive control: past, present and future. Computers & chemical engineering, Vol. 23, No. 4-5, pp. 667–682, 1999.

5 Abdul Afram and Farrokh Janabi-Sharifi. Theory and applications of hvac control systems– a review of model predictive control (mpc). Building and Environment, Vol. 72, pp. 343–355, 2014.

6 Miyata, Shohei, et al. "Fault detection and diagnosis for heat source system using convolutional neural network with imaged faulty behavior data." *Science and Technology for the Built Environment* 26.1 (2020): 52-60.

7 Sung-Hwan Cho, Young-Ju Hong, Won-Tae Kim, and M. Zaheer-uddin. Multi-fault detection and diagnosis of hvac systems: an experimental study. International Journal of Energy Research, Vol. 29, No. 6, pp. 471–483, 2005.

8 Durk P Kingma, Shakir Mohamed, Danilo Jimenez Rezende, and Max Welling. Semi supervised learning with deep generative models. In Z. Ghahramani, M. Welling, C. Cortes, N. Lawrence, and K.Q. Weinberger, editors, Advances in Neural Information Processing Systems, Vol. 27. Curran Associates, Inc., 2014.

9 Miyata, Shohei, et al. "Improving the training efficiency of automated fault detection and diagnosis for central chilled water plants by transfer learning." *Building Simulation 2021*. Vol. 17. IBPSA, 2021.

10 Li, Yanfei, and Zheng O'Neill. "An innovative fault impact analysis framework for enhancing building operations." *Energy and Buildings* 199 (2019): 311-331.

11 Chengcheng Tian, Ziwen Xing, Xi Pan, and Yafen Tian. A method for cop prediction of an on-site screw chiller applied in cinema. International Journal of Refrigeration, Vol. 98, pp. 459–467, 2019.

12 Afram, Abdul, and Farrokh Janabi-Sharifi. "Theory and applications of HVAC control systems–A review of model predictive control (MPC)." *Building and Environment* 72 (2014): 343-355.

13 W.A. Gardner. Learning characteristics of stochastic-gradient-descent algorithms: A general study, analysis, and critique. Signal Processing, Vol. 6, No. 2, pp. 113–133, 1984

REHVA Federation of European Heating, Ventilation and Air Conditioning Associations

Impact of Future Climate Change on Achieving Building Performance Standards Targets

Ahmad Faiz Khan and Amanda Webb
Department of Civil and Architectural Engineering and Construction Management, University of Cincinnati, 2600 Clifton Ave., Cincinnati, OH 45221, USA

Abstract—Building performance standards (BPS) are an increasingly popular policy that can provide significant energy and carbon savings for a jurisdiction. Future climate change is anticipated to affect building energy use, but these effects on BPS are not yet known. Therefore, the goal of this study is to evaluate the impact of future climate change on achieving BPS targets. Energy benchmarking data for two property types—offices and multifamily buildings—in New York City were combined with weather data to make change point regression models for each building. The models were then used to estimate future energy consumption in 2050 for each building using future weather data. The results show that future climate change will make it easier to achieve the BPS target for 58% of office buildings and 86% of multifamily buildings.

Index Terms—benchmarking data, building performance standards, change point regression, climate change

I. Introduction

Building performance standards (BPS) are ambitious and increasingly popular policies that require existing buildings to reduce energy consumption (or greenhouse gas (GHG) emissions) to meet a maximum set target. In 2019, Washington, DC, became the first jurisdiction in the U.S. to legislate a BPS, followed by New York City and Washington State in the same year. As of June 2023, 12 U.S. jurisdictions have passed BPS for commercial and multifamily buildings [1]. At the Federal level, the White House has launched the National BPS Coalition [2], a group of over 30 state and local governments committed to advancing BPS to reduce building emissions, and also announced a BPS for Federal government-owned buildings [3]. To support these policies, ASHRAE published a BPS technical resource guide in 2023 [4].

Local, state, and federal governments are attracted to BPS because they can provide significant energy and GHG emissions savings. The BPS in Washington, DC, is estimated to reduce citywide energy usage by over 20% [5]. New York City projects that its BPS will reduce the city's overall carbon emissions 10% by 2030 [6]. Ref. [7] found cumulative GHG emissions savings for a prospective BPS in Seattle ranging from 12 to 34%. Ref. [8] examined potential BPS impacts in 10 U.S. cities and reported that there would be a 25-45% reduction in building energy use from meeting BPS targets.

However, this prior work does not account for the impacts of future climate change on achieving BPS targets. BPS targets are long-term initiatives, and jurisdictions typically set multiple, decreasing targets over a 20- or 30-year time horizon. At the same time, many prior studies have shown that building energy use will change over time due to future climate change. Most studies predict an increase in annual energy use for buildings located in warmer climates, and an annual decrease for buildings in colder climates [9–11], with the magnitude of change varying across the studies. For example, Ref. [9] analyzed an office building under future climate in different U.S. climate regions and predicted that annual energy use would decrease by 10% or more in cold climates and increase by more than 20% in tropical climates. Given the significant financial and technical resources that BPS will require within a jurisdiction, it is imperative to find out how future climate change will impact buildings' ability to meet their BPS targets.

A key challenge in analyzing BPS under climate change is estimating future energy performance for an entire jurisdiction of buildings. Most prior studies on buildings and future climate change (including [9–11] noted previously) used physics-based building simulation tools to model one or more prototypical buildings in a climate. Simulation tools pose a challenge for analyzing climate change impacts in large portfolios of buildings, as the numerous required input parameters (e.g., building envelope parameters, internal heat gains, occupancy and equipment schedules, HVAC system specifications) are often not known. In contrast, data-driven modeling requires only past utility data and weather data to build a statistical model for predicting building energy consumption, and a subset of prior studies have used this alternative approach. For example, Ref. [12] used change point regression models to predict future energy consumption of a supermarket in the United Kingdom. Ref. [13] used the eXplainable artificial intelligence (XAI) model to predict long-term cooling energy consumption under different climate change scenarios. Data-driven methods hold significant potential for analyzing urban building portfolios in the U.S., as most jurisdictions also have mandatory benchmarking ordinances requiring buildings to report their metered energy use on an annual basis. Yet, these data-driven modeling methods have seen little application to this benchmarking data to date.

The goal of this study is to evaluate the impact of future climate change on achieving BPS targets. In this study, data-driven models—specifically, change point regression models— were developed using publicly-available benchmarking data for office and multifamily buildings in New York City. The models were used to estimate the future energy consumption of each building under future climate change, and the impact on each building's ability to achieve its BPS targets was assessed. This study makes two novel contributions to the research literature. First, it advances our understanding of BPS by considering them under future climate change. Second, it represents a novel application of data-driven urban building energy modeling to local benchmarking data.

Email addresses: khan3af@mail.uc.edu (A. F. Khan), webb2al@ucmail.uc.edu (A. Webb)
Based on MS thesis accepted 9 May 2023

II. METHODS

The methodology used in this study consisted of four major steps. First, change point regression models were created using energy benchmarking data for office and multifamily buildings of New York City for the year 2019. The next step was to project energy consumption for the year 2050 by inputting future weather data under different warming percentiles of a climate change scenario RCP8.5 in change point regression models. Third, the future GHG emissions for the year 2050 were calculated based on predicted energy use. The last step was to compare the present and projected carbon emissions intensity in the year 2050 for buildings with the BPS target.

A. Benchmarking Data

In this study, two sources of benchmarking data were used for monthly energy consumption and floor area of buildings. For monthly energy consumption data, the Local Law 84 2020 data for the calendar year 2019 [14] (monthly benchmarking data, from here) was used. Monthly benchmarking data includes property ID, property name, parent property ID (if any), parent property name (if any), month, natural gas use (in kBtu), and electricity use (in kBtu). The monthly energy use data, specifically electricity and natural gas use data, was used for the calendar year 2019 to build change point regression models. The floor area of buildings was obtained from 2018 Energy and Water Data Disclosure for the calendar year 2017 [15] (annual benchmarking data, from here), which provides annual energy data, but not monthly energy data. To use the floor area of buildings from the 2017 annual benchmarking data in 2019, it was assumed minimal new construction, renovation, demolition, or vacancies occurred in 2019. New York City was used as a case study in this research because it is the only jurisdiction that provides open access to monthly energy consumption data for its buildings.

B. BPS Target

In its Local Law 97 of 2019 [16] (LL97), New York City uses the carbon emissions intensity in $tCO_2e/m^2/yr$ as a key metric. The standard covers all buildings that exceed 2,322.6 m^2. In December 2022, New York City updated the targets for different time periods based on different property types [17]. For the calendar years 2050 or later, it set a carbon emissions intensity of 0.00 $tCO_2e/m^2/yr$ for all ENERGY STAR Portfolio Manager property types to make them carbon neutral.

For this study, the indirect and direct GHG emissions factor were obtained from ENERGY STAR Portfolio Manager's Technical Reference for Greenhouse Gas Emissions [18]. Since future GHG emissions factors for electricity and natural gas are not available and these are required to calculate carbon emissions intensity for buildings in 2050, it was assumed that they would be the same as in 2019. For 2019, direct GHG emissions factor for the U.S. was 0.18122 kg/kWh, and indirect GHG emissions factor for New York City was 0.28466 kg/kWh.

C. Weather Data

Instead of using actual weather data for New York City for the year 2019, typical meteorological year (TMY3) data was used for New York's J.F.K International Airport. This is because the future weather data for the year 2050 was generated using this TMY3 weather file. Average monthly temperatures were computed from the hourly dry-bulb temperature values in the TMY3 file.

Future weather data for the year 2050 was obtained through the WeatherShift [19] tool. It has been used in several previous studies [20] to analyze the impact of future climate change on building energy usage. It uses the "morphing" method developed by Belcher et al. [21] to downscale the outputs of 14 Global Circulation Models (GCMs) available under the fifth assessment report (AR5) [22] of the Intergovernmental Panel on Climate Change (IPCC).

WeatherShift provides projected future weather data using a TMY3 file for a location for three future time periods relative to the baseline period 1976-2005, and it uses two emission scenarios referred to as representative concentration pathways (RCPs) from the IPCC's AR5: RCP4.5 (moderately aggressive mitigation) and RCP8.5 (business as usual). It also gives an option to select the warming percentile for each scenario. For this study, future weather data for the year 2050 was obtained from the WeatherShift tool based on the RCP8.5 scenario under all warming percentiles. All warming percentiles were analyzed, and the 50^{th} percentile results are presented here, with results for other percentiles indicated in the text as ranges. RCP8.5 was selected instead of RCP4.5 because recent data suggest that the changing climate is more closely aligned with this scenario, according to the WeatherShift team. The average monthly temperatures for 2050 were then calculated from the hourly dry-bulb temperatures in the 2050 weather file. The difference between the average monthly temperatures in 2019 and 2050 is shown in Fig. 1.

D. Data Cleaning

The monthly and annual benchmarking data were cleaned and filtered prior to analysis. First, duplicate observations were removed based on property IDs. Second, primary property types other than office and multifamily residential (multifamily, from here) were filtered out. These two property types were selected because they comprise a large proportion of buildings in New York City, and multifamily buildings are of special interest in a BPS due to potential equity concerns [23]. Third, buildings with floor area less than 2,322.6 m^2 were removed, as LL97 covers only buildings that are greater than this threshold. Finally, buildings with incomplete utility data, i.e., less than all 12 months of both electricity and natural gas for 2019, were removed. After all the data cleaning, 9,760 multifamily and 433 office buildings were left for analysis out of a total of 27,968 buildings in monthly benchmarking data.

E. Change Point Regression Models

Change point regression (also known as segmented or piecewise regression) models the relationship between a dependent variable (e.g., electricity or natural gas consumption) and one or more independent variables (e.g., temperature) while allowing for distinct response functions over different ranges of

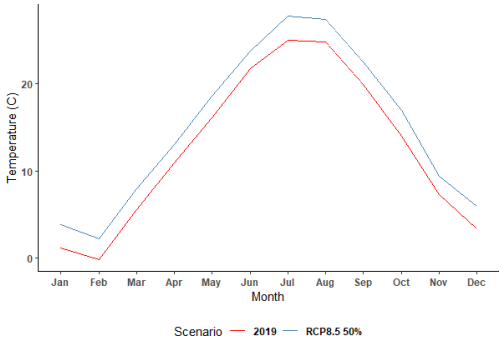

Figure 1. Variation of average monthly temperature for the years 2019 and 2050 under warming percentile RCP8.5 50%.

the independent variable(s). The boundaries between the segments where the model response changes are called "change points." This method is well-suited to modeling building energy use, which is often characterized by a weather-independent base load and a weather-dependent variable load (e.g., heating or cooling). This concept is illustrated in Fig. 2, which shows a three-parameter cooling (3P-C) and a four-parameter cooling (4P) model with a change point, base load, and weather-dependent slope representing cooling. The application of change point models for estimating building energy use is detailed in ASHRAE Guideline 14 [24].

For each building that was left in the dataset after data cleaning, change point regression models were developed using the average monthly temperature (in C) as the independent variable and their monthly electricity and natural gas consumption (in kWh) separately for the year 2019 as the dependent variable. The models were built using the "nmecr" R package [26] using 12 data points for each model. Both three-parameter (3-P) and four-parameter (4-P) models were tried for each building to determine which model best fits the data. However, for several buildings, the 3-P heating model could not be built. Therefore, 4-P models were built for all 433 office buildings, and 9,759 out of 9,760 multifamily buildings in the dataset.

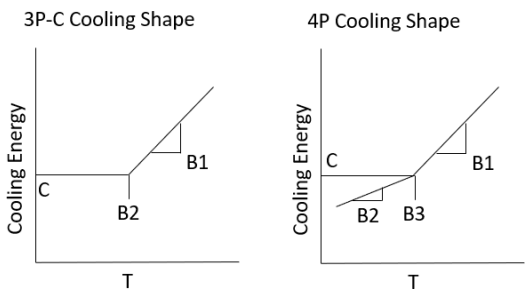

Figure 2. Three- and four-parameter change point regression models for cooling (Image Source: [25])

Two metrics were then used to evaluate the performance of each model: adjusted R^2 and the coefficient of variation of the root mean square error (CV(RMSE)). ASHRAE Guideline 14 sets a recommended maximum CV(RMSE) of 25%, and it was assumed a threshold of more than 0.7 for adjusted R^2. Only models meeting these two performance thresholds were used for further study. After applying these filters on the 4-P models for both types of buildings, 157 office buildings and 7,019 multifamily buildings were left for further analysis.

Future energy consumption was predicted from 4-P models that left after applying performance filters on all buildings using the projected average monthly temperature for the year 2050. After projecting energy consumption using 4-P models for the year 2050, it was found that for some office buildings, there was either an increase or a decrease in both electricity and natural gas usage to occur in 2050 compared to that of 2019. These buildings — 15 in number for all warming percentiles, but 14 for 75th percentile — were dropped out from further analysis because both electricity and natural gas cannot increase or decrease together with an increase in temperature. Similarly, for some of the multifamily buildings, there was either an increase or a decrease in use of both fuels, and for a few other buildings, electricity was decreasing, while natural gas was either increasing or not changing in 2050 compared to 2019. In total, these buildings — 154-180, depending on the warming percentile — were dropped out from further analysis. Finally, 142-143 out of 433 office buildings and 6,839-6,865 out of 9,760 multifamily buildings were left depending on different warming percentiles and analyzed for 2050.

F. Feasibility of Achieving BPS Target

The GHG emissions for the year 2050 were calculated from the projected electricity and natural gas consumption using the same GHG emissions factor as in 2019. The impact of future climate change on the feasibility of achieving BPS target for New York City was measured by comparing the present and projected future carbon emissions intensity in 2050 with the BPS target 0.00 $tCO_2e/m^2/yr$.

III. RESULTS

Each of the percentile values of carbon emissions intensity (tCO2e/m2/yr) are greater for office buildings compared to multifamily buildings in 2019, hence, they need to reduce their carbon emissions intensity more compared to latter to achieve the BPS target for the year 2050 (Fig. 3). The middle value in both boxes of Fig. 3 represent the median, and the lower and upper bounds of the box represent the 25th and 75th percentile values respectively. The lower and upper whiskers of each box represent the 10th and 90th percentile values (the lower and upper whiskers of all boxplots in this paper represent 10th and 90th percentile values). The red line on the boxplot shows the BPS target for all office and multifamily buildings for New York City for the year 2050. The higher carbon emissions intensity for office buildings compared to multifamily buildings is partially due to the reason that for around 75% office buildings, more than 50% energy usage comes from electricity, while for about 75% multifamily buildings, more than half energy usage

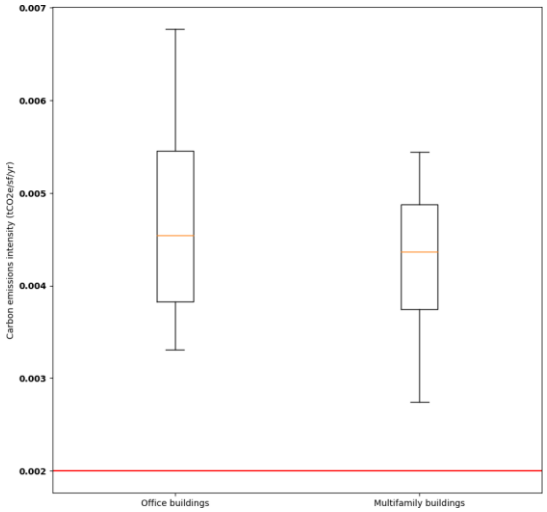

Figure 3. Variation of carbon emissions intensity for office and multifamily buildings in 2019.

comes from natural gas; and electricity consumption has a higher GHG emissions intensity than natural gas consumption.

The projection of future energy use in 2050 using the change point models shows that under all warming percentiles electricity consumption will increase, while natural gas consumption will decrease in 2050 compared to that in 2019. This is illustrated in Fig. 4 only for 50th percentile. Fig. 4 plots the percentage change in electricity (blue), natural gas (orange), and total energy (violet) in 2050 compared to 2019 for each building in the dataset. Each building is represented as a bar on the x-axis. Positive values represent an increase from 2019 and negative values represent a decrease.

From Fig. 4, it can be estimated that electricity use would increase due to the increased need for cooling, while natural gas use would decrease due to the decreased need for heating. Even though electricity use would increase, and natural gas use would decrease for both property types, out of 143 office buildings, the overall energy consumption would decrease in 2050 for 68-70% of buildings depending on future warming percentile. This is because the increase in cooling use — which leads to an increase in electricity use — in summer months would be outweighed by the decrease in heating use — which leads to a decrease in natural gas use — in winter months. There are 26-29% of office buildings for which overall energy would increase depending on future warming percentile. For these buildings, the increase in cooling use would overcome the decrease in heating use. Lastly, there are 3-5% office buildings, depending on future warming percentile, for which there would not be any change in overall energy. For these types of buildings, the increase in cooling use would be counterbalanced by the decrease in heating use. Similarly, out of 6,839-6,865 multifamily buildings, depending on future warming percentile, overall energy would decrease for 88-89% of buildings; it would increase for 10-11%;

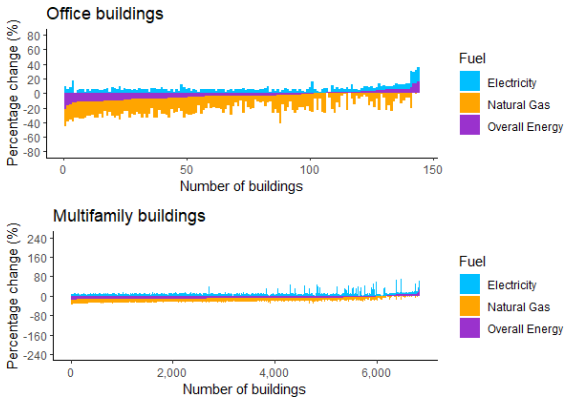

Figure 4. Variation of percentage change in electricity, natural gas, and overall energy from present condition under scenario RCP 8.5 50% for individual office and multifamily buildings.

and it would not change for 0.5-1% of buildings. The reason for increase, decrease, or no change in overall energy is the same as it is for office buildings.

For both property types, it can also be noted that there are a few high spikes in percentage change in both electricity and natural gas consumption for some of the buildings. Regarding high increase in electricity use, it was either almost constant or showed no significant difference between each month in 2019; however, for temperature greater than 21.11°C (Jun, Jul, and Aug), electricity use was increased drastically. Therefore, these buildings have greater electricity use even for only a few months in 2050. Similarly, regarding a high decrease in natural gas usage in 2050, for some of the buildings in 2019, natural gas consumption was almost zero or a constant to a number greater than zero for almost the whole year and abnormally high only in winter season; for some of the other buildings, it was almost constant for almost the whole year and declined in the summer season; and, for a few other buildings, it was drastically reduced with an increase in temperature in 2019.

For both property types, indirect carbon emissions intensity would increase, direct carbon emissions intensity would decrease, and total carbon emissions intensity would decrease for most buildings in 2050 compared to 2019 (Fig. 5). Fig. 5 shows a boxplot of the percentage change in indirect, direct, and total carbon emissions intensity for each building from 2019 to 2050. Positive values represent an increase from 2019 and negative values represent a decrease. Examining these results with respect to Fig. 4 suggests that indirect carbon emissions intensity would increase due to an increase in electricity usage, while direct carbon emissions intensity would decrease due to a decrease in natural gas use. From Fig. 5, it is evident that indirect carbon emissions intensity would increase less compared to the decrease in direct carbon emissions intensity; consequently, the total carbon emissions intensity would decrease for most of the buildings.

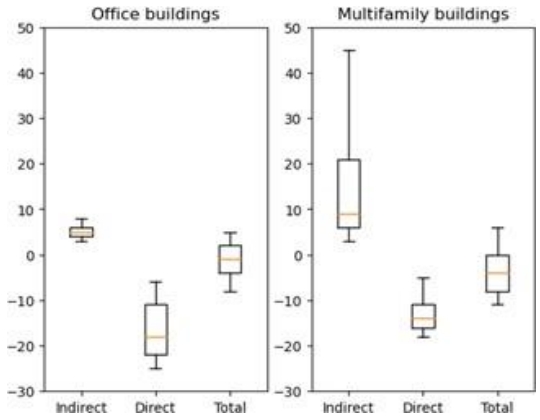

Figure 5. Variation of percentage change in indirect, direct, and total carbon emissions intensity from present condition under scenario RCP 8.5 50% for office and multifamily buildings.

For most buildings, future climate change would make it easier to achieve the BPS target than it was in 2019. Table 1 shows the percentage of buildings for which it would be easier to meet the target (percentage decrease in total carbon emissions intensity), and harder to meet the target (percentage increase in total carbon emissions intensity). For 51-58% of office buildings, it is anticipated that it would be easier to meet the target, and for 31-37% of office buildings, climate change is projected to make it more difficult to achieve the BPS target, depending on warming percentile. For 8-14% of office buildings, climate change may not have any impact on achieving the BPS target (Table 1). Similarly, for 84-86% of multifamily buildings, climate change is projected to make it easier to achieve the BPS target compared to the present condition, for 13-15% of multifamily buildings, climate change is anticipated to make it more difficult to achieve the BPS target, and for only 1-2% of multifamily buildings, climate change may not have any impact on achieving the BPS target (Table 1).

IV. CONCLUSION AND POLICY IMPLICATIONS

A. Conclusion

This study used benchmarking data for two property types — offices and multifamily residential buildings — in New York City to assess the impact of future climate change on achieving BPS target set for 2050 according to Local Law 97 [16]. The results show that climate change would facilitate achieving the BPS target for 51-58% of office and 84-86% of multifamily buildings, depending on different future warming percentile.

For both property types, electricity use would increase, while natural gas use would decrease in 2050 compared to 2019 assuming the current heating and cooling fuel sources do not change in the future. Given the increased need for cooling energy and decreased need for heating energy in future climate change, this result is unsurprising. Several prior studies have claimed the same result [9–13]. For New York City, it would require increasing the cooling system fuel use and decreasing the heating system fuel use in 2050. Further, for both property types, the rate of increase in electricity and decrease in gas is increasing as the temperature gets warmer for each warming percentile. Ref. [10–11] also found the same for different climate change scenarios.

TABLE I.
PERCENTAGE OF BUILDINGS WITH VARIATION IN TOTAL CARBON EMISSIONS INTENSITY IN 2050 COMPARED TO 2019 UNDER SCENARIO RCP 8.5 50% FOR OFFICE AND MULTIFAMILY BUILDINGS

Property Type	**Emissions increase**	**Emissions decrease**	**Emissions unchanged**
Office	32%	58%	10%
Multifamily	13%	86%	1%

In addition to the change in individual fuel use in 2050 compared to 2019, the overall energy usage would change as well, claimed by several existing studies [9–11]. In this study, for 68-70% of office and 88-89% of multifamily buildings, overall energy usage would decrease; and for 26-29% of office and 10-11% of multifamily buildings, it would increase. Ref. [11] also claimed since the US is a country that requires more heating than cooling, climate change would be a net energy saver for it.

The total carbon emissions intensity for 51-58% of office and 84-86% of multifamily buildings is anticipated to decrease, while it is increasing in the future for 31-37% of office and 13-15% of multifamily buildings. This means that climate change would expedite achieving the BPS target for New York City for more than 75% multifamily and a few more than half office buildings.

This study has several limitations. First, the results of this study could be different for a warm-climate zone. Considering future climate change in a warm-climate zone, there could be more increment in electricity use due to cooling but not any significant decrease in natural gas use due to heating compared to in a cold- or mixed-climate zone. As a result, there could be an increase in indirect carbon emissions intensity, consequently, the total carbon emissions intensity could increase. Therefore, climate change could make it difficult to achieve a BPS target in a warm-climate zone.

Second, this study does not consider the effects of meeting the interim targets that are set for New York City for the time periods before the year 2050 and the renovations that would be done in buildings to achieve them. However, applying the renovations would require energy audit data for buildings which could not be easy to get compared to getting only monthly benchmarking data for a jurisdiction.

Third, this study assumed that the floor area of buildings would be the same in the future. However, it is possible that many buildings will undergo renovation or an addition in the near future. Considering a change in floor area of buildings, the carbon emissions intensity would change and could lead to different results.

Fourth, this method does not consider any other weather parameters in making change point regression models (e.g.,

solar radiation, wind, etc.). Fifth, it was assumed that buildings will not be electrified, and that space heating will continue to be done by natural gas. Finally, it was assumed that the electric grid would not change in the near future. Therefore, it was assumed that GHG emissions factors would not change both for electricity and natural gas. However, the electric grid could get improved and produce less carbon emissions from electricity compared to what it is producing now. Consequently, the indirect carbon emissions, and as a result, the total carbon emissions would get reduced.

B. Policy Implications

The findings in this study have two broader implications for developing a new BPS for a jurisdiction. First, policymakers may want to set less stringent BPS targets for office buildings than multifamily buildings considering climate change in a jurisdiction located in cold- or mixed-climate if the key metric is carbon emissions intensity. This is because climate change could make it harder to achieve a BPS target for a lot of office buildings, and achieving a lower target could be easier for them. The second implication is that in establishing and/or updating a BPS target for a jurisdiction in the near future, policymakers may not want to use GHG emissions intensity as a key metric. This is because it could be difficult to project the GHG emissions factors that would be generated from either electricity or natural gas, and hence, it would be difficult to know the achievability of the targets considering climate change. On the other hand, using site EUI as a key metric for a BPS target could be considered.

While the results of this study indicate that climate change would make it easier for most multifamily and a few more than half office buildings to achieve the BPS target for New York City, future work could consider three aspects: (i) whether there is an inflection point for temperature below which climate change would expedite and above which climate change would not assist to achieve the BPS target; this could be done by considering future weather data for different time periods and interim BPS targets for a jurisdiction, (ii) the extent to which these findings differ in other climate zones, and (iii) whether the same results can be achieved considering the advanced climate models such as Shared Socioeconomic Pathways (SSPs) of IPCC's AR6 [27] . Generalization of the results of this study for all different climate zones considering advanced climate change scenarios could provide a clearer picture to policymakers for establishing and/or updating the BPS targets in many jurisdictions.

REFERENCES

1 https://www.imt.org/wp-content/uploads/2022/06/IMT-BPS-Map-CURRENT-06292023-CHECK-COMMS-BEFORE-USE.png (accessed July 16, 2023).

2 https://www.whitehouse.gov/climate/ (accessed May 01, 2023).

3 https://www.whitehouse.gov/briefing-room/statements-releases/2022/12/07/fact-sheet-biden-harris-administration-announces-first-ever-federal-building-performance-standard-catalyzes-american-innovation-to-lower-energy-costs-save-taxpayer-dollars-and-cut-emi (accessed May 01, 2023).

4 ASHRAE *Building Performance Standards: A Technical Resource Guide*. 2023

5 https://www.governor.wa.gov/sites/default/files/documents/clean-buildings-policy-brief-bill-signing.pdf (accessed May 01, 2023).

6 https://www.nyc.gov/assets/nycaccelerator/downloads/pdf/ClimateMobilizationAct_Brief.pdf (accessed May 01, 2023). National Renewable Energy Laboratory (NREL), «Energy Plus,» 30 September 2020. [Online]. Available: https://energyplus.net/. [Last access: 5 November 2020].

7 T. Walter and P. Mathew, "GHG policy impacts for Seattle's buildings: targets, timing, and scope," *Buildings and Cities*, 2(1), pp. 283-301, doi: https://doi. org/10.5334/bc.81.

8 A. L. Webb and C. McConnell, "Evaluating the feasibility of achieving building performance standards targets," *Energy Build.*, vol. 288, p. 112989, 2023, doi: 10.1016/j.enbuild.2023.112989.

9 D. B. Crawley, "Estimating the impacts of climate change and urbanization on building performance," vol. 1493, 2008, doi: 10.1080/19401490802182079.

10 P. Shen, "Impacts of climate change on U.S. building energy use by using downscaled hourly future weather data," *Energy Build.*, vol. 134, pp. 61–70, 2017, doi: 10.1016/j.enbuild.2016.09.028.

11 B. Bass and J. New, "How will United States commercial building energy use be impacted by IPCC climate scenarios ? ," *Energy*, vol. 263, no. PE, p. 125945, 2023, doi: 10.1016/j.energy.2022.125945.

12 M. R. Braun, H. Altan, and S. B. M. Beck, "Using regression analysis to predict the future energy consumption of a supermarket in the UK," *Appl. Energy*, vol. 130, pp. 305–313, 2014, doi: 10.1016/j.apenergy.2014.05.062.

[13] D. Chakraborty, A. Alam, S. Chaudhuri, and H. Başağaoğlu, "Scenario-based prediction of climate change impacts on building cooling energy consumption with explainable artificial intelligence," *Appl. Energy*, vol. 291, no. February, p. 116807, 2021, doi: 10.1016/j.apenergy.2021.116807.

14 https://data.cityofnewyork.us/Environment/Local-Law-84-2020-Monthly-Data-for-Calendar-Year-2/evu4-6zyr (accessed May 01, 2023).

15 https://www1.nyc.gov/html/gbee/html/plan/ll84_scores.shtml (accessed May 01, 2023).

16 https://www1.nyc.gov/assets/buildings/local_laws/ll97of2019.pdf (accessed May 01, 2023).

17 https://www.nyc.gov/assets/buildings/rules/1_RCNY_103-14.pdf (accessed May 01, 2023).

18 https://portfoliomanager.energystar.gov/pdf/reference/Emissions.pdf (accessed May 01, 2023).

19 R. Dickinson and B. Brannon, "Generating future weather files for resilience," *36 th Int. Conf. Passiv. Low Energy Archit. Cities, Build. People Towar. Regen. Environ.*, no. July 2016.

20 L. Troup and D. Fannon, "Morphing climate data to simulate building energy consumption," *ASHRAE IBPSA-USA Build. Simul. Conf.*, pp. 439–446, 2016.

21 S. E. Belcher, J. N. Hacker, and D. S. Powell, "Constructing design weather data for future climates," *Build. Serv. Eng. Res. Technol.*, vol. 26, no. 1, pp. 49–61, 2005, doi: 10.1191/0143624405bt112oa.

22 https://www.ipcc.ch/report/ar5/syr/ (accessed May 01, 2023).

23 Z. Hart, R. Gahagan, C. Majersik, J. Miller, and B. Neely, "Understanding the Housing Affordability Risk Posed by Building Performance Policies."

24 ASHRAE Guideline 14-2014.

25 M. T. Paulus, D. E. Claridge, and C. Culp, "Algorithm for automating the selection of a temperature dependent change point model," *Energy Build.*, vol. 87, pp. 95–104, 2015, doi: 10.1016/j.enbuild.2014.11.033.

26 https://kw-engineering.com/nmecr-nmec-r-package-tool-energy-efficiency-project-savings-measurement-verification-analysis-amv/ (accessed May 02, 2023).

27 https://www.ipcc.ch/ar6-syr/ (accessed May 01, 2023).

REHVA
Student Competition
Other Participants' Contribution

Tamanna Verma	**UK**
Florian Stucki	**Switzerland**
Mike Schoch	**Switzerland**
Said Bolluk	Türkiye
Johannes Simola	**Finland**
Richárd Kiss	**Hungary**
Serhan Yüksel	**The Netherlands**
Martín Bizkarra Belategi	**Spain**
Danijela Srećković	**Serbia**
Andrei Magureanu	**Romania**
Angelika Václavová	**Slovakia**

Evaluating the impact of luminance contrast on task performance whilst working on fixed and portable digital screens in a computer library

Student: Tamanna Verma, Email: tamanna.verma.22@ucl.ac.uk
Supervisors: Dr. Constantin-Cosmin Ticleanu, Email: c.ticleanu@ucl.ac.uk, Dr. Villian Lo., Email: villian.lo@ucl.ac.uk
Institute: UCL Institute for Environmental Design and Engineering (IEDE), The Bartlett, UCL Faculty of the Built Environment, Central House, 14 Upper Woburn Place, London WC1H 0NN
Approved date by the institute: 8th November 2023

Abstract—This study aims to evaluate the impacts of lighting on task performance while working on both a computer and a tablet in a digital library. Participants were assigned tasks to perform on both the computer and tablet at three different positions. The study evaluated the participants' performance based on time and accuracy. The findings indicated that luminance contrast for the screen area had a significant impact on the time taken to complete tasks, while scores did not show significant variation across devices and positions.

Index Terms— Computer and tablet screens, luminance contrast, performance.

I. Introduction

In recent years, there has been a significant shift in educational environments, with students transitioning from traditional paper mediums to digital devices like tablets and iPads. Boyce [1] discusses the transition from paper to electronic displays at workplaces and the need for luminaires that consider the physical properties of digital screens. This trend presents new challenges in lighting design, particularly in shared spaces like libraries where lighting is designed for paper-based reading, raising concerns about its impact on the visual performance of tablet users. Many students commonly use two screens simultaneously: a fixed desktop and a portable device like a tablet or iPad, replacing paper. This dual-screen setup may influence productivity and task performance [2] if lighting is not designed considering the reflective properties and orientations of both types of screens.

A. Luminance

Luminance plays a significant role in designing work environments and directly impacts performance when using digital screens [3]. Wallach's [4] research revealed that people do not perceive absolute luminance. Instead, our perception of brightness is based on the relative luminance of two adjacent areas in our field of view. This is a critical factor in determining the adaptation state of our eyes and task visibility [3].

B. Luminance contrast

Luminance contrast plays a crucial role in object visibility, indicating the difference in luminance between an object and its surrounding background. [5], [6]. Higher luminance contrast enhances visibility, but lighting conditions can affect contrast by causing disability glare or introducing veiling reflections [3]. Practical adjustments, like altering lighting positions and leveraging colour contrast, enhance visibility, especially in low luminance contrast situations [6], [7], [8], [9]. The calculation of luminance contrast remains the same regardless of the

- source of luminance, whether it's from a reflective surface, a self-luminous source like a visual display terminal (VDT screen), or a combination of both [10]. The degree of contrast between a visual target and its background significantly influences performance on visual tasks [6].

- *C. Lighting of Workstations with Display Screen Equipment*

- The luminance level of computer screens can vary significantly, ranging from 2-3 cd/m^2 for dark background screens to around 300 cd/m^2 for white background screens [11]. However, the reflection on a computer display can have three negative effects: it can decrease on-screen contrast, create a conflict for the user's attention between the actual display and its reflections, and prompt changes in focus due to the varying distances between the display and the reflected images [12]. Viewing distance and screen angle have a significant impact on visual performance and fatigue when using VDT screen [13].

- *D. The Emergence of Tablets*

Technological advancements in electronic communication tools are driving a shift from paper books to electronic devices, such as eBooks and tablets [14]. Screen glare due to flexibility in screen orientations and increased neck strain due to downward gaze are potential issues [15]. Na et al. [16] research has investigated the effects of adaptive display luminance [16], luminance contrast [17], and luminance disparity [18] on visual comfort during smartphone reading. It has been found that adjusting the luminance of the tablet display to a level higher than that of the surrounding ambient light can improve performance [14], [19]. Increased ambient lighting can cause screen images to appear faded, while decreased lighting can increase contrasts within a task area [19], which is desirable for improving performance.

E. Bridging the Gap: The Current Study

In many real-world tasks, performance is determined by both accuracy and speed in completing the required work [5]. By evaluating task performance based on scores and time while using digital screens, this research contributes to our understanding of how luminance contrast affects performance. Therefore, the core research question is:

"How does luminance contrast impact task performance on computers (fixed screen) and tablets (portable screen) in a library environment?"

II. Methodology

In this study, we designed an experiment with two tasks to evaluate how lighting affects task performance. A

luminance camera was used to measure luminance to assess the impact on efficiency based on scores and time across all devices.

A. Experiment setup

This research was designed to evaluate the performance on two types of digital screens—a computer screen and a tablet (like an iPad)—within an environment controlled by artificial lighting.

Figure 1. Device positions for computers and tablets

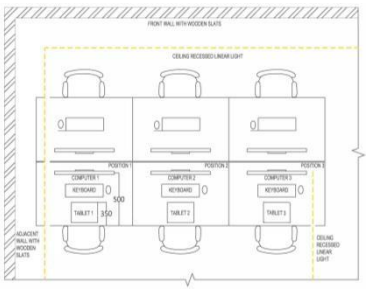

Figure 2. Plan showing the seating positions used for the experiment in the Student Centre

Location and Workstation: The workstation had three computer setups. The locations of these positions, labelled Position 1, 2, and 3, are shown in Fig. 1 and Fig. 2. Position 1 was adjacent to the wall which will also have light reflected from it on to the table and screens. A single wheeled, padded chair with adjustable seat height and fixed arm location was used.

Screens' Characteristics: The computer screen had matte finish with 23.8-inch diagonal IPS widescreen with WLED backlighting and an anti-glare LCD. The 11-inch iPad Pro display had LED-backlit Liquid Retina with 2388x1668 resolution. The screen had a glossy finish.

Lighting and screen brightness levels: The experiment utilized existing lighting conditions, including ceiling recessed linear lights with diffusers. Positions 1 and 3 had lights directly above them, whereas position 2 did not. Desk lamps were off for the duration of the experiment. The brightness levels for both the computers and the tablet were set to 100% brightness throughout the study.

Computer and Tablet Placement: Computers were vertically aligned to the table, situated 500mm from the edge. Tablets were set horizontally 300mm from the edge at all three computer locations, marked on the desk to ensure consistency. For brevity, computer and tablet positioned at Position 1 were referred to as computer 1 and tablet 1, and similar naming was used for other position 2 and 3.

Computer Alignment and Eye Level: Computers were positioned 120mm above the floor adhering to standards, which often recommend eye level to be at or slightly below the top of the viewing screen [10].

The chair's height was adjusted to maintain a consistent viewing angle, following ergonomic guidelines. Participants were also instructed to maintain an arm's length distance from the screens.

B. Tasks

The two digital tasks designed for this study were created using HTML, CSS, and JavaScript; and hosted on GitHub pages for accessibility across devices. To make the tasks more challenging, a contrast was created using a dark grey background with lighter grey numbers. The colour contrast variations used in these tasks were informed by Rea [6], who used a similar technique for paper-based tasks. The number of correct, incorrect, and missed responses were recorded for both tasks. The task also recorded the time taken for completion. Both tasks in this study measured accuracy and time taken.

C. Questionnaire/Survey

An online survey was designed to collect information about demographics, lighting preferences, mood assessment, task performance, and lighting satisfaction.

D. Participants

27 participants were recruited comprised of undergraduate and postgraduate students within the age range of 18 to 44 years.

E. Procedure

The participants were randomly assigned to one of three positions to minimize the transfer of skills (practice effect) across multiple devices. This randomization ensured an equal distribution of individual differences, enabling variations in the outcomes to be attributed to the experimental manipulation rather than underlying participant differences [20]. Firstly, participants were asked to complete a pre-task questionnaire. Then they performed tasks 1 and 2 on the computer and then repeated the same tasks on the tablet at the same position. After completing both tasks, they were randomly asked to perform the same two tasks at the remaining two positions. After completing the tasks across all positions, participants filled out the remaining sections of the questionnaire.

F. Luminance calculation

Luminance values were obtained using high dynamic range (HDR) photography, which captures wide luminance variations across multiple exposures [21]. Images were taken for each computer and tablet screen in all three predetermined positions, providing a view representative of what participants would experience. In total, six sets of images were captured, two for each position. Processed images (see Fig. 3 and Fig. 4) provided luminance values for each pixel within the image. Maximum and minimum luminance values were computed for the screens and tasks areas across all computers and tablets in three different positions (see Table I). The corresponding luminance contrast values for both the screen and task areas were derived by dividing the maximum by the minimum luminance, and these results are also presented in the same table (see Fig. 3 and Fig. 4 for reference to screen and task areas).

'Screen contrast' refers to the luminance contrast within the screen area, accounting for the luminance of reflected lighting. 'Task contrast' refers to the luminance contrast between the elements related to the task (such as text, images) and their background within the screen area.

TABLE I:
SCREEN AND TASK LUMINANCE VALUES ON COMPUTER AND TABLET SCREENS AT THREE POSITIONS

		Computer			Tablet		
		1	2	3	1	2	3
Screen Luminance cd/m²	Min	4.4	2.8	3.5	1.9	1.7	2.1
	Max	235.5	241.6	248.8	162.6	115.1	276.3
	Contrast (max/min)	53.6	86.4	70.2	86.7	67.7	132.8
Task Luminance cd/m²	Min	45.1	49.5	50.9	47.2	49.5	55.6
	Max	76.8	81.8	83.7	75.1	102.9	105.0
	Contrast (max/min)	1.7	1.7	1.6	1.6	2.1	1.9

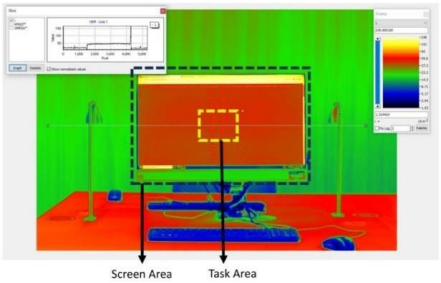

Figure 3: Luminance in the field of view of the computer

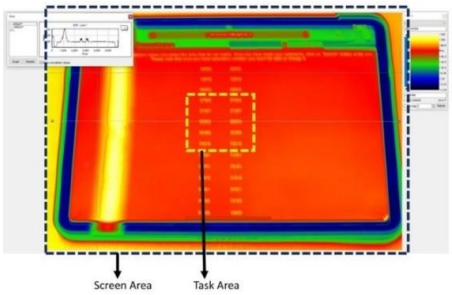

Figure 4: Luminance in the field of view of the tablet

III. DATA PRESENTATION

In the experiment, two key metrics were measured for each task—namely, the score and the time taken (in seconds). An overall score was calculated as an index of task performance incorporating both measures.

A. Pre-Task Mood Assessment

Overall, the data shows that participants were generally interested, excited, alert, attentive and active before starting the tasks. They felt low levels of distress and irritability on average.

B. Analysing accuracy and time between digital screens and seating positions

The normality of the distribution of task scores and times on different devices was assessed using the Kolmogorov-Smirnov and Shapiro-Wilk tests. Results indicated non-normal distribution for Task 1 and Task 2 scores across all computers and tablets (all p-values < 0.05). However, task times displayed mixed results, with most data having p-values > 0.05, except for specific instances (Computer 2 Task 2 time, p = 0.031; Computer 3 Task 1 time, p = 0.038; Tablet 3 Task 2 time, p = 0.001). Due to the non-normality of variables, Friedman test analyses were conducted (See Table II).

Friedman test for task 1 scores: In the evaluation of Task 1 scores for computers and tablets across different positions, no statistically significant differences were found, indicating that varied luminance levels did not substantially impact performance accuracy. However, minor variations in mean ranks were observed, with Computer 2 and Tablet 2 showing slightly higher scores.

Friedman test for task 2 scores: Similarly, in the evaluation of Task 2 scores, no statistically significant differences were found across devices. Consistency was observed in scores across computers, while slight variations among tablets might be attributed to participants' preference for physical keyboards during the typing for task 2.

Friedman test for task 1 time: Regarding completion time for Task 1, statistically significant differences were found across devices (see Table II), indicating the impact of device type and lighting conditions on performance efficiency. Tablets exhibited faster completion times compared to computers. Computer 3 had the longest duration (mean rank: 4.70), while Tablet 1 had the shortest (mean rank: 2.30). Post-hoc test was done to evaluate specific pairwise differences across all devices. The Wilcoxon Signed Ranks test suggested significantly shorter Task 1 times on tablets compared to computers (all $p < 0.05$).

Friedman test for task 2 time: For Task 2 completion time, statistically significant differences were found across devices, with computers associated with faster times compared to tablets. Tablet 3 had the longest completion time, possibly due to its horizontal orientation increasing glare susceptibility from the light above it. Wilcoxon test was done to determine the specific pairwise differences.

TABLE II:
FRIEDMAN TEST FOR TASK SCORES AND TIME ACROSS ALL 6 DEVICES (N=27)

	Score		Time	
	Task 1	Task 2	Task 1	Task 2
Chi-Square	9.398	9.622	34.767	49.497
df	5	5	5	5
Asymp. Sig.	.094	.087	<.001**	<.001**

C. Assessing relationship between luminance contrast and task performance

Average scores vs Screen luminance contrast: Fig. 5, reveals a weak negative correlation ($R^2 = 0.4511$) between screen contrast and average task scores, with higher contrasts associated with lower scores. But there's substantial scatter, indicating other factors impacting scores apart from contrast.

Average scores vs Task luminance contrast: Fig. 6 shows no meaningful relationship between task contrast and performance scores, as the variables seem entirely unrelated based on the negligible R^2 value and random scatter of data points.

Average time vs Screen luminance contrast: Fig. 7 shows a positive trend between screen contrast and average task time, indicating that higher contrasts led to longer average times. Despite some scatter in the data, the R^2 value of

0.4295 revealed a moderate positive correlation, suggesting that screen contrast accounted for 42.95% of the variance in average times. In summary, higher screen contrast corresponded to slightly longer completion times on average.

Average time vs Task luminance contrast: Fig. 8 scatterplot displays an upward trend between task contrast and average time, signifying that higher task contrast relates to longer times. With an R^2 value of 0.5647,

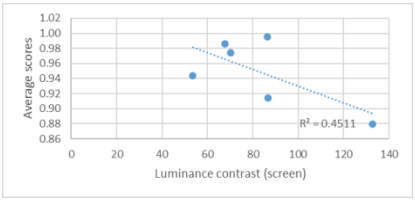

Figure 5. Scatterplot showing the relationship between screen luminance contrast and average scores

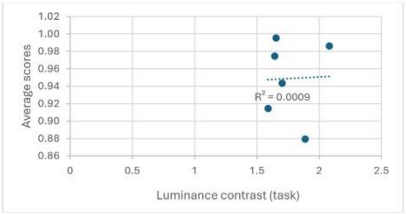

Figure 6. Scatterplot showing the relationship between task luminance contrast and average scores

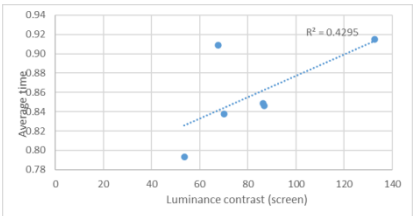

Figure 7. Scatterplot showing the relationship between screen luminance contrast and average time

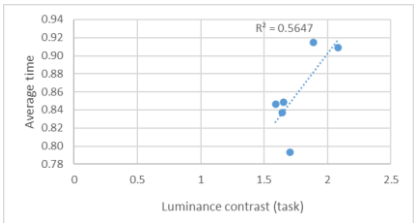

Figure 8. Scatterplot showing the relationship between task luminance contrast and average time

indicating a moderately strong positive correlation, this implies that higher task contrast corresponds to longer average completion times.

Interestingly, the results indicated that participants performed better on tablets for Task 1, as evidenced by higher scores and shorter completion times, while for Task 2, participants performed better on computers. The study revealed that lighting conditions had a notable impact on task completion time but did not significantly affect task accuracy.

IV. DISCUSSION

Previous research has explored the impact of luminance contrast on performance for paper and computer devices [22], this study fills a gap by including tablets as a replacement for paper tasks.

A. Luminance contrast and task performance

The luminance around a computer screen can diminish its visibility (known as disability glare), cause feelings of discomfort (termed discomfort glare), and create temporary adaptation challenges when shifting focus between two different luminance levels [11]. Research has shown that combining lower ambient illumination with higher display contrast improves visual recognition performance and is subjectively preferred [23]. The overall finding in this study highlights a distinction between screen luminance contrast and task luminance contrast in their effects on performance, including accuracy and time. In a past study Slater [24] evaluated contrast with the conclusion that "the greater the contrast reduction required to bring a task to threshold, the greater its visibility."

Screen luminance contrast

In terms of screen luminance contrast, it was found that higher levels worsened performance on both tablets and computers. Higher screen contrast resulted in reduced scores and longer completion times. This might be attributed to the brighter areas on screens causing discomfort and distraction, affecting focus, and diligence. The surrounding luminance influences visual performance by causing disability glare which produces a veiling luminance on the retina [25]. An ideal setup should minimize glare by maintaining surrounding luminance at the same level or slightly lower than the task area [11]. Therefore, lower luminance contrast on the screen is suggested for better performance. Additional evidence from Rea's [26] study indicates that the luminance distribution outside the task area impacts task visibility. It's noteworthy that it's reflected glare that increases this contrast and makes it more difficult to perceive task details. Hence, lower luminance contrast for the screen area is recommended for improved readability and task efficiency.

Task luminance contrast

On the other hand, when considering task luminance contrast, the results showed that an increase in task contrast led to a decrement in performance across devices. There was no strong correlation between scores and higher task contrast, but higher task contrast was associated with longer completion time, hence, reducing performance. This finding contradicts with existing literature suggesting that higher task contrast should improve performance [5], [27]. Previous studies have indicated that task performance depends on the amount of contrast in the task, regardless of how it is achieved under realistic conditions [6]. Higher task contrast generally leads to more accurate and efficient task completion, while lower task contrast may result in errors and longer completion times [10]. The discrepancy in the results regarding task contrast and performance could be attributed to various factors that require further exploration. Possible factors are discussed below.

B. Screen orientation and task performance

Performance might also be influenced by factors other than task contrast: like, device orientation during the experiment. In the current study, the difference in screen orientation might have potentially affected performance due to variations in luminaire angle in relation to each device's orientation, resulting in reflections or glare. The orientation of the screen plays a significant role in how light interacts with the device's surface. When a device is

positioned horizontally, the angle at which light hits the screen differs from when it is positioned vertically. This variance in luminaire angle can lead to reflections or glare, which may impact visibility and task performance. Boyce [1] talks about limiting the luminaire's luminance at angles that are above 55° or 65° for direct lighting, assuming ceiling-mounted luminaires and vertical or nearly vertical display orientation. While these recommendations are well-founded for single-screen setups, they may not fully apply to the more complex and diverse multi-screen arrangements that characterize modern workspaces.

In a study, Rea [6] explored how performance on paper tasks was affected not just by contrast, but also by factors like "…angle of illumination on the task, degree of vertical polarization of the illumination, orientation of the workstation relative to the illumination, […] viewing angle." These factors collectively impacted task performance in conjunction with contrast. Similarly, in the current study, the varied screen orientations may have influenced the participants' task performance due to the varied angles of illumination on both screens. This is particularly relevant in spaces like libraries where the luminaire cannot be controlled by the user and the screens are oriented differently. The limitation of the luminance of the luminaire above specific angles may differ from the suggested standard, highlighting a potential gap in existing lighting design standards that do not fully account for the needs of varied screen orientations.

C. Adaptation luminance

The transient adaptation factor quantifies the temporary reduction in contrast sensitivity when an observer shifts their gaze from a task to irregularities in the surrounding luminance and then returns to the task [25]. In this study, variability between devices might have also influenced performance, especially when transitioning between different luminance contrasts. For instance, in Tablet 3, the screen luminance was notably influenced by glare from an overhead light source, hence impacting the scores. This finding aligns with prior research indicating that substantial luminance differences are frequently viewed negatively, producing glare and reduced visibility due to temporary adaptation shifts [28]. Importantly in the current study, adaptation is not only between a screen and its background but involves two screens plus the background. This continuous adaptation across three luminance levels suggests an optimal ratio may exist between them. This should be consistent with standards recommending a 3:1 luminance ratio [10] between a screen and its background. Overall, by minimizing high variability in luminance across screens and surroundings can reduce visual strain and improve user performance.

D. Effect of character size and luminance contrast on performance

Computers showed an increase in performance with higher task contrast—a finding absent in the tablets across three positions. This difference in outcomes might be attributed to the varied screen sizes: a larger computer monitor compared to a smaller tablet. This can affect not only the display size of characters but also the perception of the surrounding luminance. A previous study on visual fatigue of VDT operators noted similar effects when comparing an LCD TFT and a CRT screen due to their size differences [29]. If a task is visible due to contrast, its apparent size also affects visibility [5]. Research by Weston [30] demonstrates that contrast and size are interdependent in their effects on visual acuity. The study revealed that increasing an object's size improves its visibility more for low-contrast objects compared to high-contrast ones [30]. In this study, text/alphabet size of the tasks varied between computer and tablet when measured due to screen size adaptability for the same kind of tasks. The text size was smaller on tablets compared to computers. Hence, this size discrepancy and contrast could have influenced overall performance outcomes between the two devices.

E. Comparing performance on computers and tablets

Computers had higher screen luminance values, while tablets had higher screen contrast, particularly Tablet 3 with the highest screen contrast which could be due to the orientation and reflection from the above light. This variation in luminance and screen contrast could have a significant impact on performance, as the overall score was lower on Tablet 3. The overall performance was better on computers compared to tablets at all three positions. Computer 1 had the highest overall score, while among the tablets, Tablet 2 had the highest score. The reason for this difference could be attributed to the absence of ceiling light directly above Tablet 2, resulting in no glare or discomfort. Research by Kojima et al. [31] found that iPad readability was highest under low lighting conditions but declined as illuminance levels increased. This suggests that lighting designed for vertical digital screens may or may not align with tablet or portable digital devices. Therefore, it is crucial to consider lighting design that accommodates different device orientations.

F. Critical Considerations and Limitations

One potential limitation is the homogeneity of the study environment. Since the study was conducted in a specific setting, generalizing the findings to other scenarios, like well-lit offices or dimly lit rooms, might be tenuous. Additionally, the nature and complexity of the tasks administered could play a significant role in device preference. User feedback indicates intuitive, responsive touch controls of tablets may provide a more seamless user experience compared to traditional mouse and keyboard interfaces on computers, facilitating certain tasks like scrolling. This suggests that differences in interface paradigms between devices could modulate the impact of variable task contrast on performance. Exploring the role of other external factors like ambient lighting, tablet screen orientations, use of task lighting on desks, or even device-specific settings could provide a comprehensive picture. From a practical standpoint, findings underscore the need for device manufacturers and lighting designers to be cognizant of luminance contrast implications.

V. CONCLUSION

The analysis yielded several key findings.

Task luminance contrast: The luminance contrast within the task area did not significantly affect accuracy but showed a strong correlation with time.

Screen luminance contrast: Lower luminance contrast for screen area was found to be associated with faster completion times, which is a noteworthy finding.

Inter-Subject Variability: Individual differences among subjects also played a significant role in performance, with task times strongly correlated by subject and scores showing a lesser correlation.

Influence of Lighting Conditions: Optimal lighting conditions were suggested to be those that did not create high screen contrast on the screen.

Tablet vs. Computer: Task performance on tablets was more disrupted by screen contrast compared to computers, potentially due to subjects adjusting their positions to avoid reflections/shadows, leading to potential errors and longer completion times.

Practical Implications: Lighting conditions that maintain high task luminance contrast and low screen luminance contrast would be optimal. Tablet 2 was identified as a favourable device due to its higher task contrast and lower screen contrast. In conclusion, this study contributes to the understanding of how luminance contrast, influences task performance on computers and tablets in a library environment. The findings provide valuable insights for designing optimal lighting conditions in digital task environments.

REFERENCES

[1] P. Boyce, *Human Factors in Lighting*. CRC Press, 2014.

[2] J. A. Veitch and G. R. Newsham, "Determinants of Lighting Quality II: Research and Recommendations." Aug. 12, 1996.

[3] Society of Light and Lighting, *SLL Code for Lighting*. CIBSE, 2012.

[4] H. Wallach, "Brightness constancy and the nature of achromatic colors," *J Exp Psychol*, vol. 38, no. 3, pp. 310–324, Jun. 1948.

[5] R. G. Hopkinson and J. B. Collins, *The ergonomics of lighting*. Macdonald & Co., 1970.

[6] M. S. Rea, "Visual Performance with Realistic Methods of Changing Contrast," *Journal of the Illuminating Engineering Society*, vol. 10, no. 3, pp. 164–177, Apr. 1981.

[7] A. A. Eastman and W. B. DeLaney, "Visibility of office-type tasks under various lighting materials-Part I," *Illum Eng*, vol. 61, no. 5, pp. 366–378, 1966.

[8] P. R. Boyce, "Variability of contrast rendering factor in lighting installations," *Lighting Research & Technology*, vol. 10, no. 2, pp. 94–105, Jun. 1978.

[9] B. M. O'Donell, E. M. Colombo, and P. R. Boyce, "Colour information improves relative visual performance," *Lighting Research & Technology*, vol. 43, no. 4, pp. 423–438, Sep. 2011.

[10] D. DiLaura, K. W. Houser, R. G. Mistrick, and G. R. Steffy, "The Lighting Handbook: Reference and Application, Illuminating Engineering Society of North America." Illumination Engineering NY, 2011.

[11] J. E. Sheedy, R. Smith, and J. Hayes, "Visual effects of the luminance surrounding a computer display," *Ergonomics*, vol. 48, no. 9, pp. 1114–1128, Jul. 2005.

[12] M. S. Rea, "Solving the problem of VDT reflections," *Progressive Architecture*, vol. 72, no. 10, p. 35+, 1991.

[13] K.-K. Shieh and D.-S. Lee, "Preferred viewing distance and screen angle of electronic paper displays," *Appl Ergon*, vol. 38, no. 5, pp. 601–608, 2007.

[14] H. Yu, T. Akita, T. Koga, and N. Sano, "Effect of character contrast ratio of tablet PC and ambient device luminance ratio on readability in low ambient illuminance," *Displays*, vol. 52, pp. 46–54, Apr. 2018.

[15] W. Osterhaus, H. Hemphälä, and P. Nylén, "Lighting at computer workstations," *Work*, vol. 52, pp. 315–328, 2015.

[16] N. Na and H.-J. Suk, "Adaptive display luminance for viewing smartphones under low illuminance," *Opt Express*, vol. 23, no. 13, pp. 16912–16920, 2015.

[17] N. Na and H.-J. Suk, "Adaptive luminance contrast for enhancing reading performance and visual comfort on smartphone displays," *Optical Engineering*, vol. 53, no. 11, p. 113102, Nov. 2014.

[18] N. Na, K. Choi, and H.-J. Suk, "Adaptive luminance difference between text and background for comfortable reading on a smartphone," *Int J Ind Ergon*, vol. 51, pp. 68–72, 2016.

[19] J.-G. Chen, S.-K. Wu, H.-P. Chiu, C.-N. Tu, and C.-H. Liu, "Evaluation of Three Tablet Computers at Two Levels of Ambient Illumination," *Int J Hum Comput Interact*, vol. 32, no. 5, pp. 394–401, May 2016.

[20] J. A. Veitch and G. R. Newsham, "Lighting Quality and Energy-Efficiency Effects on Task Performance, Mood, Health, Satisfaction, and Comfort," *Journal of the Illuminating Engineering Society*, vol. 27, no. 1, pp. 107–129, Jan. 1998.

[21] M. N. Inanici, "Evaluation of high dynamic range photography as a luminance data acquisition system," vol. 38, no. 2, pp. 123–136, Jun. 2006.

[22] J. A. Veitch and G. R. Newsham, "Exercised control, lighting choices, and energy use: An office simulation experiment," *J Environ Psychol*, vol. 20, no. 3, pp. 219–237, Sep. 2000.

[23] M. Te Chen and C. C. Lin, "Comparison of TFT-LCD and CRT on visual recognition and subjective preference," *Int J Ind Ergon*, vol. 34, no. 3, pp. 167–174, Sep. 2004.

[24] A. I. Slater, "A simple contrast reducing visibility meter," *Lighting Research & Technology*, vol. 7, no. 1, pp. 52–55, 1975.

[25] A. W. Levy, "The CIE visual performance system," *Lighting Research & Technology*, vol. 10, no. 1, pp. 19–27, Mar. 1978.

[26] M. S. Rea, "Behavioral Responses to a Flexible Desk Luminaire," *Journal of the Illuminating Engineering Society*, vol. 13, no. 1, pp. 174–190, Oct. 1983.

[27] M. S. Rea and M. J. Ouellette, "Relative visual performance: A basis for application," vol. 23, no. 3, pp. 135–144, Sep. 1991.

[28] S. Kokoschka and P. Haubner, "Luminance ratios at visual display workstations and visual performance," vol. 17, no. 3, pp. 138–144, Sep. 1985.

[29] A. Wolska and M. Świtula, "Luminance of the Surround and Visual Fatigue of VDT Operators," *International Journal of Occupational Safety and Ergonomics*, vol. 5, no. 4, pp. 553–580, Jan. 1999.

[30] H. C. Weston, "Rationally Recommended Illumination Levels," vol. 26, no. 1 IEStrans, pp. 1–16, Mar. 1961.

[31] T. Kojima, S. Sano, N. Ishio, T. Koizuka, and M. Miyao, "Verification of the minimum illuminance for comfortable reading of an e-paper," in *Lecture Notes in Computer Science*, Berlin, Heidelberg: Springer Verlag, 2013, pp. 348–355.

SPONSORED BY:

REHVA Federation of European Heating, Ventilation and Air Conditioning Associations

EUROVENT CERTIFIED PERFORMANCE www.eurovent-certification.com

The impact of Thermal Energy Storages in thermal networks on decarbonisation and grid relief

Authors: F. Stucki BSc. & M. Schoch BSc. ***Year:*** March 2023 ***Institute:*** Lucerne School of Engineering and Architecture HSLU (IGE) ***Supervisors:*** Dr. W. Villasmil (HSLU)

Abstract- The expansion and operation of thermal networks play a central role in achieving the European climate goal of net-zero by 2050. This study focuses on the influence of thermal energy storage (TES) systems on decarbonisation and grid relief in such thermal networks.

The study analyses the substitution of fossil peak load energy with the energy balance method to reduce carbon dioxide (CO_2) emissions. The impact of TES volume and base load capacity on peak load energy consumption is quantified. Grid relief is examined through a simulation using the Dymola modelling language. Thermal energy storage units are placed in a decentralised manner in the distribution network to assess their impact on the pressure drop in the distribution pipes. Both calculations are based on adjusted data from the district heating network of the waste-to-energy plant in Buchs SG, Switzerland (32 MW thermal capacity).

The results of the study indicate that TES can make a significant contribution to achieving climate change targets. Although TES with smaller volumes have the greatest relative impact on peak load substitution (t_{CO2}/m^3_{TES}), the CO_2 emissions continue to decrease steadily with increasing storage volume.

The decentralised placement of TES has a significant impact on grid relief. By discharging TES, local pressure losses can be reduced by more than 50%. The duration of the relief depends on the TES volume and the chosen charging strategy.

The economic analysis shows that in Switzerland large-scale storage facilities can be amortised within 20 years for complete decarbonisation, provided that there is a difference of 7.6 Rp./kWh (equivalent to 0.076 €/kWh) between the price of utility energy of base and peak loads. However, from a purely economic point of view, the optimal TES volume is much smaller, about 1.1% of the volume required for full decarbonisation.

***Index Terms*—thermal energy storage, decarbonization, district heating network, pressure drop, peak load, Modelica, grid relief**

I. INTRODUCTION

Buildings in Switzerland account for approximately 40% of the country's total energy demand. The use of fossil fuels is responsible for one third of the domestic CO_2 emissions [1]. This places Switzerland on a par with the European Union, where buildings also account for 40% of the total energy demand and 36% of total greenhouse gas emissions [2].

To achieve the Swiss and European climate goals of net-zero by 2050, it is crucial to decarbonise the heat supply. The aim is to shift the supply of heat to buildings from a reliance on fossil fuel-based heating systems to a predominant use of electric heat pumps and district heating networks [3]. At present, thermal networks provide only 6% of Switzerland's heat supply [4]. However, according to calculations by the association “Thermische Netze Schweiz”, up to 38% of Switzerland’s heat demand could be met in an economically and ecologically viable manner through the use of thermal networks [5].

Connecting to a district heating network does not automatically guarantee that the heat supplied is from renewable energy sources. Fossil fuels such as gas and oil still account for a substantial 31% of the total energy in district heating networks in Switzerland [6]. This energy is mainly used to cover peak loads during periods of low ambient temperatures. Therefore, replacing peak load energy is a crucial step towards the complete decarbonisation of thermal networks. District heating operators are making significant efforts to implement this substitution economically and technically. One promising solution to this challenge could be the integration of thermal energy storage systems. TES can substitute peak load energy with base load energy by charging during periods of low heat demand and discharging during periods of higher demand. This approach exploits demand fluctuations and achieves a smoothing of the power generation profile. In this way, TES enables optimised use of CO_2-neutral base load energy. Using the same approach, TES can also help to minimise hydraulic pressure losses in the distribution network. In this case, TES are integrated in a decentralised manner, i.e. directly at the consumer level. As a result, at times of high demand, the entire amount of energy doesn't have to be supplied by the main generation source, but can be provided by the decentralised TES [7].

In district heating networks, TES in the form of water-filled steel tanks are the most economical form of thermal energy storage (TES) due to their high technology readiness level and widespread use. Consequently, this study focuses on TES with sensible heat storage.

The purpose of this work is to demonstrate the extent to which TES can solve the identified challenges and provide insight that primarily benefit the operating companies.

II. METHODS

A. Research Approach

The investigation follows a systematic procedure, as illustrated in Figure 1. Initially, data from an actual district

heating network is analysed. The basic data obtained is then cleaned and supplemented with other necessary data.

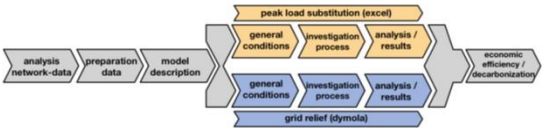

Figure 1. Methodical approach of calculations

A representative and simplified district heating network has been modelled on this data. The simplifications were chosen to ensure that the results are as general as possible and therefore transferable to other networks. Using this generic network, a static energy balance calculation for peak load substitution and a dynamic simulation for grid relief were carried out. The investigations into grid relief were conducted using the object-oriented computer language "Modelica" (Dymola environment version 2023x).

The results of both calculations form the basis of the economic and ecological analysis. Finally, the results are critically reflected upon and summarised.

B. Primary data

This study is based on consumption data from the district heating network in Buchs SG (Switzerland) for the year 2022. The network is supplied by a waste incineration plant. The heat load pattern is of particular importance to the investigation. In the absence of individual consumer load profiles, these had to be generated. First, all network consumers were grouped into clusters based on usage and location. Each cluster represents a larger number of buildings with similar usage patterns. A load profile was then generated for each cluster using the open-source tool "Freeplan" from the Technical University of Dresden [8]. The 18 clusters were then connected to the network as individual consumers. The locations of the individual clusters (e.g. industrial) were determined according to reality. This resulted in the network plan depicted in Figure 2.

The sections of the pipeline selected for analysis in the grid relief investigation are marked by three blue magnifying glasses. These include the main pipeline from the waste incineration plant and the two supply lines to the villages of Buchs and Grabs. These sections are considered relevant in the network due to their location and high utilisation. Therefore, the investigation focused on the pressure loss behaviour in these sections.

To verify the constructed network, the generated profile was compared with the actual load profile. The main focus is on the power peaks in winter and the base load in summer. The critical peaks are comparable both in terms of annual progression and in terms of daily and weekly patterns. An annual energy deviation of +10% is caused by an increased heat demand in the generated load profiles in autumn. This deviation is considered tolerable and has therefore not been adjusted further.

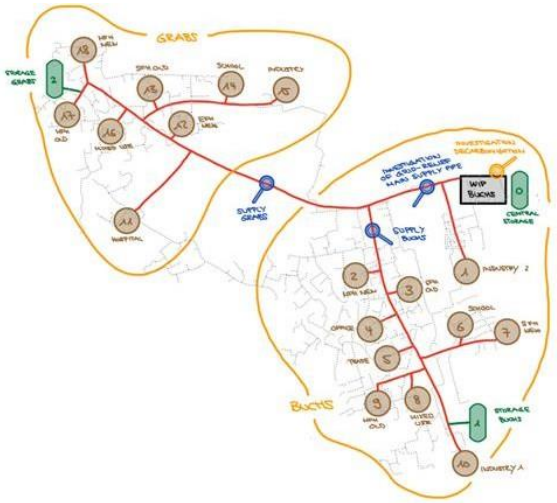

Figure 2. Simplified network layout for simulation

C. Model description

The generated network was used to carry out two considerations: peak load substitution and grid relief. To simplify the calculations, several general simplifications were made, which are described below.

The model considers heat generation as a black box that can provide heat at the required temperature level. It is assumed to be a bivalent system, where the peak load is supplied by fossil energy (natural gas). Heat is stored without phase change using water as a medium, which is stored in appropriate tanks. The study assumes unlimited space availability. External heat losses from distribution lines and storage units are excluded to keep the system and the calculations manageable. For these reasons, seasonal energy storage systems that transfer energy between summer and winter are not considered or are only considered in a simplified manner.

The calculations are based on the assumption of an energy balance. The energy taken from the grid must be replenished elsewhere in the same proportion. The first priority is to meet the heat demand with the base load (BL). If the demand exceeds the BL, the TES provides support by discharging. Finally, as the last priority, the peak load (PL) is used to meet the demand. It is assumed that the storage is only charged with the BL due to the decarbonisation objective. Furthermore, the storage is managed without the use of predictive control. It is assumed that the supply temperature (90 °C) and return temperature (60 °C) remain constant. The resulting temperature difference of 30 K can be assumed to be a suitable value for district heating networks [9].

1) Peak load substitution

Based on the simplified energy balance analysis, the impact of storage volume and the power ratio between BL and fossil PL on the required peak energy is examined. The location of the storage volume in the network (central/decentral) is not a decisive factor, as long as the TES is optimally charged and discharged. Based on these calculations, a ratio between BL power and PL power is established, which is then used for the dynamic evaluation of decentralised storage units. Additionally, for PL substitution, it is assumed that the stratification

(ΔT°=°30°K) in the storage is perfect, allowing the volume to be fully utilised at 100%.

2) Grid relief

This analysis focuses on grid relief and the reduction of specific pressure loss in pipelines. Due to the size and complexity of the model developed, the simulation period was limited to three months (January to March). These winter months are crucial for grid relief. Figure 3 shows the hydraulic setup of the model, with the BL boiler on the left and a central storage on its right. The PL boiler is then integrated in series to the main flow. From there, the energy is transported to the consumers or to the decentralised TES. Only pumps are used as actuators. This is due to the functionality of the "Dymola" software. Valves multiply the number of mathematical equations due to their complex modelling. As a substitute, pumps are used, which are tight when stationary. All controls were programmed individually for each part of the system. The use of PID controllers was avoided to prevent unwanted dynamics.

In contrast to peak load substitution, this calculation defines a power ratio between BL and PL. A base load power coverage of 60% was chosen. According to the calculations conducted, this practical ratio leads to an annual BL energy of 95% and a PL energy of 5%. It's essential to note that the power coverage must be considered individually for each system.

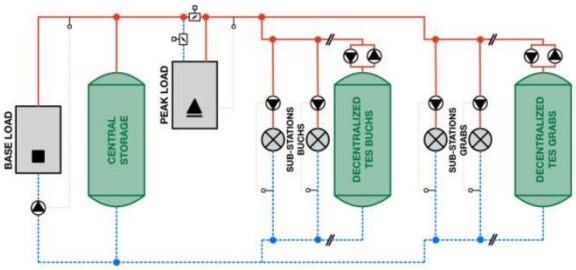

Figure 3. Schematic structure of the model

III. DATA PRESENTATION & DISCUSSION

A. Peak load substitution

The study aimed to investigate the proportion of fossil PL energy that could be substituted by TES. The following results address the research question of the extent to which TES influences the reduction of CO_2 emissions.

Figure 4 displays the results of the peak load substitution (y-axis) for various TES volumes (x-axis, up to 100,000 m³) and power distributions. The curves indicate the energy share of the PL under different power ratios between BL and PL. The total energy consumption (PL + BL) is 103.3 GWh/a. It is evident that as the TES volume increases, the curves approach the value of 0% PL energy. The power ratio between PL and BL is a crucial factor. The higher the BL power chosen, the lower the TES volume required for complete PL substitution. The power ratio of 60% used for the following grid relief analysis, achieves complete substitution of PL energy with a TES volume of 70,120 m³, corresponding to a storage capacity of 2,385 MWh at the chosen temperature difference of 30 K. This is equivalent to the consumption of approximately six cold winter days in the analysed network and 2.3% of the annual energy consumption.

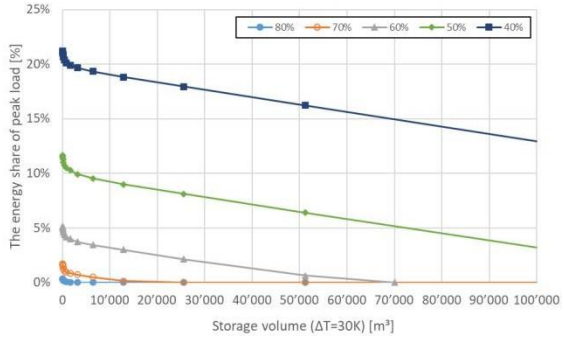

Figure 4. Peak load energy as function of TES up to 100'000 m³ (ΔT = 30 K) for investigated base load ratios in %

To enhance comprehension of the curve progression in Figure 4, Figure 5 displays the proportion of PL energy for TES volumes up to 70,000 m³ at a 60% BL power ratio. A more pronounced decrease in PL energy is observed at with moderate TES volumes. The rate of change (steepness) of the curve decreases continuously. In this case, for TES volumes between 6,400 m³ and 40,000 m³, an almost linear behaviour is observed (coefficient of determination > 0.99). The findings indicate that the substituted PL energy per cubic metre decreases as the TES volume increases. The initially greater decrease in PL energy can be attributed to the fact that TES are particularly effective with oscillating load profiles around the BL. It is important that TES can be both charged and discharged.

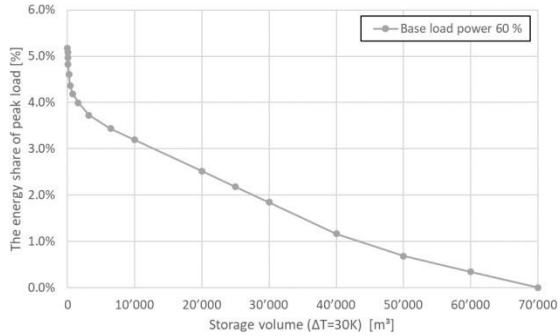

Figure 5. Peak load energy as function of TES up to 70'000 m³ (ΔT = 30 K) for base load ratio of 60%

B. Grid relief

The second research question focuses on the impact of decentralised placement of thermal energy storage on the hydraulic distribution network. Decentralised energy injection during periods of high demand aims to relieve the distribution network. The results of three selected distribution lines are then presented and analysed: the supply lines to the villages of Buchs and Grabs, and the main distribution line near the power plant site (refer to Figure 2).

Figure 6 illustrates the behaviour of the specific pressure loss (Pa/m) in the main distribution line over a 7-day period in winter season for two scenarios, with and without TES. The blue curve represents the baseline scenario without significant TES volume (50 m³). The red curve shows the pressure loss with a decentralised TES volume of 6,400 m³. The corresponding state of charge (SoC) of the TES is shown by the dashed red line. During the period considered, the decentralised TES in Buchs is discharged (red dashed line) due to higher demand than the capacity of the BL.

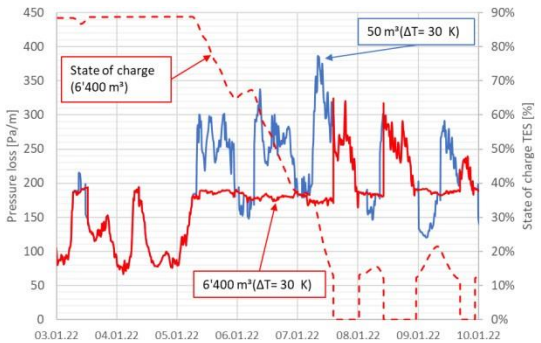

Figure 6. Specific pressure loss in main distribution pipe during TES discharge

Without grid relief, the main pipe near the heat power plant, which is considered a critical point, reaches a specific pressure loss of almost 400 Pa/m. In the variant with a decentralised TES volume of 6,400 m³, the TES is initially charged at the beginning of the period. From 05.01.2022, it supplies energy to the network with only a few interruptions. The energy demand is covered by both the centralised BL and the decentralised TES. The pressure loss in the pipeline remains constant at around 180 Pa/m, which is a reduction of more than 50% compared to the baseline. This relief is maintained until the TES is unloaded. Once the TES is discharged, all the heat is supplied by the power plant, and the critical section of the pipeline is no longer relieved. Therefore, the TES no longer affects the network. To avoid this, a different charging strategy could be used, where the TES is charged with PL energy in a predictive manner. This would allow the pipeline segment to be continuously relieved.

Figure 7 displays the same parameters as in Figure 6, but with a period of lower heat demand. The state of charge (red dashed line) continuously rises to around 88% (maximum charge due to stratification). The energy required for charging is provided by the BL. It can be observed that the pressure loss in the distribution line (red solid curve) occasionally exceeds the baseline (blue curve) where no charging is required. However, the pressure loss of max. 200 Pa/m is never exceeded, even with active TES charging.

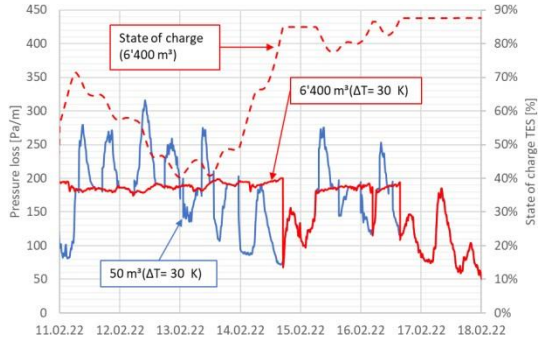

Figure 7. Specific pressure loss in main distribution pipe during charging of decentralized TES

For the main distribution line near the power plant, it doesn't matter whether the decentralised TES is located in Grabs or in Buchs. However, it can have an impact on the peripheral distribution lines. Depending on the volume and location of the TES, the hydraulic conditions can either improve or deteriorate. Figure 8 shows the specific pressure loss in the supply line to Buchs when the TES is also located there. In addition to the baseline scenario (blue) and the 6,400 m³ TES (red), an additional 100,000 m³ TES sufficient to fully replace the PL is shown in yellow. Due to the high energy share in Buchs, a similar behaviour to the main distribution line is observed. As the TES volume increases, the pressure loss trend becomes more consistent. With complete PL substitution, the pipe section can be continuously relieved, never exceeding a pressure loss of more than 200 Pa/m.

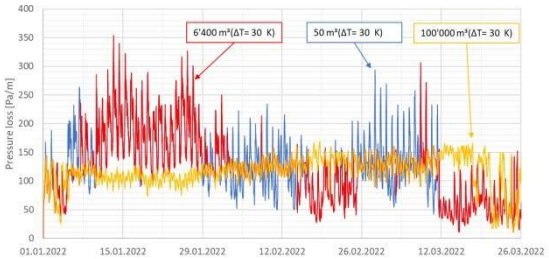

Figure 8. Specific pressure loss in supply pipe to Buchs with decentralized TES over 3 winter months

In contrast, Figure 9 visualises the specific pressure loss in the Grabs supply line when the decentralised TES is placed in Grabs. The yellow curve indicates that the hydraulic behaviour worsens above a certain TES volume. In this scenario, a negative pressure drop occurs at a volume of 50,000 m³.

This can be interpreted as a change in the flow direction within the supply pipeline. Energy is being transported from the TES in Grabs back through the supply line to Buchs. The demand in Grabs is therefore lower than the discharge capacity of the decentralised TES. However, as these lines are designed for the lower consumption in Grabs, the specific pressure loss increases excessively. Therefore, it's important to consider the demand of each specific region when positioning the TES. Ideally, the TES should be located close to the actual energy demand. Consumers with high heat demand, such as hospitals or industrial facilities are particularly suitable candidates for a near placement of a TES.

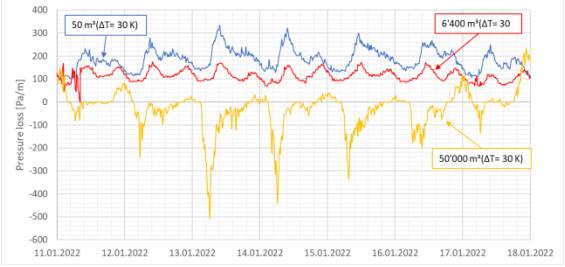

Figure 9. Specific pressure loss in supply line to Grabs with decentralized TES over 3 winter months

In summary, correctly placed TES can smooth hydraulic fluctuations and allow for more consistent network utilisation. Moreover, the performance of the network can be enhanced, and more consumers can be supplied.

C. Economic viability

The preceding calculations and findings are put into an economic context. This involves correlating the investment costs of the thermal energy storage with the reduced operating costs due to the savings from the fossil peak load (natural gas).

The economic viability calculation heavily depends on the investment costs of the storage units. These costs were calculated based on previously realised projects, predominantly in Denmark, and adjusted upwards by a factor of 2.5 to match the price level in Switzerland [10,11]. The exchange rate between the Swiss franc and the euro was set at 1 CHF = 1 € as of May 2023 [12]. The calculations are based on a payback period of 20 years and an interest rate of 3%. The cost of generating BL and PL energy also plays a crucial role. Figure 10 shows the price difference between BL and PL energy at which a TES becomes economically viable.

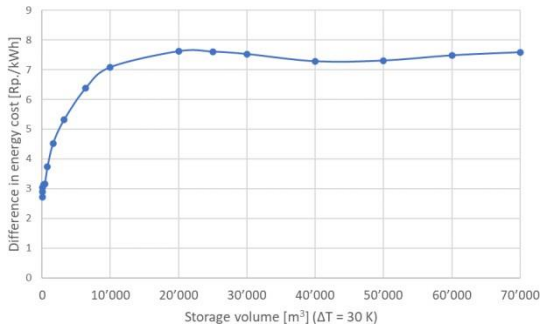

Figure 10. Required price difference between useful energy BL /PL for an amortization in 20 years, < 70,000 m³ TES (ΔT = 30 K)

The graph displays the minimum required TES volume for a 20-year payback on the x-axis, while the y-axis represents the energy price differential at the level of final energy (including system efficiencies). All points lying above the curve are therefore profitable. It is evident that TES volumes up to approximately 400 m³ will amortise within 20 years at an energy price differential of 3 Rp./kWh. For volumes exceeding 20,000 m³, the difference is approximately 7.5 Rp./kWh. This convergence can be explained by the almost linear behaviour of both the investment costs and the peak load savings within this range.

Based on these results, the economically optimal TES volume was determined using a fixed price difference. In Figure 11, a price difference of 6 Rp./kWh was assumed. This energy price difference is achieved, for example, with a wood heating system with a chip price of 5 Rp./kWh and an efficiency of 70%, compared to a gas heating system with a gas price of 11.2 Rp./kWh, with condensing technology and an efficiency of 85%. Given the increase in gas prices from the end of 2021 to mid-2023, such a price difference is realistic [13]. In Figure 11, the annual capital cost of the investment (orange) and the annual energy cost (blue) move in opposite directions. Using the mentioned fundamentals, an optimum of total costs appears at a TES volume of around 800 m³ (grey).

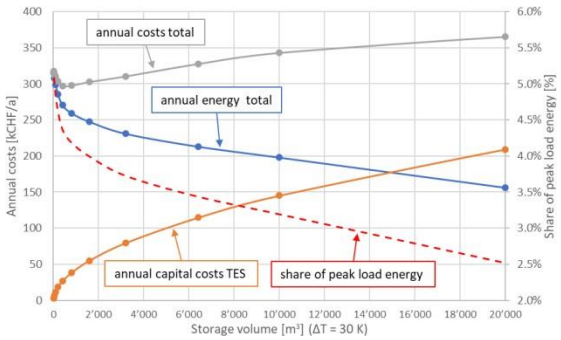

Figure 11. Annual costs at a 6 Rp./kWh price difference in useful energy prices BL/PL

D. Decarbonisation

Figure 12 displays the result of the decarbonisation analysis. It is evident that even moderate TES volumes have a significant impact on decarbonisation, similar to the peak load energy substitution. The blue curve shows the reduction in CO_2 emissions from natural gas (0.230 kg CO_2-eq./kWh), as a function of TES volume, without considering the additional base load energy required and its greenhouse gas emissions. The orange curve shows the result if the BL is supplied with wood chips (0.011 kg CO_2-eq/kWh). The higher the environmental impact of base load generation, the lower the actual CO_2 savings. For a waste-to-energy plant with low CO_2 emissions per kWh (0.003 kg CO_2-eq/kWh), the result is almost identical to the scenario without considering the base load [14].

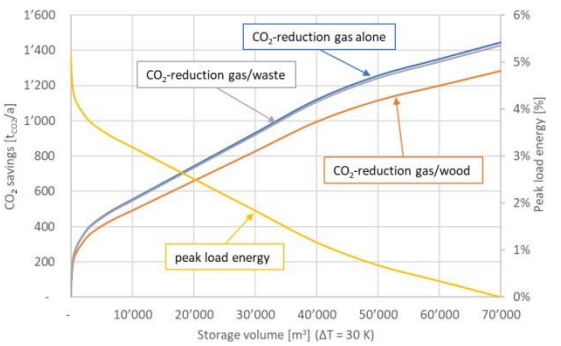

Figure 12. CO_2-reduction depending on the TES size (ΔT = 30 K) and energy source

In the example with the most economical TES size of 800 m³, the CO_2 emissions of a waste-to-energy plant are reduced by 274 tonnes per year. This is approximately equivalent to the CO_2 emissions of 59 single-family homes heated with natural gas [15]. With the chosen power ratio of 60%, the complete substitution of peak load energy results in a CO_2 saving of 1,439 tonnes per year, which is comparable to the CO_2 emissions of approximately 400 single-family homes.

IV. CONCLUSION

In conclusion, thermal energy storage systems in thermal networks provide both environmental and economic benefits. It has been shown that the largest relative reductions in peak load energy (and hence CO_2 reductions) can be achieved with minimal TES volumes. Consequently, as the TES volume increases, the reduction per cubic metre of storage steadily decreases. Beyond a certain volume, the reduction is almost linearly proportional to the storage content. The power ratio between base load and peak load has a significant impact on the required peak load energy and the corresponding volume of the TES.

To relieve the grid, it is important to consider not only the size of the TES but also the charging strategy used. A decentralised TES can significantly reduce the specific pressure loss in the main distribution line during active discharge, but it cannot provide relief at the point of full discharge. The strategy of exclusively charging the TES with base load energy results in large storage volumes, in this case, 100,000 m³. It was furthermore recognised that the location of a decentralised TES is of paramount importance. It should be located where the thermal energy is effectively needed.

Research has been shown that above a certain TES volume, the price difference between base load and peak load energy required for a cost-effective investment remains almost constant. This means that larger TES volumes (> 20,000 m³) can be operated economically with a constant payback period. Smaller volumes prove to be economically viable even with minimal price differentials. While they provide an efficient means, they do not provide a complete substitution for CO_2 emissions.

Given sufficient space and a significant energy price difference between base load and peak load, full decarbonisation through TES is advisable and must be considered when designing a district heating network.

ACKNOWLEDGEMENT

We would like to express our gratitude to Willy Villasmil and Stefan Mennel from the Institute for Building Technology and Energy (IGE) of the Lucerne University of Applied Sciences and Arts. We are also thankful to Urs Brunner from the “Verein für Abfallentsorgung” association (operator of the waste incineration plant) for his active support and the provision of helpful basic data. Their support has significantly contributed to the success of this work.

REFERENCES

1 Bundesamt für Energie. (2023a). *Gebäude*. Accessed on https://www.bfe.admin.ch/bfe/de/home/effizienz/gebaeude.html (06.05.2023).

2 European Commison. (2023). *Commission welcomes political agreement on new rules to boost energy performance of buildings across the EU.* Aufgerufen von https://ec.europa.eu/commission/presscorner/detail/en/ip_23_6423 (10.02.2024).

3 Bundesamt für Energie. (2021). *ENERGIEPERSPEKTIVEN 2050 +: Technischer Bericht*. Accessed on www.bfe.admin.ch (03.05.2023).

4 International Renewable Energy Agency. (2017). *Renewable Energy in District Heating and Cooling: A sector roadmap for REmap*. Accessed on https://www.irena.org/-/media/Files/IRENA/Agency/Publication/2017/Mar/IRENA_REmap_DHC_Report_2017.pd (20.03.2023).

[5] Sres, A. (2014). Weissbuch Fernwärme Schweiz – VFS Strategie: Langfristperspektiven für erneuerbare und energie-effiziente Nah- und Fernwärme in der Schweiz. Accessed on https://www.fernwaerme-schweiz.ch/fernwaerme-deutsch/Dienstleistungen/Weissbuch.php (30.03.2023).

[6] Sres, A. (2014). Weissbuch Fernwärme Schweiz – VFS Strategie: Langfristperspektiven für erneuerbare und energie-effiziente Nah- und Fernwärme in der Schweiz. Accessed on https://www.fernwaerme-schweiz.ch/fernwaerme-deutsch/Dienstleistungen/Weissbuch.php (30.03.2023).

[7] Verband Fernwärme Schweiz. (2020). *Leitfaden Fernwärme / Fernkälte*. Accessed on https://www.fernwaerme-schweiz.ch/fernwaerme-franz/Dienstleistungen/Leitfaden_Fernwaerme_Fernkaelte_200918.pdf (22.03.2023).

[8] Technische Universität Dresden. (2023). FreePlan (Version 2.5) [Computer software]. Accessed on https://tu-dresden.de/ing/maschinenwesen/iet/gewv/ressourcen/dateien/forschung_und_projekte/projekte/Poster_Matthees_FreePlan_ohne_QR_A4.pdf?lang=de

[9] QM Fernwärme; Schweiz. (2017). Planungshandbuch Fernwärmehttps://www.gbv.de/dms/tib-ub-hannover/100641844x.pdf

[10] Duran Adroher, N., Lüchinger, R., Villasmil, W. & Worlitschek, J. (2022). Saisonale Wärmespeicher. Accessed on https://www.aquaetgas.ch/energie/fernw%C3%A4rme/20221026_ag11_saisonale-w%C3%A4rmespeicher/ (08.05.2023).

[11] Ramboll. (2015). WÄRMESPEICHERUNG IN FERNWÄRMENETZEN: Möglichkeiten und Grenzen. Accessed on www.ramboll.com/energy (03/05/2023).

12 ESTV, E. S. (2023). Aktueller Monatsmittelkurs. Accessed on https://www.estv.admin.ch (11.05.2023).

13 Statista. (2023). Schweiz - Gaspreis nach Verbrauchertyp & Monaten 2023 | Statista. Accessed on https://de.statista.com/statistik/daten/studie/1023989/umfrage/preis-fuer-gasl-in-der-schweiz-nach-verbrauchertyp/ (20.05.2023).

14 KBOB. (2022). Ökobilanzdaten im Baubereich. Accessed on https://www.kbob.admin.ch/kbob/de/home/themen-leistungen/nachhaltiges-bauen/oekobilanzdaten_baubereich.html (12.05.2023).

15 WWF Schweiz. (2023). Gebäudesanierung und Heizsysteme | WWF Schweiz. Accessed on https://www.wwf.ch/de/unsere-ziele/gebaeudesanierung-und-heizsysteme (29.05.2023).

SPONSORED BY:

REHVA
Federation of European Heating, Ventilation and Air Conditioning Associations

Urban Building Energy Modeling: Integrating Dynamic and Data-Driven Models for Time- Series Analysis

Said Bolluk – Özyeğin University, Istanbul
Senem Seyis – Özyeğin University, Istanbul
Ece Kalaycıoğlu Özdemir – Özyeğin University, Istanbul
Reyhan Aydoğan – Özyeğin University, Istanbul

***Abstract*—This study addresses a critical gap in Urban Building Energy Modeling (UBEM) by introducing an innovative hybrid approach that combines dynamic and statistical models. Previous hybrid studies faced challenges in result validation, model calibration, and delivering predictions at high temporal resolution. To fill this gap, this study presents an integrated UBEM for time-series analysis. The methodology involves creating a dynamic model for 13 buildings on a university campus, with key parameters calibrated. This calibration reduces the simulation's monthly Coefficient of the Variation of the Root Mean Square Error (CV-RMSE) from 0.139 to 0.106 at the campus level. The calibrated dynamic model's hourly energy consumption data is then incorporated into a statistical model, a Long Short-Term Memory (LSTM) network utilized in time-series regression. This statistical model predicts hourly energy consumption with an average R-squared value of 0.915.**

***Index Terms*—Building Energy Consumption, Machine Learning, Time Series Analysis, Urban Building Energy Modeling.**

INTRODUCTION

Different modeling approaches have been introduced to the literature in recent years to understand the energy consumption patterns of urban building stocks. In this sense, Swan and Ugursal classified these approaches into two types: top-down and bottom-up [1]. The top-down examines the overall energy consumption of urban building stocks to create long-term plans considering urban planning and economic and technological growth strategies in cities. Since the goal is to understand general trends, the input data for top-down models can be broad. This can include basic information for a district, like demographics (e.g., household income or employment rate), climate conditions, and general statistics from the construction industry (e.g., rental prices and construction costs) [1].

On the other hand, the bottom-up approach focuses on understanding the factors influencing the energy consumption of urban building stocks [1]. Its goal is to develop energy reduction strategies for individual buildings or groups of buildings at the urban level. This method demands in-depth insights into regional climatic conditions and the characteristics of the buildings and occupants within the chosen district. Bottom-up urban building energy models can identify potential energy savings through retrofitting strategies across building, occupant, and grid components [2]. However, the efficacy of these models may introduce uncertainty when selecting the most suitable model for an urban-level investigation.

For instance, statistical bottom-up models leverage machine learning algorithms to predict building energy consumption. Even with this, they may overlook thermal interaction among buildings and need help accurately predicting energy use at higher resolutions (e.g., hourly consumption). This limitation arises from the challenge of integrating time-dependent variables like climate data and building operational schedules into statistical models [3]. Conversely, dynamic bottom-up models, employing computational fluid dynamics or more simplified methods [4], facilitate realistic energy simulations. Plus, dynamic models can be the key to reproducing high-resolution validation data from the existing resources since high temporal resolution energy consumption data are rarely found in UBEMs at high temporal (e.g., hourly) and spatial (e.g., building level) resolutions. However, dynamic models demand considerable computational resources and time investment [5].

Typically, UBEM studies use a single bottom-up approach tailored to the study's purpose and scope [6]. While some studies explore a hybrid approach by combining dynamic and statistical models, these efforts often suffer from shortcomings such as parameter calibration deficiencies [7], inadequate model validation [8], predictions at low temporal resolution [9], or improper utilization of dynamic models [10]. It is evident that there is a need for a novel hybrid approach in UBEM when considering the powerful elements of statistical and dynamic models. Hence, this study proposes a novel approach that integrates the statistical and dynamic models to propose a robust UBEM. In this sense, a university campus is selected for the case study. A dynamic model of the buildings in the selected campus is created, and its essential parameters are calibrated to reduce simulation errors. Subsequently, this dynamic model generates synthetic hourly energy consumption data, which is used to validate the statistical model. Finally, the statistical model conducts a time-series analysis to predict the hourly energy consumption of the buildings.

METHODOLOGY AND RESULTS

DYNAMIC MODEL

The selected area for the case study is the Özyeğin University campus in Istanbul. There are thirteen conditioned buildings with different use types on the campus. Clustering buildings into archetypes with similar energy characteristics is very important when working at the urban level. Thus, thirteen buildings were clustered into four archetypes: academic building, dormitory, social building, and sports center. The Urban Modeling Interface (UMI), developed by MIT Sustainable Design Lab [11], was selected to perform dynamic energy simulations. UMI is integrated to a computer-aided design (CAD) software called Rhinoceros 3D [12] and it requires three main types of input data. These are building templates, building geometries, and weather data. A building template is text-based data that includes the essential characteristics of the building, such as the building envelope properties, zone conditioning details, HVAC details, domestic hot water (DHW) details, and building operational schedules. The input of a building template should represent the selected building to ensure the accuracy of the energy simulation. In this sense, necessary permissions to collect the available building data were obtained from the deanery. Two energy audit reports were conducted on campus in 2014 and 2020. These reports contain essential information about the energy performance of the buildings. In addition, the campus buildings' project plans, including architectural, electrical, and mechanical plans, were used to identify and characterize buildings.

The next step is to create a 3D model of the campus. Yandex Map Constructor was employed to create building footprints. Once each building footprint was extracted as a map layer, the final map file was extracted as a GEOJSON file. This file was then inserted into the UBEM.io tool, an online platform to create UBEMs [13]. A GIS interface in UBEM.io ensured that the buildings were in valid coordinates and that the footprints were not overlapping. Then, building heights were inserted into UBEM.io, and a UMI file was obtained. Figure 1 shows the 3D model of the campus building in Rhino. The final input of the campus model is the weather data. There are multiple weather stations near campus. The hourly weather data between September 2018 and September 2023 was obtained from the Turkish State Meteorological Service (TSMS). This data includes temperature, relative humidity, dew point temperature, wind direction and speed, sun exposure intensity, and total precipitation at the hourly resolution within the given years.

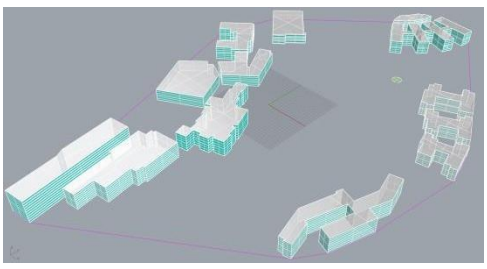

Figure 1. 3D campus model in Rhino

This study's validation data comprises metered data, which includes the natural gas and electricity consumption of the buildings. UMI considers various end-uses to calculate the buildings' energy consumption. Among these, cooling, equipment, and lighting energy uses are powered by electricity, while heating and Domestic Hot Water (DHW) are fueled by natural gas. Despite small air conditioners cooling the offices of dormitory staff, it was assumed that the dormitory buildings did not need cooling. The electricity and natural gas consumption are measured monthly in kWh. These consumption titles were aggregated under a final target end-use called Total Operational Energy (TOE). Minor discrepancies in modeling may cause slight variations in the gross floor area of buildings in the dynamic model compared to the original. To address this, interpreting simulation results in terms of energy use density rather than exact use in kWh can be beneficial. Therefore, TOE was presented as energy use intensity, which is the building energy consumption per gross floor area (GFA) (kWh/m2). The available weather data spans from September 2018 to September 2023. Hence, the average metered data during this period was used to generate the validation data for the dynamic model.

Some of the simulation parameters were extracted from energy audit reports. For instance, these reports provide detailed and consistent thermal transmittance values (U-Value) for each archetype, even though only the ground U-Value has a notable variation among the buildings within the same archetype. Assigning precise values to each parameter from these reports is challenging. For instance, equipment power density (EPD) and lighting power density (LPD) may vary across different zones within a building. Similarly, determining the infiltration rate, which denotes the amount of outside air that enters a building through cracks or openings, is complex due to its varying impact on different areas of the building shell and core. Hence, parameters with inherent uncertainties require careful examination. However, considering the vast number of uncertain parameters, a feature importance analysis should be performed to select which parameters influence the building's energy consumption most. This led us to conduct a Sensitivity Analysis. Two distinct values for all thirteen parameters, resulting in 8192 scenarios, were simulated using UMI. Subsequently, a linear regression model was constructed to observe the relationship between the parameter combinations and the simulated TOE. Linear regression models seek to determine the coefficients of input variables by assessing their impact on the target variable. In this case, the regression model's input variables are the simulation parameters, while the target variable is the simulated TOE. Let us assume a linear regression model with n parameters according to the target TOE. For a given scenario, if x_i is an input variable, a_i is the coefficient of that input, and a_0 is the intercept that represents the bias in the regression model with a standard normal distribution, then this model can predict the target y using Equation 1:

$$y = a_0 + \sum_{i=1}^{n} a_i x_i \qquad (1)$$

In Equation 1, the coefficients were scaled between zero and one to compare the features' importance better. This metric is called relative feature importance (RFI). According to the RFI and correlation values in Table 1, the first five parameters represent most of the variations in the target TOE. Thus, DHW Flow Rate, Heating Set Point, LPD, EPD, and Infiltration were selected to be calibrated using the monthly metered data. The rest of the parameters were assigned to the archetypes using the exact values from the energy audit reports and the project plans.

TABLE I.
SENSITIVITY ANALYSIS RESULTS

Parameter Name	***RFI***	***Correlation***
DHW Flow Rate	0.255	0.595
Heating Set Point	0.234	0.545
LPD	0.159	0.371
EPD	0.159	0.369
Infiltration	0.089	0.208
Occupant Density	0.032	0.074
Cooling Set Point	0.030	0.069
Heating Coefficient of Performance	0.020	0.046
Cooling Coefficient of Performance	0.009	0.022
Scheduled Ventilation ACH	0.007	0.017
Ground R-Value	0.006	0.013

The possible values of the selected parameters were derived from either the energy audit reports or the literature. For example, the maximum and minimum infiltration ratios were set to 0.5 and 0.1 since the campus buildings are relatively new and designed to be energy efficient. Similarly, using the literature, upper and lower limits were determined for EPD [14] [15] [16], LPD [14] [17] [18], and DHW flow rate [14] [19] [20]. Finally, the upper and lower values for the heating set point were determined from the building operational schedules in the energy audit reports. Distinct values of each parameter from their possible value ranges were tested in calibration. Thousands of scenarios with different parameter combinations were simulated in UMI, and their results were evaluated for each archetype at the monthly resolution. In this sense, an error metric called the Coefficient of the Variation of the Root Mean Square Error (CV-RMSE) was used to evaluate the scenario results (Equation 2).

$$CV - RMSE = \frac{\sqrt{\frac{1}{N}\sum_{t=1}^{N}(r^t - y^t)^2}}{\bar{r}} \qquad (2)$$

For a given archetype, r^t represents the monthly target TOE obtained from the metered data, $\bar{r}$ is the average TOE of the monthly metered data, y^t is the monthly simulated TOE, and N is the total number of monthly observations, which is twelve, in Equation 2. CV-RMSE decreases as the monthly simulation errors get smaller and more consistent. Hence, it simultaneously evaluates the stability and accuracy of building energy simulation. Consequently, scenarios exhibiting the lowest monthly simulation errors were identified as the optimal parameter combination for each archetype. The dynamic model was then characterized with optimal parameter combinations. This constituted the calibrated model. The monthly simulation error of the calibrated model was measured at the archetype and campus levels. The comparison between the baseline and calibrated models at multiple spatial resolutions is provided in Table 2.

TABLE II.
MONTHLY SIMULATION ERRORS

Model	**CV-RMSE (Archetype Level)**	**CV-RMSE (Campus Level)**
Baseline Model	0.226	0.139
Calibrated Model	0.169	0.106

STATISTICAL MODEL

Since the monthly simulation error of the calibrated model at the campus level is under 15%, which is a reasonable limit according to a relevant ASHRAE Standard [21], the calibrated model was assumed to be capable of creating hourly energy consumption data for the campus buildings. Hence, the calibrated dynamic model was utilized to create hourly energy consumption data, which served as the validation data of the statistical model. Many data-driven models can predict building energy consumption effectively. However, the objective of this study is to predict the hourly energy consumption, which is a highly time-dependent work. For example, the energy consumption of a building at a specific time step can be influenced by the energy consumption for the previous time steps, as well as fluctuations in the weather data from the previous hours can also affect the upcoming consumption. Therefore, the LSTM model was selected as the statistical model. LSTM models are known for their powerful capabilities in time series analysis with capturing long-term dependencies and patterns in sequential data. Unlike typical feed-forward models, which only consider observations at a given time t, LSTM models retain memory of temporal changes and incorporate them into predictions (Equation 3).

$$y^t = f(x^t, h^{t-1}) \qquad (3)$$

As seen from Equation 3, the activation function in the LSTM models included a memory term h^t when predicting the desired output y^t. This term allows the LSTM to understand the interaction between inputs and targets from a time perspective. Therefore, LSTM models are called sequential models. The sequence length that the LSTM model must cover is uncertain and could be

determined after intensive trials. For example, the sequence length of three comprises the state of the last three hours. This might be helpful when the data does not include long-term patterns, and the targets should be evaluated at small intervals. On the other hand, a sequence length of 24 hours can allow the daily patterns in data to be observed while keeping the hourly patterns. However, as the sequence length increases, the meaning from the small-time intervals vanishes, and the models start capturing the long-term patterns. Also, increasing the sequence length complicates the model structure and yields longer training times. Therefore, the sequence length should be selected carefully.

A single LSTM model was created for each building, which makes 13 models in total. The energy audit report provides the building characteristics, such as GFA, envelope properties, HVAC details, and building operational schedules. However, since each LSTM model includes only one building, most characteristics become impractical in training. For example, let us consider the AB1 building. 8,760 hourly energy consumption was obtained from the UMI simulation using the calibrated model. Some of the input data for AB1, including the U-Value, EPD, LPD, or Heating Set Point, will be static features. This means that these features will be the same for 8,760 observations. The models cannot derive information without variance in the input data. Therefore, all the static features become ineffective. On the other hand, building operational schedules (e.g., heating schedules) and weather data (e.g., temperature) are inputs that change over time. Therefore, the building operational schedules and the weather data formed the primary input source of the LSTM model. The building operational schedules involved the heating, cooling, DHW use, equipment use, lighting use, and occupancy schedules. Meanwhile, the weather data included dry bulb temperature, dew point temperature, relative humidity, wind direction, wind speed, hourly total global solar radiation, sun exposure intensity, and liquid precipitation depth.

However, excluding the static features causes the loss of a massive amount of information since the targets, which are the hourly energy consumption, are shaped by the building characteristics. To that end, the building operational schedules and weather data were combined with the building characteristics. For example, the EPD obtained from the calibrated model was multiplied by the hourly equipment use schedules to create a new feature called Equipment Load Density. This provided an EPD changing over time. The same procedure was repeated for the LPD, DHW Flow Rate, and Occupant Density by utilizing their operational schedules. Additionally, the heating and cooling set points were made functional with the hourly weather data and the building operational schedules for zone heating and cooling. In this way, the heating and cooling setpoints, which are static features, were transformed into features that change over time. The input data was divided into training, validation, and test sets following standard practice in machine learning, with the training set comprising 80% of the observations and the validation and test sets having 10% each. The training and validation sets were utilized for model training to determine optimal hyperparameters over the validation curve (Figure 2). The validation curve in Figure 2 summarizes the hyperparameter tuning process of a sample LSTM model based on the learning rate and the number of epochs. The number of epochs refers to the iterations over the entire dataset during training, while the learning rate determines the step size in updating model weights. In the validation curve, the continuous red represents the training loss, whereas the dashed blue line represents the validation loss. Notably, the slope of the validation loss diminishes as the number of epochs increases. After about 150 epochs, the validation loss stays the same. In contrast, the training loss consistently decreases with the growing number of epochs. This is because the model learns more and more from the training data and starts overfitting. Consequently, this might cause the trained model to lose its generalization capacity and the reduction of the validation loss to be either stopped or reversed.

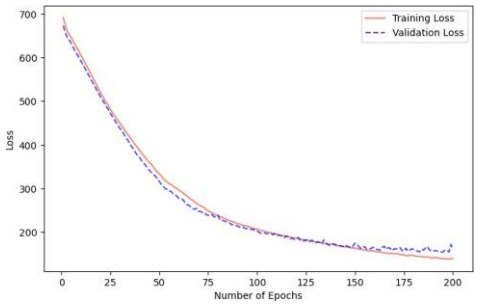

Figure 2. Validation curve of a sample LSTM model

The performance of the trained models was evaluated on the test data using the Coefficient of Determination (R-squared) and Mean Absolute Error (MAE). R-squared measures the proportion of variance in the target variable that can be predicted from the input variables (Equation 4):

$$R^2_{t=1}(r^t, y^t) = 1 - \frac{\sum^N (r^t - y^t)^2}{\sum_{t=1}^N (r^t - \bar{r})^2} \qquad (4)$$

In Equation 4, for a given hour t, r^t represents the target consumption obtained from the calibrated dynamic model, $\bar{r}$ is the average of the targets, and y^t is the predicted consumption of the LSTM model, and N is the total number of observations in our case. An R-squared value of 1 indicates a perfect prediction, meaning that the model's input variables explain all variance in the target variable. In contrast, an R-squared value of 0 suggests that the model explains no variance. The following regression evaluation metric, MAE, measures the average magnitude of errors between predicted and actual values in a dataset. For a given hour t, in our case, where r^t represents the target hourly consumption, y^t denotes the predicted consumption of the LSTM model, and N is the total number of observations in Equation 5:

$$MAE(r^t, y^t) = \frac{1}{N} \sum_{t=1}^{N} |r^t - y^t| \qquad (5)$$

The performance of the LSTM models is illustrated in Table 3. Overall, the regression results are promising. The LSTM models of dormitory buildings and the sports center outperformed the other models. Average R-squared values for the academic buildings are 0.839, whereas the average R-squared value for dormitories is 0.993. This is followed by an average of 0.830 and 0.916 for the social building and sports center. A possible reason for the high accuracy of the dormitory models is that there might be more minor variations in the characteristics of the buildings included in the dormitory archetype. Notably, the proposed LSTM models were equipped only with the non-static features from the building operational schedule and weather data. Integrating the building characteristics, such as envelope properties and HVAC details, can enormously increase the regression performance. However, such static features require different algorithmic approaches when developing time-series models. Overall, the LSTM models yielded an average of 0.915 R-squared value in predicting the hourly energy consumption. This study's evaluation of the LSTM models equipped only with the non-static feature set at the hourly resolution proves that there is still room for improvement.

TABLE III.
EVALUATION OF THE HOURLY PREDICTIONS OVER THE TEST SETS

LSTM ID	***R-squared***	***MAE***
AB1	0.841	166.913
AB2	0.848	137.246
AB3	0.836	69.623
AB4	0.822	212.508
SCOLA	0.849	58.711
OM	0.830	109.739
SM	0.916	27.625
Y1	0.997	8.512
Y2	0.997	6.098
Y3	0.993	7.481
Y4/5	0.991	31.664
Y6	0.982	41.777
GH	0.996	3.711

DISCUSSION AND CONCLUSION

There are examples of studies integrating dynamic and statistical models in UBEM. However, these studies usually suffer from shortcomings such as parameter calibration deficiencies [7], inadequate model validation [8], predictions at low temporal resolution [9], or improper utilization of dynamic models [10]. Thus, there is a need for a novel hybrid approach in UBEM. In this sense, this study developed a hybrid approach by integrating the substantial elements of different modeling techniques in UBEM. First, a calibrated dynamic model created consistent synthetic hourly energy consumption data. The synthetic data then formed the statistical models' validation data. The statistical model performed a time-series analysis and reasonably predicted the hourly energy consumption of the buildings. The proposed approach showed that hybrid modeling techniques can be valuable in UBEM. The calibration of dynamic models, as in this study, can be valuable in creating synthetic hourly data when the available metered data is at lower temporal resolutions. Transforming non-static features of the buildings into time-dependent features by utilizing the building operational schedules proved the importance of occupant-related parameters in UBEM. Similarly, this study emphasizes the value of feature extraction in machine learning based on the solid performance of the LSTM models in predicting hourly energy consumption.

Within the scope of this study, the proposed hybrid model can optimize the building's energy efficiency design by exploring various configurations in the building envelope and operational details and minimizing energy consumption and the resultant environmental impact. For example, different values for the building insulation or various scenarios on the zone conditioning scenarios can be tested over the proposed model, and these results can identify the necessary action to reduce energy consumption. Likewise, the impact of climate change on the observed area can be foreseen and mitigated as the proposed model can utilize the weather data effectively. Moreover, the proposed hybrid model can evaluate the energy reduction strategies at the urban level. Hourly synthetic energy consumption data enable understanding of the deviations in the building energy consumption patterns within higher temporal resolutions. These patterns can be combined with the building characteristics, and the determinant parameters shaping the building energy demand can be extracted. In addition, the proposed hybrid UBEM can guide urban planners in detecting districts with high energy demands and generating energy-efficient interventions for urban building stocks. Such observation and control power allow urban planners to identify areas where energy resources are under significant pressure or where potential inefficiencies occur. Urban planners can also evaluate the potential return on investment for implementing energy-efficient measures in specific areas by utilizing the proposed hybrid model.

Time-dependent features were utilized in creating individual LSTM models, while static features, such as window-to-wall ratio (WWR), infiltration rate, and occupant density, were discarded. As a future work, a joint LSTM model, integrating the input data of all 13 buildings, can utilize the static features left behind. Each building will have its building characteristics in the joint model. Therefore, static feature columns will exhibit variations and be valuable in the joint model. Thermal interaction between the campus buildings is another question to consider in future works. Besides the static features from the building characteristics and the time-dependent features, such as building operational schedules and weather data, the location and the three-dimensional interaction between the campus buildings can be valuable. For example, the surrounding buildings can influence solar radiation on a building's surface. Likewise, the wind effect in outdoor corridors formed by building settlement causes significant changes in the temperature of the building facades. New features can be created to enhance the prediction capacity of the statistical model considering the thermal interaction between buildings. For instance, a

location feature can be added to the statistical model that holds insights into the building's latitude, longitude, and altitude. Another future research direction could be developing an automated decision tool to evaluate scenarios and achieve energy reduction, such as modifying building envelope properties or operational schedules. This tool can accurately predict the impact of any alteration in building characteristics by appropriately incorporating the energy-related parameters of the buildings and climate conditions within the statistical model.

REFERENCES

1 Swan, L. G., & Ugursal, V. I. (2009). Modeling of end-use energy consumption in the residential sector: A review of modeling techniques. Renewable & Sustainable Energy Reviews, 13(8), 1819–1835. https://doi.org/10.1016/j.rser.2008.09.033

2 Hong, T., Chen, Y., Luo, X., Luo, N., & Lee, S. H. (2020). Ten questions on urban building energy modeling. Building and Environment, 168, 106508. https://doi.org/10.1016/j.buildenv.2019.106508

[3] Fathi, S., Srinivasan, R., Fenner, A. E., & Fathi, S. (2020). Machine learning applications in urban building energy performance forecasting: A systematic review. Renewable & Sustainable Energy Reviews, 133, 110287. https://doi.org/10.1016/j.rser.2020.110287

4 Booth, A., Choudhary, R., & Spiegelhalter, D. (2012). Handling uncertainty in housing stock models. Building and Environment, 48, 35–47. https://doi.org/10.1016/j.buildenv.2011.08.016

5 Kazmi, H., Fu, C., & Miller, C. (2023). Ten questions concerning data-driven modelling and forecasting of operational energy demand at building and urban scale. Building and Environment, 239, 110407. https://doi.org/10.1016/j.buildenv.2023.110407

6 Ang, Y. Q., Berzolla, Z., & Reinhart, C. (2020). From concept to application: A review of use cases in urban building energy modeling. Applied Energy, 279, 115738. https://doi.org/10.1016/j.apenergy.2020.115738

7 Yi, C. Y., & Peng, C. (2019). An archetype-in-neighbourhood framework for modelling cooling energy demand of a city's housing stock. Energy and Buildings, 196, 30–45. https://doi.org/10.1016/j.enbuild.2019.05.015

8 Ali, U., Bano, S., Shamsi, M. H., Sood, D., Hoare, C., Zuo, W., Hewitt, N., & O'Donnell, J. (2024). Urban building energy performance prediction and retrofit analysis using data-driven machine learning approach. Energy and Buildings, 303, 113768. https://doi.org/10.1016/j.enbuild.2023.113768

9 Brøgger, M., Bacher, P., & Wittchen, K. B. (2019). A hybrid modelling method for improving estimates of the average energy-saving potential of a building stock. Energy and Buildings, 199, 287–296. https://doi.org/10.1016/j.enbuild.2019.06.054

10 Roth, J., Martin, A., Miller, C., & Jain, R. K. (2020). SynCity: Using open data to create a synthetic city of hourly building energy estimates by integrating data-driven and physics-based methods. Applied Energy, 280, 115981. https://doi.org/10.1016/j.apenergy.2020.115981

[11] Reinhart, C., Dogan, T., Jakubiec, A., Rakha, T., & Sang, A. (2013). UMI – an urban simulation environment for building energy use, daylighting and walkability. Building Simulation Conference Proceedings. https://doi.org/10.26868/25222708.2013.1404

12 McNeel, R. (2008). Rhinoceros: NURBS modeling for Windows. Robert McNeel & Associates, 862.

13 Ang, Y. Q., Berzolla, Z., Letellier-Duchesne, S., Jusiega, V., & Reinhart, C. (2022). UBEM.io: A web-based framework to rapidly generate urban building energy models for carbon reduction technology pathways. Sustainable Cities and Society, 77, 103534. https://doi.org/10.1016/j.scs.2021.103534

14 Deru, M., Field, K., Studer, D., Benne, K., Griffith, B., Torcellini, P., Liu, B., Halverson, M. A., Winiarski, D., Rosenberg, M., Yazdanian, M., Huang, J., & Crawley, D. B. (2011). U.S. Department of Energy Commercial Reference Building Models of the National Building Stock. https://doi.org/10.2172/1009264

15 Mahajan, V., Srinivasan, R. S., Chini, A. R., & Ries, R. (2017). Space-Level Plug-Load densities of educational buildings on university campuses. Journal of Energy Engineering-asce, 143(2). https://doi.org/10.1061/(asce)ey.1943-7897.0000388

16 Chang, R., & Crawley, D. (2018, September). Influence of Plug and Process Loads and Occupancy on Ultimate Energy Savings – a New Approach. 2018 Building Performance Analysis Conference and SimBuild Co-Organized by ASHRAE and IBPSA-USA, 8, 713–720. Retrieved from https://publications.ibpsa.org/conference/paper/?id=simbuild2018_C099.

17 Ashrae. (2020). ANSI/ASHRAE/IES Standard 90.1-2019: Energy Standard for Buildings Except Low-Rise Residential Buildings. ASHRAE.

18 Agency, U. S. E. P., & of Energy, U. S. D. (2006). 6. Lighting. Retrieved from http://www.energystar.gov

19 Murakawa, S., Nishina, D., Takata, H., & Tanaka, A. (2005). An Analysis on the Loads of Hot Water Consumption in the Restaurants.

20 Pérez-Lombard, L., Ortiz, J., & Pout, C. (2008). A review on buildings energy consumption information. Energy and Buildings, 40(3), 394–398. https://doi.org/10.1016/j.enbuild.2007.03.007

21Ashrae, A. G. (2002). Guideline 14-2002: Measurement of Energy and Demand Savings. ASHRAE, Atlanta.

SPONSORED BY:

REHVA Federation of European Heating, Ventilation and Air Conditioning Associations

EUROVENT CERTIFIED PERFORMANCE www.eurovent-certification.com

Enhanced commissioning process to guarantee high performance of hybrid systems in large commercial buildings

Johannes Simola[1, 2], Risto Kosonen[1], and Simo Kilpeläinen[1]
[1] Aalto University, Otakaari 4, 02150 Espoo, Finland [firstname.lastname@aalto.fi]
[2] Lassila & Tikanoja Oyj, Valimotie 27, 00380 Helsinki, Finland [firstname.lastname@lassila-tikanoja.fi]
The Master's Thesis upon which this article is based was accepted at Aalto University in September 2023.

***Abstract*—To achieve the set climate targets, energy-efficient and environmentally friendly heating and cooling systems are needed in buildings. For that reason, hybrid heating systems and energy recycling systems are becoming more popular. Hybrid systems are complex, and it has been noticed that they often have shortcomings in their actual operation. The hypothesis assumed for non-optimal performance is a deficient commissioning process.**

This study focuses on the analysis of how the actual commissioning process of hybrid systems is carried out and how the quality of the commissioning process is affected by the performance of the system. In the literature review, the suitability of different international and Finnish guidelines for commissioning of complex hybris systems are investigated. The main research method was site visits of the case buildings and interviews of the keypersons involved design process of those buildings. Also, the measurement data of the hybrid system was analyzed if the relevant data was available. Based on the findings, suggestions for Finnish commissioning process improvement are proposed.

Hybrid heating systems are life-cycle investments, and their operation should be continuously monitored to verify correct system operation and energy savings. In several studies, commissioning process is one of the most effective ways to reduce a building's energy consumption, and to guarantee high performance of HVAC systems. However, in Finland, the commissioning process is not standardized, and international guidelines are generally not implemented in practice. Finnish practice focuses only on the testing and handover phases. This is not enough to guarantee the designed targets. The analysis carried out clearly indicates that predesign phase and ongoing commissioning should be added to the Finnish instructions. The well-commissioned buildings are in general reached better the set targets than commissioning process was not done properly. Also, the contract form has a direct connection to the result and system operation. Hybrid systems contracted with one proficient contractor operated much better than in buildings where responses are divided with several contractors.

***Index Terms*— HVAC commissioning process, hybrid heating system, heat pump, district heating**

Introduction

Building sector is one of the most significant energy consumers in the Europe. In many countries, heat is mainly produced with the help of fossil fuels. To reach the climate targets, the primary energy consumption of the buildings must be reduced, and efforts must be made to use decarbonized heat production methods. Using waste heat and using renewable energy sources (RES) with heat pumps (HPs) are effective ways to reduce heating power demand and energy usage. With the help of hybrid heating systems, which combine different heat generation methods, it is possible to achieve low carbon dioxide (CO_2) emissions. However, to reach the full potential of these systems, operation should be always guaranteed.

For that reason, the combined heat pump and district heating (hybrid systems) are coming more popular. Those hybrid heating systems are more complex when they use several heat sources. Commissioning process becomes very important to guaranteeing the cost saving and environmental saving potential brought by the new hybrid heating systems.

Several guidelines have been made to guarantee the operation of the heating, ventilation, and air conditioning (HVAC) systems in buildings. For example, HVAC testing and handover instructions by Rakennustietosäätiö (RT) in Finland [1-2], Commissioning process standard and guideline by American Society of Heating, Refrigerating and Air-Conditioning Engineers (ASHRAE) [3-4] and HVAC Commissioning process guidebook by the Federation of European Heating, Ventilation and Air Conditioning Associations (REHVA) have been published [5].

Current guidelines, however, do not directly apply to complex hybrid systems, and it is important to be able to identify the most crucial points. Consequently, guidelines would be needed to ensure the operation of the hybrid heating systems, which are generally perceived as complex to design and operate. According to different interviews, suspicions have been raised that the hybrid heating systems do not work as designed or deficiencies have been detected in their operation.

This research focuses on the commissioning process of the hybrid heating systems covering the whole life cycle. The hypothesis of the study is that the commissioning process is the main challenge. For that reason, designing and technical aspects of the hybrid heating systems are not focused.

All phases from design to actual operation of the hybrid heating systems are analyzed. With the checklist, interviews of the key personnel related to the conducted commissioning process of hybrid heating systems are performed. These key personnel included the property owners, user organizations, designers, supervisors, and contractors. With the help of the checklist and interviews, similarities and differences between the commissioning process conducted were searched for. As a conclusion, key findings are summarized, and proposals are made to improve the commissioning process of the hybrid heating systems.

To analyze the commissioning process and how it could be improved in Finland, the following research questions were formed:

- How is the commissioning process of hybrid heating systems currently done and how the quality of process effects on the performance of the hybrid systems?
- How is the targeted system performance reached with currently implemented processes?
- What are the challenges to enhance commissioning process and how the commissioning process should be improved?

I. HYBRID HEATING SYSTEMS

A. Commonly used hybrid heating systems

Hybrid heating system is a system where several different heat sources are connected, see Fig.1. Examples of those include heat pumps (HPs), heat recovery, thermal energy storage tanks, heat exchangers, district heating (DH), electric boilers, combustion boilers and geothermal wells. Hybrid heating systems aim to use most the available waste heat to achieve the lowest possible greenhouse gas emissions.

Figure 1. Hybrid heating system with multiple heat exchangers and heat sources.

There are numerous options for HP integration in building energy system, for example ground source heat pumps (GSHP), outdoor air to water heat pumps (AWHP) and exhaust air heat pumps (EAHP). GSHPs are often the first choice. However, the lack of free land area is a challenge for building geothermal wells. Hence, hybrid systems with AWHPs have also become common in urban buildings. Currently, the popularity of energy recycling is on the rise and the growth is accelerating due to the increased energy prices, see Fig. 2.

Figure 2. Heat pump operating as an energy recycling heat pump in a hybrid heating system.

In buildings with several heat sources, heat production can be adjusted according to the cheapest energy carrier that covers the heating power requirement. In many hybrid heating system cases, it does not make economic sense to produce peak power with a heat pump, and thus DH or an electric boiler is needed for top up heating power. The concept of the hybrid heating systems depends greatly on the type of the building. In different types of buildings, the possibilities of utilizing waste heat vary greatly. In general, supermarkets and industry have usually waste heat available for use, and it is advantageous to get most of the energy recycled. In Fig.3, an example of view of building automation system of energy recycling hybrid heating system with DH.

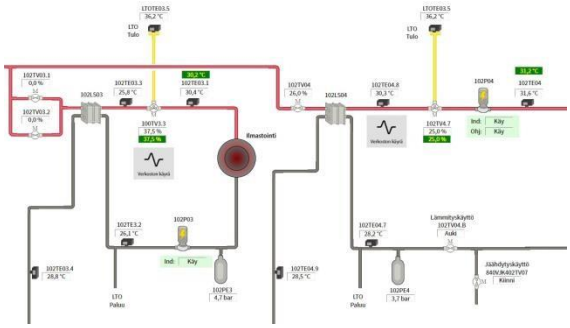

Figure 3. Monitoring view of DH-hybrid heating system.

II. METHODS

The research in this master's thesis was based on the analysis of the commissioning process of eight complex hybrid systems. The common denominator between the case buildings was that the construction process of the hybrid heating system was completed within a few years. All the case buildings were located in Southern Finland and equipped with modern automation systems. Selected case buildings included different hybrid heating systems based on HPs and DH. Most of the HPs were traditional liquid to liquid HPs but there were also some case buildings with AWHPs.

Hybrid heating system implementation, operation, and the commissioning process were detailed analysed in the case buildings. Information and design material related to the hybrid heating system project were also analysed if they are available. With the help of created checklist focusing on separate phases of the project and the analysis of the overall operation, the key personnel of the case buildings' hybrid heating systems were interviewed. Thus, an insight of the implementation and commissioning process of the hybrid heating system, from predesign to system operation and follow up was obtained. Interviewed stakeholders included HVAC designers, consultants, supervisors, equipment suppliers, customer representatives and contractors. Also, the measurement data of the hybrid system was analysed if the relevant data was available. However, in many case buildings, the measured data was not systematically collected and monitored.

Before the interview, it was emphasized to the participants that the names and exact information of the case buildings would not be published, so that they would speak openly and the real problem areas of the hybrid heating systems commissioning process could be clearly noticed. The research was focused on the commissioning process and hence opinions on the design technical aspects of the systems or equipment choices were not asked.

Based on the differences between the form of contract (one responsible company or divided responses), success of the implementation methods and commissioning process were also evaluated.

HVAC process description of the Finnish RT instruction cards in quality assurance, reception procedure the tasks of the documentation instruction [1-2] were used to compile the checklist which was used in the case building research and interviews. The ASHRAE Commissioning Process guidelines [3-4] and REHVA HVAC Commissioning Process guidebook [5] were also reviewed during the development of the checklist. In addition, the checklist was also made to include hybrid heating system specific properties, because the previous mentioned guides did not include hybrid systems directly.

A. Site-related assesment methods

The stages of the commissioning process carried out in the case buildings were compared with the stages given in the guidelines RT, ASHRAE and REHVA [1-5]. With the information from the guidelines, analysis was then made about the importance of the various stages in relation to the commissioning process. The calculated energy consumption in the design phase was compared to the actual energy consumption in the case buildings' hybrid heating systems and an effort was made to evaluate how well the systems operate in the case buildings. The quality of the case buildings' commissioning process was mapped by finding out different completed commissioning measures. The roles of persons in the hybrid heating system projects, were also assessed.

The checklist was used to collect hybrid heating system commissioning information as detailed a level as possible. To get a comprehensive insight of the hybrid heating system projects commissioning process, the checklist included points related to project planning, predesign phase, design phase, hybrid heating system construction, testing, follow up and monitoring. The checklist also included questions related to opinions of experts in the HVAC field. With the various questions and answers, information about the quality of the commissioning process implementation in the different case buildings in Finland could be obtained.

The checklist started with a description of the type and intended use of the case building. It was also determined in the beginning, whether the case building was a new construction project or a renovation project. In some buildings only the heating system had been constructed/renovated. Based on information collected, the size of the project was classified to be either small or large.

After finding out the basic information of the project, the checklist included questions related to the hybrid heating system implementation and commissioning process, from the project predesign phase till to the warranty period and ongoing commissioning of occupied buildings. The checklist phase steps and the most important questions in separate phases are presented in Fig. 4.

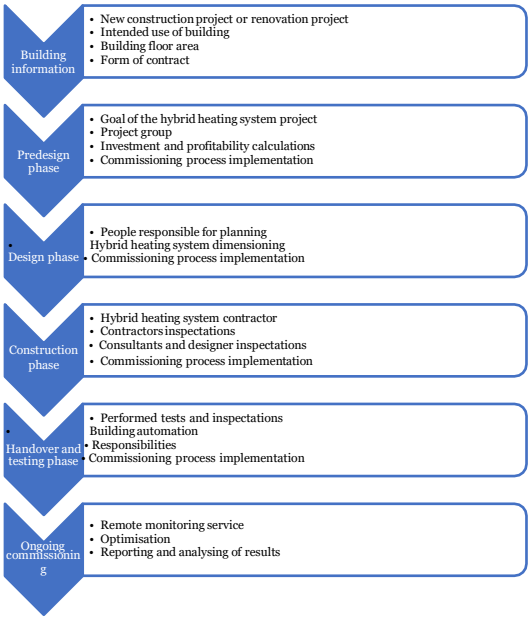

Figure 4. Basic information collected of the case buildings.

B. Analyzed case buildings

The eight case buildings that were the subject of the research and interviews varied in gross floor area between 9000 m^2 and 100000 m^2. The types of properties included residential buildings, office buildings, schools, shopping centers and multi-purpose buildings.

Contract models and commissioning process responsibilities varied between case buildings. Four of the case buildings, and the other four buildings were renovation projects. In each case building, an energy-efficient solution had been the main driver, when the hybrid heating system were selected.

The hybrid heating system of all case buildings included at least two or more heat sources, see Table 1. Free cooling either from geothermal well field or outside air was also implemented into all case buildings. HP and DH were also in every case building, and district cooling (DC) connection was in four case buildings. The basic principle of each system was to use the HP to produce as much basic heating energy as possible and the remaining top up heating with DH.

The power dimensioning of the HPs in the buildings was ranging between 20-50% of the buildings peak power demand and the designed annual energy coverage was between 50-98%, depending on the case building. Depending on the use of the building, domestic hot water production was mainly done with DH in the case buildings. The quantifiable reason for this was the building user dependent high need for domestic hot water or the waste heat available for the use of the HPs. Domestic hot water is usually heated to higher temperature than the heating network and depending on the heat source, it is not necessarily smart to produce domestic water only with a heat pump. The size of the building area limited the number of geothermal energy wells, and thus GSHP capacity, in three case buildings.

TABLE I.
A DESCRIPTION OF THE CASE BUILDINGS IS PRESENTED.

Case building No.	Building type	Building size	Hybrid heating system model
1	New residential building with grocery store and few business spaces	9000m²	GSHP with grocery store waste heat and wastewater heat recovery. Free cooling with wells. DH as top up heating and DC as top up cooling.
2	New School building	9000m²	GSHP with DH. Free cooling with wells.
3	New School building	10000m²	GSHP with DH. Free cooling with wells.
4	Renovated Apartment building area	29000m²	GSHP with DH. Free cooling with wells.
5	Shopping centre	100000m²	HP with grocery store waste heat recovery, exhaust air heat recovery, cooling network waste heat recovery. DH as top up heating.
6	Renovated commercial building	12500m²	AWHP with booster HP. DH as top up heating.
7	New apartment building with offices and market	14000m²	HP with DC return connection. DH as top up heating and DC as top up cooling. Area heating and cooling network.
8	Combination of office/education buildings properties	33000m²	AWHP low temperature area heating and cooling network. DH as top up heating and DC as top up cooling.

III. COMMISSIONING IMPLEMENTATION IN CASE BUILDINGS

The commissioning process is not as well known in Finland as it is described in the ASHRAE and REHVA guidelines [3-5]. In Finland, it is understood purely as the testing and handover phase. The reason for this is related to the instructions in the Finnish RT HVAC commissioning guidelines, where the commissioning process is started during the construction phase [1-2].

When the commissioning process is not started earlier than the construction phase, it cannot address the errors and problems that appear in the project predesign and design phases. In all the case buildings investigated in this study, the RT instructions on HVAC commissioning process were at least partially followed in the operational verification. The RT instructions guidelines on commissioning are quite comprehensive and considers also heating and cooling systems, but they are not detailed for hybrid systems. However, it was possible to notice from the case buildings that they had not been implemented as comprehensively as stated in the instructions [1-2]. Some of the process steps were clearly omitted in the case buildings.

Regarding the case buildings' hybrid heating systems, the commissioning process was performed in different ways. There did not seem to be a clear uniform commissioning way between the case buildings. The methodology of the implemented commissioning process was very much depending on the people involved in the hybrid heating system project. Some of the case buildings, where a hybrid heating system project group was implemented already in the project predesign phase, worked exemplary. When the overall responsibilities of the involved people had been defined, the commissioning process had been carried out with higher quality. In case buildings 2,3 and 4 the implementation of the hybrid heating system was subcontracted in the building construction project, and the

commissioning process was mainly a responsibility of the general HVAC supervisor, who was also the supervisor of another HVAC systems. In case building 4 where hybrid heating system implementation was carried out by HVAC supervisor, many problems were found in the operational tests. Problems generally led to repairs during the warranty period. Deficient commissioning processes were carried out in case buildings 2,3 and 4. Rest of the case buildings included few exemplary and good commissioning implementations. Only in the case building 4 commissioning implementation was poorly done. The professional skills of the people involved in the hybrid heating system commissioning process can be considered to have a direct connection to the commissioning implementation and hybrid heating system operation.

It could be noticed that the title of commissioning provider is quite often confused with HVAC supervisor in Finland. In the case buildings, it was noticed that the qualification of HVAC supervisors is not necessarily sufficient to supervise the implementation of complex hybrid heating systems.

IV. DISCUSSION

International commissioning guidelines compiled by ASHRAE and REHVA are very comprehensive, but many people working in the field of HVAC technology in Finland have probably never heard of these. The benefits of commissioning process starting from the project predesign phase should be made better known to the professionals of the Finnish HVAC and building industry. There are a lot of relevant inspections in the RT instructions available in Finland. However, the commonly used Finnish RT instructions should be updated. Involving commissioning provider from the beginning of the project and predesign phase inspections should be added to the Finnish instructions first.

The implementation of the hybrid heating system project is largely in the hands of the end user. The building owner/investor should be informed the worth to invest in hybrid heating system commissioning process. Hybrid heating systems are life-cycle investments and thus the correct operation of the equipment must be guaranteed throughout its life cycle for the savings to be realized. It is senseless to invest in an expensive hybrid heating system equipment if all its possible benefits are not reached.

Commissioning process costs are small compared to the savings produced during the life cycle of a large hybrid heating system. Therefore, desire and expertise are needed on the customer side right from the beginning of the energy efficient heating project.

The responsible contractor of the hybrid heating system should be a professional contractor who is responsible for the implementation and operation of the entire hybrid heating system. The contractor should understand the equipment installation and system operation. Hybrid heating system contract should not be divided into shared contracts. Hybrid heating system projects should be implemented as overall responsibility contracts.

Using prefabricated systems has been found to reduce installation mistakes. The flow of the information and cooperation between owner/investor, supervisors, equipment manufacturers, designers and contractors are especially important part towards high performing hybrid heating systems. The hybrid heating systems can be made to work when the overall responsibilities and the responsibilities of the parties involved to project are precisely defined. Here are a few ways as an example:

- The project should have a competent commissioning provider who should guide the entire project from predesign to ongoing commissioning.
- One proficient contractor should be responsible for the entire hybrid heating system installation.
- The whole system could be based on a life-cycle responsibility model, in which the property owner buys ‘’heat as a service’’ from the hybrid heating system owner/implementer.

Finding qualified and professional commissioning provider is also a challenge. The commissioning provider should be an experienced specialist in HVAC and automation systems and understand the complete operation of the hybrid heating system equipment (HPs, DH, DC, automation). A classification system should be developed for evaluating the competence of the commissioning provider, where is analyzed commissioning provider’s previous references and experience in similar projects.

The lack of education of the hybrid heating systems in Finland are also a big challenge. There is no direct education for HPs and hybrid heating systems at any level. Hence, there are a lot of self-taught people working in the field and the instructions are partly incomplete. It has also been noticed that not all HVAC designers have the required skills to design hybrid heating systems. Education related to hybrid heating systems should be improved.

A. Reliability of results

One of the biggest challenges is to justify monetary how much improved commissioning process will enhance the performance of the hybrid heating systems. To clarify this, more hybrid heating system case buildings and measurement data on the actual system operation is needed. In this study measurement data of the systems was not very widely available and in some of the case buildings necessary data was not available.

The results of the study correspond to the view of people working in the field, and guidelines, publications and literature research also support these findings. It can therefore be stated that the conclusions can be considered dependable even with the limited amount of tangible measured data available for this study.

B. Further research, documentation and work on guidelines

In the future, the topic could be studied more by testing international commissioning process practice in hybrid heating systems. In these projects, the commissioning process should be systematically conducted in a comprehensive manner, from the project predesign phase

to ongoing commissioning with professional commissioning provider.

The results could be examined for the benefits brought by comprehensive commissioning process weighed against the additional costs arising from commissioning implementation. The hybrid heating system projects implemented according to the international commissioning process guidelines should be compared to the current situation in Finland. The points of inspection could be for example the number of errors detected in the testing and handover phase, and how much energy and emissions could be saved if the system was made to operate optimally directly from the start.

It would also be necessary to make guidelines/classification for the evaluation of the commissioning provider. For example, it could be defined what training requirements, what kind of system knowledge and what references are required from the commissioning provider.

V. CONCLUSIONS

HVAC systems have become even more complex with increasing utilization of waste heat and system electrification. Complex HVAC systems bring challenges for the control of the different sub-systems. Complex systems such as hybrid heating systems with heat pumps and energy recycling do not always work as they should. In this work, the hypothesis was that not well-done commissioning process is the main reason for non-optimal operation. The objective of this thesis was to analyse the actual commissioning process of hybrid systems and effect of the actual performance of the systems. Further, it is proposed how the existing process should be developed.

From the case buildings analysed, it was noticed that the commissioning process is currently implemented in many ways and a uniform manner could not be found between case buildings. The commissioning process was mainly focused on the testing and handover phases, which resulted in warranty-period repairs being carried out in several case buildings. In three case buildings hybrid heating systems worked very well. In all the other five case buildings, problems were found that affected the operation of the system. The most common problems were related to heat collection, automation, or installation errors. The main reason for the problems was the lack of overall responsibility and an inadequate commissioning process without a commissioning provider.

The form of the contract also had a major impact on hybrid heating system operation. The hybrid heating systems contracted by one proficient main contractor worked well. Systems contracted as a shared contract with several sub-contractors were unclear and there were problems with the responsibilities, operation, and coordination of the hybrid heating system. Also, the professional skills and earlier references of the people participating in the process (designers, supervisors, contractors) were found to have a direct connection to the operation of the system.

In the case buildings, hybrid heating systems were working better according to design if the project and responsibilities of the stake holders were clearly defined. It was especially important that responsible people were included from the project predesign to the end of the project. The system should be monitored after the project is completed to ensure designed operation. Ongoing commissioning and comprehensive monitoring of the hybrid heating systems are particularly important to verify that energy is produced and used in an optimal way. Ensuring the hybrid heating system operation also supports the maximizing of environmental benefits, when all the environmental and energy saving potential can be achieved. Thus, complex hybrid heating system projects should have experts who ensure the correct operation of the system from the project predesign phase to ongoing commissioning and life cycle monitoring.

As a development proposal, adding the project predesign phase, design phase and ongoing commissioning phase based on the international guidelines of ASHRAE and REHVA, to Finnish RT instructions would make them more useful. The guidelines do not include hybrid heating systems and it would be beneficial that the guideline involved a comprehensive commissioning process for hybrid heating systems. The process should emphasize the importance of the commissioning provider and the determination of the owner project's requirements before the project implementation.

ACKNOWLEDGEMENT

Special thanks to Prof. Risto Kosonen and D.Sc. Simo Kilpeläinen for their good advice and guidance. Thanks also to everyone who participated in the interviews and case building visits. This study is funded by TALOTEKNIIKKA 2030 programme.

REFERENCES

1 Finnish Building Information Foundation RTS. (2018). RT 10-11301, Talotekniikan laadunvarmistus- ja vastaanottomenettely.

2 Finnish Building Information Foundation RTS. (2018). RT 10-11302, Talotekniikan laadunvarmistus- ja vastaanottomenettely, tehtävät ja dokumentointi.

3 ASHRAE. (2018). Commissioning Process for Buildings and Systems, ANSI/ASHRAE/IES Standard 202.

4 ASHRAE. (2019). The Commissioning Process, ASHRAE Guideline 0.

5 REHVA. (2019). REHVA Guidebook No. 27 - HVAC Commissioning Process.

SPONSORED BY:

REHVA Federation of European Heating, Ventilation and Air Conditioning Associations

EUROVENT CERTIFIED PERFORMANCE www.eurovent-certification.com

Investigating the on-site consumption of PV system production in residential buildings

Gyula Richárd Kiss [1] - Dr. Miklós Horváth[1]

[1] Budapest University of Technology and Economics, Faculty of Mechanical Engineering, Department of Building Services and Mechanical Process Engineering

***Abstract* — The focus of this article rises from the substantial growth in installed solar PV capacity, which is disrupting the stability of the electric grid. Integrating renewable energy systems poses a challenge because of the restricted ability to regulate the electricity grid, stemming from insufficient and readily accessible storage solutions. Consequently, our primary aim is to enhance on-site consumption of PV-generated electricity, thereby reducing the negative effect of the increased PV capacity. This objective can be realized through the implementation of smart control mechanisms and the adoption of energy storage technology. Our study investigates the impact of battery storage on the on-site utilization of PV system output across various HVAC systems and battery configurations. We analyze the interaction between different types of batteries, the size of PV systems, and annual electricity consumption patterns. By leveraging our findings, it becomes possible to assess the viability of different battery setups in relation to household consumption habits and PV system specifications.**

***Index Terms*— solar power generation, residential building, battery, battery storage, building simulation.**

Introduction

In our study we've investigated battery storage for household PV systems and its effects on different technical building systems and batteries. We aim to address the interactions between batteries, solar PV systems, annual electricity consumption and hourly electricity consumption profiles. Our work provides the foundations to determine – based on the consumption of a family house – which system will have an impact on the utility bills, so that users can choose the best solution for them.

I. LITERATURE REVIEW

A. Design of solar systems

Solar PV systems can be divided into three groups, depending on whether they are connected to the public electricity grid and whether the system has electricity storage. Thus, we can define on-grid, off-grid and hybrid systems. In grid-connected systems, there is usually no battery storage, in which case the electricity is stored by the electricity grid. In an off-grid system, there is no connection to the grid thus electricity storage is required. hybrid systems can be split into two subsystems with and without feedback. [1].

B. Solutions to increase on-site use and storage of solar electricity

The generated electricity is best used locally, so we need to match our consumption patterns to the energy generation, considering the power available and the performance of the equipment we use. The main objective is to reduce the amount of electricity drawn from the grid as much as possible, to limit the necessary drawdown to the evening or in the shaded periods and to operate mainly only those consumers whose operation is essential, e.g. refrigeration, heating system, electrical equipment and lights. This can be easily achieved with smart home control, for which there are already many industry solutions available today.

Another type of storage is to "cool" or "heat" using the excess energy available. This can mainly be the case in the following situations:

- DHW production;
- building mass tempering;
- heating/cooling thermal storage.

The energy produced and not consumed can also be stored in the form of electricity for later use with the installation of batteries. For battery energy storage, an important parameter is the electricity distribution scheme and the length of time we want to operate the system. There are different schemes to choose from, e.g. peak-shaving, SUB (solar-utility-battery), SBU (solar-battery-utility). The battery charging can be prioritized as well, whether it should be solar, grid or combined. In our study, only solar energy was used to charge the battery.

In our research, we looked at battery storage and consumption optimization in more detail and examined their interactions.

C. Battery types

In order to operate off-grid or hybrid systems batteries needed to be installed The batteries have to be connected in series and in parallel to achieve the correct operating voltage and capacity. The resulting battery pack must be optimised to maximise its lifetime. Their lifetime and price vary depending on whether we are talking about lead-acid, gel and unsaturated glass-fibre (AGM), Li-ion or LiFePo4 (LFP) batteries, their lifetime and price also increasing in that order [2]. Inverters of different power ratings may have different battery packs with different terminal voltages, the most common being 12 V, 24 V, 48 V systems, but it should be noted that the higher the terminal voltage, the lower the currents required to serve the given power, thus reducing the wire cross-sections, which can lead to cost efficiency as well as system safety. We studied the 48 V systems, since this is where the highest charging power is available, and the most common battery types: lead-acid, AGM, LFP. [2]

Lead-acid batteries have a very short life, while Li-ion batteries have a long life, but are sensitive to temperature, which is overcome by the more recently used LiFePo4

(LFP) battery. At a maximum of 50% immersion, it can last about 200 cycles and is highly susceptible to rapid degradation and sulphation. There is also a maintenance-free version that does not require topping up with distilled water.

AGM batteries should be charged up to a maximum of 50%, at which point they will last an average of 1000 cycles, and at 100% discharge this is reduced to a few hundred cycles.

Li-ion batteries should be submerged to 80% of their maximum capacity, avoiding the risk of deep discharge (DoD). The ideal temperature range is 15-35 °C. The chance of self-discharge is low, they are fast to charge and discharge and have a long life. [3]

Since the rates and times of solar generation and consumption do not overlap, we need to include storage, the proportions of which are shown in Figure 1. [3]

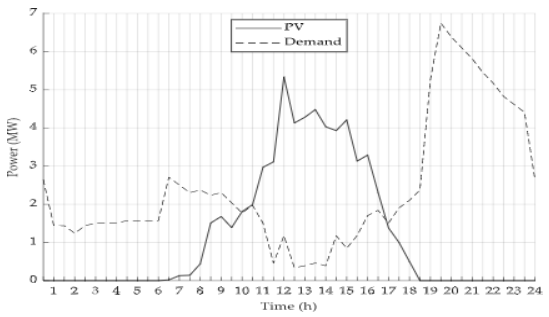

Figure 1. Solar PV system and power consumption per day [3]

When charging series and parallel connected batteries, an imbalance in the charge between the cells can occur and a charge balancer should be used to avoid this. The battery manage system (BMS) eliminates the difference in charge between the different battery units, thus increasing the battery pack life as there is no overcharge or deep discharge in the individual cells. It is recommended to keep the DoD between 50-80%. [4].

Another important characteristic of batteries is their charge and discharge rate, which is characterised by the C-rate. "*The capacity of batteries is usually defined in 1 C, which means that a fully charged battery with a capacity of 1 Ah should provide 1 A for one hour.*"[5] TABLE I. shows the recommended C-ratio and life expectancy of different types of batteries at the given C values. [5]

TABLE I.
C-RATIO AND LIFE EXPECTANCY OF DIFFERENT TYPES OF BATTERIES [5]

Type	Capacity	Charging C-rate	Discharging C-rate	lifecycle
lead acid	35-40 Wh/kg	0,5-1 C	1 C	<350
NiMH	60-120 Wh/kg	0,7-1 C	1-15 C	500-2000
Li-ion	100-265 Wh/kg	0,7-1 C	1 C	400-1200
LiFePO4	90-120 Wh/kg	1 C	1-25 C	1000-2000

II. BRIEF BUILDING DESCRIPTION, ELECTRICAL PROFILES

A. Simulation model of the building

Based on the residential typological surveys carried out in Hungary, we can distinguish 23 residential building types, of which we worked with type 4, built between 1945 and 1959, but the studies can be carried out for any building type following the process below. [6]

The simulation was carried out using DesignBuilder v7 [7], in which a model of the building was created based on the available data. The available data were the floor areas of each room, the masonry, the layering of the slabs and their properties, and the size, orientation and properties of the windows and doors. The resulting model is shown in Figure 2.

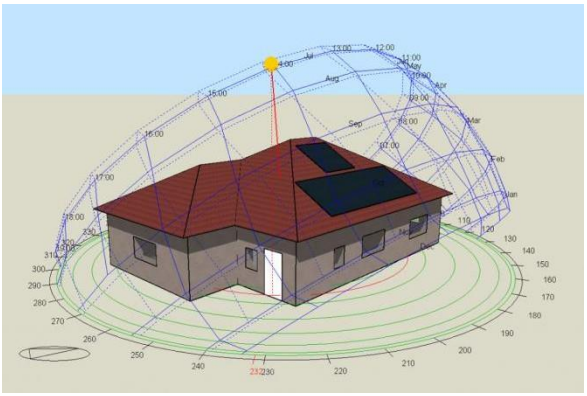

Figure 2. Figure, Image of a building model built in DesigneBuilder v7

For the simulation, the DHW requirements were determined according to the Hungarian regulations (TNM Decree 7/2006) [8], which were entered in the program as a function of the floor area of the bathroom and kitchen. The occupancy schedule was taken according to the standard MSZ-EN-16798-1_2019, assuming a single-family case and considering working days and holidays. The infiltration was set to 0.7 1/h based on building typology data, considering the air leakage from the unsealed air duct. The air exchange schedule was modelled differently in winter and in summer: in the summer period above the minimal airchange an intensive night ventilation was added. The weather data (typical meteorological year) were provided based on GPS coordinates N47.430, E19.182 and considering the time period 2005-2020. For heating, an operative temperature of 20 °C was set, while the setback was 16 °C. For cooling, the operative temperature was set at 26 °C and the setback was 32 °C.

B. Heat generators and heat transmitters

The building was tested in an uninsulated condition, our heating and DHW producer was in one case a 10 kW heat pump with a 300 l buffer tank, which was heated in winter and cooled in summer, our heat emitter was a fan coil system, as this type of heat exchanger is the easiest to install in this building during a renovation to provide both cooling and heating. In another case, it was a condensing combi gas boiler and radiator. These variable parameters were simulated using the DesigneBuilder v7 program at a resolution of a full year, yielding 8760 data points, which were imported into the System Advisor Model v2021

(SAM) [9] program where the solar PV system and battery storage were simulated.

C. Electricity profiles

One of our input parameters was the different household electricity consumption profiles. This was an attempt to model the impact of different user habits. Different profiles imply different power demands in the same hour. The nature of the profiles we have defined is shown in Figure 3. , which were prepared by László Czétány and colleagues for the domestic building stock. [10]

The CI profile has an annual electricity consumption of 2814 kWh/yr, while the CII and CIII profiles have a consumption of 2364 kWh/yr and 3092 kWh/yr respectively. The annual consumption is adjusted by the specific consumption per floor area of the profiles, which for this building is given in TABLE II.

Figure 3. Solar PV system and power consumption per

TABLE II.
ANNUAL AND SPECIFIC CONSUMPTION FOR DIFFERENT CONSUMPTION PROFILES

profile	CI	CII	CIII
annual consumption	2814 kWh	2364 kWh	3092 kWh
specific consumption	5,95 W/m²	4,67 W/m²	4,87 W/m²

III. THE CASES EXAMINED

A. The solar system designs under study

Our variable parameters were the consumption data, which were derived from the heat production and consumption profile data described earlier. These were used to investigate the distribution of solar energy consumed locally, electricity consumed from the battery and electricity purchased from the grid for different battery types and capacities. The battery variants we studied are shown in TABLE III.

TABLE III.
1. THE BATTERY TYPES AND CAPACITIES WE TESTED.

Lead Acid	5 kWh	10 kWh	15 kWh	20 kWh
AGM				
LFP				

In SAM, you can set the right electrochemical model for each type of battery. To do this, you need to know the cell allocation, capacity, nominal, discharged and fully charged voltage ranges, allowable charge and discharge currents, and energy density of the battery. Based on these, the program can also calculate the battery life, number of cycles, discharge depth and battery temperature.

The parameters we recorded, according to the data provided by the manufacturer, for batteries with a capacity of 5 kWh and different electrochemical types are shown TABLE IV.

TABLE IV.
2. THE PROPERTIES WE HAVE INCLUDED DEPENDING ON THE BATTERY TYPES

Electrochemical type		**Lead Acid**	**AGM**	**LFP**
Design performance	kW	1,2	1,2	2.56
Design capacity	kWh	5	5	5
Design voltage	V	48	48	51,2
Cell voltage	V	12	12	3,2
Cell capacity	Ah	110	110	100
Cell resistance	Ohm	0,25	0,25	0,002
Discharged voltage	V	12	12	2,7
Nominal Voltage	V	12,7	13	3,2
Exponential voltage	V	12,9	14,5	3,6
Charged voltage	V	13,2	14,8	3,7
Energy density	Wh/kg	60	43	56,26

The simulations were started with fully charged batteries, with a maximum charge of 95% and a minimum charge of 10%, thus increasing their life expectancy. The simulation duration was set to 20 years.

IV. RESULTS

A. Testing the lifetime of different battery types

The lifetime was examined assuming the input data given above. Figure 4. illustrates that the lifetime decreases very drastically with an Acid battery, with a lifetime of only 4 years and a significant decrease in the usable capacity and thus in the amount of electricity that can be drawn from it, year by year. AGM batteries have a lifetime of only 1 year more, i.e. 5 years, but unlike an acid battery, you can draw almost as much power from it in the first two years, and then it loses capacity drastically. LFP batteries, on the other hand, can deliver almost constant energy over their entire lifetime, which can exceed 30 years if there is no cell failure. As capacities increase, lifetimes are only slightly extended. It is striking that the 10 kWh LFP battery can provide nearly 600 kWh more electricity per year compared to the 5 kWh LFP battery. This is because the 5 kWh capacity battery is not able to accommodate the summer solar peak, so less solar energy is stored in the battery.

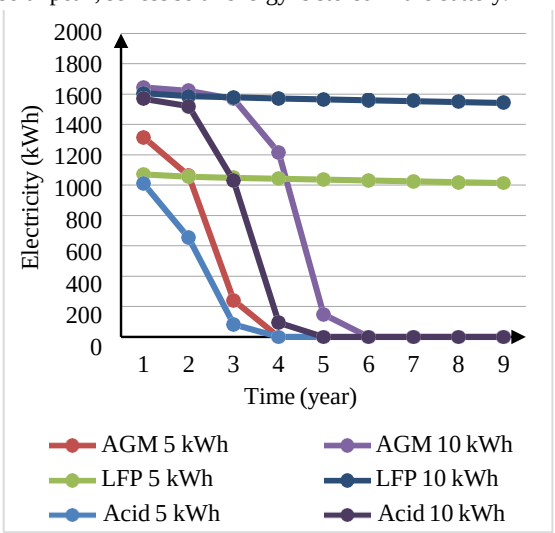

Figure 4. The electricity used from batteries over the years

In all of our simulations we found that the 5 kWh battery had significantly more cycles compared to the 10, 15,

20 kWh capacity batteries, but we did not observe such a difference in cycles between the 10, 15 and 20 kWh batteries. Battery manufacturers often specify the warranty period of their products in years or cycles, so for a 5 kWh battery this may be less. This is illustrated in Figure 5.

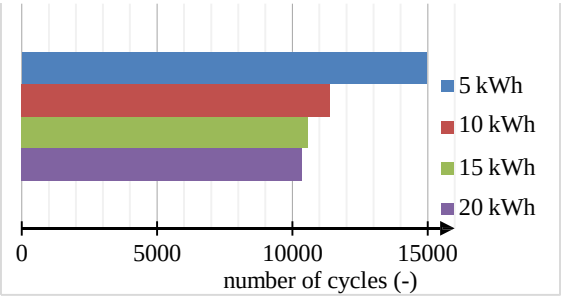

Figure 5. Number of cycles of LFP batteries of different capacities over 10 years

Looking at the different cases, based on 5-10 kWh batteries, we obtained a best-case lifetime of 5-6 years for acid, of which 2-3 years can be calculated for cost analysis, for the reasons mentioned above. In case of the AGM battery, the total lifetime is 5-7 years, but only 4-5 years can be considered for cost analysis. For LFP batteries, even with a 20-year simulation, they would still have 88-90% of their rated capacity but would require replacement or repair in case of cell failure, which can be costly if it is needed after the manufacturer's warranty period.

As the LFP battery has the longest lifetime and can extract nearly the same amount of energy over the years, we will focus on this type of battery in the following.

B. 4.2. Factors affecting the amount of electricity used locally by solar panels

Figure 6. shows the amount of electricity used locally per year for solar panels in different orientations. The building under study has a default south orientation, and the diagram shows that the highest amount of electricity used locally is in this case. All other orientations have significantly lower energy use. With an eastern orientation, we can use more electricity locally in the winter months compared to a western orientation, but this is reversed in the summer when we can use more electricity locally with a western orientation.

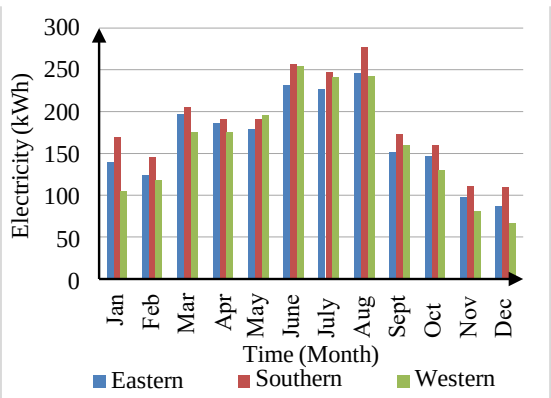

Figure 6. Variation of annual in-situ solar energy as a function of different orientations

C. Impacts of solar PV systems with different outputs

A solar PV system with a maximum capacity of 4 kWp can be installed on the roof of the building, but for the sake of interest, we have theoretically investigated how the ratio of solar energy used locally, electricity drawn from the battery and electricity drawn from the grid varies for different installed capacities of solar PV systems. We have also examined how the amount of solar energy lost varies compared to the net metering, this loss coming from conversion on the one hand and from the finite capacity of the batteries on the other.

Figure 7. and Figure 8. show the winter electricity distribution of the 4 and 8 kWp solar PV system. The C1 profile simulated system has the above mentioned HVAC design and 15 kWp LFP battery with a test period of 20 years. The inverter efficiency and battery charge are also marked in the figures. It can be clearly observed that the solar energy used in the 8 kWp system is unchanged compared to the 4 kWp system, but the difference in the amount of energy used from the battery is very significant between the two systems, in favour of the 8 kWp system. Since the amount of electricity used from the battery has increased and the amount of solar energy used locally is unchanged, the difference reduces the amount of electricity used from the grid. The inverter efficiency did not change significantly or fluctuate during the period studied.

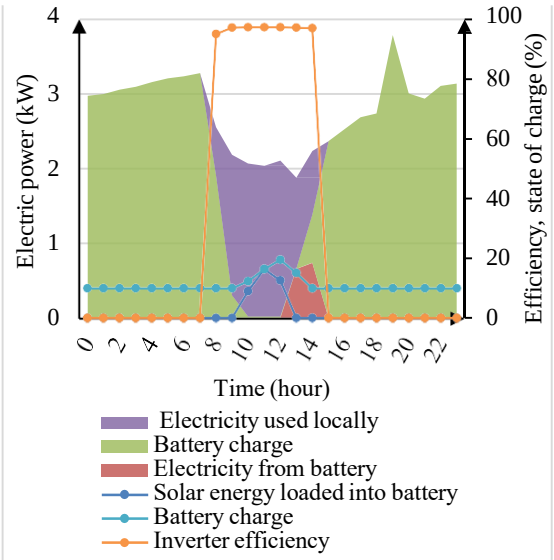

Figure 7. Distribution of electricity from a 4 kWp solar PV system in winter

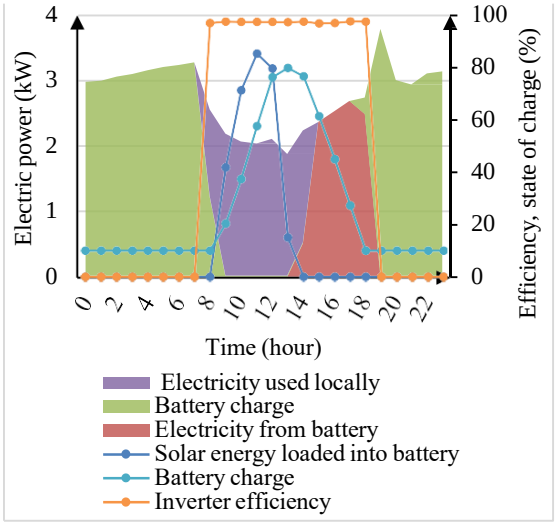

Figure 8. Distribution of electricity from an 8 kWp solar PV system in winter

Figure 9. and Figure 10. show our system in the summer case. It can be clearly seen that there is no significant difference between the 4 and 8 kWp systems in the summer case, both can fully meet the demand. In the 8 kWp case the amount of solar energy used locally is higher, but in the 4 kWp case this difference is easily compensated by the battery. In summer, the fluctuations in inverter efficiency are already noticeable, caused primarily by the charging and discharging of the battery. It can be clearly observed that as the battery charge decreases, the inverter efficiency starts to decrease. The C1 profile is nicely plotted over the time period studied. Between 8 pm and 2 am the peak caused by DHW is seen, which also appears between 5 am and 7 am in the morning.

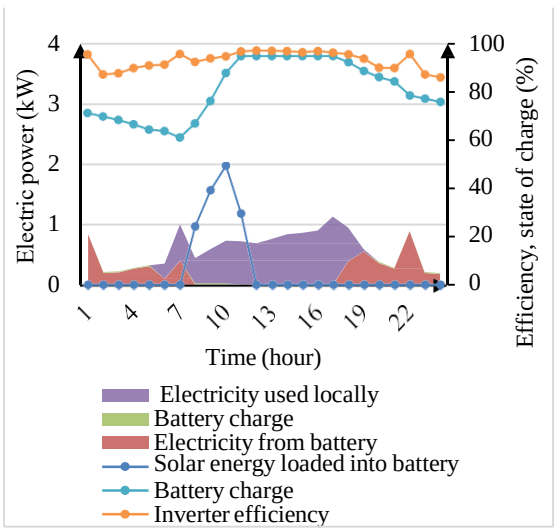

Figure 9. Distribution of electricity for a 4 kWp solar PV system in summer

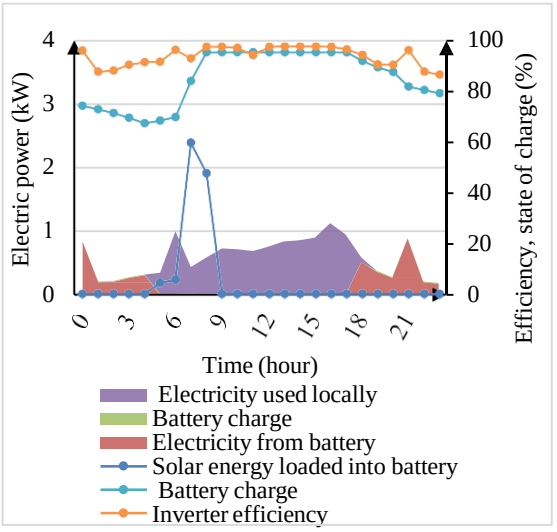

Figure 10. Distribution of electricity from an 8 kWp solar PV system in summer

Significant differences were found between the amount of solar energy used locally, especially in the winter months. This is due to the fact that the power consumption of the heat pump is very high during this period, so the higher capacity solar PV system can more easily serve this higher power demand, while in spring and autumn, due to the reduced electricity demand, there is less difference between the installed capacities compared to the winter case. In the summer case, when cooling demand also appears in the consumption data due to the heat, there is also a big jump, but compared to the winter case, the difference between 4, 6 and 8 kWp systems is smaller in summer. From this we conclude that there is not enough consumption demand, leaving the 6 and 8 kWp solar PV systems underutilized, as all three systems show a large jump compared to 2 kWp, so 2 kWp is not enough for this consumption, these are shown in Figure 11.

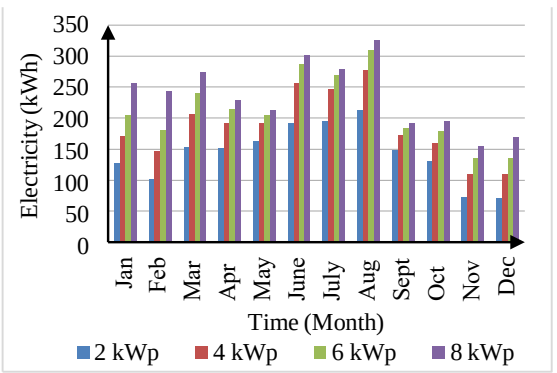

Figure 11. Annual solar energy used on-site based on the installed capacity of the solar PV system.

D. Impact of different consumption profiles

Since the maximum solar capacity that can be installed on the type 4 house, we studied is 4 kWp, we have used this as a basis for the rest of our calculations.

We considered it very important to examine the impact of consumption profiles, as this is determined by the basic

user habits. The simulation was performed for an uninsulated building, assuming a condensing combi gas boiler and a 10 kWh LFP battery. In this case, the electricity consumption is exclusively the consumption from the household. In the case of the CII consumption profile, the annual battery state of charge was significantly higher, due to the fact that the consumption demand was shifted, mainly in the afternoon and evening hours, and the power demand was not high, so that the battery could be charged while the sun was shining. However, the solar energy consumed locally was significantly lower for the CII profile than for the CI and CIII profiles, precisely because of the afternoon peak demand. For the CII profile, the battery could be used more often due to the high hourly charge, hence the DoD percentage was higher here and this is the reason why the battery capacity loss is highest for this profile. The annual power consumption of CI and CIII profiles is significantly higher than that of CII profile. Since in winter there is a drop in solar PV generation, which prevents the batteries from recharging, the electricity drawn from the grid is very high. In summer there is no significant difference between the profiles. These are illustrated Figure 12.

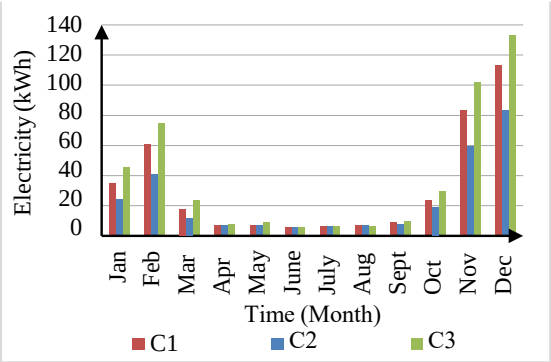

Figure 12. Annual electricity drawn from the grid, based on consumption profiles.

V. SUMMARY

In our study, we investigated the impact of different battery, solar PV systems and consumption profiles on electricity use and battery lifetime. There was significant variation in degradation between battery types. Acid batteries fail very quickly, with a lifespan of 3-4 years, but can only provide a steady supply of energy for 1-2 years. AGM batteries can have a lifetime of 5-6 years, but these batteries can only provide nearly the same energy for 3- 4 years. LFP batteries have been simulated to have a lifetime of more than 30 years, based on the input parameters and have been able to deliver constant energy throughout their lifetime. Based on our simulations, the optimal battery capacity under the considered boundary conditions is 5 kWh.

Consumption profiles have a significant impact on the amount of electricity used on site. Consumption adapted to the duration and scale of solar generation will result in more solar energy used locally.

A larger PV system is particularly useful during the winter months, when there are fewer hours of sunshine, while in summer the output of the different systems is more balanced, with significantly more production relative to consumption. Higher capacity solar systems can charge batteries to a greater extent, so for the same consumption profile, the amount of solar energy used locally was also higher in absolute terms for the higher kWp systems, especially in the winter months.

A further area of research could be how electricity use can be improved by matching consumption to solar generation, thereby increasing the amount of solar energy used locally, which can be best achieved through smart controls and smart buildings. Investigating the payback of a solar PV system without back-feeding or batteries based on consumption data.

REFERENCES

[1] Energy Education, ‘Photovoltaic system’, 2022, Accessed: Oct. 22, 2022. [Online]. Available: https://energyeducation.ca/encyclopedia/Photovoltaic_system

[2] P. J. Kollmeyer and T. M. Jahns, ‘Aging and performance comparison of absorbed glass matte, enhanced flooded, PbC, NiZn, and LiFePO4 12V start stop vehicle batteries’, *J Power Sources*, vol. 441, p. 227139, Nov. 2019, doi: 10.1016/J.JPOWSOUR.2019.227139.

[3] P. Boonluk, S. Khunkitti, P. Fuangfoo, and A. Siritaratiwat, ‘Optimal siting and sizing of battery energy storage: Case study seventh feeder at nakhon phanom substation in Thailand’, *Energies (Basel)*, vol. 14, no. 5, 2021, doi: 10.3390/en14051458.

[4] M. O. Qays, Y. Buswig, M. L. Hossain, and A. Abu-Siada, ‘Active charge balancing strategy using the state of charge estimation technique for a PV-battery hybrid system’, *Energies (Basel)*, vol. 13, no. 13, 2020, doi: 10.3390/en13133434.

[5] Off-grid Solar, ‘Akkumulátor C-ráta (C-rate)’. Accessed: Dec. 02, 2022. [Online]. Available: https://offgridsolar.hu/wiki/akkumulator-c-rata/

[6] Csoknyai Tamás, Farkas János, Formanek László, and Horváth Miklós, *Épülettipológia tanulmány,*. Budapest, 2015.

[7] DesignBuilder Software Ltd., ‘DesignBuilder’, 2022, Accessed: Feb. 25, 2024. [Online]. Available: https://designbuilder.co.uk/

[8] Magyar Közlöny, ‘TNM Decree 7/2006’, 2006, Accessed: Feb. 25, 2024. [Online]. Available: https://njt.hu/jogszabaly/2006-7-20-6F

[9] National Renewable Energy Laboratory (NREL), ‘System Advisor Model (SAM)’, 2022, Accessed: Feb. 25, 2024. [Online]. Available: https://sam.nrel.gov/

[10] Czétány László *et al.*, ‘Development of electricity consumption profiles of residential buildings based on smart meter data clustering, Energy and Buildings. 252 (2021)’. Accessed: Nov. 10, 2022. [Online]. Available: https://doi.org/10.1016/j.enbuild.2021.111376

Effectiveness of window signalling systems in open-plan workplaces: evidence from field work

Author: S. (Serhan) Yüksel MSc **Year:** June 2023 **Institute:** Delft University of Technology (TUD)
Supervisors: P. (Pedro) de la Barra Luegmayer MSc, Prof. A.C. (Atze) Boerstra, Dr. A. (Alessandra) Luna-Navarro

Abstract — Occupants are often unaware of window-opening strategies that can enhance their well-being and reduce energy consumption. Window feedback systems that indicate when to manually operate a window have become a strategy for enhancing the indoor climate, occupant satisfaction and energy efficiency. These systems are recognized for providing the comfort benefits of manual window controls while providing the efficiency benefits of completely automated windows. However, there is a lack of evidence to what extent window feedback systems are able to guide occupants towards an effective window operation for both energy and comfort.

This research proposes a new window feedback system based on indoor air quality, thermal quality and energy performance. Results from preliminary testing and deployment are also presented to investigate the effectiveness of the light window feedback system. As part of the testing, both an existing and a new situation were analysed in an open-plan workplace for six weeks. The existing situation served as a benchmark for the new situation in which the window feedback system was implemented. The outcome of the research shows that ambient light window feedback systems can improve the indoor environment and occupant satisfaction in open-plan workplaces. Objective measurements reveal an improved indoor temperature, relative humidity and CO_2 concentration. Furthermore, it shows a reduced ineffective window opening time by 55%. Subjective measurements validate the objective measurements by showing a higher satisfaction of the thermal environment and indoor air quality. In addition, subjective measurements reveal that a majority of the respondents understand the system, act according to the provided feedback and are satisfied with the implementation. As a result, the improvement of the indoor environment and corresponding satisfaction can be related to the window feedback system. The outcome of this research provides also design requirements for further development of the light window feedback system and its algorithm.

***Index Terms* — behaviour, energy efficiency, feedback, indoor climate, satisfaction, window**

I. Introduction

Energy efficiency has been recognised as an important strategy to minimise climate change. One significant barrier to energy-efficient buildings is the lack of understanding about the real functioning of a building once it is built. The predicted energy use of buildings does frequently not match the real energy use and is caused by several factors such as construction and weather conditions. Several studies argue that the occupant's behaviour could also be a reason for this mismatch [1] [2]. It appears that occupants influence energy consumption by using different interfaces such as windows, window shades, thermostats and lighting controls [3].

A. Research problem

Especially window opening behaviour can have a significant impact on energy consumption since it is directly related to the thermal environment, indoor air quality, energy efficiency and occupant's satisfaction [4]. Despite the importance of window operation, occupants are often unaware of window-opening strategies that can enhance their well-being and reduce energy consumption. Both manual and automated window control have their flaws. Automated window control provides more energy efficiency but comes at the expense of occupants' comfort, satisfaction and productivity. Manual window control provides a wider comfort band but bears the risk of inefficient energy use. A feedback system for manual window control could be a compromise in which occupants get the ability to satisfy their comfort, while being informed about the impact of window operation on the indoor climate and energy efficiency to enhance their behaviour [3] [5]. However, there is a lack of evidence to what extent window feedback systems are able to provide successful cooperation between occupants and windows which enhances energy efficiency, satisfaction levels and their well-being.

B. Status quo of research in window feedback systems

The impact of window feedback systems on the indoor environment and/or occupant satisfaction is rarely evaluated in the literature. Only six case studies were found in which none conducted both objective and subjective measurements to validate the results. Only the study of Ref. [6] focused on subjective measurements and revealed considerations for implementing a window feedback system. According to their findings, window feedback has the most influence when it is clearly visible, the logic behind it is understandable, and when it is linked with motivational factors that promote comfort and energy efficiency. Other studies conducted objective measurements and lacked support to relate the results of the indoor environment to the window feedback. In addition, these studies had limitations regarding the test group size, window feedback system design and data collection.

C. Research goal and scope

This study aims to (i) gain evidence on the effectiveness of window feedback systems in improving the indoor climate and occupant satisfaction, (ii) and provide design guidelines for the further development of these systems. This is achieved by collecting objective and subjective data

from an existing and new situation in an open-plan workplace for six weeks. The existing situation served as a benchmark for the new situation in which an ambient light window feedback system was implemented.

II. METHODOLOGY

A. *Description case study*

The experimental study was performed in the building technology studio of the TU Delft's faculty of architecture and the built environment. This studio is located on the West wing of the second floor and functions as an open-plan workspace for both students and professors. The studio is characterized by its narrow plan, multiple façades, many (tilted openable) windows, international-originated occupants and peak periods with high volumes of users. The heating is controlled by radiators and the ventilation is regulated by mechanical in and outlets. The studio does not have an air conditioning system. Measurements were performed in the middle section of the studio, as shown in Figure 1, and represents a typical open-plan workplace.

Figure 1. Photo of the investigated middle section of the building technology studio. The table numbers correspond with Figure 2.

B. *Experimental design*

Objective and subjective measurements were conducted from 3 to 21 April 2023 for the existing situation, and from 24 April to 12 May 2023 for the new situation. This period was characterized by its varying warm and cold weather with sunny and rainy days. Everyday data was collected from 9:00 till 19:00. No data was collected during the weekends, holidays and incidentally other days. Occupants were informed about the window feedback system before the implementation in the new situation.

The objective measurements served to analyze and compare the indoor environment in both situations. These measurements included monitoring the indoor and outdoor temperature, relative humidity (RH), Particulate Matter 2.5 ($PM_{2.5}$) and Particulate Matter 10 (PM_{10}). In addition, the indoor carbon dioxide (CO_2), window operation and convector operation were monitored. The data of the sensors were collected by a Raspberry Pi 4 model B and were sent through a connector called WeMos D1 mini pro. This connector was attached to each sensor and created its own network together with the Raspberry Pi. Figure 2 provides an overview of the sensor placement with the corresponding parameters. This figure shows that the indoor temperature, RH and CO_2 concentration were measured on both room level (table 3) and desk levels (table 1 and 2) to enable a comparison between both. The CO_2 sensors were placed at breathing height and placed away from the windows to avoid inaccuracies.

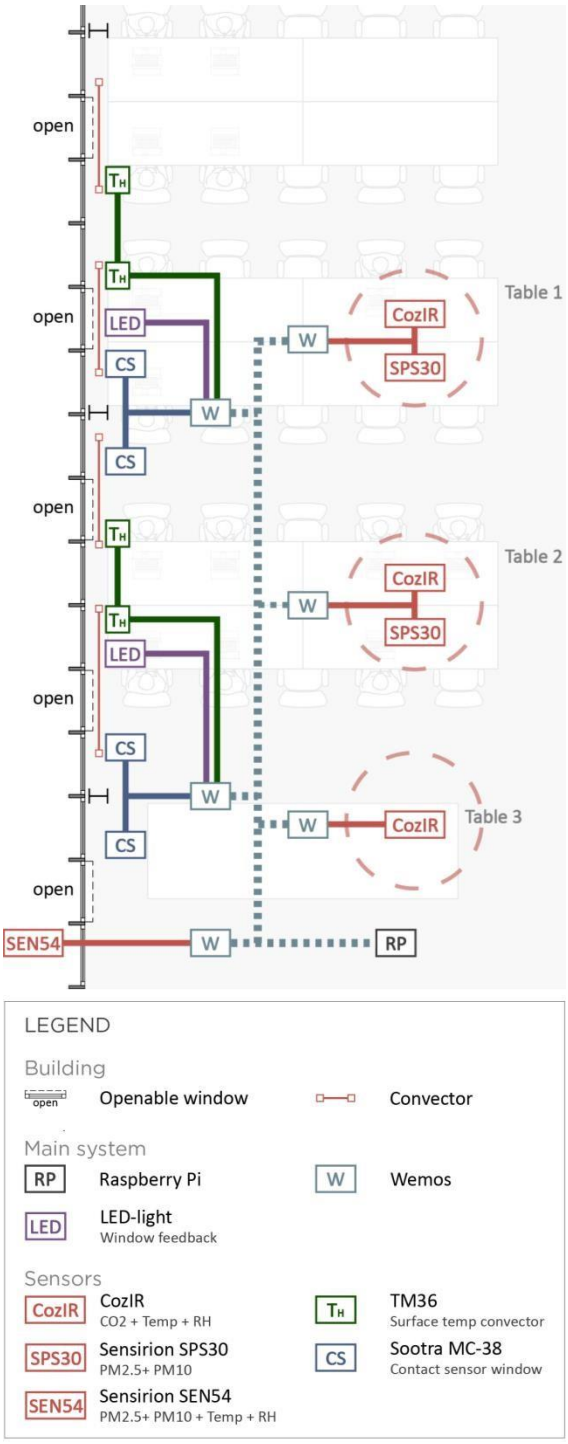

Figure 2. Plan indicating the placement of sensors, window feedback systems and other hardware with corresponding connections.

Subjective measurements served to analyze and compare the occupant's perception in both situations, and to validate the results of the objective measurements. These measurements were conducted in the form of surveys and aimed to record the occupant's perception of the indoor air quality, thermal environment, window operation, and the window feedback system. The existing situation received 37 respondents and the new situation 22 respondents.

C. Window feedback system design

The implemented window feedback system in the new situation comprises an algorithm and light interface design in which both are based on literature research. The light interface design, as shown in Figure 3, consists of three colours that are displayed by a vertical LED strip and are explained by a legend and QR code. The system was positioned in a central spot in the studio near an openable window to enhance the visibility, and to create a stronger association between the light and window opening.

The algorithm design, as illustrated in Figure 4, consists of hierarchically arranged domains containing one or more parameters. These domains, indicated by colours, encompass energy, weather conditions, indoor air quality, outdoor air quality and thermal comfort. The hierarchical structure is based on two design principles:

Principle 1: *To enhance energy efficiency, the window should be closed when the outdoor temperature is colder and should be open when the outdoor temperature is warmer. This principle can be overruled when occupants' comfort or health is at stake.*

Principle 2: *The health of occupants is more important than energy efficiency and occupants' comfort.*

It should be noted that principle 1 was specifically introduced for the experiment's context and is not representative for buildings with air conditioning or periods of the year with high outdoor temperatures.

The selected parameters in the algorithm's domains are based on the most important parameters that affect the window operation in offices and includes the temperature, CO_2 concentration, PM concentration, wind velocity, rainfall, and heating installation [3] [4] [7] [8]. The indoor and outdoor temperature are used in determining the energy efficiency and predicting the thermal comfort according to the adaptive model class I from EN 15251. The CO_2 concentration functions as an indicator of ventilation levels and the possible accumulation of pollutants. The threshold of the CO_2 concentration is in line with the ISHREA 10001 and EN 15251 category III. The PM concentration is used as an indicator of outdoor air quality since it is primarily produced by fuel-powered vehicles and a wide range of industrial processes [9]. The thresholds of the PM concentrations are in line with Ref. [10]. The threshold for the wind velocity is based on Ref. [7].

D. Limitations

It is important to acknowledge that the experimental design has several limitations. This includes the assumption of a micro-climate that is not affected by adjacent areas and the limited duration of the experiment which is not sufficient to take seasonal variations into account. In addition, the mean radiant temperature was not

Figure 3. Designed and implemented window feedback system with corresponding legend and QR code

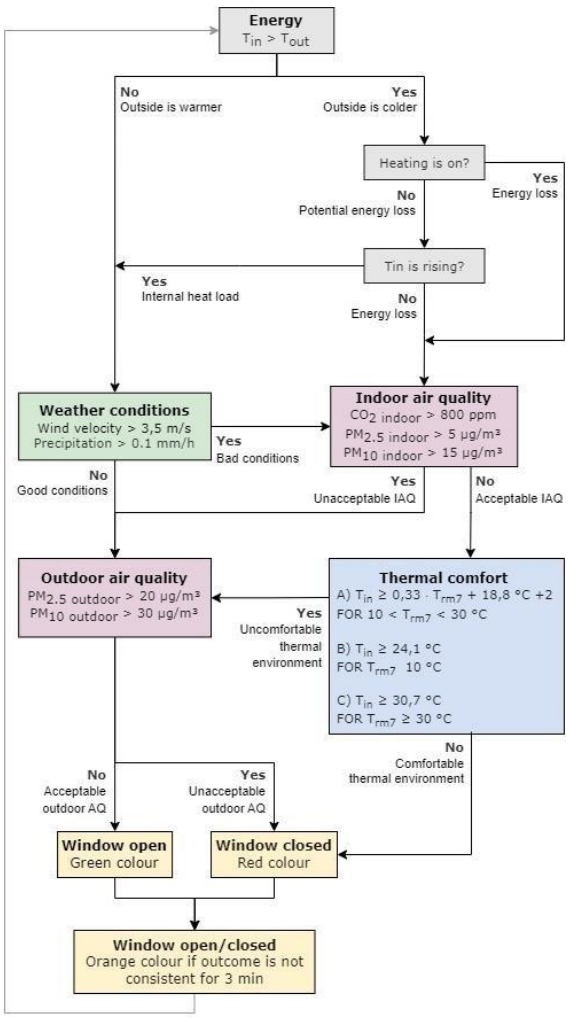

Figure 4. Flowchart of the design algorithm depicting hierarchically arranged domains with corresponding parameters and thresholds

measured and resulted in an approximation of the operative temperature. Furthermore, the sun radiation and outdoor noise were not included in the algorithm and could have provided a more accurate outcome. Another limitation of the algorithm is that outdoor air quality has more significance than indoor air quality, which does not always hold true. For example, when both the indoor and outdoor air quality are exceeded and the indoor air quality is more of a concern.

III. RESULTS AND DISCUSSION

A. *Existing situation*

The objective measurements for the existing situation are illustrated as orange boxplots in Figure 5. These orange boxplots show that all indoor environmental parameters excluding the PM_{10} concentration surpass their respective thresholds for extended periods. The mean exceedance per workday during the existing situation is 1 h 53 min for the CO_2 concentration, 2 h 19 min for the indoor temperature, 1 h 19 min for the indoor RH and 10 min for the indoor $PM_{2.5}$ concentration. This unsatisfactory environment corresponds with the subjective measurements in which a majority of the respondents were not satisfied with the indoor air quality and thermal environment as shown in figure 6 and 7. A majority of the respondents indicated 'sun radiation' as the main reason for their thermal discomfort, followed by 'heating/cooling system does not respond quickly enough' and 'Air too dry'. The sun radiation could be an important reason for the indoor temperature exceeding its respective threshold, together with the outdoor temperature and internal heat produced by high occupancy levels (indicated by the CO_2 concentration). The experienced dry air can be attributed to the low indoor relative humidity and could have caused the symptoms 'eye irritation / dry eyes', 'nose irritation' and 'sore throat', which a significant number of respondents reported.

The objective measurements also revealed an average window opening time of 48 minutes during the existing situation. The subjective measurements showed that a majority of the respondents were not satisfied with the window control despite many openable windows and the relatively close proximity for operation (an average distance of 4 meters). According to four respondents, this poor perception can be attributed to the inclination of the windows. They expressed that the inclined position is not

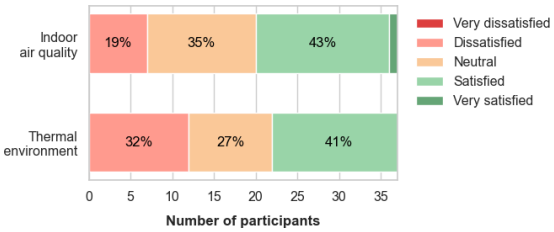

Figure 6. Satisfaction levels of the indoor air quality and thermal environment during the existing situation

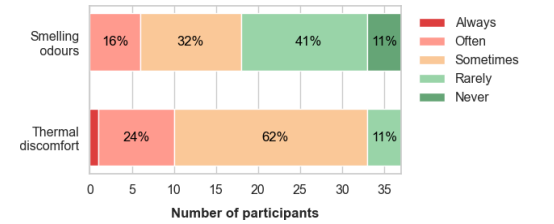

Figure 7. Frequency of discomfort related to the indoor air quality and thermal environment during the existing situation.

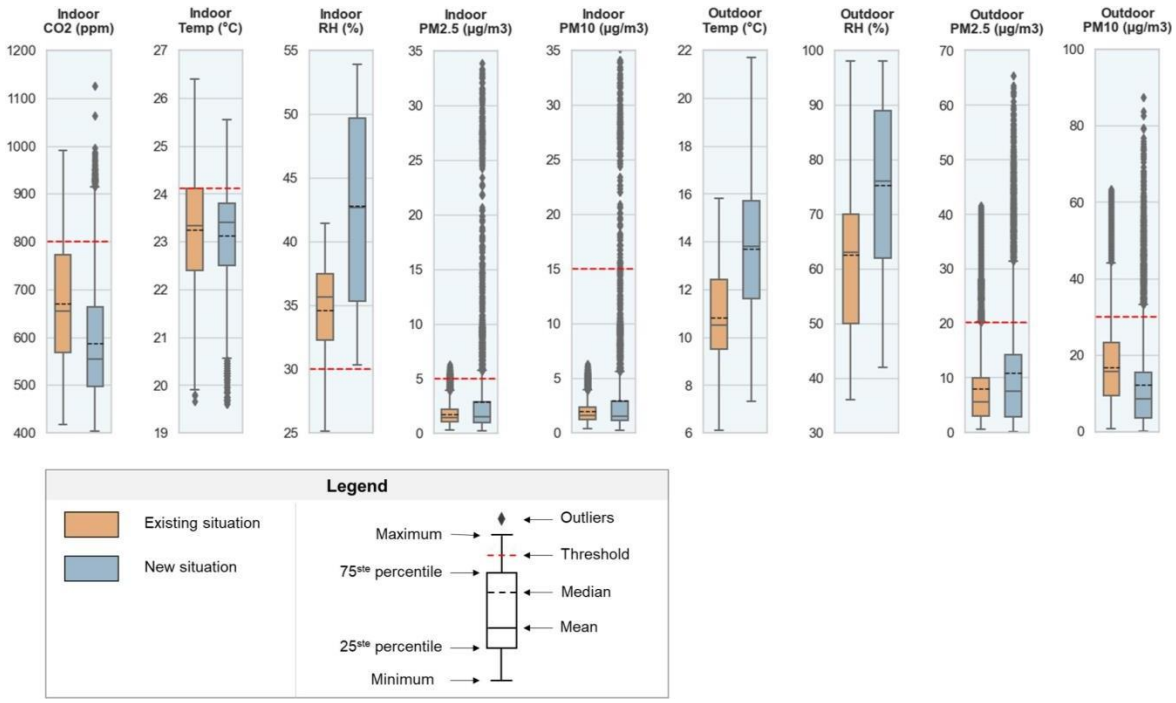

Figure 5. Visualization of the objective measurements for the existing and new situation for each parameter by boxplots and corresponding legend.

effective enough to improve the indoor environment. The respondents also indicated their reasons for window operation. The main reason for window opening is 'for fresh air', followed by 'To be cooler', 'to increase the air movement' and 'To feel a connection with outdoors'. The main reason for window closing is 'to feel warmer', followed by 'the draft was uncomfortable', 'to prevent rain from entering inside', and 'to reduce outdoor noise. These reasons do align with the results of Ref. [6].

The subjective measurements also indicate that most respondents do consider others before operating a window, but are more hesitant to question others before operating a window or to express their dissatisfaction with the window state.

B. New situation

The objective measurements for the new situation are illustrated as blue boxplots in Figure 5. These blue boxplots show that all indoor environmental parameters excluding the relative humidity surpass their respective thresholds for extended periods. The mean exceedance per workday during the new situation is 38 min for the CO_2 concentration, 52 min for the indoor temperature, 1 h 19 min for the indoor $PM_{2.5}$ concentration and 19 min for the indoor PM_{10} concentration. The exceedance of the indoor PM concentration can be related to the high outdoor PM concentration and the window opening time of 4 h 39 min as an average per workday.

C. Comparison of existing and new situation

Table 1 enables a comparison between the existing and new situation by providing the mean exceedance per workday for each parameter in both situations. It also includes the mean per workday for the window opening time and the ineffective window opening time. The latter is defined as the time in which the window state is not according to the outcome of the designed algorithm.

Table 1 shows an improved CO_2 concentration, indoor temperature and relative humidity in the new situation. This improvement corresponds with the higher satisfaction levels in the new situation regarding the indoor air quality and thermal environment as shown in figure 8 and 9. However, it should be taken into account that the new situation had 15 fewer respondents than the existing situation. Table 1 shows also a deterioration of the indoor $PM_{2.5}$ and PM_{10} concentration and can be related to the higher outdoor $PM_{2.5}$ and PM_{10} concentration. All changes in the new situation can be related to the increased window opening time which was 4,81 times higher than the existing situation.

Table 1 shows also a 55% decrease of the ineffective window opening time in the new situation, despite the increased indoor particulate matter. This suggests an improvement of the window opening behaviour and can be explained by the window feedback system. According to the subjective measurements of the last survey, the window feedback system had a significant influence on the improved window-opening behaviour. A majority of the respondents indicated that they understood the system, did act according to the provided feedback and were satisfied with the implementation. In addition, a majority indicated to have trust in the system and its ability to improve indoor air quality, thermal environment, energy efficiency and social interaction between users. However, it should be considered that the new situation had higher outdoor temperatures, which could have been another significant reason for the increased window opening time.

Respondents also indicated their preferences regarding the window feedback system design, A majority of the respondents would prefer a parameter display in addition to the window feedback system, and would not prefer a feedback message to their phone or computer. About one-third of the respondents would prefer to receive feedback when only an action is required.

TABLE I.
COMPARISON BETWEEN THE EXISTING AND NEW SITUATION IN TERMS OF THE MEAN EXCEEDANCE PER WORKDAY FOR EACH PARAMETER AND (INEFFECTIVE) WINDOW OPENING TIME

Parameter	**Exceedance existing situation** [Mean per day]	**Exceedance new situation** [Mean per day]	**Ratio** [New related to existing]
Indoor CO2	1 h 53 min	38 min	- 66%
Indoor Temp.	2 h 19 min	52 min	- 63%
Indoor RH	1 h 43 min	-	- 100%
Indoor PM2.5	10 min	1 h 19 min	+ 690%
Outdoor PM2.5	50 min	1 h 47 min	+ 114 %
Indoor PM10	-	19 min	-
Outdoor PM10	49 min	1 h 12 min	+ 47%
Window opening time	48 min	4 h 39 min	+ 481%
Ineffective window opening time	2 h 51 min	1 h 17 min	- 55%

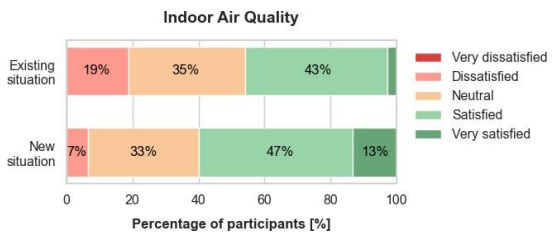

Figure 8. Comparison of the existing and new situation regarding the satisfaction levels of the indoor air quality.

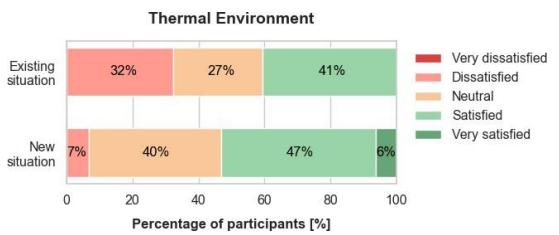

Figure 9. Comparison of the existing and new situation regarding the satisfaction levels of the thermal environment.

IV. CONCLUSION

By conducting an experiment, this research investigated the influence that ambient light window feedback systems can have on the indoor climate and

occupants' satisfaction in open-plan workplaces. The research focused on determining the effectiveness of these systems and on establishing design guidelines for further development.

The experiment took place inside the building technology studio of TU Delft's faculty of architecture and lasted for 6 weeks. During this period, the first three weeks consisted of measuring the existing situation. In the remaining three weeks, a window feedback system was implemented to identify its influence compared to the existing situation. Both objective and subjective measurements were conducted during the existing and new situation.

For the existing situation, the objective measurements suggest that the indoor environment can be improved on several aspects including the temperature, relative humidity, CO_2 concentration and particulate matter concentration. This is in agreement with the subjective measurements of the first survey in which a majority of the respondents experienced discomfort related to the indoor air quality and thermal environment.

For the new situation, the objective and subjective measurements suggest that the indoor environment improved compared to the existing situation. The window opening time increased by 481% while the ineffective window opening time was reduced by 55%. Specifically, the temperature, relative humidity and CO_2 concentration improved. As an exception, the particulate matter concentration deteriorated. All changes can be related to the increased window opening time.

According to the subjective measurements of the last survey, the window feedback system had a significant influence on the increased and effective window opening time. A majority of the respondents indicated that they did understand the system, did act according to the provided feedback and were satisfied with the implementation. In addition, a majority of the respondents indicated to have trust in the system and its ability to improve indoor air quality, thermal environment, energy efficiency and social interaction between users. However, it should be considered that the new situation had higher outdoor temperatures, which could have been another significant reason for the increased window opening time. Nevertheless, this study shows that ambient light window feedback systems can be promising inside open-plan workplaces. In addition, the following design recommendations are made for further development of the algorithm and window feedback system:

- Include the indoor mean radiant temperature, outdoor noise and solar radiation as parameters in the algorithm for a more accurate outcome;
- Reconsider the importance of the outdoor air quality in the algorithm. Currently, the outdoor air quality has a higher importance than the indoor air quality which may not be correct in certain scenarios. For example, when both the indoor and outdoor air quality are exceeded and the indoor air quality is more of a concern.
- Include a parameter display. This is preferred according to the subjective measurements.
- Do not include blinking lights or feedback messages to phones/computers. This is not preferred according to the subjective measurements.

REFERENCES

1 Buso, T., Fabi, V., Andersen, R. K., & Corgnati, S. P. (2015). Occupant behaviour and robustness of building design. *Building and Environment*, *94*, 694–703. https://doi.org/10.1016/j.buildenv.2015.11.003

2 Mahdavi, A., et al. (2021). The Role of Occupants in Buildings' Energy Performance Gap: Myth or Reality? *Sustainability*, *13*(6), 3146. https://doi.org/10.3390/su13063146

3 Day, J. K., et al. (2020). A review of select human-building interfaces and their relationship to human behavior, energy use and occupant comfort. *Building and Environment*, *178*, 106920. https://doi.org/10.1016/j.buildenv.2020.106920

4 Liu, Y., et al. (2022). Rethinking the limitations of research on occupants' window-opening behavior: A review. *Energy and Buildings*, *277*, 112552. https://doi.org/10.1016/j.enbuild.2022.112552

5 Bordass, B., Leaman, A., & Bunn, R. (2007). Controls for End Users: A guide for good design and implementation.

6 Ackerly, K., & Brager, G. (2013). Window signalling systems: control strategies and occupant behaviour. *Building Research &Amp; Information*, *41*(3), 342–360. https://doi.org/10.1080/09613218.2013.772044

7 Fabi, V., Andersen, R. V., Corgnati, S., & Olesen, B. W. (2012). Occupants' window opening behaviour: A literature review of factors influencing occupant behaviour and models. *Building and Environment*, *58*, 188–198. https://doi.org/10.1016/j.buildenv.2012.07.009

8 Fabi, V. (2013). Influence of Occupant's Behaviour on Indoor Environmental Quality and Energy Consumptions. In *A Roadmap to predict the unpredictable energy-related occupant behaviour*.

9 Abdul-Wahab, S. A., Chin Fah En, S., Elkamel, A., Ahmadi, L., & Yetilmezsoy, K. (2015). A review of standards and guidelines set by international bodies for the parameters of indoor air quality. *Atmospheric Pollution Research*, *6*(5), 751–767. https://doi.org/10.5094/apr.2015.084

[10] World Health Organization [WHO]. (2021). WHO global air quality guidelines: Particulate matter (PM2.5 and PM10), ozone, nitrogen dioxide, sulfur dioxide and carbon monoxide. *WHO*.

SPONSORED BY:

Atecyr

ATECYR'S APPLICANT

Developing a Predictive Control System for Optimal Chiller Operation

Martin Bizkarra Belategi [1, 2] – mbizkarra001@ikasle.ehu.eus.

Supervisors: Estibaliz Pérez Iribarren [1] – estibaliz.perezi@ehu.eus; Iker González Pino [1] – iker.gonzalezp@ehu.eus;
Saioa Herrero López [2] – saioa.herrero@tekniker.es.

[1] Department of Energy Engineering, University of the Basque Country UPV/EHU. Bilbao, Spain.
[2] Tekniker Research and Technology Centre. Eibar, Spain.

Master's thesis, October 2023.

***Abstract*— In a world where decarbonisation is an urgent priority, the building sector plays a pivotal role in mitigating carbon emissions. To meet this challenge, it is necessary to adapt HVAC systems and develop advanced controllers, of which Model Predictive Control (MPC) stands out. This work focuses on the development of an MPC designed to optimise the operation of a refrigeration plant. To achieve an accurate controller, detailed models of the main components of the system, such as the chiller and the thermal energy storage tank, have been integrated into a simplified, control-oriented plant model. Various options have been analysed to eliminate the need for binary variables and conditional structures in the model. The developed MPC belongs to the field of non-linear programming and aims to minimise consumption or cost and to guarantee demand coverage. The controller has been tested on a digital twin of the plant, and calculations have been performed to determine the energy and cost savings achieved.**

***Index Terms*— CasADi, Electric chiller, Modelling and simulation, Model Predictive Control, Non-linear programming, Water tank.**

I. INTRODUCTION AND CONTEXT

In the context of growing awareness of the climate crisis, profound changes in the way we produce and consume energy have become inevitable. One of the key sectors in need of urgent transformation is the energy sector, as carbon emissions from energy production and consumption account for a significant share of our global emissions. Reducing and decarbonising thermal energy consumption in the tertiary and residential sectors is crucial. These sectors have significant heating and cooling needs, which are often met by non-renewable energy sources.

Meeting these challenges requires innovative solutions that not only reduce thermal energy consumption, but also enable more efficient and sustainable use of thermal energy. This decrease involves the development of effective thermal energy storage systems and advanced control strategies that optimise the operation of thermal systems. Such an approach can improve energy efficiency and decrease carbon emissions linked to heating and cooling in buildings and industrial systems.

This work is part of the BEST-Storage research project [1]. BEST-Storage is an acronym for Building Energy Efficient System through short and long spectrum Thermal Energy Storage. It is a project funded by the European Union's Horizon Europe initiative, and its objective is to develop thermal energy storage technologies that are adapted optimally to each type of energy demand. The project aims to innovate high-energy-density storage solutions for both the short and long term. These technologies will be integrated into intelligent building energy management systems, including Model Predictive Controllers (MPC), to reduce operating costs in short-term applications.

MPC is an advanced process control method that uses dynamic models of the process to optimise the current state while considering future states [2]. This is achieved by solving an optimisation problem for a finite time horizon (consisting of several intervals) and implementing only the control action corresponding to the first interval. Once that interval has elapsed, the horizon moves forward and the optimisation problem is solved again, and the control action for the next interval is applied again. This process is repeated, shifting the horizon one interval forward in each calculation.

A. Objectives and Scope

The aim of this work is to develop an MPC system that can optimise the operation of a refrigeration system. The primary objective is to create an accurate and robust controller that minimises energy consumption and costs while also ensuring optimal coverage of the thermal demand. This is achieved by creating detailed models of the main system components, such as the chiller and storage tank, and implementing advanced control strategies within the framework of Non-Linear Programming (NLP).

In this regard, the goal is to develop an MPC for a cooling plant like the one that will be used as a prototype in BEST-Storage, using water instead of a phase change material as the thermal fluid.

Considering the characteristics and requirements of the future prototype plant, the components of a simplified system are defined in *I.C.* The development of the models of the main components of the chilled water plant is explained in *II.B.* The forecasted variables' models, such as cooling load demand, ambient temperature, and electricity tariff, are explained in *II.C.* Based on these models, a control algorithm is designed to minimise the operating cost and cover the demand under certain supply conditions. This is explained in II.D. To assess the control algorithm's performance, we simulate it using a digital twin of the plant. The results obtained in these simulations are presented in *III.* This approach will provide relevant results and conclusions that will help in the development and optimisation of the prototype's controller.

B. Analysed Alternatives

In complex refrigeration systems that involve generation, distribution, and multiple equipment, an optimal controller must determine which components should be active (chillers on or off), how to operate the thermal storage (charge or discharge), and what the optimal output of each piece of equipment should be, based on the outlet tempera- ture and mass flow [3].

In this case, the controlled cooling system is less complex as the controller does not control the distribution, and the system has only one generator. Therefore, there are two binary variables: one to determine the chiller's state (on/off) and the other to decide whether to charge or discharge the tank. This requires the development of a program with in- teger variables. The models used to represent the plant and its components and the MPC objective function have non- linear characteristics. As a result, the program falls into the category of Mixed Integer Non-Linear Programming (MINLP) problems. This type of problems can be challeng- ing, and only a few freely available solvers can handle it. Using binary variables results in an exponential growth of potential solutions as the prediction horizon increases. Due to the prediction horizon and granularity needed for this case, the computational cost would be excessively high.

However, linearising the equations governing the system and developing a MILP-type problem is not feasible due to the strong non-linearity of the chiller model, which would result in a considerably inaccurate representation. As a result, we have chosen an NLP-type problem to develop the MPC. We employed various mathematical functions to model the hybridity of the system at the cost of adding non-linearities to it.

C. Case Study Description

The case study examines the cooling plant of a test bed in the BEST-Storage project. We simplified the system and adapted to use water as the thermal fluid. It consists of three parts defined by the three main components (Fig. 1): pro- duction (electric chiller), storage (water tank), and consumption (heat exchanger).

The project brief for BEST-Storage set two essential requirements for the size and operation of the plant: the chiller must have a power of 3 kW, and the storage capacity must be 9 kWh (equivalent to 3 hours at maximum power). To ensure that the MPC developed in this work had a similar operating mode (including charge and discharge cycles, control, and prediction times, etc.) to that of the original project, it was necessary to maintain these conditions and adapt them to the properties of the water.

The selected chiller must meet specific requirements, in- cluding a supply temperature of 5°C, variable capacity, availability of a communication module, and sufficient known operating points. After considering these factors, we chose the Climaveneta i-BX/004 4.3 kW as the best option. This non-reversible air/water chiller with an inverter fulfilled all the necessary characteristics. The manufacturer provided operating data for the unit at various outlet temperatures, ambient temperatures, and partial loads.

We selected a stratified chilled water tank to store the 9 kWh as a thermal gradient. Duty cycle temperatures of 5-10°C were considered, resulting in a minimum volume of 1560 litres. The reference tank used is the Lapesa Geiser Inertia 1500 litre cylindrical tank with direct loading and unloading.

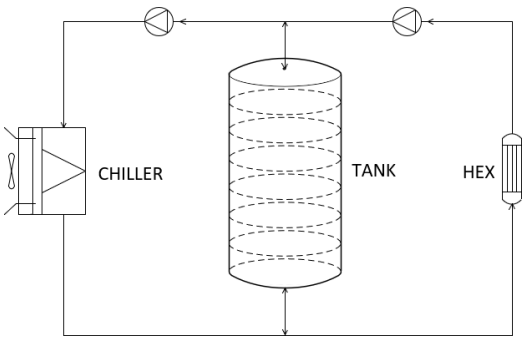

Figure 1: Diagram of the simplified cooling plant.

II. METHODS

A. Software used

MATLAB was used as an interface for developing the optimisation code, modelling components and predictions, and performing digital twin simulations. In addition, the open-source tool CasADi was used to solve the MPC optimisation problems online. CasADi utilises a symbolic work environment to implement Automatic Differentiation methods for obtaining necessary information such as gradients and Jacobian matrices [4]. This information is then used to solve optimisation problems using various algorithms. The IPOPT solver is used for this purpose due to its public license, inclusion in the CasADi package, and suitability for the formulated problem.

B. Modelling the System

The cooling system was modelled by first modelling its main components and then integrating them into a simplified plant model. A state-of-the-art analysis of control-oriented models was conducted to determine the most suitable model for the problem. A combination of physical and grey box models was used to create the model of the plant.

1) Electric Chiller

The electric chiller was modelled using the DOE-2 methodology, which is currently employed in the DOE-2 and EnergyPlus simulation programs [5]. This method consists of a grey box or hybrid model that includes three primary functions: a binary quadratic curve (1) representing the cooling capacity as a function of evaporator and condenser temperatures; a binary quadratic curve (2) representing the full load efficiency as a function of evaporator and condenser temperatures; a quadratic curve (3) reflecting the efficiency as a function of part load percentage (4). The chiller's electrical power consumption in any operating condition is calculated by multiplying the reference electrical power with the product of three functions defined by 13 parameters (5).

$$CAPFT = a_1 + b_1 \cdot T_{evap} + c_1 \cdot T^2_{evap} + d_1 \cdot T_{cond} + e_1 \cdot T^2_{cond} + f_1 \cdot T_{evap} \cdot T_{cond} \quad (1)$$

$$EIRFT = a_2 + b_2 \cdot T_{evap} + c_2 \cdot T^2_{evap} + d_2 \cdot T_{cond} + e_2 \cdot T^2_{cond} + f_2 \cdot T_{evap} \cdot T_{cond} \quad (2)$$

$$EIRFPLR = a_3 + b_3 \cdot PLR + c_3 \cdot PLR^2 \quad (3)$$

$$PLR = \dot{Q}/(\dot{Q}_{ref} \cdot CAPFT(T_{evap}, T_{cond})) \quad (4)$$

$$P = P_{ref} \cdot CAPFT(T_{evap}, T_{cond}) \cdot EIRFT(T_{evap}, T_{cond}) \cdot EIRFPLR(\dot{Q}, T_{evap}, T_{cond}) \quad (5)$$

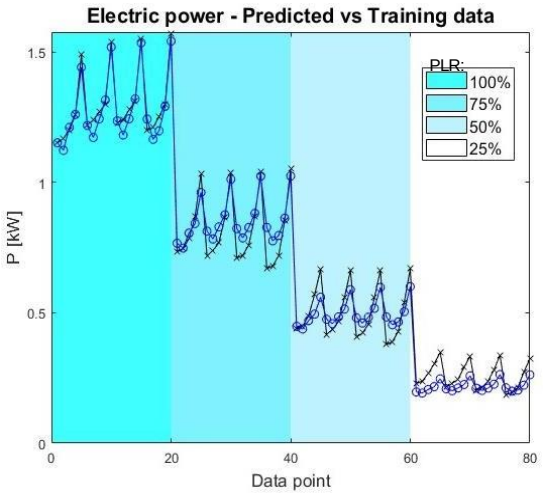

Figure 2: Chiller model results, training data (black) vs predicted (blue) electric power.

The 13 parameters defining these functions were determined by applying regression methods to the data set provided by the manufacturer. The operating data, which includes cooling capacity and Energy Efficiency Ratio (EER), is available for 20 temperature pairs and 4 partial load states, resulting in a total of 80 operating points. The model was validated using training data, which indicates lower reliability at low partial loads (Fig. 2). The error coefficients, when compared to the training data, were as follows: $R^2 = 0.987$; RMSE = 0.098.

2) Water Tank

The water tank was modelled using an approach based on the fundamental laws of heat transfer. The developed model is one-dimensional and represents a tank that is divided into equal-sized segments. The most common and documented method for modelling the tank was chosen [6], which involves discretisation on the vertical z-axis, with N segments of equal volume and height Δz (Fig. 3). This approach transforms the partial differential equation defined by 1D energy conservation over a control volume of thickness *dz* into a set of ordinary differential equations (ODEs), one for each segment of the tank. Equations (6) to (8) represent the temperature of the tank's bottom, middle and top segments at the time interval *t+1*. In this case, the tank was divided into 20 segments (*N=20*). While increasing the discretisation enhances the model's accuracy, it also increases the computational cost of the optimisation problem, so it is necessary to find a suitable balance.

$$T_{t+1_1} = T_{t_1} + \frac{\Delta t}{\rho Cp V_{seg}} \cdot (\dot{m}_{up} Cp (T_{chiller} - T_{t+1_1}) + \dot{m}_{down} Cp (T_{t+1_1} - T_{t+1_1}) + \dot{Q}^{amb}_{1} - \dot{Q}^{diff}_{1}) \quad (6)$$

$$T_{t+1_i} = T_{t_i} + \frac{\Delta t}{\rho Cp V_{seg}} \cdot (\dot{m}_{up} Cp (T_{t+1_{i-1}} - T_{t+1_i}) + \dot{m}_{down} Cp (T_{t+1_{i+1}} - T_{t+1_i}) + \dot{Q}^{amb}_{i} + \dot{Q}^{diff}_{i-1} - \dot{Q}^{diff}_{i}) \quad (7)$$

$$T_{t+1_N} = T_{t_N} + \frac{\Delta t}{\rho Cp V_{seg}} \cdot (\dot{m}_{up} Cp (T_{t+1_{N-1}} - T_{t+1_N}) + \dot{m}_{down} Cp (T_{t+1_N} - T_{return}) + \dot{Q}^{amb}_{N} + \dot{Q}^{diff}_{N-1} - \dot{Q}^{amb}_{N}) \quad (8)$$

The enthalpy flux expression in each segment varies depending on the tank's mode of operation, whether it is loading or unloading. To represent these modes without including binary variables or events in the code, we used the logistic function, which is continuous and differentiable. We defined two auxiliary variables that take values of 0 or 1 depending on the direction of flow through the tank (10), (11), indicating whether it is flowing up or down.

$$\dot{m}_{tank} = \dot{m}_{chiller} - \dot{m}_{load} \quad (9)$$

$$\dot{m}_{tank} > 0 \rightarrow \dot{m}_{up} = \dot{m}_{tank} \cdot up = \frac{\dot{m}_{tank}}{1+e^{-\mu * \dot{m}_{tank}}} \quad (10)$$

$$\dot{m}_{tank} < 0 \rightarrow \dot{m}_{down} = \dot{m}_{tank} \cdot down = \frac{\dot{m}_{tank}}{1+e^{\mu * \dot{m}_{tank}}} \quad (11)$$

To integrate the tank model into the MPC, a time discretisation is required in addition to the spatial discretisation. The set of ODEs was integrated using the backward Euler method (12), which is more stable than the standard Euler method for the discretisation times used in the MPC. In the digital twin, the MATLAB *ode15s* integrator was used to simulate the dynamics of the tank. The system of equations is stiff, and a variable step integrator is required to obtain accurate simulations.

$$T_{t+1_i} = T_{t_i} + \Delta t \cdot F_i(T_{t+1}, \dot{m}_i, T^{in}_i)_i \quad (12)$$

Additionally, the digital twin model incorporates a correction for the thermal inversion of the tank caused by buoyancy forces. This correction was implemented using the differentiable approximation of the Max function, *LogSumExp* (13), as proposed in [7]. This model was developed to be included in the MPC. However, it affected the convergence of the solver negatively, and was finally only included in the digital twin.

$$\dot{Q}^{diff}_i = G_i \cdot (T_i - T_{i+1}) = G_i \cdot (log(1 + exp(-\mu \cdot (T_i - T_{i+1})))/\mu + \Delta \cdot (T_i - T_{i+1}) \cdot log(1 + exp(\mu \cdot (T_i - T_{i+1})))/\mu) \quad (13)$$

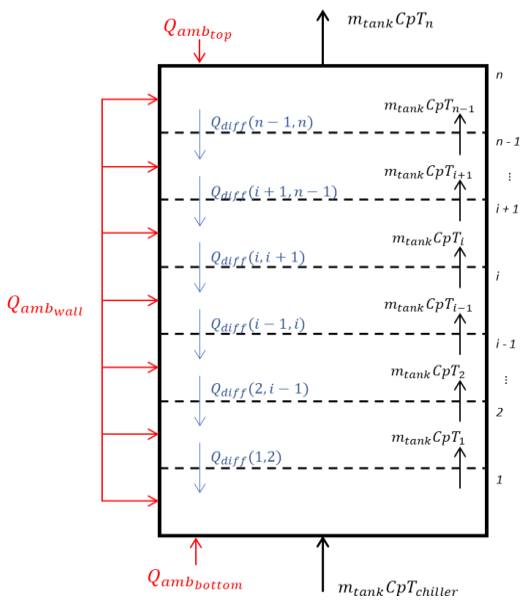

Figure 3: Mass and energy flow representation for the tank model (upwards flow).

3) Heat Exchanger

The heat exchanger connected to the consumer circuit was physically modelled with an ideal efficiency of 100%. The flow rate from the tank to the heat exchanger varies to maintain a constant temperature difference of 5°C in the heat exchanger.

The three components were integrated into a plant model, with mass and energy balance equations added to the nodes at the inlet and outlet of the tank. These equations are dependent on the tank's flow direction, and so the auxiliary variables mentioned above were used.

C. Modelling the Forecasts

The MPC requires forecasts of a few variables to predict the evolution of the system and calculate the cost function over the entire horizon. These variables include the ambient temperature, cooling power demand, and electricity tariffs. The forecasts provided to the MPC are also used for vali- dation in the digital twin. The aim of the work is to test the controller algorithm, so the forecasts do not need to be highly accurate.

The temperature of the environment was modelled as a sinusoidal function with a 24-hour period, centred at 21ºC, and an amplitude of 5ºC, with a maximum at 15:00. The cooling power demand's daily profile was modelled as a normal distribution with a peak power of 5 kW at midday and an amplitude of 8 hours. The electricity contract of the building where the prototype will be installed was used as a reference. Its tariffs vary periodically according to the month and the time of day.

D. Controller Development

The developed controller consists of an Optimal Control problem with finite receding horizon to plan the chiller's operation, aiming to cover the demand and minimise oper- ating costs or maximise efficiency. The controller incorpo- rates a plant model to predict the system's future evolution and considers restrictions in the control and output varia- bles. Therefore, a Model Predictive Control is necessary. The MPC solves an optimisation problem with non-linear constraints and a non-linear objective function in each in- terval, using a multiple-shooting resolution approach. The multiple-shooting approach has the following formulation:

$$\min_{x_k,u_k} \quad J(x_k,u_k) \tag{14}$$

$$s.to. \quad x_{k+1} = F(x_k,u_k) \quad , \quad k = 1,\dots,hp \tag{15}$$

$$h(x_k,u_k) \leq 0 \quad , \quad k = 1,\dots,hp \tag{16}$$

$$B(x_1,x_{hp+1}) = 0 \tag{17}$$

1) System Variables

The control variables (u) of the problem are the water temperature at the chiller outlet and the mass flow rate of the generation circuit. The state variables (x) of the problem are the temperatures of each tank segment. The output variables (y) of the problem are the supply water temperature and the electrical power consumed by the chiller. The control and state variables are the decision variables of the problem to be solved. To increase flexibility in the problem and restrict the supply temperature, an auxiliary slack variable was declared. Additional optimisation variables were necessary to model the system without errors.

2) Constraints

The system variables are subject to several constraints. First, the state update equation (which models the tank dynamics) imposes first-order dynamic constraints (15). Second, the trajectory constraints limit the operating range of the control and output variables of the system (16), such as the operating limits of the chiller and the supply conditions. Finally, the measured values of the state variables impose the boundary constraints (17) –in this case only the initial boundary constraint is considered–.

The flow rate through the chiller and the cooling capacity supplied by it can take values between 0 and the maximum limit, as the lower limits were not restricted. The reason for this is that it was not possible to model the range of these semi-continuous variables without resorting to MINLP formulations.

3) Objective Function

The MPC outputs are calculated by minimising an objective function that represents the operating strategy for the controller. A multi-objective function was used to optimise several criteria simultaneously (18). The objectives include minimising economic cost or maximising energy efficiency, keeping the supply temperature below 7ºC, and avoiding abrupt changes in the operation of the chiller. It is possible to choose which objectives to consider and to give them different weights (w_i) according to their importance. These objectives are represented mathematically by cost functions and summed into a single function the solver attempts to minimise. To add different cost functions in the same objective function we applied a scale normalisation.

$$\tilde{J} = Consumption + Cost + Track\,T + Variation \tag{18}$$

$$\tilde{J} = w_1 \sum_{k=1}^{hp} \frac{P_{el_k}}{P_{el_{MAX}}} + w_2 \sum_{k=1}^{hp} \frac{P_{el_k} \cdot €_k}{P_{el_{MAX}} \cdot €_{MAX}} + w \sum_{k}^{3} \frac{slack_k}{\Delta T_{MAX}} + w \sum_{k=1}^{4} \frac{(u_{k+1} - u)^2}{\Delta u_{MAX}^2}$$

4) Parameters

To complete the configuration of the MPC, certain parameters must be defined. The most important ones are the prediction time/horizon –*hp* = 12 hours– and the control time –*tc* = 15 minutes–. In this case, the problem was formulated with a control horizon that is the same length as the prediction horizon. This configuration resulted in a total of 144 intervals to be considered, resulting in an optimisation problem with 3620 variables and 4198 constraints.

III. Data Presentation and Discussion

We implemented the MPC in a digital twin of the plant in MATLAB to virtually validate it. The developed program follows the flowchart shown in Fig. 4.

During the development of the controller, we carried out repeated simulations to validate or discard different configurations (models, implementation methods, constraints, cost functions, target weights, parameters, etc.). Finally, we obtained a controller that operated the plant as desired. We compared the performance of the system to a base case (BC), which involved a chiller directly coupled to the demand. Savings were calculated this way. This comparison, although unfair, was enough to assess the general performance of the chiller.

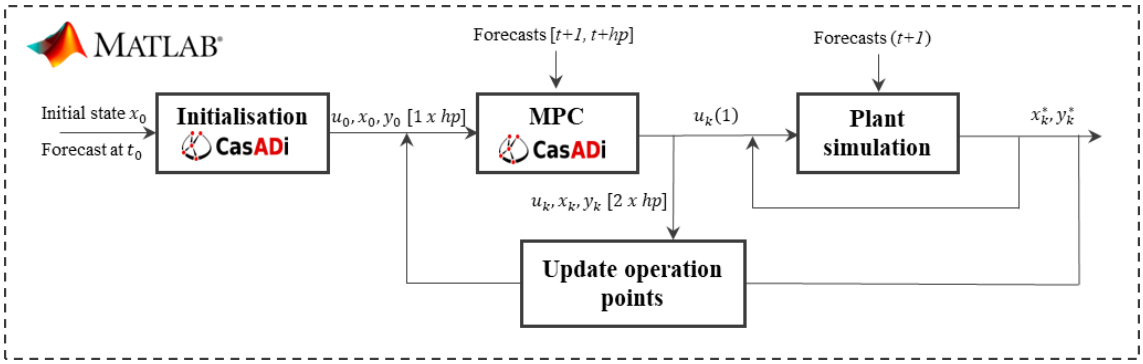

Figure 4: Flowchart of the main program used to simulate the system.

As mentioned earlier, the user has the option to choose between minimizing energy consumption or operating costs. In the first scenario, during a 7-day simulation period, the system achieved a median EER of 4.43. When compared to the base case (BC), the controller was able to save up to 14.4% in energy. However, the savings were considered insufficient, even though the MPC's logic was sound. The reason for this was due to the limited capacity of the tank, which was only 9 kWh, and hence, the controller had little room to shift and shave a peak cooling power of 5 kW. Therefore, to further evaluate the controller's performance, we decided to double the tank's capacity. With this increased capacity, we were able to achieve an energy consumption that was 16.9% lower than the BC and a median EER of 4.57.

We also modified the configuration for the controller that aims to minimize economic costs to determine the impact of a larger tank capacity on its performance. With the original configuration, the economic cost for the MPC was 22.9% lower than for the BC. With the new configuration, the cost was 29.7% lower.

Fig. 5 displays the simulation results for the controller that aims to minimize the operating costs (double capacity configuration). Fig. 5. a) shows that the supply temperature drops below 7ºC when there is a cooling demand, and the chiller outlet temperature has a smooth profile with no abrupt changes. Fig. 5. b) shows the tank's temperature gradient over height and time, illustrating how the controller charges and discharges the energy storage. During the charging cycle, the tank is cooled below 7ºC, allowing the system to operate at higher temperatures when the prices are higher. Fig. 5. c) displays the demanded and generated cooling power, along with the mass flow rate in both circuits. The cooling power profile is shifted to the morning hours when ambient temperatures and electricity prices are lower, and the profile's peak is shaved by working at lower partial load ratios to achieve higher efficiency values. The chiller's mass flow rate profile is remarkably smooth. Finally, in Fig. 5. d), the operating cost and the consumed electric power over the 2 days are illustrated, with most of the energy consumed during the period of lowest energy prices.

IV. CONCLUSIONS

This thesis presents the development of a robust Nonlinear Model Predictive Control formulation for a cooling plant. The plant consists of a chiller and tank system. We have modelled the chiller using a grey-box approach. To avoid the use of integers, we have modelled the semi-continuous variables of the chiller as continuous. We have modelled the water tank using a 1D physics-based approach. The hybrid behaviour of the tank has been modelled using the logistic function. We have implemented the dynamics of the tank using a multiple-shooting formulation.

The controller solves a multi-objective optimisation problem to calculate the optimal control trajectory. It aims to: 1) minimise energy consumption or economic cost; 2) minimise the deviation of the supply temperature from the reference conditions; and 3) ensure a smooth operation. The system anticipates the cooling demand and charges the tank efficiently working at partial loads and low outdoor temperatures. The MPC charges the tank during periods of lower electricity prices to minimise costs. At the same time, the controller ensures that the flow temperature remains below 7ºC. All of this is achieved without any significant variation in the control variables.

We evaluated the controller in a digital twin of the plant, and the results showed that the models and algorithms used were effective from a control performance standpoint. Simulations showed promising results, with energy savings of up to 19.9% and a reduction in economic costs of up to 29.7%. However, it's important to note two things. First, we calculated the savings against a base case that did not include the tank or a control strategy. To analyse the real potential of this control method, we need to compare it with a more traditional rule-based control for the same setup. Second, we have not tested the controller in a real environment yet, so the predictive performance of the models is still unknown.

The development of the alternative controllers or models analysed in this thesis is left to future research. On the one hand, alternative options for modelling the hybridisation of the tank should be researched. On the other hand, it is necessary to develop a programme that considers the operating limits of the chiller as well as the on and off states of the chiller. To achieve this, three approaches can be followed: 1) to deepen the available modelling techniques to incorporate these considerations in an NLP; 2) to develop a MINLP program, with binary variables to represent the limits and states, and then to solve the problem using a solver such as

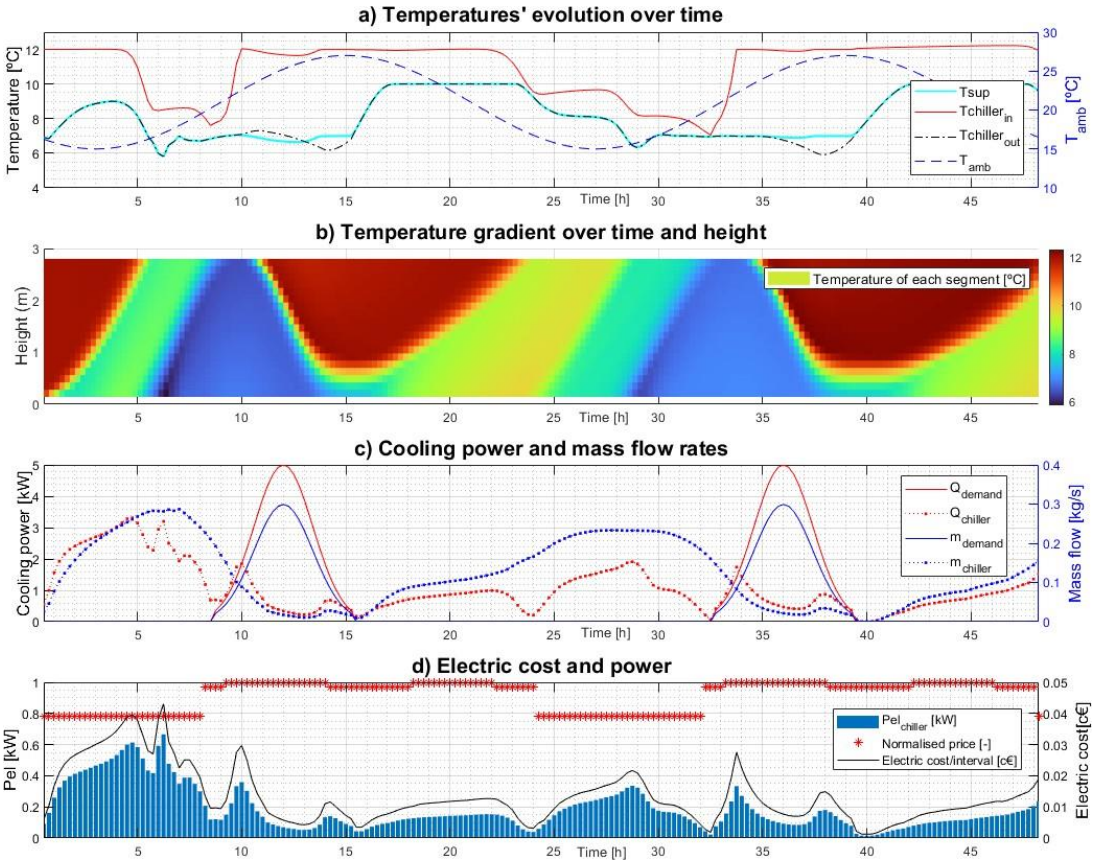

Figure 5: Simulation results for 2 days with the economic MPC.

Bonmin together with a higher capacity processor; 3) to develop a better postprocessing algorithm that considers the limits without affecting the performance of the controller.

Finally, the MPC developed in this thesis will be adapted for implementation in the prototype of the BEST-Storage project. The adapted controller will be tested in the prototype installation, which will allow to evaluate its control and prediction performance in a real environment and to adjust the parameters for optimal operation.

ACKNOWLEDGEMENT

1. This work was carried out within the framework of the project BEST-Storage, which has received funding from the European Union's Horizon 2020 research and innovation programme under grant agreement nº101096516.
2. The master's thesis was conducted at the Research and Technology Centre Tekniker, supervised by researcher Saioa Herrero López.

REFERENCES

[1] EU Cordis (2022). "Building Energy Efficient System through short and long spectrum Thermal Energy Storage". https://doi.org/10.3030/101096516

2 Pérez Soler, E. (2011). "Control predictivo sujeto a restricciones poliédricas no convexas: solución explícita y estabilidad", unpublished. Universitat Politècnica de València. http://hdl.handle.net/10251/9315

3 Conejo, A.J., Baringo, L. (2018). Unit Commitment and Economic Dispatch. In: Power System Operations. Power Electronics and Power Systems. Springer, Cham. https://doi.org/10.1007/978-3-319-69407-8_7

4 Andersson, J.A.E., Gillis, J., Horn, G. et al. CasADi: a software framework for nonlinear optimization and optimal control. Math. Prog. Comp. 11, 1–36 (2019). https://doi.org/10.1007/s12532-018-0139-4

5 Hydeman, M. & Jr, K.L. & Dexter, A.L. (2002). Tools and techniques to calibrate electric chiller component models. ASHRAE Transactions. 108. 733-741.

6 Untrau, A., Sochard, S., Marías, F., Reneaume, J., Roux, G., & Serra, S. (2023). A fast and accurate 1-dimensional model for dynamic simulation and optimization of a stratified thermal energy storage. Applied Energy, 333, 120614. https://doi.org/10.1016/j.apenergy.2022.120614

[7] Lago, J., De Ridder, F., Mazairac, W., & De Schutter, B. (2019). A 1-dimensional continuous and smooth model for thermally stratified storage tanks including mixing and buoyancy. Applied Energy, 248, 640–655. https://doi.org/10.1016/j.apenergy.2019.04.139

SPONSORED BY:

Sizing Methods for the Ground-Embedded Heat Exchanger of a Geothermal Heat Pump

Student: Danijela Srećković
Supervisor: Full Professor Miloš Banjac
University of Belgrade, Faculty of Mechanical Engineering, Kraljice Marije 16
danijelasreckovic27@gmail.com, mbanjac@mas.bg.ac.rs
September, 2023

***Abstract*— The stable, long-term, and sustainable use of geothermal heat pumps primarily depends on the correct sizing of the ground-embedded heat exchanger. It should be dimensioned in such a way that it is not too large, and that over the decades of utilization to come, it ensures neither a significant increase nor decrease in the temperature of the soil in which it is installed. With the aim of bringing this issue closer to engineering practice, for the case of vertically buried heat exchangers, recognized and accepted models for their dimensioning are presented, as found in the professional literature. A quality check of their predictions is performed on a specific example, highlighting inconsistencies and significant discrepancies in the results that arise from their use.**

***Index Terms*— geothermal heat pump, vertical embedded heat exchanger, analytical sizing method sizing, numerical sizing method.**

Introduction

The continuation of increase in energy demand, the depletion of conventional energy reserves such as oil, coal, and natural gas, and global warming as a consequence of using these energy sources, imperatively impose requirements for the utilization of renewable energy sources. Therefore, finding new and improving existing methods of their use, as well as optimizing already existing ones, currently represent a priority engineering challenge.

When it comes to meeting heating needs, which often contribute to over 50% of the energy balance of each country, the use of heat pumps powered by electricity obtained from renewable energy sources can be one of the optimal solutions. This is particularly true for so-called ground source heat pumps (GSHP), where they utilize the earth, or underground water, as the heat source or sink (Fig. 1).

Heat pump systems that utilize groundwater as a heat source, also known as open-loop systems (Fig. 1), first began to be used in the late 1940s. In these systems, groundwater serves as a source or sink of heat. The groundwater is pumped from a sealed well and, by flowing through a heat exchanger, transfers heat to or from the heat pump. After this process is completed, the thermally depleted water is returned to the ground by discharge into a so-called return or injection well.

The subject of this paper are heat pumps that utilize the ground as a heat source. The transfer of thermal (internal) energy within the soil occurs through the mechanism of heat conduction, assuming that the influence of groundwater movement is neglected. Due to the high thermal capacity of the soil, the impact of surface phenomena on soil temperature is negligible. Thermal diffusivity and fluid flow velocity are dominant physical quantities that significantly affect the heat transfer process: their values vary depending on the type of soil, so it is necessary to define the physical characteristics of the soil as accurately as possible. The process of transferring heat from the ground to the heat pump is achieved through a heat exchanger, which typically consists of high-density polyethylene pipes buried in vertical boreholes or horizontal trenches.

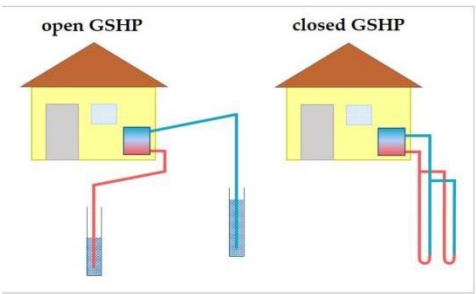

Figure 1. Types of ground sources heat pump systems

When harnessing the Earth's heat through a Ground Source Heat Pump (GSHP) system, several interconnected components work together to facilitate efficient heating. At the heart of the system is the heat pump itself, which consists of a compressor, condenser, expansion valve, and evaporator. These components manipulate the refrigerant to extract heat from the ground and distribute it into the building.

The process begins with vertical borehole heat exchangers (VBHE), which are designed to tap into the Earth's geothermal energy. These heat exchangers typically consist of one or more vertical boreholes drilled into the ground, reaching depths of approximately 100 to 150 meters. Each borehole contains a series of pipes through which a water-antifreeze mixture circulates.

As the water-antifreeze mixture flows through the boreholes, it absorbs heat from the surrounding soil. This heat transfer occurs due to the relatively stable temperature of the Earth at deeper depths. The absorbed heat causes the

water-antifreeze mixture to increase in temperature, making it an effective medium for transferring thermal energy.

Simultaneously, the heat pump's refrigerant circulates in a closed loop within the system. The refrigerant absorbs the thermal energy from the water-antifreeze mixture as it passes through the evaporator coil located in the boreholes. This absorption of heat causes the refrigerant to evaporate, transforming into a low-pressure, low-temperature gas.

The compressor within the heat pump then compresses the low-pressure refrigerant gas, raising its temperature and pressure. The high-temperature, high-pressure refrigerant gas then flows into the condenser coil, where it releases its heat to a third working fluid – typically water.

The water, now heated by the refrigerant, circulates through a separate water circuit within the building. This heated water is distributed to various heat exchangers located in rooms or spaces that require heating. These heat exchangers transfer the thermal energy from the water to the indoor air, effectively warming the building.

Finally, the refrigerant, having released its heat, condenses back into a liquid state within the condenser coil. The liquid refrigerant then passes through an expansion valve, where its pressure and temperature are reduced, preparing it to repeat the cycle by returning to the evaporator coil in the boreholes.

In summary, the GSHP system utilizes vertical borehole heat exchangers to extract geothermal heat from the Earth, transferring it to a refrigerant within the heat pump. This heat is then distributed throughout the building via a water circuit, providing efficient and sustainable heating.

These heat pumps, due to their exceptional energy efficiency, simplicity, and durability of the systems, as well as decentralized application, are recognized as one of the most promising technologies in terms of economic and energy savings. Supporting this is the fact that their global implementation records an annual growth of over 10% [2].

For the safe and long-term application of these facilities, special attention should be paid to the sustainability of their operation. In other words, the ground-coupled heat exchangers need to be properly dimensioned to ensure that over the decades of operation, there is neither a significant increase nor a significant decrease in the temperature of the soil in which they are placed.

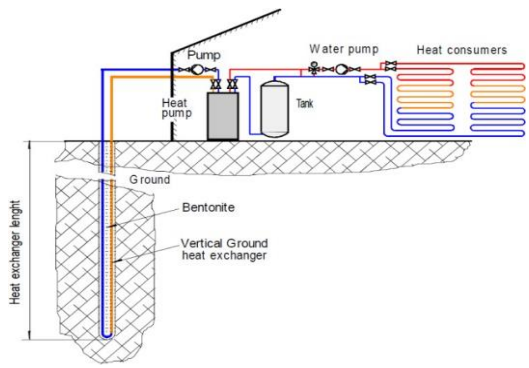

Figure 2. Scheme of a heating system with a geothermal heat pump and a vertically buried heat exchanger [1]

With the idea of bringing this issue closer to engineering practice, for the case of vertically embedded heat exchangers (Figure 3), recognized and accepted models for their dimensioning are presented, as found in the professional literature. Two relevant analytical methods were selected for analysis, and their results were compared with numerical solutions. On a specific example, their prediction reliability was verified, highlighting inconsistencies and significant mutual deviations in results arising from their use.

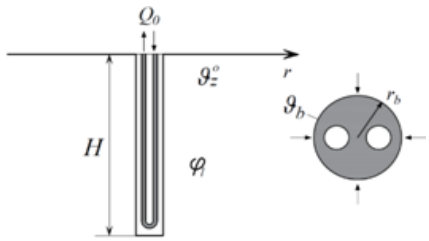

Figure 3. Schematic representation of a typical vertical borehole

I. HEAT TRANSFER THROUGH A GROUND-EMBEDDED HEAT EXCHANGER

To understand the complex phenomena occurring during the transfer of heat between the ground as a heat source and the working fluid, it is necessary to form a model and apply basic principles of thermodynamics to it. The direction of heat flow depends on the operating modes of the heat pump. In the winter period, the heat pump extracts heat from the ground, and then the temperature of the ground is higher than the temperature of the working fluid flowing through the pipe in the ground. The most intensive exchange occurs at the beginning of the pipe of the heat exchanger because there is the greatest difference between the temperature of the ground ϑg and the temperature of the working fluid at the entrance to the heat exchanger ϑi, while the temperature of the fluid at the exit of the heat exchanger ϑo is almost equal to the temperature of the ground (Figure 4a). On the other hand, in the summer period, heat is transferred to the ground because in this mode of the heat pump, the temperature of the working fluid is higher than the temperature of the ground (Figure 4b). In the next chapter, we will discuss the winter operating mode of the heat pump, through the basic principles of thermodynamics.

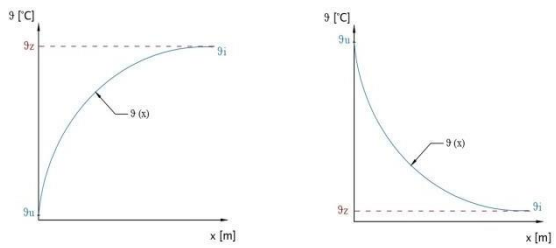

Figure 4. a) winter operating mode b) summer operating mode

A. *Heat Transfer Model*

Before analyzing the heat transfer process through the vertically buried heat exchanger in the ground, the following assumptions are introduced:

-The process is steady-state.

-The temperature of the ground is higher than the temperature of the working fluid ($\vartheta_g > \vartheta$).

-The temperature of the ground is considered to be approximately constant.

-The influence of groundwater is neglected.

For a infinitesimally small control volume, we can establish mass and energy balance equations (First Law of Thermodynamics). After suitable transformations, employing Fourier's law and Taylor series expansion, we derive a second-order differential equation that describes the intricate process of heat transfer.

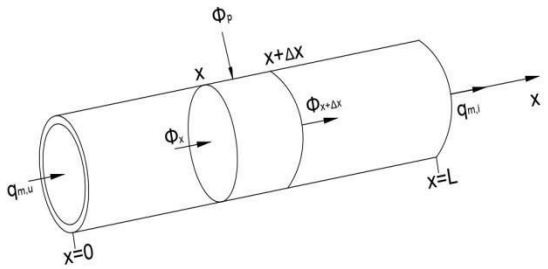

Figure 5. The model of the pipe of the heat exchanger through which the working fluid flows

$$\lambda \frac{\partial^2 \vartheta}{(\partial x)^2} = -4kL\left(\frac{d_o}{d_i^2}\right)\left(\vartheta_g - \vartheta\right) + \rho w_f c_p \frac{\partial \vartheta}{\partial x} \qquad (1)$$

B. Thermal resistances to heat transfer through a ground embedded heat exchanger in the ground

To install a vertical heat exchanger in the ground, it is necessary to provide a borehole of sufficient depth L and diameter d_b. Figure 3 shows a so-called "U-tube" placed in a borehole filled with backfill, typically bentonite. The heat transfer process from the ground to the working fluid, or vice versa, needs to be examined through thermal resistances in order to determine the heat transfer coefficient k.

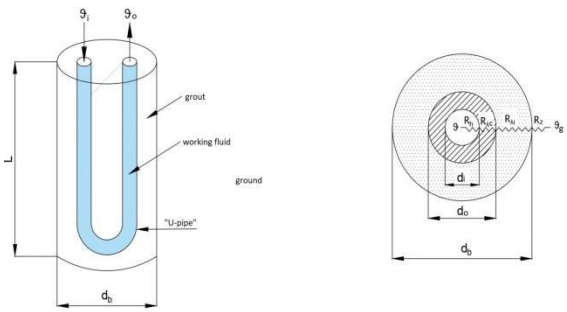

Figure 6. Single “U-pipe” and thermal resistances

$$R_{tot} = \frac{1}{h_i A_i} + \frac{1}{2\pi\lambda_p}\ln\frac{d_o}{d_i} + \frac{1}{2\pi\lambda_i}\ln\frac{d_b}{d_o} + R_g \qquad (2)$$

II. ANALYTICAL SIZING METHODS OF GROUND-EMBEDDED HEAT EXCHANGER

A. IGSHPA method

The IGSHPA method is an analytical approach for determining the dimensions of a vertical, ground-embedded heat exchanger, recommended by the International Ground Source Heat Pump Association. According to this method, specific lengths of the heat exchanger are determined to meet the heating requirements during the winter operating mode of the heat pump, as well as the lengths needed to fulfill the cooling needs during the summer operating mode of the heat pump [3]. Formulas for calculating these lengths are provided as follows:

$$L_h = \frac{\Phi_h (R_b + R_g F_h)}{\vartheta_0 - \vartheta_{\min}} \cdot \frac{COP_h - 1}{COP_h} \qquad (3)$$

$$L_c = \frac{\Phi_c (R_b + R_g F_c)}{\vartheta_{\max} - \vartheta_0} \cdot \frac{COP_c - 1}{COP_c} \qquad (4)$$

This analytical method does not require any iterative procedure; rather, after determining all necessary parameters, the required length is directly obtained. The larger of the obtained lengths is adopted. The initial step in dimensioning using this method is to determine the maximum thermal load of the building during the winter/summer period, similar to the approach taken in thermal engineering calculations. To obtain the peak thermal load on the ground, the expression is multiplied by a factor that encompasses the $COP_{h/c}$. The values of borehole resistance are determined based on geothermal tests and depend on the material and type of pipes, as well as the filling used in the borehole. The soil resistance is determined using either the infinite line source model (ILS) or through measurements at the location itself. The temperature of the thermally undisturbed soil is also determined through measurements at the borehole location or the borehole field.

B. ASHRAE method

The ASHRAE method for dimensioning a vertical, ground-coupled heat exchanger is a method recommended by the American Society of Heating, Refrigerating and Air-Conditioning Engineers . Similar to the IGSHPA method, this approach involves the specific determination of the length of the heat exchanger required to meet the heating needs during the winter operating mode of the heat pump, as well as the length needed to fulfill the cooling requirements during the summer operating mode of the heat pump [4]:

$$L_h = \frac{\Phi_y R_{g,y} + \left(\Phi_{l,h} - W_h\right)\left(R_b + PLF_m R_{g,m} + R_{g,d} F_{sc}\right)}{\vartheta_0 - \frac{\vartheta_{f,in} + \vartheta_{f,out}}{2} - \vartheta_p} \qquad (5)$$

$$L_c = \frac{\Phi_y R_{g,y} + \left(\Phi_{l,c} - W_c\right)\left(R_b + PLF_m R_{g,m} + R_{g,d} F_{sc}\right)}{\vartheta_0 - \frac{\vartheta_{f,in} + \vartheta_{f,out}}{2} - \vartheta_p} \qquad (6)$$

The transience (non-stationarity) of the process is encompassed by incorporating so-called impulses (daily $R_{g,d}$, monthly $R_{g,m}$, and annual $R_{g,y}$) into the calculation, which effectively represent the thermal resistances of the ground during the corresponding time periods (impulses). This dimensioning approach requires an iterative calculation since certain parameters appearing in equations (5) and (6) depend on the length of the buried vertical heat exchanger. The ASHRAE method includes the mutual influence of neighboring boreholes, further complicating the dimensioning process but making it more precise. As a result, this calculation method is often applied.

Similar to the IGSHPA method, the larger of the obtained values is adopted as the relevant length of the heat exchanger.

C. *Earth Energy Designer*

EED is a software package developed by the Swedish company BLOCON. The entire theoretical foundation of this software is based on the Eskilson theory, which he developed in his doctoral dissertation [5]. The essence of the calculation is based on determining g-functions, which depend on the geometry of boreholes, their spacing, and the depth of the boreholes themselves. The EED model utilizes precalculated values of g-functions using the Superposition Borehole Model (SBM) numerical model. Calculated values of g-functions for over 800 different configurations are integrated into the software, allowing EED quick access during calculations [6].

The mentioned numerical model is a three-dimensional model based on the superposition of a numerical axisymmetric solution for each borehole. The software provides the necessary borehole depth, the change in the average fluid temperature over a specified time period, and the option to optimize the selected configuration as a calculation solution. The EED software employs the Finite Line Source (FLS) model, considered the most accurate among traditional soil models, as it can account for axial effects of heat transfer processes over longer time periods. Eskilson initially proposed the general solution for the Finite Line Source model [5], later developed by Zeng [7], considering the impact of the finite length of the borehole and the surface of the soil as boundaries.

III. CALCULATION OF THE HEAT EXCHANGER

The comparative assessment of the quality of analytical methods (IGSHPA and ASHRAE) and the numerical EED method for sizing a vertical ground-embedded heat exchanger was evaluated using the example of utilizing geothermal energy for heating and cooling the SIV 3 building in New Belgrade. The calculation was conducted for the purpose of creating an appropriate study within the Project "Energy Efficiency Renovation of Central Government Building - Feasibility Study on EE Renovation of SIV 3 building," implemented by the United Nations Development Programme (UNDP) in Serbia.

Through a detailed energy audit of the building, carried out as part of the Energy Efficiency Study, it was determined that the annual heating demand for this building is 3412 MWh/year, the annual cooling demand is 1850 MWh/year, and the hot water consumption needs are 183 MWh/year. In addition, the review found that the heating power of the heating system is 4,136 MW, and the cooling power of the cooling system is 2200 MW.

The available space for installing geothermal probes, located in the green area in front of the SIV 3 buildings, is depicted in Figure 7. It consists of two plots - Field I with dimensions of 82.4 m x 73.6 m and Field II with dimensions of 73.6 m x 23.5 m.

Through conducted research, specifically Thermal Response Tests on two boreholes, "Geco-inženjering" d.o.o. established that the average temperature of the soil layer at a depth of 125 m is 18.83°C, and its (average) thermal conductivity has a value of $\lambda = 1.87$ W/m·K.

Figure 7. Available surface for the borehole field at the SIV 3 location

Using the previously mentioned data, a calculation was performed to determine the necessary dimensions for a ground-embedded heat exchanger that would sustainably utilize the earth as a heat source or sink. With the IGSHPA method, it was determined that the total required length of the vertical, ground-embedded heat exchanger should be 49,667 m. Using the ASHRAE method, the calculation yielded a required length of 113,420 m for the heat exchanger. Finally, the numerical EED method calculated that the necessary length of the heat exchanger is only 30,628 m.

Assuming that the numerical EED method provided the most accurate results, it can be concluded that the IGSHPA method predicts dimensions for the heat exchanger that are about 62% larger than necessary. Additionally, despite being more complex than the IGSHPA method and encompassing transient heat exchange processes more comprehensively, the results obtained with the ASHRAE method are higher than those obtained with the EED method by 2.7 times. A graphical representation comparing the results of the two analytical methods and one numerical method for sizing is shown in Figure 8.

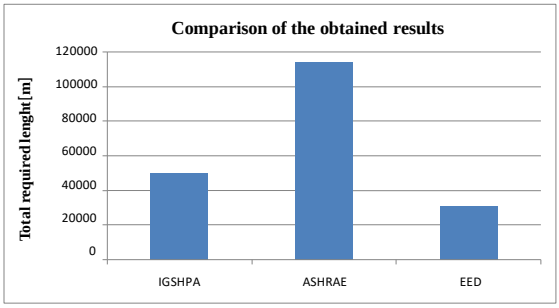

Figure 8. Graphical Comparison of Results from Two Analytical and One Numerical Sizing Methods

The differences observed in the results of calculations made by the IGSHPA method and the numerical EED method can primarily be attributed to inaccuracies in adopting specific values in the relevant analytical equations of EED method. Additionally, differences arise due to the inherent limitations of all analytical approaches to accurately capture the intricate dynamics of the heat transfer process and the mutual interactions of the surrounding wells. Notably, the absence of a representation for borehole thermal resistance in the IGSHPA method equation additionally raises suspicion about the precision of this calculations.

Similarly, the differences in results obtained by the ASHRAE method and the numerical EED method stem from the former's reliance on adopting critical parameters such as the penalty temperature of the fluid traversing the exchanger, fluid temperatures, and thermal resistances of the soil across diverse temporal intervals. Although ASHRAE provides guidelines for the adoption and calculation of these parameters, the instructions may lack the necessary precision, requiring using additional data sources and, in some instances, on-site measurements.

It is also noteworthy that both analytical methods incorporate constant values for maximum thermal loads during both heating and cooling phases, which indicates a potential overestimation of exchanger dimensions. Neither analytical method considers borehole configuration, exchanger pipe geometry within the borehole, the nature of the working fluid including its physical and chemical properties, nor the dynamic nature of the thermal load over specific time intervals-aspects comprehensively addressed by the numerical EED method.

IV. VERIFICATION OF SYSTEM SUSTAINABILITY

In addition to sizing, the EED software enables the validation of the system's sustainability throughout the operational period. In order to prevent significant disruptions to soil temperature during the operational period, it is essential for diagram illustrating the base load throughout the year should exhibit a more uniform profile in both heating and cooling modes (Figure 9).

Through the executed simulation of the heating/cooling system operation in the EED software, data on monthly temperature distributions of the fluid under typical loads for the next 25 years of operation were obtained. The simulation indicates that the minimum average fluid temperature after 25 years of system operation will be 10 °C (end of January). The end of August is anticipated as the period when, after 25 years of operation, maximum average fluid temperatures can be expected, reaching 29°C according to the model (Figure 10).

Figure 11 depicts the determination of the optimal borehole depth for a given configuration, aiming to ensure a reliable operation of the system.

To obtain the results in the EED software shown in Figures 9, 10, and 11, input data regarding the soil characteristics, dimensions, and material of the probe, as well as the working fluid flowing through the embedded heat exchanger, are essential. The parameters utilized were adopted based on investigations conducted by "Geco-inženjering" d.o.o., and the well configuration was adjusted to the available surface area (Figure 7).

The examination was conducted with a borehole diameter of 152 mm, utilizing Double U type pipes with an outer diameter of 32 mm. The thermal conductivity of the pipe material is 0.42 W/ m·K, while the thermal conductivity of the filling material is 0.8 W/ m·K. The working fluid applied in the software analysis is 25% monoethylene-glycol.

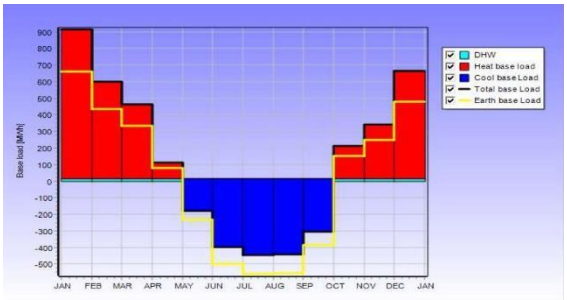

Figure 9. Base load throughout the one year

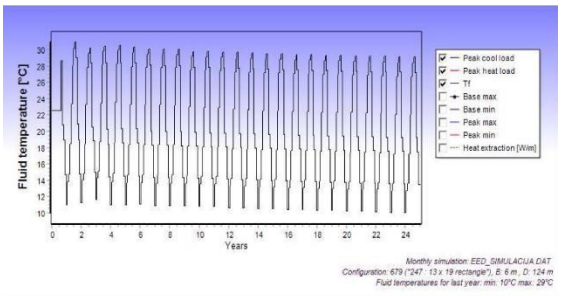

Figure 10. Presentation of fluid temperature variations under base load over 25 years of operation

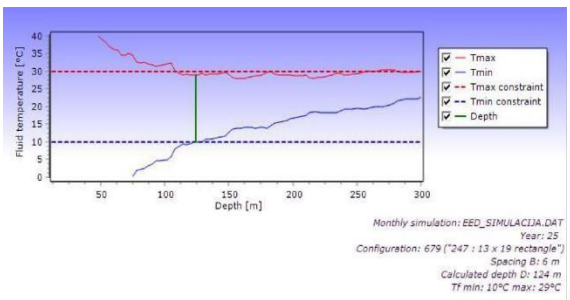

Figure 11. Presentation of determining the required borehole depth

V. CONCLUSION

Despite being more straightforward for utilization and recommended by reputable professional associations such as IGSHPA and ASHRAE, analytical methods for sizing ground-coupled heat exchangers in geothermal heat pump systems fail to provide sufficiently accurate results to endorse their use in engineering calculations. When applied to a real-world case of sizing a vertical ground-coupled heat exchanger for utilizing geothermal energy to heat and cool the SIV 3 building in New Belgrade, the dimensions calculated by the IGSHPA method were 62% larger than those obtained by the numerical EED method. In the case of the ASHRAE method, the calculated dimensions were even 2.7 times larger than the results obtained by the EED method. Simultaneously, although using commercial software and embedded numerical models likely yields more accurate results, there is no means of independently

verifying their accuracy, relying instead on trust in the expertise of their creators.

Given the increasing adoption of geothermal heat pumps and the growing need for quick, simple, yet sufficiently accurate and reliable calculations, further work is essential in refining existing analytical expressions or creating new ones for sizing ground-coupled heat exchangers in geothermal heat pump systems. These new models should take into account the dynamics of daily and seasonal loads, the arrangement and influence of neighboring boreholes, the type of working fluid, and more.

REFERENCES

1 Banjac, M. J., *et al*., Experimental determination of thermal conductivity of soil with a thermal response test, *Thermal science*, 2012, Vol. 16, No. 4, pp. 1117-1126, https://doi.org/10.2298/TSCI100627156B

2 Rosenow J., D. Gibb, N. Thomas, Lowes R., *Heating up the global heat pump market*, Nature Energy, 2022

3 Xuedan Z., Z. Tintian, Bingxi L., J. Yiqiang, *Comparison of Four Methods for Borehole Heat Exchanger Sizing Subject to Thermal Response Test Parameter Estimation*, School of Energy Science and Engineering, China. Energies, 2019, 12, 4067

4 *** *Geothermal Energy*, ASHRAE Handbook.

5 Eskilson P., *Thermal analysis of heat extraction boreholes*, Doctoral Thesis, University of Lund, 1987.

6 BuildingPhysics.com (https://buildingphysics.com/download/eedfaq.pdf)

7 Zeng H., Diao N., Fang Z., *Heat transfer analysis of boreholes in vertical ground heat exchangers*, International Journal of Heat and Mass Transfer, 2003.

NOMENCLATURE

$COP_{h/c}$	- coefficient of performance [-]
$F_{h/c}$	- run fraction for heating/cooling mode [-]
F_{sc}	- short circuit loss factor [-]
$L_{h/c}$	- required design length for heating/cooling mode [m]
PLF_m	- part load factor [-]
R_b	- borehole thermal resistance [mKW^{-1}]
R_g	- ground thermal resistance [mKW^{-1}]
$R_{g,d}$	- effective thermal resistance of ground (daily pulse) [mKW^{-1}]
$R_{g,y}$	- effective thermal resistance of ground (annual pulse) [mKW^{-1}]
R_{tot}	-total thermal resistance [m^2KW^{-1}]
h_i	- heat transfer coefficient $\lceil \lfloor Wm^{-2}K^{-1} \rfloor \rceil$
A_i	-the inner surface of the pipe $\lfloor m^2 \rfloor$
λ_p	-thermal conductivity of the pipe $\lceil \lfloor Wm^{-1}K^{-1} \rfloor \rceil$
d_i	-inner diameter of the pipe $\lfloor mm \rfloor$
$R_{g,m}$	- effective thermal resistance of ground (monthly pulse) [mKW^{-1}]
$W_{h/c}$	-power input at design heating/cooling mode [kW]
$\Phi_{h/c}$	-design load for heating/cooling mode [kW]
Φ_y	- net annual average heat transfer to the ground [kW]
$\Phi_{l,h/c}$	- heat pump power in heating/cooling mode [kW]
$\vartheta_{f,in/out}$	- liquid temperature at heat pump inlet/outlet [°C]
$\vartheta_{max/min}$	- maximum/minimum fluid temperature [°C]
ϑ_o	- undisturbed ground fluid temperature [°C]
ϑ_p	- temperature penalty [°C]
d_o	-out diameter of the pipe $\lfloor mm \rfloor$
λ_i	- thermal conductivity of the grout $\lfloor Wm^{-1}K^{-1} \rfloor$
w_f	-fluid flow rate $\lfloor ms^{-1} \rfloor$
ρ	-density $\lfloor kgm^{-3} \rfloor$
L	-length of the borehole $\lfloor m \rfloor$

Quantitative modeling and economic assessment of a 5GDHC network in Cluj-Napoca

Student: Ș. Andrei MĂGUREANU
Teachers: lecturer PhD. eng. Constantin CILIBIU
lecturer PhD. eng. Andrei M. BOLBOACĂ

Faculty of Building Services Engineering, Technical University of Cluj-Napoca

***Abstract*— Fifth-generation district heating and cooling (5GDHC) networks present an innovative approach to addressing the escalating global energy demand by promoting reductions in greenhouse gas emissions and enhancements in energy efficiency. This study explores the viability and potential of a conceptual 5GDHC network situated in Cluj-Napoca, Romania. The network is distinctively integrated with groundwater thermal energy storage and features a significantly oversized horizontal thermal collector constructed from uninsulated plastic pipes, alongside decentralized energy production mechanisms. Such systems hold the potential to act as a vanguard for climate action initiatives, offering substantial benefits not only to the urban area of Cluj-Napoca but also contributing significantly to the environmental strategies of Romania.**

***Index Terms*— 5GDHC, greenhouse gas emissions, groundwater thermal energy storage, horizontal thermal collector, uninsulated plastic pipes, decentralized energy production, climate action initiatives.**

I. INTRODUCTION

The last century's energy transition marked a significant shift towards the adoption of innovative production technologies, such as renewable sources. The core objective behind embracing new energy sources is to mitigate environmental impact, targeting both reduction in greenhouse gas emissions and increase in production efficiency. However, the urgent issue of climate change, now more apparent than ever, encounters the obstacle of a world with escalating energy demands, a trend set to continue in the foreseeable decades.

1.1. Background

Previous publications have provided clear examination of the evolution of district heating systems ([1],[2],[3]), starting with the first generation which utilized high-temperature steam for distribution. The transition to second and third generations marked the replacement of steam with pressurized hot water. Progressively, the strategy shifted towards reducing the network's distribution temperature while incorporating emerging technologies such as renewable energy, waste heat utilization and micro cogeneration plants. The advancement to the fourth generation saw reduction in thermal levels, enabling said integration, including solar and geothermal energy.

The new generation of thermal grids distinguishes itself from its predecessors through the following key advancements [4]:

- The implementation of grid temperatures that closely match ground temperatures to minimize thermal losses
- The ability to address to different loads: heating and cooling
- Energy sources having low temperature difference with the ambient temperature
- Integration with the power grid, facilitating the thermal storage of excess electrical energy produced from renewable sources
- 100% renewable energy target

Interest in the potential of next-generation thermal grid applications has significantly grown across European nations, evidenced by the variety of research endeavors both underway and completed. This enthusiasm towards development is supported by the availability of market-ready, established technologies, which allows for the swift launch of pilot projects.

Several projects have been implemented across Europe, with notable examples in Glasgow and Paris documented in references [4], [5], and [6]. The scalability of 5GDHC is increasingly supported by such projects and individual case studies demonstrating the viability of such expansions.

1.2. Aim of the research

As urban populations grow, there's an inevitable rise in energy demand and greenhouse gas emissions. The trend of global urbanization is projected to continue, with the urban population share growing from its current 54% to an estimated 68% by 2050 [7]. This increase will further intensify the energy and environmental challenges faced by urban centers.

A zero-carbon city can be defined from the perspective of energy production and use, as a city that generates as much or more carbon-free sustainable energy as it uses [8]. NetZeroCities is a project that is part of the Horizon 2020 Research and Innovation Programme in support of European Union's Green Deal. NetZeroCities has been designed to help cities overcome the current structural, institutional and cultural barriers they face in order to achieve climate neutrality by 2030 [9]. This initiative has the goal of achieving 100 smart and climate-neutral cities by 2030 and Cluj-Napoca was selected to be part of it in 2022, positioning the city as an European frontrunner in adopting green transition strategies. In support of this mission, Cluj-Napoca City Hall, through the "Clujul Verde" initiative, is dedicated to enhancing urban quality of life. This commitment is evident in efforts to modernize and expand green spaces, improve pedestrian infrastructure, promote eco-friendly public transportation, and most importantly, the shift toward sustainable energy solutions.

The aim of this work is therefore to propose an innovative 5GDHC grid model that aligns with previously mentioned initiative. This model integrates technologies

like thermal energy storage and decentralized, sustainable energy production, leveraging local energy sources without disrupting the natural balance. The proposed design is envisioned as a functional pilot cluster that could lead to a broader network of interconnected systems in the future. This paper's methodology was designed to be both practical and economically viable, while still offering holistic strategies for identifying and addressing challenges within the system's implementation.

II. METHODOLOGY

The model simulates the energy dynamics of a 5GDHC system, focusing not only on the aspects of energy consumption and production but also on maintaining the environmental equilibrium, which such systems might otherwise disrupt. A combination of empirical models [10, 11,12] and simulation programs [13] has been used and referenced in this study to achieve this objective.

2.1. Efficiency of the existing system

This system was conceived as an alternative to the significantly inefficient current central heating system, the District Heating Plant (DHP) in the Mărăști district of Cluj-Napoca. The existing DHS infrastructure includes an older setup with a 116 MWt overheated water boiler, complemented by a newer cogeneration installation. This modern setup features three cogeneration units, each with 1.5 MWe and 1.6 MWt thermal output, alongside four hot water boilers with capacities of 8, 14, 16, and 24 MWt.

In table I, annual values are presented, calculated using a mathematical model based on TMY (Typical Meteorological Year), for delivered heat, heat produced, and contained heat in the natural gas [14].

TABLE I. ANNUAL VALUES OF THE ENERGY BALANCE COMPONENTS

Delivered heat (MWh)	Produced heat (MWh)	Contained heat (MWh)
35383	72210	90262

According to [14], the distribution efficiency is 49%, which means that less than half of the produced thermal energy is delivered to the consumers. These losses can be attributed entirely to the high temperature of the fluid and the faulty insulation of the distribution system.

The overall efficiency of the existing system is 39%, indicating a loss of 61% caused by production and transportation. In addition to distribution losses, this value includes inefficiencies in the fuel burning processes and losses through radiation from equipment.

The annual level of CO_2 emissions for the existing system is 21121 tCO_2.

2.2. Geographical context

The geographical coordinates of Cluj-Napoca are 46°46′N 23°35′E, situating the city in the northwestern part of Romania. The prevailing ground type is clay under natural conditions, with a relative humidity of around 80% ([15], [16]). Based on data presented in [15], [16] and [17], the thermal properties of this soil type at an average temperature of 11.85 °C and at depths of 2 to 5 meters are defined as follows: thermal conductivity λ=1.16 W/mK and thermal diffusivity α=7.009·10^{-7} m^2/s.

Geotechnical and hydrogeological studies conducted by the Cluj-Napoca Water Company ([18], [19]) and provided to the author, reveal characteristics of the local aquifer as follows: the aquifer table is situated at a depth of 60 meters, where its temperature is 8 °C, with a potential extraction flow rate of 980 liters per second.

The data presented above holds relevance to this paper, considering that the implementation of this 5GDHC network leverages the two local and natural energy sources: the ground and the aquifer.

2.3. Model configuration

This study aims to propose an alternative to the existing inefficient heating system in the Mărăști district of Cluj-Napoca. It implies a distribution system with a total length of 90 km for the supply pipe and an equal length for the return pipe. This network is designed to be installed at the depth of 4 meters.

Previously indicated, the study leverages both the aquifer and the ground as unconventional, centralized energy sources, complemented by heat pumps serving as decentralized sources, where each decentralized station is comprised of one reversible heat pump for heating and cooling, and an additional heat pump for domestic hot water (DHW). This ensemble of energy sources is engineered to provide at least an equivalent amount of energy as currently delivered by natural gas combustion at the DHP, thus the calculated heating power requirement for a single apartment is 1.7 kW, with the method presented in [20], while the demand for DHW is calculated at 2.5 kW. By employing the previously stated values and incorporating data from [14], the resulting values were derived and are now provided:

TABLE II. SUMMARY OF UNITS

	Value
Total number of apartments	4440
Total number of buildings	222
Total number of heating/cooling Heat Pumps	444
Total number of DHW Heat Pumps	444

The calculation algorithm [20] used for determining the necessary power values inherently tends toward oversizing. This approach not only facilitates the addition of new consumers in the short term but also accommodates an increased number of users following the rehabilitation of apartment blocks over the longer term, without alterations to the energy sources.

The supply network spans a total of 90 km, divided roughly equally into two, with each part supplying one half of the total consumers. The supply pipeline is doubled by the return pipes. The network is constructed using PE100 pipes with outer diameter of 800 mm and inner diameter of 705 mm and with nominal pressure of 10 bar. The supply pipe maintains an annual average temperature of 7 °C, whereas the return pipe operates at 2 °C, so that the highest temperature in the network is equal to the lowest temperature the ground can naturally reach. This 5 °C temperature differential is strategically maintained to ensure the coefficient of performance (COP) of the heat pumps is not adversely affected. According to the equation of continuity, the flow rate is 445.81 liters per second in each section, with corresponding velocity of 1.75 m/s.

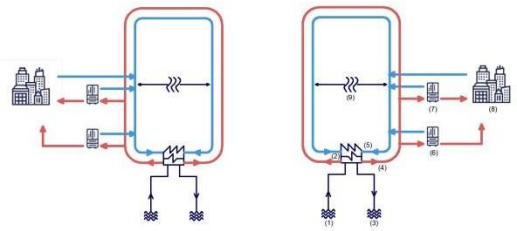

Figure 1. Diagram depicting the functioning of the 5GDHC model

In Figure 1, the diagram illustrates the components of the system as follows: Component 1 represents the aquifer section from which water is extracted; Component 2 is the heat exchanger; Component 3 denotes the section where water is re-injected into the ground; Component 4 is identified as the supply pipe; Component 5 corresponds to the return pipe; Component 6 is the heat pump designated for domestic hot water (DHW) production; Component 7 is the heat pump used for heating purposes; Component 8 represents the consumers and Component 9 is the ground yielding thermal energy to the return pipe.

4. The centralized plant

The employment of groundwater as one of two secondary heat sources within the presented system, while offering certain benefits, also entails potential risks stemming from one primary trigger: gas exsolution over a long-term perspective.

The following set of analyses aims to give a better understanding of the phenomena under consideration, with the objective of creating remedial strategies based upon rigorous mathematical and thermophysical models.

1. Relevance of gas solubility

The relations between gases and chemical precipitation holds importance in any groundwater-based system, particularly the interactions between oxygen O_2 or carbon dioxide CO_2 and other elements, as the two aforementioned gaseous species affect the chemical equilibria of many compounds [17]. Henry's law states that gas solubility in water is dependent on pressure, concentration and temperature [21]. This has significant implications on groundwater-based systems, where the extraction of water from an aquifer induces a decrease in hydrostatic pressure, culminating in CO_2 oversaturation. The resultant exsolution of CO_2 instigates chemical disequilibrium within the aquifer, leading to elevated pH levels. This shift facilitates the onset of precipitation reactions, altering both the chemical composition of the groundwater and the functioning of the system. This phenomenon is further examined in the specific literature [22].

For a comprehensive evaluation of the risks associated with gas exsolution within a system, it is imperative to examine how the design of the system impacts groundwater pressure throughout its operation. To accurately account for the impacts of the parameters, it is essential to consider the piping system's size, length and roughness, as well as the elevation relative to the reference point. Moreover, energy losses through the system must be considered. These factors are expressed in relation (1), an adaptation of Bernoulli's equation for the hydraulic system (rearranged after equation (2) in [11])

$$\frac{p_2}{\rho g} = \frac{p_1}{\rho g} + \alpha_1 \frac{V_1^2}{2g} - \alpha_2 \frac{V_2^2}{2g} + (z_1 - z_2) + h_{pump} - h_{losses} \quad (1)$$

Where p denotes the hydrostatic pressure (Pa), V the mean groundwater flow velocity (m/s), g the gravitational acceleration (m/s^2), ρ the density of groundwater (kg/m^3), z the elevation (m) and α the correction factor for turbulence in pipes. 1 and 2 are arbitrary location within the system. The terms $p/\rho g$ are pressure heads, $V^2/2g$ are velocity heads, h_{pump} is the hydraulic head supplied by the submersible pump and h_{losses} is the sum of all frictional losses. All terms are measured in m.

Equation (1) states that hydrostatic pressure is converted into potential and kinetic energy. In the context of gas solubility effects, these transformations should be regarded as pressure losses. For a better relevance to our system, the following assumptions are made: point 1 is strategically located at the water table within the aquifer, meaning that the velocity of water (v_1) is negligible and the reference elevation being in fact z_1, thus equal to 0. At this location, pressure naturally equilibrates to the atmospheric pressure, serving as a referenece point again, so $p_1 = 0$. Inside the pipe, the mean velocity can be represented as Q/A. So, the new equation is ([11]):

$$\frac{p_2}{\rho g} = h_{pump} - h_{losses} - z_2 - \alpha \frac{Q^2}{2gA^2} \quad (2)$$

This equation describes the total pressure of water in an arbitrary point in the system. Given the premise that all head losses are compensated for by the submersible pump, it establishes a state of dynamic equilibrium, where h_{pump}=h_{losses}. The equation can also be used to describe the power needed to circulate groundwater.

$$P = \frac{\rho g Q h_{pump}}{y} \quad (3)$$

where η is the coefficient of efficiency. Equation (2) serves as a basis for tracking the pressure along the system during operation, thereby facilitating an understanding of the potential of gas exsolution.

2.4.2. The design concept

The proposed design assesses the pressure variable. The purpose of such a system is to supply adequate thermal energy to the heat exchanger while avoiding the occurrence of gas exsolution. This is achievable by ensuring a continuous increase in pressure throughout the system, rather than allowing for drops in pressure.

A design concept which incorporates an adequate approach to pressure and temperature management in the system has been previously described in [11]. The same concept will be tested for the case study in Cluj-Napoca. Data that is necessary for the implementation is extracted from ref. [18], [19] and includes the value of the possible flow rate within the system at 10 l/s and depth of the aquifer set at 60 meters, which will serve as a reference plane for calculations.

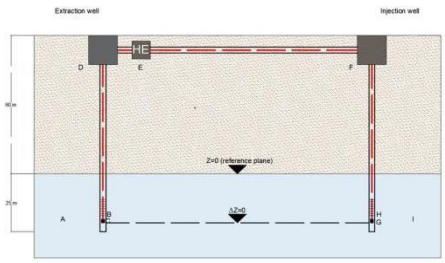

Figure 2. Geothermal substation layout

In figure [2], the system is depicted as a sequence A-I which represents different components and locations within the system. Points A and I are situated in the aquifer, in the vicinity of the production and injection well, respectively. Point C (25m) is the submersible pump, and B denotes the production well screen. D represents the housing of the production well, leading to point E, the heat exchanger, and further along to F, the injection well housing. The distance between D and E is kept relatively short, to avoid vacuum pressure forming in the heat exchanger. Point H is the injection well screen and G the outlet pipe within the injection well, placed at the same depths as their counterparts.

Gas exsolution occurs when the hydrostatic pressure in point A or I fall beneath the partial pressure of CO_2 in water. A thorough understanding of the chemical equilibrium between CO_2, bicarbonate HCO_3 and carbonate CO_3^{-2} is needed. In the absence of such specific data, a conservative and safe approach is to maintain the hydrostatic pressure at the depth of A and I constant.

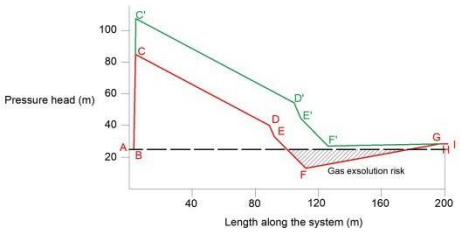

Figure 3. HGL for the design concept

Using formula (2) and noted considerations, it is possible to construct a Hydraulic Grade Line (HGL) for the system which specifically addresses the risk of CO_2 exsolution. The resulting graph (figure 3) indicates that in the absence of a mechanism to maintain a steady pressure above the threshold where exsolution becomes a risk, there is hazard that CO_2 will exsolve.

To manage this risk, a backpressure valve is installed at the exit point of the injection pipe (G). For this system, the pressure of the valve has been determined to be approximately 2 bars, which means that point F in the system would remain safely above the threshold.

2.5. Thermal capacity of the ground

The ambient temperature network functions as a thermal collector by transporting a secondary agent for water-water heat pumps. Determining the correct amount of energy that can be extracted from the ground requires a careful balance. It's essential to size the loop system adequately to prevent overcooling during the winter months. To ensure so, two important parameters are considered: thermal diffusivity and thermal conductivity. For the region of Cluj-Napoca, reference values have been previously presented in section 2.2. Using these values, it is possible to calculate the volumetric heat capacity of the soil:

$$C_v = \frac{\lambda}{a} \left[\frac{J}{m^3 K}\right] (4)$$

Both λ and α are dependent on ground temperature. For thermal diffusivity, a straightforward variation equation can be defined:

$$\lambda = \lambda_0 + b(T - T_0) (5)$$

Where λ represents the thermal diffusivity at a given temperature T, and λ_0 is the thermal diffusivity at a reference temperature T_0, with b acting as the variation factor. Another workpaper [23] investigates the variation of thermal conductivity with temperature for a soil composition closely resembling that found in Cluj-Napoca, focusing specifically on the positive temperature range of 1-5 °C. Drawing from these findings, we consider the coefficient of variation, b, to be equal to 0.01 per 1 °C increment. Consequently, over an annual cycle, λ ranges from 1.11 to 1.20 W/mK.

Reference [12] provides an equation to describe how thermal diffusivity varies in relation to both depth and temperature:

$$\alpha_z = \frac{\omega}{2}\left(\frac{z}{\ln \frac{T_p}{T_H + T_m}}\right) (6)$$

According to [12], temperature variation is conceptualized as a harmonic function over time, implying its similarity to a periodic wave oscillating around the average temperature. Despite its simplicity, this model effectively captures the fundamental characteristics of seasonal temperature fluctuations. Therefore, in equation (6), ω is angular frequency (rad/s), in our case $2\pi/365 \cdot 24 \cdot 3600$, T_m (°C) the annual average temperature, T_p (°C) the monthly amplitude, T_H (°C) the maximum temperature of the soil that takes place during the annual cycle. Thus, α fluctuates between $9.52 \cdot 10^{-7}$ and $5.34 \cdot 10^{-7}$ m^2/s throughout a year.

Employing equations (5) and (6), alongside soil temperature data sourced from [24], enables the calculation of the annual variation of the volumetric heat capacity C_v in relation to temperature for Cluj-Napoca, specifically at a depth of 2 meters.

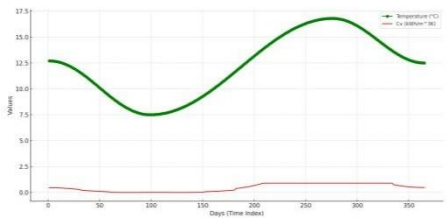

Figure 4. Volumetric heat capacity variation with temperature in an annual cycle

Based on the data presented in figure 4, the daily average thermal capacity of the ground per unit volume—prior to altering its temperature by 1 degree—during Romania's heating season, where at depths of 4 meters the average temperature is 11.58 °C, is 0.452 kWh/m³K.

With the aforementioned variable established, it becomes possible to formulate an equation for calculating the total amount of heat that can be extracted from the ground:

$$Q_{ground} = \pi L x (d + x) \cdot C_v (7)$$

Where L is the total length of the system, x the distance from the pipe that is capable of heat loss and d the of the pipes.

Assuming x is roughly 1 meter, according to equation (7), the volume of soil impacted by thermal exchange is 508680 m^3 and Q_{ground} is 229.92 MWh/K.

To determine the heat transfer between the ground and the thermal agent, it is essential to calculate the heat flow between them, which relies on the total thermal resistance.

$$q = \frac{\Delta t}{R_t} \quad (8)$$

$$R_t = R_1 + R_2 + R_3 \quad (9)$$

In (8), q is the heat transfer between the thermal fluid and the ground (W/m) and Δt (°C) is the temperature difference between the ground and the fluid.

In equation (9), R_t (mK/W) represents the total thermal resistance. The components of the resistance are as follows: R_1 (mK/W) denotes the resistance to heat transfer via conduction between the ground and the pipe's exterior. R_2 (mK/W) signifies the resistance to heat transfer via conduction from the exterior to the interior of the pipe. Finally, R_3 (mK/W) represents the resistance to heat transfer via convection between the pipe's interior and the working fluid.

$$R_t = \frac{1}{2\pi\lambda_g}\ln\left(\frac{2h}{d_e} + \sqrt{\left(\frac{2h}{d_e}\right)^2 - 1}\right) + \frac{1}{2\pi\lambda_{PE}}\ln\left(\frac{d_e}{d_i}\right) + \frac{1}{\pi d_i \alpha_i} \quad (10)$$

In (10), λ_g (W/mK) is thermal conductivity of the ground, same as λ from (5), h (m) is the depth of the pipe, d_e (m) is the outer diameter of the pipe, λ_{PE} (W/mK) is the thermal conductivity of the pipe's material, in this case high-density polyethylene PE100, d_i (m) is the inner diameter of the pipe and α_i (W/m^{2}K) is the forced convection factor. Out of these values, α_i is the only one not readily available.

In order to determine α_i, we need to compute a function of variables, specifically the Reynolds, Nusselt and Prandlt numbers.

$$\alpha_i = \frac{Nu \cdot \lambda_w}{d_i} \quad (11)$$

$$Nu = 0.021 \cdot Re^{0.8} \cdot Pr^{0.43} \cdot \left(\frac{Pr}{Pr_p}\right)^{0.25} \cdot \varepsilon_L \quad (12)$$

$$Pr_p = f(t_p) \quad (13)$$

$$Pr = f(t_w) \quad (14)$$

$$Re = \frac{w \cdot d_i}{u} \quad (15)$$

In equation (11), λ_w=0.55675 (W/mK) is the thermal conductivity of water at the average temperature of 2.5 °C. In (12), ε_L=1 (-) is a factor dependent on the length of the network. In (13) and (14), t_p (°C) and t_w (°C) represent the temperatures on the interior side of the pipe's wall and of the water, respectively. In equation (15), w (m/s) is the velocity of water and v (m^2/s) the kinematic viscozity of water.

It is now possible to determine the value of q, representing an instant measurement of thermal energy transferred from the ground to the thermal agent per meter of pipe, which at the average temperature of 11.85 °C for the ground and 4.5 °C for the water is 18.44 W/m.

$$Q_t = q \cdot L \quad (16)$$

Equation (16) details Q_t, representing the rate of thermal exchange between the ground and the entire system, which is 1659.6 kW for the previously mentioned average value of q.

$$r_{ne} = \frac{V_w \cdot c_w}{Q_t} \quad (17)$$

Equation (17) specifies the total time needed, τ_{nec} (h/K), accounting for the rate of thermal exchange, to increase the temperature by 1 degree across the entire network, which is 24.56 h/K. The value for the numerator term in this case is 40772.19 kWh/K and it represents 17.76% of the total energy required to change the surrounding ground's temperature by 1 degree.

Based on the analysis, it is reasonable to conclude that, without considering electrical power or other variables, it would take approximately 5 days to elevate the return pipe's temperature back to the supply pipe's value, without causing the ground temperature to drop by even one degree. However, it's important to remember that the ground in the system serves as an auxiliary energy source, and the representation of energy transfer is not linear.

Data obtained from source [24] and illustrated in Figure 4 provide the minimum soil temperature value in an annual cycle. By considering this value as the lower limit for the degree of temperature decrease in the ground, given that the ground can naturally replenish that energy, it becomes feasible to calculate the total amount of energy that can be extracted from the ground without disrupting the natural equilibrium.

2.6. Energy consumption

The total energy consumption is directly linked to the required heating power of the system and is computed as an hourly sum of the total power consumption needed to maintain the temperature inside the apartments constant at 20 °C, amidst lower external temperatures. The total yearly value, expressed in MWh, is 20128.75.

The total yearly energy consumption for DHW production, based on measured values from [14], is 15255 MWh.

Considering a qualitative adjustment of the thermal agent's temperature based on external temperatures, the seasonal Coefficient of Performance (COP) for space heating is 3.36. For hot water, maintaining a constant temperature of 45 °C, the seasonal COP is 3.79. Combined, these efficiencies yield an annual electrical energy output of 10015.89 MWh.

The hydraulic load loss for water circulation through the loop has been determined to be 1.21 mH_2O/km, resulting in

a total loss of 5.44 bar over 45 km. Accordingly, one circulation pump with a nominal power of 315 kW and an effective power of 275.8 kW needs to be installed at each of the two parts of the network.

The energy extraction capability from the two sources is calculated hourly, compared with the thermal energy demand for heating and hot water. The analysis assumes a minimum sustainable and environmentally safe ground temperature of 7.5 °C—corresponding to the annual cycle's natural low and the supply pipe's temperature. This induces thermal equilibrium-like state, halting ground energy extraction and prompting a switch to aquifer-sourced thermal energy via heat exchangers. Among the 98 boreholes in the target area, a maximum of 43 boreholes are utilized for energy extraction, a value reached on the 49th day of the year. For these, with a flow rate of 10 l/s and a necessary hydraulic load of 111 mH2O, installing 43 submersible pumps, each with a nominal power of 18.5 kW and an effective power of 15.58 kW, is requisite.

Therefore, the overall energy consumption of the pumps accounts for variations in energy extracted from the two primary sources and the flow rates in both areas. The outcomes reveal annual consumptions of 671.28 MWh for circulation pumps and 2541.58 MWh for submersible pumps, accumulating to a total of 13,229.15 MWh for the whole system, including the heat pumps' consumption.

With these values, it is possible to compute the system's overall performance by considering the total thermal energy delivered compared to the total electrical energy consumed, inclusive of the electrical energy for the pumps. The resulting overall efficiency ratio is 2.67.

The system's primary energy is considered in report to the electrical energy sourced from the national grid. Utilizing a conversion factor from [25], the primary energy output is determined to be 33072.13 MWh. The equivalent CO2 emissions conversion factor, also from [25], indicates emissions of 3538.71 tonnes of CO2, which is 5.96 times lower than the current emissions from the District Heating Plant (DHP) system in Cluj-Napoca.

III. ECONOMICAL PERSPECTIVE

The current cost of thermal energy stands at 0.138 €/kWh. The cost for the proposed system is derived by multiplying the total electrical energy used by 0.168 €/kWh, the rate for one kWh of electrical energy, and then dividing by the total thermal energy output. We added an additional 30% to account for indirect costs such as maintenance and operational expenses, leading to a final cost of 0.081 €/kWh. The system is expected to have a lifespan of 25 years. With a total investment of 30,775,517 €, calculated at 0.40 €/m², the annual savings are projected at 1,993,672.61 €, derived from the cost differential per kWh between the existing and the concept systems. For the Net Present Value (NPV) calculation, we used a 4% discount rate, reflecting the low-risk nature of the investment given the mature technologies employed, reliance on stable grid electricity, and the increasing demand for electricity. The resulting NPV is 369,765.86 €, and the payback period is estimated at 15.43 years. The cost of each unit of saved energy is calculated at 0.093 €/kWh, with a cost-to-benefit ratio of 0.98.

IV. CONCLUSIONS

In conclusion, the proposed 5GDHC system for Cluj-Napoca is a technical innovation, showcasing integration of aquifer thermal storage and ground thermal energy. This system leverages a uniquely designed horizontal thermal collector constructed from uninsulated plastic pipes, strategically oversized to enhance the effective surface area for heat exchange. This setup ensures efficient thermal interaction with the surrounding soil, effectively reducing energy losses typically associated with heat transfer.

From a scientific perspective, the system leverages thermal dynamics to optimize energy usage. The ground and aquifer thermal energy sources are calibrated to maintain a near-ambient operational temperature, which significantly diminishes thermal losses and improves the overall energy efficiency of the system. The integration with low-temperature district heating and cooling technology is pivotal, allowing for the utilization of renewable energy sources, which further minimizes the environmental impact.

Economically, while the system demands an upfront investment of €30,775,517, it demonstrates substantial operational savings with an estimated annual saving of €1,993,672.61. The financial analysis shows a calculated Net Present Value (NPV) of €369,765.86, with a return on investment period of 15.43 years. The technical advancements contribute to these economic benefits by reducing maintenance costs and enhancing the energy yield per unit input.

Overall, this 5GDHC system represents a pioneering step towards sustainable urban energy solutions in Cluj-Napoca, combining scientific methodologies with practical, scalable technology to achieve significant reductions in greenhouse gas emissions and advance towards a zero-carbon urban environment.

V. REFERENCES

1 Henrik Lund, Poul Alberg Østergaard, Miguel Chang, Sven Werner, Svend Svendsen, Peter Sorknæs, Jan Eric Thorsen, Frede Hvelplund, Bent Ole Gram Mortensen, Brian Vad Mathiesen, Carsten Bojesen, Neven Duic, Xiliang Zhang, Bernd Möller, The status of 4th generation district heating: Research and results, Energy, Volume 164, 2018, Pages 147-159, ISSN 0360-5442

2 Henrik Lund, Neven Duic, Poul Alberg Østergaard, Brian Vad Mathiesen, Future district heating systems and technologies: On the role of smart energy systems and 4th generation district heating, Energy, Volume 165, Part A, 2018, Pages 614-619, ISSN 0360-5442

3 Abdur Rehman Mazhar, Shuli Liu, Ashish Shukla, A state of art review on the district heating systems, Renewable and Sustainable Energy Reviews, Volume 96, 2018, Pages 420-439, ISSN 1364-0321

4 https://5gdhc.eu/

5 https://www.clydegateway.com/

6 https://epa-paris-saclay.fr/nos-missions/amenager-durablement/le-reseau-dechange-de-chaleur-et-de-froid-de-paris-saclay-un-modele-innovant-au-service-de-la-transition-energetique/

7 Duan Z., Kim S., Progress in Research on Net-Zero-Carbon Cities: A Literature Review and Knowledge Framework. Energies 2023, 16, 6279.

8 https://en.wikipedia.org/wiki/Zero-carbon_city

9 https://netzerocities.eu/the-nzc-project/

10 A.M. Măgurean, Three-dimensional numerical model for heat transfer dynamic analysis for the building-soil interaction by applying the similarity theory, Thermal Science and Engineering Progress, Volume 43, 2023, 102013, ISSN 2451-9049,

11 Gjengedal, S.; Stenvik, L.A.; Storli, P.-T.S.; Ramstad, R.K.; Hilmo, B.O.; Frengstad, B.S. Design of Groundwater Heat Pump Systems. Principles, Tools, and Strategies for Controlling Gas and Precipitation Problems. Energies 2019, 12, 3657.

12 Andújar Márquez JM, Martínez Bohórquez MÁ, Gómez Melgar S. Ground Thermal Diffusivity Calculation by Direct Soil Temperature Measurement. Application to very Low Enthalpy Geothermal Energy Systems. Sensors (Basel). 2016 Feb 29

13 https://acad.npro.energy/

14 Local Strategy of the Thermal Energy Supply Service for Consumers in Cluj-Napoca Municipality for the period 2021 – 2031 and outlook for 2050

15 Tudor P. Todoran, Mugur C. Balan, Long term behavior of a geothermal heat pump with oversized horizontal collector, Energy and Buildings, Volume 133, 2016, Pages 799-809, ISSN 0378-7788

16 M.C. Balan, T.P. Todoran, S.D. Bolboaca, L. Jäntschi, Assessments about soil temperature variation under censored data and importance for geothermal energy applications. Illustration with Romanian data, J. Renew. Sustain. Energy 5 (2013) 1–13.

17 Stumm, W.; Morgan, J.J. Aquatic Chemistry: Chemical Equilibria and Rates in Natural Waters, 3rd ed.; Wiley: New York, NY, USA, 1996

18 Hydrogeological study regarding the rehabilitation of the underground water collection system from the Florești source, Cluj-Napoca Municipality, Rev. 1 August 2015

19 Geotechnical study regarding the regional project for the development of water and wastewater infrastructure in the counties of Cluj and Sălaj, in the timeframe 2014-2020, nr. 178/28.08.2015

20 SR 1907-1:2014 Heating Plants. Design Heat Requirements Computation for Buildings. Computation Method (Romanian standard)

21 Henry, W., III. Experiments on the quantities of gases absorbed by water, at different temperatures, and under different pressures. Philos. Trans. R. Soc. Lond. 1803, 93, 29–273.

22 García-Gil, A.; Epting, J.; Ayora, C.; Garrido, E.; Vázquez-Suñé, E.; Huggenberger, P.; Gimenez, A.C. A reactive transport model for the quantification of risks induced by groundwater heat pump systems in urban aquifers. J. Hydrol. 2016, 542, 719–730.

23 Xiuling Ren, Yanhui You, Qihao Yu, Guike Zhang, Pan Yue, Mingyang Jin, "Determining the Thermal Conductivity of Clay during the Freezing Process by Artificial Neural Network", Advances in Materials Science and Engineering, vol. 2021, Article ID 5555565, 10 pages, 2021.

24 Balan, Mugur C. et al. “Assessments about soil temperature variation under censored data and importance for geothermal energy applications. Illustration with Romanian data.” Journal of Renewable and Sustainable Energy 5 (2013): 041809

25 Calculation methodologies for the energy performance of buildings, code MC 001-2022

SPONSORED BY:

Energy Audit of a Kindergarten

Ing. Angelika Václavová (angelika.vaclavova@stuba.sk)
Supervisor: doc. Ing. Michal Krajčík, PhD. (michal.krajcik@stuba.sk)
Department of Building Services, Faculty of Civil Engineering,
Slovak University of Technology in Bratislava, Slovakia, 2024

Abstract - The content of the paper is to provide an energy audit of a kindergarten building located in the town of Spišská Nová Ves, for the purposes of evaluating the current state of the building's energy economy. The assessment is based on both the thermal and technical properties of building structures, the actual energy demand for heating. At the same time, this thesis also determines the condition of the sanitary installations, as well as the electrical installations of the building. The main goals of this work are to suggest a proposal for individual measures leading to a reduction in energy consumption, their economic evaluation, and subsequently to compile a set of recommended measures with a reduction in financial requirements for the operation of the addressed object with an effective payback period.

Index Terms - energy audit, energy saving measures, economic evaluation, energy efficiency

Introduction

The energy performance of a building is the total amount of energy required to achieve all the energy needs associated with the use of the building. Energy is used to ensure the needs of building occupants with the aim of creating conditions of thermal comfort, adequate hygienic conditions and generally to improve the quality of life. The energy performance of a building can be improved by reducing energy consumption for each point of use, in heating, cooling, ventilation and lighting, through the design of energy saving measures. Before renovating a building, it is recommended to process an energy audit of the building so that building operators can avoid making a bad investment decision.

The energy audit includes an overall inspection of the building, analysis and evaluation of the current state of the building. The energy consumption has been characterized, a proposal for optimal measure has been prepared concerning the building structure or building services that can lead to an improvement of the energy efficiency of the building. The investments needed to implement the proposed measures are also evaluated, with economic payback. The design of measures can be processed in many alternatives, so the orderer of the energy audit can choose the most advantageous solution for him.

The energy audit is processed according to the methodology and requirements of Act No. 321/2014 Coll. on Energy Efficiency and in according to the Decree No. 179/2015 Coll. of the Ministry of Health of the Slovak Republic

I. DESCRRIPTION OF A CURRENT STATE OF THE SUBJECT OF THE ENERGY AUDIT

The kindergarten is located in the town of Spišská Nová Ves, in the catastral area of Spišská Nová Ves. The building is categorized as a civic facility building in the category of school or school facilities.

The "Kindergarten and Nursery School" building was built in the early 1970s and was located in the building used until today. Nowadays, the building operates only as a kindergarten for children from 2,5 - 6 years old. The character of the building is a block, it is located on flat terrain within the residential housing estate.

Figure 1 External view on the south-east side (rear entrances)

The kindergarten is a building without basement composed of three interconnected parts, with different storeys.

1. Kitchen with sanitary facilities and laundry
2. Classes with dining and social zones
3. Classes

A. Constructional-technical solution of a building

Vertical constructions (external wall): filling external walls are made of porous concrete precast panels thickness 300 mm, which were additionally insulated in 2016 by contact insulation system "ETICS", on the material based on polystyrene, type "EPS-F" thickness 140 mm. The surface treatment of the walls is solved by silicone painted plaster.

Horizontal structures (ground floor): ceilings are reinforced concrete, prefabricated. Floor covering layers vary according to the purpose of the rooms (floating floor, ceramic tiles, linoleum, carpet, etc.)

Roof structure: the roof structure of all three parts is flat, single skin made of reinforced concrete panels. The supporting structure is a prefabricated skeleton of the MS-66 system. The roof is thermally insulated by roofing aerated concrete slabs of 240 mm thickness, placed on the sloped layer made of loose perlite, thickness up to 80 mm.

Building openings: the filling constructions in the building underwent a complete replacement in 2012. Windows and entrance doors are made of plastic frame with double glazing.

B. Thermal-technical properties of a building

The following table shows the data of all the cooled envelope structures of the evaluated building through on which heat losses occur.

TABLE I.
THERMAL-TECHNICAL PROPERTIES OF STRUCTURES

Construction	Area	Heat transfer coefficient		Thermal resistance	
		U	U_{r1}*	R	R_{r1}*
	[m^2]	[$W/m^2.K$]		[$m^2.K.W^{-1}$]	
External wall	1038,0	0,19	0,22	5,41	4,4
Flat roof	1550,0	0,43	0,15	2,32	6,5
Building opening	363,6	1,2	1,7	-	-
Ground floor	1550,0	0,14	-	0,17	2,5

* required value by standard STN 73 0540 – 2 + Z1 + Z2

II. PURCHASE OF A ENERGIES AND WATER

A. Natural gas

The building takes natural gas from the company Slovak Gas Industry, a.s. Natural gas is used in the building exclusively for the needs of the kitchen. Natural gas consumption was significantly lower in 2020 due to the partial closure of the kindergarten due to pandemic COVID-19.

TABLE II.
AMOUNT AND PRICE OF THE PURCHASED NATURAL GAS

Natural gas	2020		2021		2022		Average 2020-2022
	[kWh]	[Eur]	[kWh]	[Eur]	[kWh]	[Eur]	[kWh]
Total	6 176	290	8 931	388	9 889	895	**8 332**

B. Thermal energy

The building is connected to the central heat supply from the distributor EMKOBEL a.s. From the total annual consumption, it can be stated that the kindergarten was still heated to the minimum temperature even during the closure in 2020.

TABLE III.
AMOUNT AND PRICE OF THE PURCHASED THERMAL ENERGY

Thermal energy	2020		2021		2022		Average 2020-2022
	[MWh]	[Eur]	[MWh]	[Eur]	[MWh]	[Eur]	[MWh]
Total	149	11035	170	10775	158	11164	**159**

The purchased heat is used exclusively for heating in the building. The heating system is designed with one branch as a two-pipe heating system with a temperature gradient of the heating medium of 92.5°C/67.5°C. Central heating regulation is provided by the users themselves on the heating devices. There are no fittings installed in the central heating technical room to regulate the branches. The total number of installed heating elements is 98, made up of original cast iron radiators.

Figure 2 Heat transfer station of Kindergarten

C. Electrical energy

The kindergarten is supplied from the distribution system of the company Eastern Slovak Energy a.s. The most important appliances of the kindergarten are lighting, kitchen equipment, and electric water heaters.

TABLE IV.
AMOUNT AND PRICE OF THE PURCHASED ELECTRICITY

Electricity	2020		2021		2022		Average 2020-2022
	[kWh]	[Eur]	[kWh]	[Eur]	[kWh]	[Eur]	[kWh]
Total	20174	3541	21392	3976	20840	7852	**20 802**

Hot water is prepared in local electric storage heaters at the point of consumption. The heaters supply hot water to the sanitary and hygiene spaces, the kitchen, and the laundry.

The installed lighting of the building is made up of original bulbs as well as already reconstructed LED luminaires. The total installed lighting power is approximately 9.73 kW. The total number of luminaires installed in the building is 333. The electricity consumption for lighting accounts for almost 47 % of the total average electricity consumption for the kindergarten building (average in 2020-2022).

D. Drinking water

The water supplier is Podtatranská water operating company, a.s. The cold-water supply to the building is from the public water supply. From the point of view of the assessment of possible savings measures, the audit further assesses only the consumption for water and sewerage, not including the amount for water from surface runoff.

TABLE V.
AMOUNT AND PRICE OF THE PURCHASED DRINKING WATER

Drinking water	**2020**		**2021**		**2022**		**Average 2020-2022**
	[m^3]	[Eur]	[m^3]	[Eur]	[m^3]	[Eur]	[m^3]
Total	384	847	411	910	544	1 256	446

The sanitary installations in the object have been completely reconstructed. The installed washbasin taps and shower heads are mostly without energy-saving solutions. The installed toilet bowls are with two-stage flushing.

III. ASSESMENT OF A CURRENT STATE

The invoiced amount of energy consumption is based on standardised input parameters in terms of day degrees and indoor and outdoor ambient temperatures. The following table summarises the average amount of fuel, energy and water inputs to the building for the years 2020-2022, where the price in 2022 excluding VAT has been considered.

TABLE VI.
STRUCTURE OF ENERGY INPUT DATA

Form of energy/ medium	**Unit**	**Amount**	**Calorific value** [GJ/unit.]	**Energy content** [MWh]	**Annual costs** [€]
Electricity	MWh	21	1,00	21	7 838
Thermal energy	GJ	572	3,60	159	11 263
Natural gas	MWh	8	0,90*	8	754
Drinking water	m^3	446	-	-	1 030
Total energy consumption				**187**	**19 855**

The following graph shows the percentage evaluation of the cost of electricity, heat, natural gas and water commodity consumption.

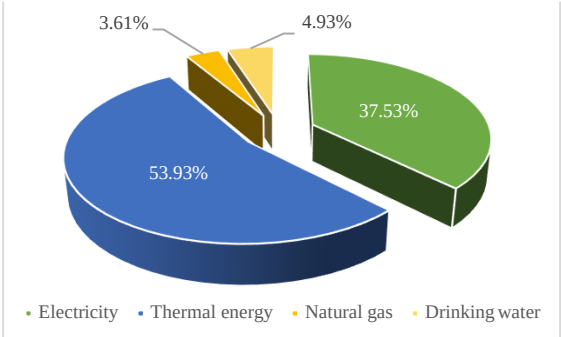

Figure 3 Commodity costs in %

The graph shows that thermal energy accounts for the dominant part of the costs, up to 54%, electricity accounts for 36% of the costs, water accounts for 5% and the rest is the cost of natural gas.

A. Energy consumption

After considering the effects of the specific climatic conditions in the given location, the heating consumption was recalculated using the day-step method (based on billing values) and the average value of the heating consumption was determined. Losses for energy conversion and distribution are also included in the total heating consumption. The average heating consumption in the years under consideration was 137,6 MWh/year.

TABLE VII.
STRUCTURE OF ENERGY INPUT DATA – CLIMATICALLY NORMAL YEAR

Form of energy/ medium	**Unit**	**Amount**	**Calorific value** [GJ/unit.]	**Energy content** [MWh]	**Annual costs** [€]
Electricity	MWh	21	1,00	21	7 838
Thermal energy	GJ	495	3,60	138	9 751
Natural gas	MWh	8	0,9	8	754
Total energy consumption				**166**	**18 343**

B. Energy demand

The calculation of the total heat demand for heating is carried out by the day-step method using the standardised input parameters for the area. The calculation of heat losses is based on the currently known and described condition of the building structures to be cooled (Table 1). The total heat demand for heating to cover heat losses through transition and ventilation was reduced by external heat gains from solar radiation and internal heat gains from electrical and thermal appliances and from metabolic heat of occupants. The heat demand for heating the building is 132,7 MWh/year.

TABLE VIII.
ENERGY DEMAND FOR HEATING

Monitored data	Unit	Calculated value
Thermal energy demand for heating	MWh/year	132,66
Thermal loss of the transmission system	MWh/year	14,95
Thermal loss from distribution systems	MWh/year	5,76
Energy consumption of the pump	MWh/year	1,86
Thermal loss from heat production	MWh/year	1,51
Energy demand for heating	MWh/year	156,8

The total energy demand for heating is equal to 156, MWh/year.

IV. ENERGY SAVING MEASURES

A. Installation of perlators and energy saving shower heads

In the sanitary installations of the building are installed mostly faucets without perlators. There are a total of 23 wash basin spout fittings and 5 showers installed in the building. As part of the proposed cost-saving measure, it is envisaged to install 23 pcs of perlators on the basin spout fittings to direct the water flow and aerate it, and consequently reduce the water flow. At the same time, it is proposed to install a total of 5 energy saving shower heads.

Economical evaluation of the measure:

- Investments: 570 €
- Water savings: 47 m^3/year
- Cost savings On drinking water: 108 €/year
- Lifetime of a measure: 15 years
- Real time payback: 6,3 years

B. Modernization of interior lighting

The measure proposes the replacement of the remaining original lighting by LED light sources, the number of 128 pcs. The measure envisages replacing only the bulbs themselves, piece by piece, without replacing the existing wiring. According to the type of operation of the kindergarten, 1 000 hours of lighting per year were considered.

Economical evaluation of the measure:

- Investments: 1280 €
- Electricity savings: 6,5 MWh/year
- Costs savings on electricity: 2460 €/year
- Cost savings on operation and maintenance 92 €/year
- Lifetime of a measure: 30 years
- Real time payback: 0,5 years

C. Hydraulic regulation and balancing of the heating system

The heating system in the kindergarten building is not hydraulically regulated. Central heating is regulated manually as needed by thermostatic heads on the end elements, which were replaced with new ones in 2019. The proposed measure envisages the installation of control valves on the main central heating branch and at the same time on the riser pipes at the foot of the risers. The currently installed thermostatic heads need to be pre-set, which will automatically restrict the heating water flow as required. The heating system is re-regulated, which prevents possible under- or overheating in the rooms, and a large consumption of pumping power.

Economical evaluation of the measure:

- Investments: 3430 €
- Thermal energy savings: 4,1 MWh/year
- Cost savings on thermal energy: 293 €/year
- Cost savings on operation and maintenance 92 €/year
- Lifetime of a measure: 10 years
- Real time payback: 18,1 years

D. Thermal insulation measures - flat roof insulation

The roof construction does not meet the requirement of the standard for thermal protection of buildings, for this reason the roof insulation with contact insulation system (EPS) with heat transfer coefficient λ = 0.038 W/(m.K) is considered. To meet the energy criteria, the existing roof construction has to be additionally insulated with a suitable thermal insulation of at least 160 mm thickness. The heat transfer coefficient after implementation should not exceed 0,15 W/m^2.K for the roof construction.

The estimated cost of the roof insulation measure is 120 €/m2 without VAT. The cost of the material, the removal and reinstallation of the asphalt strip and the cost of the implementation work were taken into account in the price determination.

Economical evaluation of the measure:

- Investments: 186 600 €
- Electricity savings: 33,9 MWh/year
- Costs savings on electricity: 2401 €/year
- Cost savings on: operation and maintenance 1200 €/year
- Lifetime of a measure: 25 years
- Real time payback: 51 years

E. Installation of photovoltaic panels

The kindergarten has a relatively large area of unshaded roof structure where a south-facing photovoltaic power station (PV plant) can be located. The proposed measures envisage the generation of electricity by photovoltaic panels to cover the total annual electricity consumption. The system will remain connected to the distribution

system of the company Eastern Slovak Energy a.s, but photovoltaic panels will be connected to the system too.

The proposed PV power output considers synergies in the case of reducing the overall electricity consumption of the building by installing LED lighting. In the calculation was considered a monocrystalline photovoltaic module Vitovolt 300 type M335WA from the manufacturer Viessmann. The design considered placing the collectors on the flat roof of the kindergarten at an angle of 35º facing to the south. The peak power of one panel is 330 Wp with an area of 1,732 m2, and a specific power of 195,9 W/m2.

For electricity consumption, the average electricity consumption for the period 2020-2022 under review was taken into account. After retrofitting the original lighting with LED technology, the electricity consumption would be reduced by 6.528 MWh/year, i.e. a value of 14.272 MWh/year. This value has been taken into account in the design of the number of panels. The proposed number of panels to cover the energy consumption is 44 PV panels, with a total plant capacity of 14 520Wp.

Average monthly energy production data was obtained for a given kindergarten location from the Photovoltaic Geographic Information System (PVGIS) website, available at: https://re.jrc.ec.europa.eu/pvg_tools/en/.

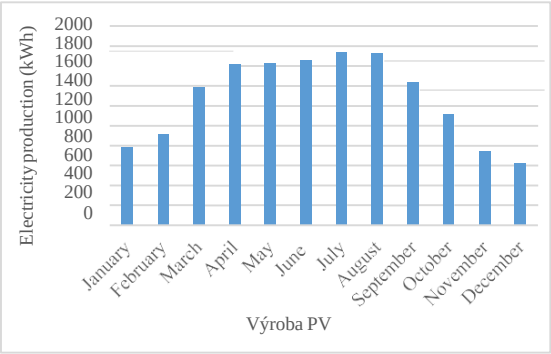

Figure 4 Electricity production (PV 14,52 kWp)

The surplus electricity generated by the PV plant is considered to be returned back to the grid. The measure assumes a purchase price of 180 €/MWh (excluding VAT) for the surplus electricity.

Economical evaluation of the measure:

• Investments:	17 400	€
• Electricity savings:	13,8	MWh/year
• Costs savings on electricity:	5197	€/year
• Cost saving on operations	560	€/year
• Proceeds for the sale of electricity:	670	€/year
• Lifetime of a measure:	23	years
• Real time payback:	3,7	years

V. SET OF RECOMMENDED MEASURES

The set of recommended measures includes all proposed measures with a payback period less than their lifetime, according to annex 4 to the Decree 327/2015 Coll. At the same time, the recommended payback period for the set of measures specified in the decree, namely 15 years, was monitored. The measure concerning the hydraulic regulation and balancing of the central heating system does not meet the payback requirement, but it was also included in the measure set, due to the obligation to ensure and maintain a hydraulically regulated heating system according to Act No. 321/2014 Coll.

The set of recommended measures included:

- Installation of perlators and energy saving shower heads
- Modernization of interior lighting using LED technology
- Hydraulic regulation and balancing of the central heating system
- Installation of photovoltaic panels

Annual energy savings

• Energy savings:	24,4	MWh/year
• Water savings:	47	m^3/year

A. Economic assessment of the set of recommended measures

For the purposes of the calculations, 5% discount rate was considered; the compound increase in energy prices was not considered. In calculating the simple payback period of the recommended measures, the total investment cost of each measure and the savings in energy, water, operation and maintenance costs were used.

Results of the economic evaluation of the set of recommended measures:

• Investments:	22 680	€
• Cost savings on thermal and electrical energy	7950	€/year
• Cost savings on repair and maintenance:	92	€/year
• Cost savings on drinking water:	108	€/year
• Proceeds from the sale of electricity:	670	€/year
• Benefits of the implementation of the set of measures:	8820	€/year
• Real time payback	2,8	years

The following chart shows the discounted cash flow in each year, which shows the cumulative discounted cash flow. By calculating the cumulative cash flow, it was found that by the end of the third year after the application of the set of recommended measures, the investments start to be profitable.

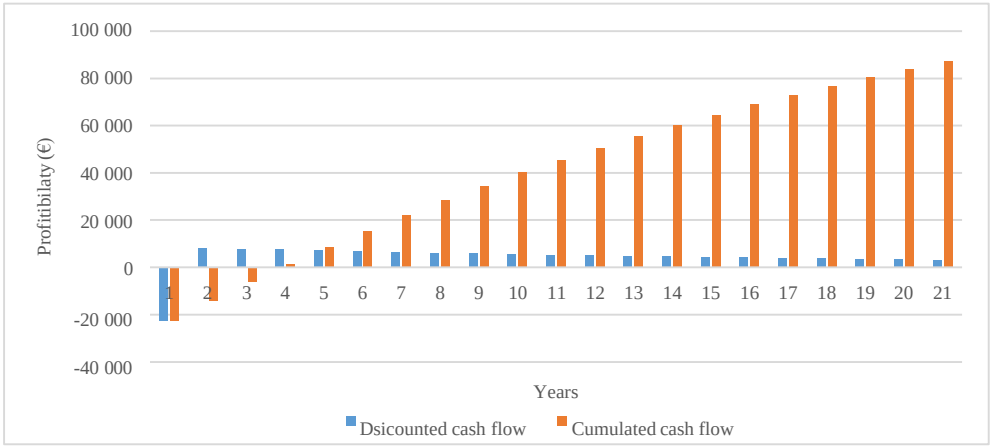

Figure 5 Discounted (cumulated) cash flow

VI. DISCUSSION

The individual cost-saving measures as well as the set of recommended measures are evaluated from both a technical and an economic point of view. The assessment was based on billing data of real consumption of heat and electricity, as well as cold water for the years 2020-2022.

The set of recommended measures consists of the measures that most affected by the deficiencies of the current energy economy and at the same time are the most beneficial. The implementation of the set of recommended measures is appropriate to carry out with regard to the time of payback of investment, the lifetime of the measures, the difficulty of implementation, the maintenance and operation of the building.

The benefit of the set of recommended measures consists in the reduction of electricity consumption by 97%, in the reduction of water consumption by 20%, in the reduction of total costs by 8 820 €/year, in the efficiency of the invested funds, where the real payback period is 2.8 years.

VII. CONCLUSION

The purpose of the energy audit is a technical and economical assessment of the energy saving potential and the proposal of measures leading to a reduction of fuel and energy consumption in the assessed building.

The energy audit is based on the assessment of the current state of the building, its construction and technological design and the assessment of the energy performance of the building. The aim was to propose energy-saving measures that will improve the energy efficiency of the building.

REFERENCES

DAHLSVEEN, T. – PETRÁŠ, D. – CHMÚRNY, I. – SMOLA, A. – LULKOVIČOVÁ, O. – FÜRI, B. – KONKOĽ, R. *Energy audit and certification of buildings.* Bratislava: Jaga Group, 2008. 163 s. ISBN 978-80-8076-063-2.

KRAJČÍK, M. – PETRÁŠ, D. – SKALÍKOVÁ, I. *Energy assessment of buildings.* Bratislava: Spektrum STU, 2019. 220 s. ISBN 978-80-227-4903-9.

CHMÚRNY, I. *Thermal protection of buildings.* Bratislava: Jaga, 2003. 214 s. ISBN 80-889-0527-3.

STERNOVÁ, Z. 2010. *Energy efficiency and energy certification of buildings.* Bratislava: JAGA GROUP, 2010. ISBN 978-80-8076-060-1

Event Pictures

The REHVA Community of Young Professionals brings together participants from past editions of the student competitions to share knowledge and best-practices .

This Book of Papers aims at concentrating the knowledge of each edition of the competition and serve as a way to commemorate the occasion.

REHVA warmly thanks all the people involved in the organisation and participation to the event.

Join the discussion on the
@RCYP Linkedin group!